

EARTHQUAKE SOURCE PARAMETERS AND ATTENUATION CHARACTERISTICS OF ARUNACHAL REGION

Ph. D. THESIS

by

ROHTASH KUMAR



**DEPARTMENT OF EARTHQUAKE ENGINEERING
INDIAN INSTITUTE OF TECHNOLOGY ROORKEE
ROORKEE-247 667 (INDIA)
APRIL, 2015**

EARTHQUAKE SOURCE PARAMETERS AND ATTENUATION CHARACTERISTICS OF ARUNACHAL REGION

A THESIS

*Submitted in partial fulfilment of the
requirements for the award of the degree
of*

DOCTOR OF PHILOSOPHY

in

EARTHQUAKE ENGINEERING

by

ROHTASH KUMAR



**DEPARTMENT OF EARTHQUAKE ENGINEERING
INDIAN INSTITUTE OF TECHNOLOGY ROORKEE
ROORKEE-247 667 (INDIA)**

APRIL, 2015

**©INDIAN INSTITUTE OF TECHNOLOGY ROORKEE, ROORKEE-2015
ALL RIGHTS RESERVED**



INDIAN INSTITUTE OF TECHNOLOGY ROORKEE

ROORKEE

CANDIDATE'S DECLARATION

I hereby certify that the work which is being presented in the thesis entitled “**Earthquake Source Parameters and Attenuation Characteristics of Arunachal Region**” in partial fulfillment of the requirements for the award of the Degree of **Doctor of Philosophy** and submitted in the **Department of Earthquake Engineering** of the Indian Institute of Technology Roorkee is an authentic record of my own work carried out during a period from December, 2011 to April, 2015 under the supervision of **Dr. S.C. Gupta**, Scientific Officer, Department of Earthquake Engineering, Indian Institute of Technology Roorkee, Roorkee.

The matter presented in the thesis has not been submitted by me for the award of any other degree of this or any other Institute.

(ROHTASH KUMAR)

This is to certify that the above statement made by the candidate is correct to the best of my knowledge.

(S.C. Gupta)
Supervisor

Dated: April , 2015

Abstract

The seismic waves produced by the earthquakes are used to study the structure and composition of the earth's interior, and the properties of earthquake source. However, to understand how the wave field is radiated from the earthquake source it is important to deduce the properties of the earthquake source as the resolution of the earth's structure requires precise knowledge of the parameters of earthquake source and path travel by seismic waves (Shearer, 1999). The parameters characterizing the source of an earthquake are called the earthquake source parameters. These parameters are computed in the time domain from the measurements of arrival times of seismic phases and in the frequency domain from the spectra of the seismic waves. In the early 1930's Richter introduced the magnitude parameter to measure the size of an earthquake using the amplitude of seismic waves. The similar work of Aki (1967) and Brune (1970) laid a strong foundation to develop the scaling laws and to compute the earthquake source parameters using the spectra of seismic waves. The earthquake source parameters can be broadly classified into two types: the kinematic parameters and the dynamic parameters (Duda, 1978). These parameters provide a great deal of information about the properties of the earthquake source, and find a large number of applications in Seismology and Earthquake Engineering. Study of seismic wave attenuation provides the information regarding the medium through which they travel and this information can be interpreted in terms of both physical properties of the geological formation as well as level of inhomogeneities present in the medium. This is important for understanding the seismotectonics and also play significance role in estimation of seismic hazard for a given region (Aki 1969, Aki and Chouet, 1975).

Himalaya mountain range is formed by the collision of Indian plate with Eurasian plate about 40 to 50 million years ago. It leads to the building of regional and local scale tectonic features. The main boundary thrust (MBT) and the main central thrust (MCT) are few of them.. The most of earthquake occurred in the Himalaya are along these tectonic features. It is important to understand the earthquake source process and predict the strong ground motion. Two main factors that plays important role in understanding the tectonics and medium properties of a region are earthquake source properties and seismic wave

attenuation. So the understating of these attributes of earthquakes is important for various purposes such as river valley projects and other construction works in the Himalayan region.

The Himalayas can be divided structurally (tectonically) from north to south as: Tibetan Himalaya (Northwest part of Arunachal Himalaya bordering Bhutan and Tibet, trending NE-SW), Higher Himalaya (limits between Tibetan Himalaya and MCT, ENE-WSW trend adjacent to Bhutan and changes to NE-SW eastward), Lesser Himalaya (limits between Higher Himalaya and sub-Himalaya, trending E-W in western part, swinging NNE-SSE till the syntaxial then NW-SE), sub-Himalaya (trending E-W near Bhutan, swings ENE-WSW towards east) and the division from east to west: The Eastern Himalaya, Central Himalaya and western Himalaya. (e.g. Gansser 1964; Le Fort 1975). In the northeastern part of India, is Arunachal Pradesh which mostly occupied by the high mountain range of eastern Himalayas. The Himalayan range enters in Arunachal Pradesh from Bhutan at the west of Kameng district, and the altitude in this region varies from 800-7,000 m above mean sea level. It runs through the northwards region over the Kangto region before ending at the easternmost part of Arunachal Himalaya, i.e. The Namcha Barwa Massif. This part of the Himalayas includes extensive faulting and over-folding as the major structural element. The regional structural trend of the eastern Himalayas is mostly E-W to ENE-WSW from Bhutan to the northeastern Arunachal Pradesh, which changes gradually to NE-SW near Siang valley and terminates against Siang fracture (e.g. Nandy 1976). Geotechnically, the Arunachal Pradesh can be divided into four geotechnical blocks: the Himalaya, the Mishimi hills, Nagapatkoi ranges of the Arkon Yomo Mountain and Brahmaputra Basin; each of these have experienced intense stages of tectonic development in response to collision of plates and uplift of the Himalayas (Kumar 1997).

From the broad description above, the study region, lower Siang of Siang valley is in Arunachal Himalaya surrounded by Main Frontal Thrust, Main Boundary Thrust in the south, Mishmi Thrust, Tidding Suture and Lohit Thrust in the east and Bame-Tuting Fault in the west. This region is in seismic zone V as per IS Code (IS 1893 (Part 1): 2002) of India. This region shows polyphase deformation, and three stages could be recognized in the region. Six major lithotectonic belts with different litho-stratigraphic settings and deformation patterns

separated from one another by regional thrust planes are present in the valley (e.g. Singh and Chowdhary 1990). Like the other parts of Himalaya, the eastern most Himalaya of Arunachal Pradesh exhibits quiet high seismicity and lies within the seismic zone V as per IS Code (IS 1893 (Part 1): 2002). Several earthquakes of smaller to moderate magnitudes have occurred in this region (Kayal, 1987). The two great earthquakes namely Shillong (1897) and Assam (1950) earthquakes having magnitudes 8.1 and 8.6, respectively, fell in close proximity to the study region. Shillong earthquake on June 12, 1897 (M_w , -8.1) located near the northern edge of Shillong Plateau while Assam earthquake on August 15, 1950, located in Mishmi hills. On September 18, 2011, the Sikkim

The present study is based on observational data and is devoted to the estimation and interpretation of source parameters and wave attenuation characteristics in the Lower Siang region of Arunachal Pradesh using the data of microearthquakes of small and moderate earthquakes. This study has been carried out with the following objectives:

- To estimate the source parameters of local earthquakes for Lower Siang region of Arunachal Himalaya and to develop the scaling relations between various source parameters.
- To estimate the focal mechanism of local earthquakes using the waveform inversion method.
- To determine the seismic wave attenuation characteristics of Lower Siang region of Arunachal Himalaya by estimating the quality factor of P-wave (Q_α), S-wave (Q_β) and coda waves (Q_c) of the local earthquakes data and to develop frequency dependence attenuation relationships for the region.
- To investigate the lapse time dependence of Q_c .
- To separate out the effect of the intrinsic and scattering attenuation from the total attenuation.

The P-wave and S-wave arrival time data of 104 local earthquakes has been measured from the digital seismograms obtained during the period from July 2011 to May 2012 from

five seismological stations. The hypocentre parameters of local earthquakes have been estimated using HYPOINVERSE computer program (Klein, 1978) integrated in SEISAN software used for the estimation of hypocentre parameters. The velocity model given by Khattri et al. (1983) used for the estimation of hypocentre parameters. The standard errors in the estimation of hypocentre parameters for these events are ≤ 0.50 sec in origin time (RMS), ≤ 5.0 km in epicentre (ERH), and ≤ 5.0 km in focal depth (ERZ).

The results on the source parameters and f_{\max} have been obtained for the Lower Siang region of Arunachal Himalaya from the analysis of 104 local earthquakes. The results showed that the values of seismic moment, Moment magnitude, the source radii and stress drops varies from 1.6×10^{18} to 3.1×10^{23} dyn-cm, 1.4 to 5.0, 157.8 to 417.1 m and 0.1 to 74 bars respectively. Except a few events, the stress drop remains constant and does not vary with focal depth. Hence no dependency of stress drops with depth is obtained for the study region that indicates that the stress drop is only the function seismic moment and fracture radius. Based on results on seismic moment and corner frequency, the scaling relation $M_0 \propto f_c^{-3.27}$ has been obtained for the study region. $\Delta\sigma$ relationships with M_0 , $\log(\Delta\sigma) = 0.1804 \log(M_0) - 2.945$ is also obtained for the study region. Satoh et al. (2000) obtained a relationship $\log(\Delta\sigma) = -2.91 \log(M_0) + 5.8$ using deep borehole data of Japan. The results obtained in present study are seems to be more realistic than Satoh et al. (2000). Satoh et al. (2000) relationship suggests stress drop increases as the seismic moment decreases. But in real scenario it is not possible because lower magnitude event can never have stress drop greater than high magnitude event.

The results have been obtained based on the comparative study of f_c and f_{\max} showed that both f_c and f_{\max} behaves in a similar manner with respect to source, focal depth and epicentral distance. From the various plots of both f_c and f_{\max} with seismic moment, focal depth, epicentral distance at different recording site showed the same amount of scatters and trends in the distribution of data. From this, it is observed that f_{\max} is having almost similar behavior to seismic moment as obtained for f_c to the seismic moment. For this it is brought out that f_{\max} is due to source process because it is affected by source as well as site in similar way as f_c and it is well known that f_c is the source property so f_{\max} is also a source effect. Both f_c and f_{\max} are found to be independent of epicentral distance and depth of occurrence. Relationship of f_{\max} with seismic moment and stress drop has also been obtained.

In the present study efforts have been made to manifest the source of non-DC (CLVD) component of MTs. from the moment tensor analysis of 104 local earthquakes. The moment tensor analysis of 41 earthquakes out of 104 earthquakes having magnitude greater than 2.5 and signal to noise ratio (SNR) greater than 6 with small epicentral distances brought out more clarity in the identification of cause of CLVD. It has also been observed that variation in CLVD caused by various source such as noise in the data, focal depth and magnitude of the event. Source depth acts a controlling factor of CLVD. For selected 41 events the high CLVD component confined to shallow depth. For high SNR the CLVD% is quite low. CLVD is also dependent on the magnitude of event. In the higher magnitude range greater than 3.5, DC% is greater than 60%. Hence most of high magnitude earthquakes are having double couple (DC) source mechanism. The appearance of CLVD in low magnitude may also be attributed to the directivity effect (Adamova and Síleny, 2010).

The seismic wave attenuation has been studied for Lower Siang region by estimating the quality factor of P-wave (Q_α) and S-waves (Q_β) in the frequency range 1.5 to 24 Hz adopting the extended coda normalization method. The estimated value of Q_α and Q_β are found to be strongly frequency dependence in the study region. Their mean values vary from 49 ± 4 at 1.5 Hz to 1421 ± 6 at 24 Hz for Q_α and from 118 ± 6 at 1.5 Hz to 2335 ± 5 at 24 Hz for Q_β . The frequency dependence Q_α and Q_β relationships are obtained as, $Q_\alpha = (25 \pm 1)f^{(1.24 \pm 0.04)}$ for P-wave and $Q_\beta = (58 \pm 1)f^{(1.16 \pm 0.04)}$ for S-wave. The comparison of Q_α and Q_β has brought out that P wave attenuates more rapidly as compared to S-wave at all frequencies.

The results obtained in the present study are found to be comparable with the other seismically active regions of the India as well as world. The comparison of Q_α and Q_β with the other seismically active regions of India showed that the region around the Lower Siang is more attenuating among almost all Indian regions except the Chamoli region which showed higher attenuation, whereas the comparison among some regions of World showed similarly increasing pattern with increasing frequency. The higher frequency dependence of attenuation describes the region is high seismically active. Also low value of Q_α and Q_β in the Lower Siang region as compared to other Indian regions indicate the high tectonic activity. Higher Q_β than Q_α for the entire frequency range indicate the crust of the Lower Siang region of Arunachal Himalaya is highly heterogeneous.

The coda waves of 104 local earthquakes have been analyzed for three lapse time windows (30, 40 and 50sec) employing the single backscattering model at seven frequency bands with a central frequency in the range of 1.5 Hz to 24.0 Hz. Obtained Results show the average variation in Q_c is from 109 ± 33 , 138 ± 42 and 162 ± 46 at 1.5 Hz to 3149 ± 923 , 3439 ± 944 , and 3889 ± 1165 at 24 Hz for lapse time windows of 30, 40 and 50 sec, respectively. The frequency dependence relationships; $Q_c=(52\pm1)f^{1.22\pm0.03}$, $Q_c=(83\pm1)f^{1.18\pm0.02}$ and $Q_c=(105\pm1)f^{1.16\pm0.02}$ are obtained for lapse time windows of 30, 40 and 50 sec respectively. So in the study region Q_c is found to be function of frequency and lapse time window and Q_c increase with increase of frequency as well as lapse time window. The increase in Q_c value with the time window is attributed to the increase in Q_c with depth because heterogeneities of the medium decreases with depth. in the frequency dependent relation given above Q_0 (Q_c at 1 Hz) value increases with the lapse time window while there is a nominal decrease in the degree of frequency dependence (η) with increasing window length. This may be due to decrease in scattering effect and hence the decrease heterogeneities of the medium with depth. The comparison of Q_c value obtained in the Lower Siang region with that obtained in other part of India and World showed that Siang region is tectonically active.

The separation of scattering (Q_s) and intrinsic (Q_i) attenuation from the S-wave attenuation (Q_β) and coda wave attenuation (Q_c) has been carried out employing the Wennerberg (1993) method and developed the frequency dependent Q_s and Q_i relations.

The Q_i and Q_s show the frequency dependent character in the frequency range 1.5 to 24 Hz. The average scattering and intrinsic relationships are obtained for the region as $Q_s=(31\pm1)f^{1.04\pm0.02}$, $Q_s=(48\pm1)f^{1.05\pm0.02}$ and $Q_s=(61\pm1)f^{1.05\pm0.02}$ and $Q_i=(68\pm1)f^{0.95\pm0.06}$, $Q_i=(134\pm1)f^{1.01\pm0.05}$ and $Q_i=(167\pm1)f^{0.96\pm0.03}$ for lapse time windows of 30, 40 and 50 sec, respectively. Both Q_c and Q_i at a given frequency increases with lapse time duration. This can be attributed to the decreases in the heterogeneities and the inter-grain fraction with increase in depth as larger the lapse time represents the characteristics of deeper depths. Q_i and Q_s comparison and values of seismic albedo shows that scattering attenuation is more prominent over intrinsic attenuation in the region over entire frequency range 1.5 to 24 Hz.

Various studies of Q in various regions of the world show high Q -value in seismically stable regions and relatively low Q value in the seismically active regions. The Q -values and

their frequency dependent relationships estimated in the present study are well correlate with highly seismically active and heterogeneous regions. The frequency dependent attenuation relations developed in present study would be useful in various scientific and engineering applications including earthquake hazard assessment, earthquake source parameter estimation and understanding the physical phenomenon related earthquake elastic energy propagation of Lower Siang region as well as other regions of Arunachal Himalaya and NE region as a whole.

ACKNOWLEDGEMENT

It is beyond any doubt that the research work is period is both the toughest and most challenging time throughout the study. This thesis is the result of the work carried out through such time, in which I received the help of several people who deserve some words of gratitude.

It gives me great pleasure to express my deepest gratitude to my Ph.D. **Dr. S.C. Gupta**, for his help, relevant literature sources and valuable comments on this document. His knowledge of seismology, as well as his suggestions on how to tackle a problem, guided me towards my research goals. His logical ideas and detailed knowledge motivated me throughout the study and more importantly building my attitude of systematic investigation of scientific problem. He inspires me very much how to express my ideas and showed me different paths to approach research problems and to accomplish final goals.

Profound gratitude is due to the faculty of earthquake engineering department, especially, **Prof. and Head Dr. M.L. Sharma, Prof. H.R. Wason, Dr. J.P. Narayan and Dr. J. Das** for their friendly guidance and technical advice throughout the research work. The technical, office and supporting staff of the department, deserve credit for their help too.

I would like to thanks **Dr. R.K. Bajpai** (Scientific Officer-G) and **Shri R.S. Soni** Head of Technology Development Division BARC Mumbai for their kind support and encouragement.

My friends and seniors help me lot while staying in Roorkee and working in BARC Mumbai. In particular, I would like to manifest my deepest thanks to **Dr. Arjun Kumar, Dr. Sandeep Sanger Dr. Vinay Kumar, Vishal Khatri, Renu Khatri, Sandeep, Dr. Himanshu Mittal Sanjay Jain, Dr. Anil Kumar Jindal, vandana Ganghas, Kamal, S.P. Singh, Mohit Matta, Manas Jyoti Gohain, Prakash Mukherjee, Prateek Srivastav and Sasank Sekher Misra** for being not only my best friends, but also for the good moments, interesting discussions and significant help in the last weeks of this research. Thank you guys! I am happy that I did not earn only prestigious degree but also sincere and everlasting friends.

Back at home in Peer Bidoli (Karnal), I would like to thank Late **Shri Ram Sarup**, My grandfather, **Smt Rampyari**, My grandmother, **Shri Suresh Kumar**, my father, **Smt. Shyamo Devi**, my mother, **Shri Ram Kumar**, my Uncle, **Smt Neeta devi**, my aunty, **Mr. Shishpal**, my younger brother and **miss Rekha**, my younger sister for the moral support, constant encouragement and blessings which provide me inner strength and encouragement since my first day in Roorkee during ups and downs of the Ph.D. This thesis is therefore, dedicated to my family especially my parents.

[Rohtash Kumar]

Contents

	Page No.
<i>Declaration</i>	<i>i</i>
<i>Abstract</i>	<i>ii</i>
<i>Acknowledgement</i>	<i>viii</i>
<i>Contents</i>	<i>x</i>
<i>List of Figures</i>	<i>xiii</i>
<i>List of Tables</i>	<i>xvi</i>
Chapter 1: INTRODUCTION	1-6
1.1 PREAMBLE	1
1.2 IMPORTANCE OF STUDY	4
1.3 RESEARCH OBJECTIVES	5
1.4 STUDY AREA	5
1.5 DATA SET	6
1.6 PLAN OF THE THESIS	6
CHAPTER 2: GEOLOGY & TECTONICS OF THE REGION AND DATA SET USED	7-23
2.1 INTRODUCTION	7
2.2 GEOLOGY OF THE REGION	8
2.3 TECTONICS OF THE REGION	11
2.4 SEISMICITY OF THE REGION	17
2.5 DATA SET USED IN STUDY	21
CHAPTER 2: ESTIMATION OF SOURCE CHARACTERISTICS	24-56
3.1 INTRODUCTION	24
3.2 EARTHQUAKE SOURCE MODELS	25
3.2.1 Seismic Wave Radiation from a Point Force	27
3.2.2 Far field body waves due to a point source	28
3.2.3 Near field of a point source field	29
3.2.4 Kinematic model of fault rupture	30

3.2.5	Rectangular fault: Haskell's model	30
3.2.6	Circular fault: Brune's model	31
3.2.7	Dynamic model of fault rupture	34
3.3	SOURCE PARAMETERS	34
3.4	ESTIMATION OF EARTHQUAKE SOURCE PARAMETERS: PROCEDURES	38
3.4.1	Baseline Correction	38
3.4.2	Seismogram rotation	39
3.4.3	Instrument corrections	42
3.4.4	Correction for Path Effect	42
3.5	DATA ANALYSIS	43
3.6	RESULTS AND DISCUSSION	46

CHAPTER 4: MOMENT TENSOR SOLUTIONS 57-74

4.1	INTRODUCTION	57
4.2	METHODOLOGY	58
4.2.1	Moment tensor source	58
4.2.2	Basic formulations	60
4.2.3	Inversion of moment tensor	62
4.2.4	Decomposition of moment tensor	64
4.3	GENERAL STEPS OF MOMENT TENSOR INVERSION	65
4.4	ISOLA	66
4.5	ANALYSIS PROCEDURE	67
4.6	DISCUSSION OF RESULTS	71

CHAPTER 5: SEISMIC WAVE ATTENUATION 75-91
CHARACTERISTICS USING BODY WAVES

5.1	INTRODUCTION	75
5.2	BASIC MATHEMATICAL FORMULATION FOR WAVE ATTENUATION	76
5.3	METHOD FOR ESTIMATION OF Q_A AND Q_B	77
5.4	ANALYSIS PROCEDURE	80
5.5	RESULT AND DISCUSSION	82

CHAPTER 6:	SEISMIC WAVE ATTENUATION	92-111
	CHARACTERISTICS USING CODA WAVE	
6.1	INTRODUCTION	92
6.2	MODELS AND METHODOLOGY	93
6.3	ANALYSIS PROCEDURE	97
6.4	RESULTS AND DISCUSSIONS	102
CHAPTER 7:	SEPARATION OF SCATTERING AND	112-124
	INTRINSIC ATTENUATIONS	
7.1	INTRODUCTION	112
7.2	METHOD FOR ESTIMATION OF Q_s AND Q_I	115
7.3	RESULTS AND DISCUSSION	116
CHAPTER 8:	SUMMARY OF RESULTS AND CONCLUSIONS	125-130
8.1	INTRODUCTION	125
8.2	SUMMARY THE RESULTS OF SOURCE PARAMETERS	126
8.3	SUMMARY OF RESULTS ON MOMENT TENSOR SOLUTIONS	127
8.4	SUMMARY OF SEISMIC WAVE ATTENUATION USING BODY WAVES	127
8.5	SUMMARY OF RESULTS ON SEISMIC WAVE ATTENUATION USING CODA WAVES	128
8.6	SUMMARY OF RESULTS ON SSEPARATION OF SCATTERING AND INTRINSIC ATTENUATIONS	128
8.7	LIMITATIONS OF THE PRESENT STUDY	129
8.8	SUGGESTIONS FOR THE FURTHER STUDY	130
	Appendix I	131
	Appendix II	136
	Appendix III	146
	Appendix IV	151
	LIST OF PUBLICATIONS	152
	Bibliography	156-193

LIST OF FIGURES

Figure No.	Details of Figure	Page No.
2.1	The geologic tectonic map of the Himalaya along- with location of study region (red box).	8
2.2	Regional geology of Arunachal Pradesh (after Geological Survey of India, 2010)	10
2.3	Regional tectonic set up of eastern Himalaya. (after Yadav et al., 2009). The box in the figure shows the study area.	12
2.4	Map showing the study area. (Tectonics after GSI, 2010)	13
2.5	Epiconenters of historical significant earthquakes occurred in NE India and its adjoining area (after Rajendran and Rajendran, 2011). The area around study region is marked by box.	18
2.6	Epiconenters of earthquakes occurred within 100 km from the center of study area during 1950 to 2010. Seismotectonic setup around study area is also shown on map (Tectonics after GSI, 2000). MBT-Main Boundary Thrust, MFT- Main Frontal Thrust, BFT- Bame Tuting Fault, LT- Lohit Thrust, TS-Tidding Suture, MT- Mishmi Thrust. (After EQ:2010-22, EQ: 2011-30)	20
2.7	Map showing epicenters of events recorded during July 2011 to May 2012 (solid circles). Tectonics after GSI (2000).	23
3.1	Far field and near field displacement relation on left two panels and far field displacement and velocity spectrum on right panel.	29
3.2	The Haskell's model is a rectangular fault with length L and width W. It ruptured with uniform velocity v living behind the slip dislocation D.	31
3.3	Brune's model of circular fault.	32
3.4	Far field average spectral density curve (After Brune, 1970)	33
3.5	Idealized shape of Fourier amplitude spectrum of acceleration time history showing the corner frequency, f_c , and cutoff frequency, f_{max} .	37
3.6	The effect of baseline error (a) original acceleration record (b) velocity record obtained after integration of acceleration record (c) displacement record obtained by integrating the velocity record (after wang et al., 2011)	39
3.7	Representation of the radial and transverse directions of seismic waves.	40
3.8	Rotation of North-South and East-West components of Seismogram towards the direction of epicentre of an earthquake by angle (ϕ).	41

3.9	An example of 3-component vertical, NS, ES and rotated SH, SV, longitudinal components of ground motion obtained after rotation.	41
3.10	Flow chart for estimation of source parameters using DEQ_EQK_SRC_PARA.	44
3.11a	An example of SH component of a seismogram of local earthquake (M_w 3.1) recorded at ADIPASI station on 29/09/2011. Showing the above displacement (left) and acceleration (right). The source model fitted for both spectra is shown in each spectrum	45
3.11 b	An example of SH component of a seismogram of local earthquake (M_w 3.1) recorded at ADIPASI station on 29/09/2011. Showing the above displacement (left) and acceleration (right). The source model fitted for both spectra is shown in each spectrum	45
3.12	Plot between source radius and seismic moment	48
3.13	Plot between stress drop and focal depth.	48
3.14	The relationship between seismic moment and corner frequency. The middle line corresponding to $\epsilon = 0.5$ shows $M_0 \propto f_c^{-3}$. (After Kanamori and Rivera, 2004)	49
3.15	Plot between seismic moment and corner frequency	49
3.16	Plot showing variation of average values of f_c and f_{max} with seismic moment.	50
3.17	Plot between focal depth and f_c and f_{max} .	51
3.18	Plot between epicentral distance (DEPI) and f_c and f_{max} .	51
3.19a	Plot of f_c and f_{max} with seismic moment at ADIPASI station	53
3.19b	Plot of f_c and f_{max} with seismic moment at AHOLI station	53
3.19c	Plot of f_c and f_{max} with seismic moment at AYENG station	54
3.19d	Plot of f_c and f_{max} with seismic moment at LEDUM station	54
3.20	Plot between f_{max} and seismic moment, M_0 . The values of f_{max} obtained from Lower Siang region of Arunachal Pradesh (NE India) (open diamonds) are overlain on results of f_{max} from worldwide values compiled by Aki (1988).	55
3.21	Relationship between stress drop and f_{max}	56
4.1	A mathematical representation of the movement on a fault during an earthquake, comprising of nine generalized couples, or nine sets of two vectors. The tensor depends of the source strength and fault orientation (After Aki and Richards, 1980).	60
4.2	Representation of isotropic, DC and CLVD components in form of real source model along-with their equivalent force and beach ball (modified after Aki and Richards, 1980).	62
4.3	Beach balls corresponding to basic elementary matrices given by Kikuchi and Kanamori (1991).	63
4.4	The correlation between observed and synthetic waveforms as a function of the trial source depth. Colors represent the DC%. (a) 18/08/2011. (b)	68
4.5	The correlation between observed and synthetic waveforms of 18/08/2011 at various trials on 2 km x 2 km grid along NS and EW directions. The colours of beach balls represent the DC%.	69

	(a) Represent the planer view of the grid. (b) Represent the side view standing EW and looking towards NS.	
4.6	Plot showing comparisons between observed (black) and synthetic waveforms (red) for four stations which are used in inversion. Variance reduction is shown in blue letters.	70
4.7	The plot between CLVD and source depth. (a) All 104 events, (b) selected 41 good events	72
4.8	Plot between SNR and CLVD%.(a) All 104 events, (b) selected 41 good events	72
4.9	The variation of DC% with magnitude.(a) All 104 events, (b) selected 41 good events	73
4.10	The variation CLVD% with magnitude.(a) All 104 events, (b) selected 41 good events	73
5.1	Example of a horizontal component (N–S) seismogram recorded at station LED with. The arrival time of P, S and Coda waves are marked. A time window of 2.56 sec is taken for all three waves.	80
5.2	Flow chart of MATLAB code used for the estimation of P and S wave analysis.	81
5.3	Coda normalized peak amplitude decay of P waves with hypocentral distance for five central frequencies at LED station and the regression lines from the least-squares best-fitted lines are also shown.	83
5.4	Coda normalized peak amplitude decay of S waves with hypocentral distance for five central frequencies at LED station and the regression lines from the least-squares best-fitted lines are also shown.	84
5.5 a	Comparison of estimated value of Q_{α} at all five stations	86
5.5 b	comparison of estimated value of Q_{β} at all five stations	86
5.6	Comparison of Q_{α} (a,b) obtained in the present study with the other regions of the Indiaand world.	87
5.7	Comparison of Q_{β} (a,b) obtained in the present study with the other regions of the India and world.	87
5.8	Comparison between average Q_{α} and Q_{β} .	90
5.9	Comparison of average value of Q_{β}/Q_{α} (at 1 Hz) obtained in the present study with different regions of the world. The solid line is corresponding to $Q_{\beta}=Q_{\alpha}$ and dashed line is theoretically derived by Sekiguchi (1991) corresponding to $Q_{\alpha}=2.25Q_{\beta}$.	91
6.1	Flow of CODAQ program used for coda wave attenuation estimation.	99
6.2	Q_c estimate of an event recorded at LED station occurred on 13/08/2011. (a) Unfiltered data trace with coda window, (b) to (h) band pass filtered displacement amplitudes of coda window at 1-2 Hz,2-4Hz,4-8Hz,6-12Hz, 8-16Hz, 12-24Hz and16-32Hz	101

respectively. Abbreviations are: P: P-wave arrival time; S: S-wave arrival time.

6.3	Plots of quality factors and central frequencies for all the five stations (a) to (e) and average with linear regression frequency dependent relationship (f), $Q_c = Q_0 f^n$ at different lapse time 30, 40 and 50 sec.	105
6.4	Plots of average quality factors and central frequencies with linear regression frequency dependent relationship $Q_c = Q_0 f^n$ at different lapse time window 30, 40 and 50 sec.	106
6.5	Q_c variation with frequency at each station for lapse time window 30, 40 and 50 sec	107
6.6	Comparison of Q_c values for Lower Siang Region of Arunachal Himalaya, India with the existing Q studies in India.	109
6.7	Comparison of Q_c values for Lower Siang Region of Arunachal Himalaya, India with the existing Q studies worldwide.	110
7.1a	Plots of average quality factors and central frequencies with linear regression frequency dependent relationship $Q_s = Q_0 f^n$	118
7.1b	Plots of average quality factors and central frequencies with linear regression frequency dependent relationship $Q_i = Q_0 f^n$ at various lapse time window	118
7.2	Average values of Q_c , Q_β , Q_s and Q_i at different frequencies for the Lower Siang region along with the least-squares best-fitted lines at different lapse time window.	120
7.3	Comparison of quality factor for scattering attenuation (Q_s) with other region of India and World.	122
7.4	Comparison of quality factor for intrinsic attenuation (Q_i) with other region of India and World.	123

LIST OF TABLES

Table No.	Details of Table	Page No.
2.1	stations locations along with the type of rock/soil	22
2.2	Velocity model used for estimation of hypocentre parameters (after Khattri et. al., 1983).	22
3.1	Historical contribution in development of source models (After Lenhardt, 2002)	26
5.1	Q_α and Q_β values along with their standard deviations at different central frequencies at five stations.	85
5.2	Average values of Q_α and Q_β along with their standard deviations at different central frequencies.	85
5.3	Frequency dependent relationships for five stations	85
6.1	Coda wave explanation models (After Herraiz and Eapinosa, 1987)	94
6.2	Various central frequencies with low-cut and high-cut frequency bands used for filtering.	98
6.3	Maximum depth of the ellipsoidal volume at various stations. Here 'A' is the average are generating coda.	102
6.4	Mean value of Q_c at each station at three lapse time windows for different frequencies along with standard errors..	103
6.5	Fitted power law for each station and mean power law for the region for different lapse time 30, 40 and 50 sec..	104
6.6	Mean value of Q_c at three lapse time windows for different frequencies along	104
6.7	Mean power law for the region for different lapse time 30, 40 and 50 sec.	106
6.8	Comparative study of observed Q_0 and n values for other regions of the India for 30 sec lapse time window.	110
6.9	Comparative study of observed Q_0 and n values for other regions of the World for 30 sec lapse time window.	111
7.1	Q_c , Q_β , Q_s and Q_i values in frequency range 1.5-24 Hz for 30, 40 and 50 sec lapse time windows.	117
7.2	Mean power laws for the region for different lapse time 30, 40 and 50 sec.	119

INTRODUCTION

1.1 PREAMBLE

Himalaya mountain range is formed by the collision of Indian plate with Eurasian plate about 40 to 50 million years ago. It leads to the building of regional and local scale tectonic features. The main boundary thrust (MBT) and the main central thrust (MCT) are few of them.. The most of earthquake occurred in the Himalaya are along these tectonic features. It is important to understand the earthquake source process and predict the strong ground motion. Two main factors that plays important role in understanding the tectonics and medium properties of a region are earthquake source properties and seismic wave attenuation. So the understating of these attributes of earthquakes is important for various purposes such as river valley projects and other construction works in the Himalayan region.

The sudden release of elastic energy from an earthquake source is the main cause disaster in any region.. The main disasters of geological origin are earthquakes, landslides, tsunamis and volcanic eruptions. Earthquake is the most dangerous among the disasters of geological origin. The earthquake produced by sudden release of stored elastic energy in the form of seismic waves. The destruction caused by an earthquake is directly related to its magnitude and indirectly related to the path travelled by the seismic waves. In order to minimize the destruction, the knowledge of its source and path travelled by seismic waves is very important.

The seismic waves originated from an earthquake source and propagate through the earth's interior contains the information of wave traveling media. The ground motion recorded at a station is the convolution of source, path and site. The nature and size of earthquake is defined by its source. As the seismic wave propagate from earthquake source to the recording station the amplitude and frequency contents modify due to the local geological structure and composition below recording station. These changes are described by the path effects. The response of uppermost layer including topography is measured by site response. Therefore, to understand the contribution of each factor affecting the seismogram it is necessary to decompose the observed seismogram into its constituents i.e. source, path and site response.

Earthquake source parameters plays an important role towards understanding the kinematic and dynamic properties of earthquake source as well as for understanding the seismotectonics of an area and hence for seismic hazard assessment. Earthquake source parameters are generally estimated from the radiated seismic wave-fields. Aki (1967) first examined the dependence of the amplitude spectrum of seismic waves on source size on the basis of two dislocation models. One model is known as ω^3 proposed by Haskell (1964) and another ω^2 model which is constructed by fitting of dislocation velocity autocorrelation function to a function decaying exponentially. Aki (1967) argued that ω^3 model does not follow the self similarity concept while ω^2 model gives a satisfactory agreement with such. Brune (1970, 1971) gives a circular source model. It consists of finite radius circular fault plane on which instantaneous shear stress pulse is applied. This model employs three independent parameters (moment, source dimension and fractional stress drop) those determine the shape of the far-field displacement spectrum of body waves. He constrained the relationship of the corner frequency to the fault radius by assuming that the effective stress was equal to the average static stress drop.

In the earthquake source models the acceleration spectrum increases with increasing frequency and become constant beyond corner frequency. This high cut off frequency was interpreted as the source effect by Ida (1973). Hanks (1982) called this cut off frequency as maximum cut-off frequency f_{\max} , above which acceleration spectral amplitudes diminish abruptly. Papageorgiou and Aki (1983a, b) attribute it to source effect and relates with size of cohesive zone or break down zone. Anderson and Hough (1984) called the high cut off decay parameter as kappa (κ) later the researchers such as Li et al. (1994), Castro et al. (2000) uses the κ and f_{\max} in same context. Anderson and Hough said that the kappa in high frequency spectra is due to the shallow depth attenuation effect below receiver. They recognized the kappa as a site effect because they observed that the κ is higher for hard rocks and lower for soft sediments. On the other hand, Su et al. (1992) analyze the data set of 132 seismometers and found that the site amplification factor increases monotonically with geologic age of the site rocks up to 12 Hz and concluded that there is no site contribution of κ upto 12 Hz.

The focal mechanism solutions of earthquakes are useful to study the nature of faulting processes operating in a seismically active area. These solutions can be obtained by various methods such as inversion of P-wave first motion polarity, amplitude inversion and moment tensor solutions (MTs). If well azimuthal coverage data is not available the polarity inversion

and amplitude inversion can't be used. In such cases we left only which on possible solution of such situation known as MTs. The MTs technique is popular for estimating source mechanism using multi-station data (Zahradnik et al. 2008). The focal mechanism solution can also be obtained even with a single-station waveform data (Langston 1981; Dreger and Helmberger 1991; Kim and Kraeva 1999; Kim et al. 2000). The single-station waveform inversion has been theoretically well explained by Dreger and Helmberger (1993) and Pinar et al. (2003). The various sensitivity tests carried by Dreger and Helmberger (1993) suggest that single station is adequate for waveform inversion. The inversion results were not degraded by the horizontal misallocation of up to 15 km for the Baja event (Dreger 1992). He also explained that the good azimuthal coverage is not required when the data used are recorded on three-component seismogram

Earthquake releases the seismic energy which is again redistributed within the earth by seismic wave refraction, reflection, diffraction, scattering and geometric spreading. The total amount of seismic energy in all these elastic processes remains conserved. The seismic energy is mainly attenuated by losing energy in the form of heat and scattering. The heat is generated due to the internal friction of medium particle and heterogeneity of the medium though causes the scattering of seismic waves. The efficiency of seismic energy propagation through a medium is commonly expressed by the dimensionless quantity called quality factor Q (Knopoff, 1964). It represents the decay of wave amplitude during its propagation in the medium. Wave attenuation is one of the most important parameter which reflects the medium characteristics travelled by seismic waves. Different quality factors are assigned to different seismic waves. Attenuation coefficient in any region can be quantified by P-wave quality factor (Q_α); shear wave quality factor (Q_β) and coda wave quality factor (Q_c). Midorikawa (1980) has suggested that S-wave is directly related to seismic hazard. The attenuation computed using coda wave (Aki & Chouet 1975; Singh & Herrmann 1983) is the combined effect of scattering and intrinsic attenuation. The simultaneous knowledge of direct S-wave attenuation (Q_t) and coda wave attenuation (Q_c) is important to estimate the intrinsic attenuation (Q_i) and scattering (Q_s). The relative contribution of scattering and intrinsic attenuation is required for appropriate ground motion simulation and tectonic interpretation (Hoshiaba 1993; Akinci et al. 1995; DelPezzo et al. 1995). Some researchers (Tsujiura, 1978; Aki, 1980) gives more importance to scattering than intrinsic

attenuation in quantification of physical properties of earth's crust while other argued that intrinsic attenuation plays more important role (Frankel and Wennerberg, 1987).

In this present study the estimation of source parameters, focal mechanisms and seismic wave attenuation characteristic will be carried out using the local earthquake data recorded by the operation of a five station local seismological network around Lower Siang region of Arunachal Lesser Himalaya.

1.2 IMPORTANCE OF STUDY

The present study is concentrated mainly on two aspects of seismology, i.e., the source and path. It includes the estimation of seismic source parameters, moment tensor analysis and the seismic wave attenuation characteristics of Lower Siang region of Arunachal Himalaya. The importance of this study is as follows:

- i) Estimation of seismic source parameters is important to understand the earthquake source processes, to simulate strong motion, to investigate attributes of seismicity and
- ii) Source parameters are also used to study spatial and temporal variation of tectonic stress from the stress drops of earthquakes, developing scaling laws, understanding earthquake rupture processes, quantifying the excitation of high frequency strong ground motion produced by large earthquakes.
- iii) The slip directions estimated from focal mechanism solutions based on moment tensor solution are very useful to infer the direction of relative plate motions. Rate and cumulative displacement of earthquakes estimated from seismic moments have been used to estimate relative velocity between plates. MTs are also useful for the discrimination of nuclear explosions from earthquakes.
- iv) Study of seismic wave attenuation is considered as one of the fundamental requirements for understanding the seismotectonics setup of a seismic region, for the estimation of earthquake source parameters, for the simulation of strong ground motion at a site due to probable earthquake source zones.

1.3 RESEARCH OBJECTIVES

The study has been carried out with the following objectives:

- i. To estimate the source parameters of local earthquakes for Lower Siang region of Arunachal Himalaya and to develop the scaling relations between various source parameters.
- ii. To estimate the focal mechanism of local earthquakes using the moment tensor solution and to identify the factors responsible for the generation of non double couple component of moment tensor.
- iii. To determine the seismic wave attenuation characteristics of Lower Siang region of Arunachal Himalaya by estimating the quality factor of P-wave (Q_α), S-wave (Q_β) and coda waves (Q_c) of the local earthquakes data and to develop frequency dependence attenuation relationships for the region.
- iv. To investigate the lapse time dependence of Q_c .
- v. To separate out the effect of the intrinsic and scattering attenuation from the total attenuation.

1.4 STUDY AREA

The Lower Siang region of Arunachal Himalaya has been selected for the present research work. This region of Arunachal Himalaya is unique and different from the other parts of Himalaya as three plates; Indian plate, Indo-Burmese plate and Eurasian plate meet at this junction. This region consists of many tectonic features, such as Main Frontal thrust (MFT) and Main Boundary Thrust (MBT), which run along almost entire Himalaya, terminates in this area of Arunachal Pradesh and makes a tri-junction with other tectonic features such as Mishmi Thrust (MT)). Lohit Thrust which is considered responsible of the Great Assam earthquake also runs only about 30 km northwest-southeast of this tri-junction. The region has experienced two 8+ magnitude earthquakes namely, the great Shillong earthquake of 1887 ($M_w = 8.0$) and the great Assam earthquake of 1950 ($M_w = 8.6$) have occurred about ~550 km southwest and ~137 km

northeast respectively of the study area. The study area lies in the seismic zone V as per Indian seismic zoning map.

1.5 DATA SET

A data set of 104 local earthquakes recorded during the period from July 2011 to May 2012 through the deploying of a five station seismological network in the Lower Siang region of Arunachal Himalaya. Two type of sensors triaxial short period seismometer and triaxial broad band seismometer have been used for collecting the local earthquake data. Out of five stations; four were operated with short period seismometer CMG-40T1 (frequency 1 to 100 Hz) and one station was operated with broad band seismometer CMG-40T. These earthquakes are having magnitude range from 1.4 to 5.0, and focal depth range 6.0 to 45.0 km.

1.6 PLAN OF THE THESIS

The present work is divided into 8 chapters. Chapter 2 present the brief description of the geology, tectonics and seismicity of the region. This chapter also includes the data set used for the study. Chapter 3, 4 contain the description of methodology and analysis procedures adopted to compute earthquake source parameters and moment tensor solutions. Chapter 5 and 6 describe the detailed account of estimation of quality factor of P-waves (Q_α), S-waves (Q_β) and Coda waves (Q_c) for the study region using microearthquake data and a brief discussion on the interpretation of the results. The methodology for separation intrinsic attenuation and scattering attenuation is discussed in Chapter 7. The summary of results and conclusions drawn from the study are presented in Chapter 8.

Geology & Tectonics of the region and Data set used

2.1 INTRODUCTION

Arunachal Pradesh is located at northeastern tip of India. It is also called the land of rising sun. It is bounded by the neighboring countries of India; Myanmar, Bhutan and China (Tibet) towards East, West and North respectively. It is located between 26°28' and 29°30' N and 91°30' and 97°25' E and occupy about 83,578 sq. km area. Most of the area of Arunachal Pradesh is inaccessible because of rugged terrains, unpredictable climatic conditions, dense impenetrable forests and poor road communications. Thus, geologically and seismically less explored area. The study region, Lower Siang is a part of Arunachal Lesser Himalaya and located between 27°30' and 29°00' N and 94°30' and 96°00' E. Fig 2.1 shows the location of study region respectively.

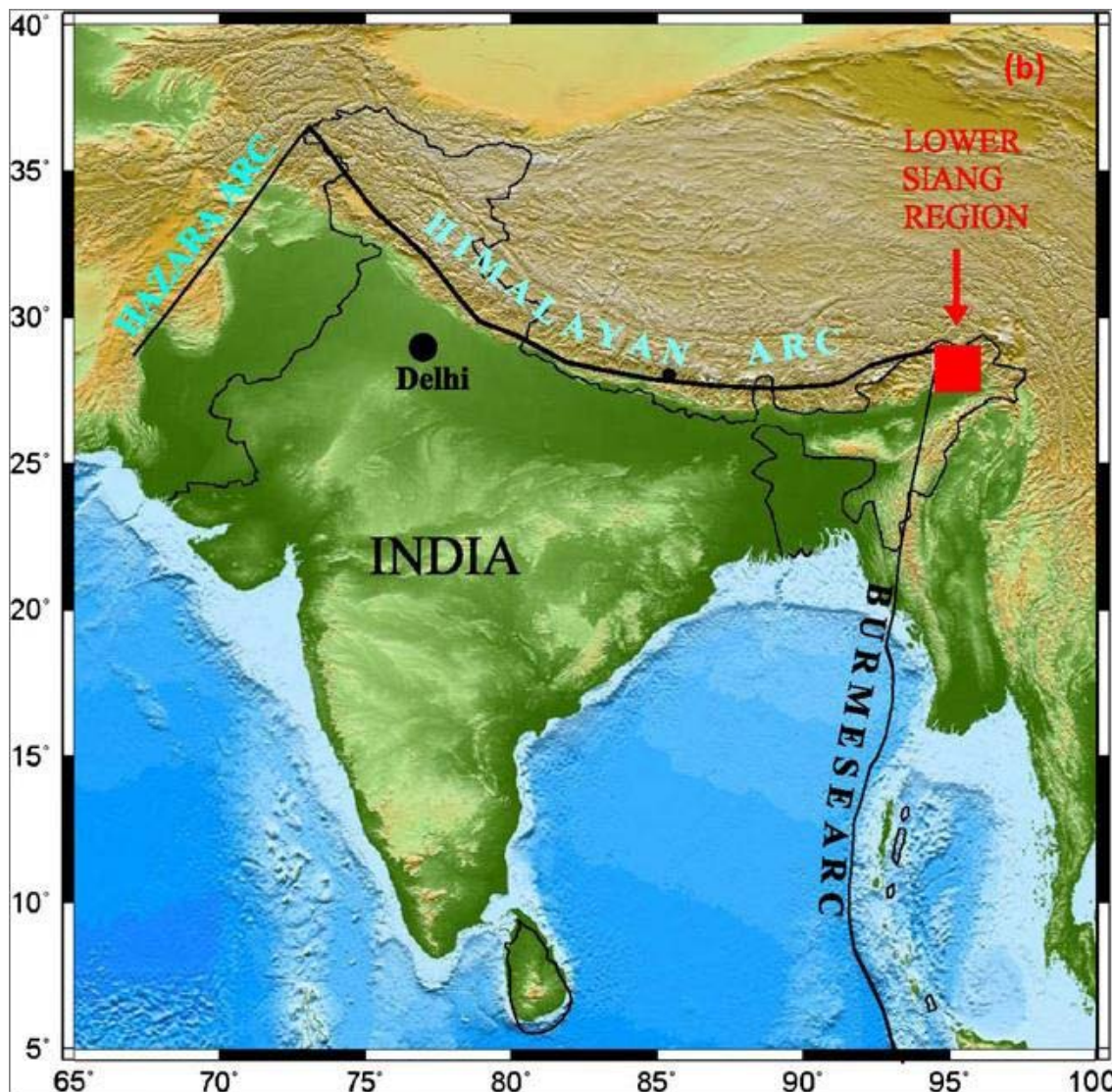


Fig. 2.1 The geologic tectonic map of the Himalaya along- with location of study region (red box).

2.2 GEOLOGY OF THE REGION

The Lower Siang is located in east Arunachal Pradesh and lies between north part of MBT to west of Mishmi thrust of Mishmi hills. High mountain ranges of Eastern Himalayas occupied most of Arunachal Pradesh. This part of the Himalayas includes extensive thrusting, faulting and over-folding as major structural elements. The regional structural trend of the Eastern Himalayas is mostly E-W to ENE-WSW from Bhutan to the north-eastern Arunachal Pradesh, which changes gradually to NE-SW near the Siang valley and terminates against the Siang fracture (Nandy, 1976; Singh, 1996). Fig.2.2 represents the regional geology of Arunachal Pradesh. The framework of regional geology is established by various researches (Singh, 1993; Kumar, 1997; GSI, 2006). The arrangement of litho-tectonic belts of Eastern Syntaxis consists of Proterozoic to

HIMALAYAN BELT SEDIMENTARY AND METAMORPHIC ROCKS			
Q ₁₂ ^a	ALLUVIUM AND RIVER TERRACE	—————	QUATERNARY
N ₁ Q ₁ S	LOWER/MIDDLE/UPPER SIWALIK (UNDIFFERENTIATED)	SIWALIK GROUP	MIDDLE MIOCENE TO LOWER PLEISTOCENE
S ₁ FD	GEKU FORMATION	YINKIONG GROUP	UPPER PALAEOCENE TO MIDDLE EOCENE
P ₁ gbh	BHARALI FORMATION	GONDWANA GROUP	PERMIAN
P ₁ gb	BICHOM FORMATION		PERMIAN
P ₁ gnd	MIRI FORMATION/ UNDIFFERENTIATED MIRI-BICHOM		PALAEOZOIC
P ₁ gob			
Pt ₁ -P ₁ J	THINGBU FORMATION		NEOPROTEROZOIC TO CAMBRIAN
Pt ₂ d	DIRANG FORMATION	—————	MESOPROTEROZOIC
Pt ₁ bcq Pt ₁ bcd	Quartzite/ Dolomite CHILLIPAM FORMATION	BOMDILA GROUP	PALAEOPROTEROZOIC
Pt ₁ bt	TENGA FORMATION		PALAEOPROTEROZOIC
Pt ₁ bk	KHETABARI FORMATION		PALAEOPROTEROZOIC
Pt ₁ s	High Grade Schist & Gneiss		SELA GROUP
IGNEOUS ROCKS			
Tu ₁ g	TOURMALINE GRANITE		TERTIARY
SP ₁ av	ABOR VOLCANICS		PALAEOCENE-EOCENE
SP ₂ v	LICHI VOLCANICS		PALAEOZOIC
B ₁ g	BIOTITE GRANITE		PALAEOZOIC
Pt ₁ gh	ZIRO GRANITE GNEISS		PALAEOPROTEROZOIC

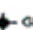
TRANS HIMALAYAN BELT SEDIMENTARY AND METAMORPHIC ROCKS		
KTtl	LIMESTONE (TIDDING FORMATION)	CRETACEOUS-TERTIARY
KTtes KTtegn	Hornblende-Mica Schist/Hornblende Gneiss (ETALIN FORMATION)	CRETACEOUS-TERTIARY
Ptys	YANG SANG CHU FORMATION	PROTEROZOIC
IGNEOUS ROCKS		
KTts	TIDDING SERPENTINITE	CRETACEOUS-TERTIARY
KTtmv	TUTING METAVOLCANICS	CRETACEOUS-TERTIARY
KTJg	LOHIT GRANITOID COMPLEX	CRETACEOUS-TERTIARY

SOUTH EASTERN ARUNACHAL PRADESH			
Q ₁₂ ^a	ALLUVIUM AND RIVER TERRACE	—————	UPPER PLEISTOCENE-HOLOCENE
N ₁ Q ₁ nd	DIHING FORMATION	NAHORKATIA GROUP	UPPER PLEISTOCENE-LOWER PLEISTOCENE
N ₁₂ nt N ₁₂ ng	TIPAM FORMATION/ GANDHIGRAM FORMATION		LOWER TO MIDDLE MIOCENE
Pg ₂₂ b	Sandstone and Coal		BARAIL GROUP
Pg ₂ d	Grey Shale with Sandstone	DISANG GROUP	MIDDLE TO UPPER EOCENE
Pd	TILUNG FORMATION	—————	PROTEROZOIC
Ptnc	NAMDHAPA CRYSTALLINE COMPLEX	—————	PROTEROZOIC

STRUCTURAL INDEX

 THRUST
  GEOLOGICAL BOUNDARY: CONFIRMED/INFERRED
  UNMAPPED AREA

MINERAL INDEX

 COAL
  LIMESTONE
  GRAPHITE
  QUARTZITE
  DOLOMITE

GEOGRAPHICAL INDEX

 STATE CAPITAL
  MAJOR TOWN
 - - - - - STATE BOUNDARY

Fig. 2.2 Regional geology of Arunachal Pradesh (after Geological Survey of India, 2010)

The major geological groups and formations in the regions are Siang Group, Siyom Group, Lower Gondawana Group, Yingkiong Formation and Siwaliks. The major rock type in Siang group are medium to high grade metamorphic rocks such as biotite gneisses, staurolite-garnet-biotite-schists, staurolite-garnet-graphitic, calc-silicate rocks, graphite schist, garnetiferous etc. the graphitic schists at Angguing are categorised by the idiomorphs of staurolite prisms. An association of graphite schists with the white marble bands is present near Yamelling (Singa). The Siyom group is presented in the Siyom valley. It comprises of limestone, black slates schistose quartzites, with phyllite, migmatites, amphibolite, gneisses, schistose quartzite and biotite schists. In the Subansiri region same litho assemblage has been acknowledging. Here the main rocks are migmatites and gneisses. These gneisses are also known as Ziro gneisses, Daporijo gneisses. At Tuting an extrusive contact has been observed. Here exposed meta volcanic rocks succeed the Siang Group. A garnetiferous zone having thickness 10-15 cm marked the contact. Tuting granites and gneisses are carried by the thrust plane against the Siang group rocks. This thrust cut off the metavolcanics beyond the Sirup Chu. The Lower Gondawana Group rocks are observed at Rylu, Ganu, Daring, Gensi and Tatamori areas. The rocks of this group are black slates, carbonaceous, grey sandstone and phyllite with coaly lenses. A transitional nature contact between Miri and Gondwana can be observed along the section of Pasihat-Rotung road where local shaling can also be observed. Yingkiong Formation occupied a large land between Yamne and Siang valleys. Here the thick succession of volcanic sediments, black shale, purple and pale green shale, siltstone and light grey sandstone are present. The Yingkiong Formation is associated with nummulitic limestone bands of lower Eocene age. Although, earlier considered age of this group was Pre-Cambrian. Siwalik belt is observed in the Sub-Himalayan zone. It is divided into three parts; Lower, Middle and Upper. Brownish grey sandstone with clay is found in Lower Siwalik. The coarse grained sandstone are found in The Middle Siwalik. The Upper Siwalik consists of boulder beds, pebbles, sands and silty clays. The Siwalik is separated by Main Boundary thrust (MBT) from the Gondwanas and Miri quartzite.

2.3 TECTONICS OF THE REGION

A regional tectonic set up of eastern Himalaya is shown in Fig. 2.3. The study area occupies 4 X 4 degree areas and details are discussed below for overall understanding of tectonic status (Fig. 2.4). As per geotectonic set-up of Arunachal Pradesh, four different identifiable geotectonic blocks exist, viz, the Himalayas, the Mishmi Hills, Naga-Patko

ranges of the ArakanYoma Mountain and the Brahmaputra Basin, each characterised by distinct stratigraphy and structure. These blocks have experienced intense stages of tectonic development and associated orogenic movements in response to collision of plates and uplift of Himalayas (Kumar, 1997).

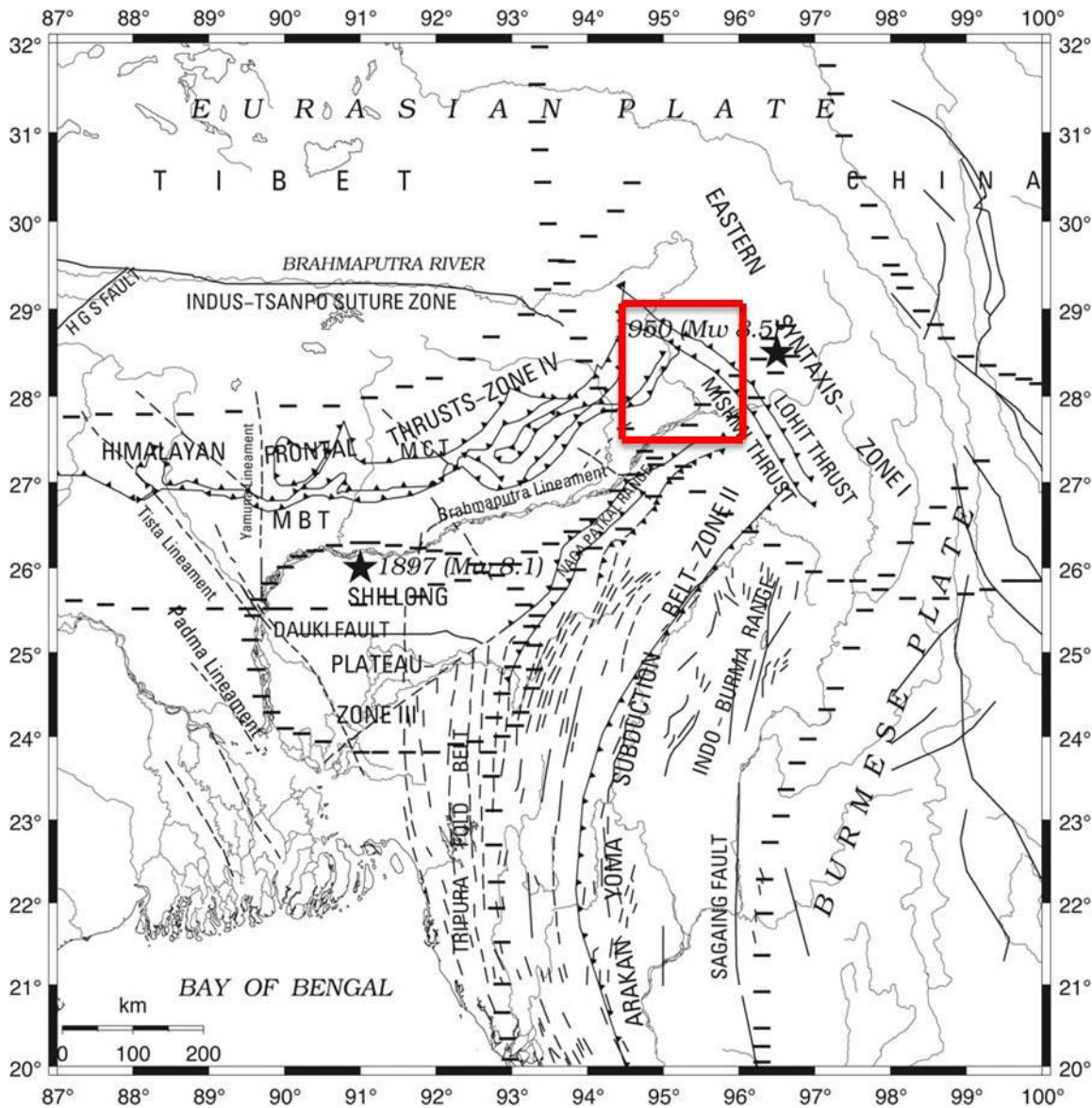


Figure 2.3 Regional tectonic set up of eastern Himalaya. (after Yadav et al., 2009). The box in the figure shows the study area.

In Arunachal Pradesh the Himalayan mobile belt forms the main and prominent geotectonic block. This block is bordered by the Central Burmese Plate towards east. The prominent tectonic feature Indus-Tsangpo Suture Zone (ITSZ) separating the mobile belt from the Indus-Shyok Belt of the Tibetan Plateau defines its northern limit. The river Tsangpo (Brahmaputra) flows along ITSZ remarkably in an E-W rectilinear valley. The

ITSZ marks the collision boundary of the Indian and Tibetan Plates. The Main Central Thrust (MCT) separates the rock units south of ITSZ. In this zone the highest-grade gneisses and metamorphites of the axial belt is separated from Precambrian sedimentary sequence and its equivalents by MCT. The Main Boundary Thrust (MBT) separates the Siwalik rocks from the pre-Tertiary rocks. Beyond MBT, different stratigraphic units are disposed in intricate thrust slices. Since the rocks of this segment range in age from Proterozoic to Cenozoic, it has undergone different stages of crustal evolution and has been subjected to orogenic movements of varying intensity from time to time. In different deformational structures, major discontinuities or unconformities the imprints of orogenic movements are identifiable (Kumar, 1997).

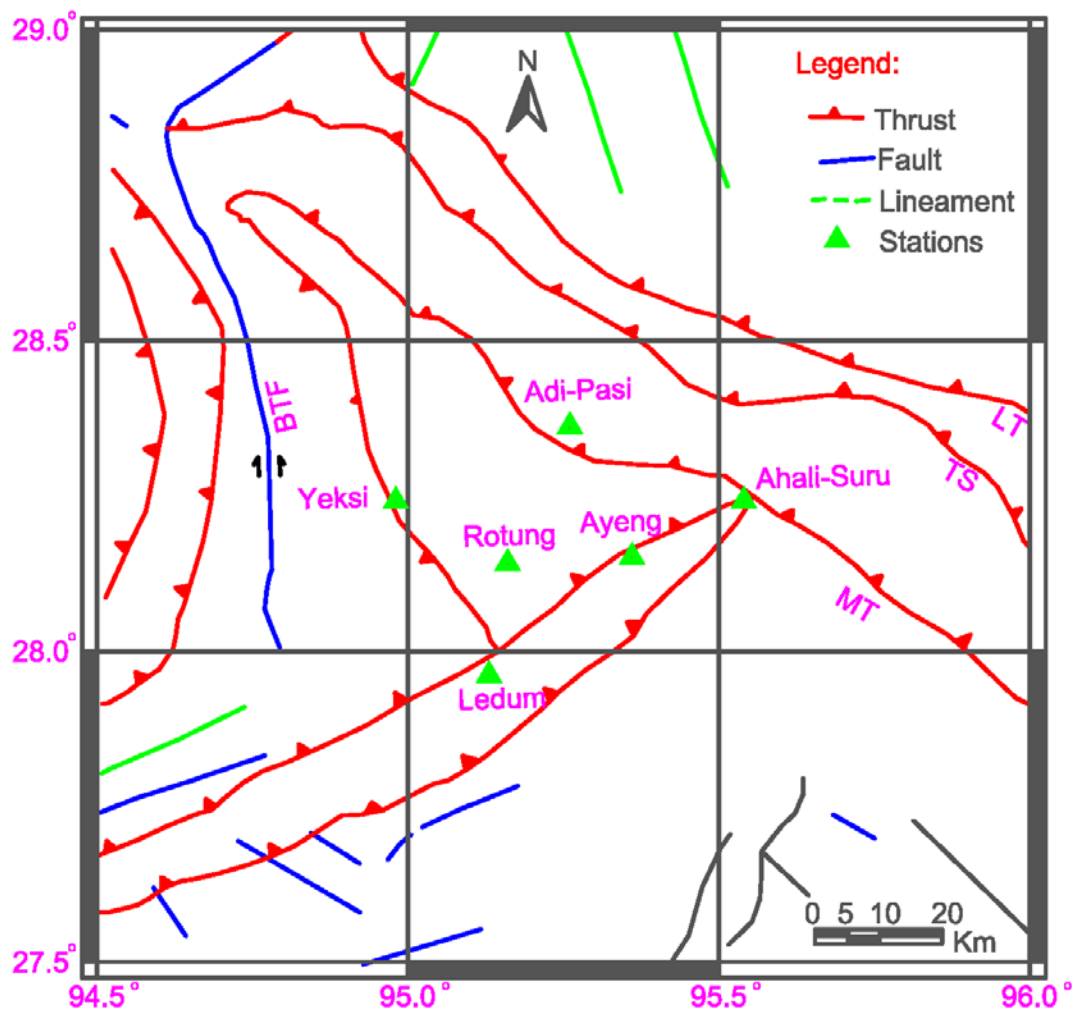


Figure 2.4 Map showing the study area. (Tectonics after GSI, 2010)

Mishmi hills, the second geotectonic block does not belong to the Indian plate and considered to be part of the Central Burmese Plate. The metasediments of this block had undergone four phases of deformation and had been intruded by granites/granodiorites and abuts against the Indian Plate along the Tidding Suture. The diorite-granodiorite crystalline complex are observed in Mishmi hill massif (Nandy, 1976) and the south-western boundary of this is marked by high angle NW-SE trending Mishmi Thrust (MT) along which this block is thrust on the adjoining rocks. The NW-SE trending metamorphic belt is in direct contact with the Brahmaputra alluvium in this region. Mishmi hills massif acts as a linkage between the Himalayan and Indo-Burman structural and stratigraphical trends in north and east respectively.

Third geotectonic block is the Naga-Patkoi Ranges, which lies in parts of Arunachal Pradesh and Nagaland. This block is made up of Paleogene-Neogene sediments unconformably overlying the concealed basement of Precambrian rocks. The basement is considered to be eastern extension of the Shillong Plateau that remained a stable landmass since Precambrian and did not receive any sedimentation during Lower Palaeozoic. Since Upper Palaeozoic its geological history is parallel to that of the Himalayan region as reflected by different orogenic events (Kumar, 1997). Sedimentation in this segment including the parts of Shillong Plateau and Mikir Hills was initiated in Lower Permian in response to two phases of the Hercynian orogeny and paleogeographic frame-work.

In front of the rising mountains during the development of the Sub-Himalayas and the Arakan-Youma mountains in Early Middle Pleistocene due to orogenic movements both in the Himalayan and Indo-Burman Mountain belt a huge depression was formed. This valley is known as the Brahmaputra Valley, was filled up by fluvial sediments during the latter part of the Quaternary period and evolved as the Brahmaputra Plain. Mathur and Evans (1964) referred the Brahmaputra Basin as the Foreland Spur.

The geological history of these four geo-physiographic divisions has evolved differently in response to various tectonic episodes. The rock assemblages of these divisions are of different ages and also differ in structural/deformational features and geological history. Further, the imprints of different orogenic episodes differ markedly in their intensity. So during specific orogenic movements the rocks are extensively deformed and re deformed. The major tectonic features are described below.

Main Central Thrust (MCT), a regional tectonic feature that traverses along the whole length of Himalayas. It has developed in response to intensive and extensive operative

compressional tectonics. This is a north dipping thrust with initial steepness and marks the tectonic boundary between the high-grade metamorphites of the Se La Group and low to medium-grade metasediments of the Dirang Formation in the Diggin Valley, in upper height of the Kamlariver and near Taliha in the Subansiri river section. Further in east, the Dirang Formation appears to get eliminated and it marks the tectonic boundary with the Bomdila Group. The MCT has been traced to Arunachal Pradesh through Nepal, Darjeeling-Sikkim and Bhutan, which abuts against the Tidding Suture in the Siang Valley (Ravi Shanker et al., 1989).

Main Boundary Thrust (MBT) is another regional tectonic feature of the Himalayas, which demarcates the tectonic boundary between the Main Himalayan Belt and the Frontal Folded Belt forming the Sub-Himalayas. It is also a north dipping thrust fault with ENE-WSW trend from the border with Bhutan in the west to Roing in the Dibang valley and does not continue southeast to join the Mishmi Thrust as visualized by Ranga Rao (1983). According to Sinha Roy (1976), the MBT flattens at depth, as indicated by the absence of Gondwana rocks in southern Bhutan and in the west-central Arunachal Pradesh. This is possibly due to the fact that the MBT merges at depth with some dislocation zones in the inner belt.

In the region of foothills of the Arunachal Himalayas, south of MBT, a thick pile of molassic sub-greywacke representing the Siwaliks are exposed. This belt is continuous all along the Himalayan foothills from Kashmir to Arunachal Pradesh. The Siwalik sequence was deposited during the Mio-Pliocene in an unstable sinking basin, developed on the downward bending plate north of the Shillong Plateau and south of rising Himalayas. The Siwaliks, are folded and thrust over by the older rocks from the north along the MBT. The lithological assemblages of the Siwaliks were also controlled by the vigour of tectonism in the source area of the rising Himalaya. The Main Frontal Thrust (MFT) marks the southern fringe of the Siwalik belt, bordering the Brahmaputra basin. The Lohit Complex, as referred by Anon (1974), exposes a thick sequence of metasediments and associated granitic and mafic rocks occur in the extreme northeastern part of the region. These rocks assemblages has a regional NW-SE trend, abutting against the Himalaya along the Tidding Suture in southeast, and in south, against the NE-SW trending Naga-Patkoi ranges along Mishmi Thrust. Tidding Suture is a NW-SE trending tectonic feature considered to mark the plate boundary between the Indian and Central Burmese Plates. It could be traced from Dhapa Bum in the southern part of the Lohit valley to beyond south of Tuting in the Siang valley in the northwest (Kumar, 1997). It

appears to abut against the Mishmi Thrust (Ranga Rao, 1983). Whereas, the Lohit Thrust runs parallel to the Tidding Suture demarcating the tectonic contact between the Tidding and the Mishmi Formations, was first identified by Nandy (1976). Mishmi Thrust plane is redefined as the tectonic contact between the Tertiary succession of Naga-Patkoï Ranges and the Bomdilla Group and the Lohit Complex of the Mishmi Hills exposed along Dapha Bum. It trends east west in the western exposed part and gradually swings southeastwards to assume NW-SE trend.

The Naga-Patkoï Ranges are subdivided into two zones/belts, viz., the Schuppen Belt and Kohima-Patkoï Synclinorium on the basis of structural elements (Mathur and Evans, 1964). The Disang Thrust is considered as the dividing line between the two structural zones, the area lying to its southeast forms Patkoï Synclinorium. Patkoï Synclinorium tectonic zone lies between the Disang Thrust and Ophiolite and Melange Zone in the east, the latter exposed in Myanmar. The rocks of the Disang Barail and the Nahorkatia groups have been folded into a number of north-easterly plunging folds, which swerve to east west and then to NW-SE trend, apparently due to younger deformational phase.

The Schuppen Belt in Naga Hills is represented by imbricate faulted belt of Cenozoic sediments forming the southeastern limit of the Brahmaputra Basin and separated from the Patkoï Synclinorium by the Disang Thrust. It is made up of eight over thrusts, one overriding the other, along which the Naga Hills have relatively moved towards northwest. The north-western most thrust is referred as the Naga Thrust. The Disang Thrust, which is quite persistent, is taken as the uppermost thrust. All these thrust plane trend in NE-SW direction, which is parallel to regional trend of the hill ranges. The Naga-Patkoï Ranges and the Brahmaputra Valley subjected to varying degrees of compression due to orogenic movements. All the deformational structures developed in the Naga-Patkoï Ranges trend NE-SW in south-western part of the ranges, but swerve to east in north and then to southeast in the upper reaches of the Nao Dihing valley before entering Myanmar, running almost parallel to the tectonic contact with the Mishmi Thrust with convexity towards north. The Brahmaputra basin is underlain by the basement rocks which in turn are covered by near horizontal to gently dipping Cenozoic sediments excepting in the eastern, most part in the Upper Brahmaputra Plain where the sediments are folded into a northwesterly plunging anticline possibly due to a southwesterly thrust from the Mishmi Hills.

2.4 SEISMICITY OF THE REGION

Arunachal Pradesh is one of the most seismically area of Himalayan terrains. The earthquake activity of this region is attributed to collision of Indian plate with Eurasian plate in north and subduction of Indian plate below the Burmese plate in the east. Most of the earthquakes observed in this region are shallow focus (40 Km). However, some intermediate focus events also occurred in the Naga Hills.

The whole NE region of India lies in the seismic zone-V, as per the Indian standard criteria for Earthquake Resistant Design of Structure IS 1893 (part-I): 2002: General provision and Buildings. Zone-v is highest earthquake intensity zone of India. On Modified Mercalli M.M. intensity scales, it is equivalent to the seismic intensity XI or more.

In the close proximity of the study region two great earthquakes namely the Shillong (1897) and the Assam earthquakes (1950) have occurred. The epicentral locations of Shillong ($M_w=8.0$) and Assam earthquakes ($M_w=8.48$) (magnitudes after Rajendran and Rajendran, 2005) are near the northern edge of the Shillong Plateau and near the Mishmi Hills respectively (Fig. 2.5). The seismicity in the Arunachal Himalaya is mainly attributed to the MBT (Verma, 1991; Verma and Kumar, 1987). However, many earthquakes also occurred near the MCT. In addition to this the seismic activity also observed along some NE trending lineaments. Few earthquakes are also occurred along several thrusts including the Lohit and Mishmi Thrusts having trend NW-SE. The epicentral location of Great Assam earthquake of 1950 lies about 100 km east of Mishmi thrust (Verma, 1991; Verma and Kumar, 1987). Large number of aftershocks of 1950 Assam earthquake were located between Tsangpo and MBT region. This is an indication of rejuvenation of tectonic activity far from main region. Here some thrusts and faults rupturing release the energy. Hence from the occurrence of such big earthquakes it can be interpreted that thrust front of The Himalaya may extend eastward into the Mishmi region. The focal mechanism of earthquakes occurred in eastern Himalaya suggest the association of earthquakes with prevailing compressional tectonics in the region. Verma and Kumar (1987) and Verma (1991) showed that most of earthquake processes are of thrust type and only few are of shearing motion type. Molnar (1987) based on the information of Oldam (1899) suggested that 1897 Shillong earthquake has been occurred due to the under-thrusting of Indian continent. Southward overthrusting which produces horst type of structure is the cause of Shillong earthquake (Mukhopadhyay, 1990). Bilham and England (2001) suggested that a structure bounded by two reverse faults as a

cause of earthquake is suggested by. Severe and Armbruster (1981) suggest that the Assam earthquake (1950) can be considered as the locus of all the great earthquakes occurred in Himalaya and it is resulted from the detachment along the Himalayas. Another cause of this earthquake was suggested by Chen and Molnar (1990). They explain that it is due to shallow- dipping thrust plane. Fig 2.5 shows locations of the historical significant earthquakes occurred in India and its adjoining area.

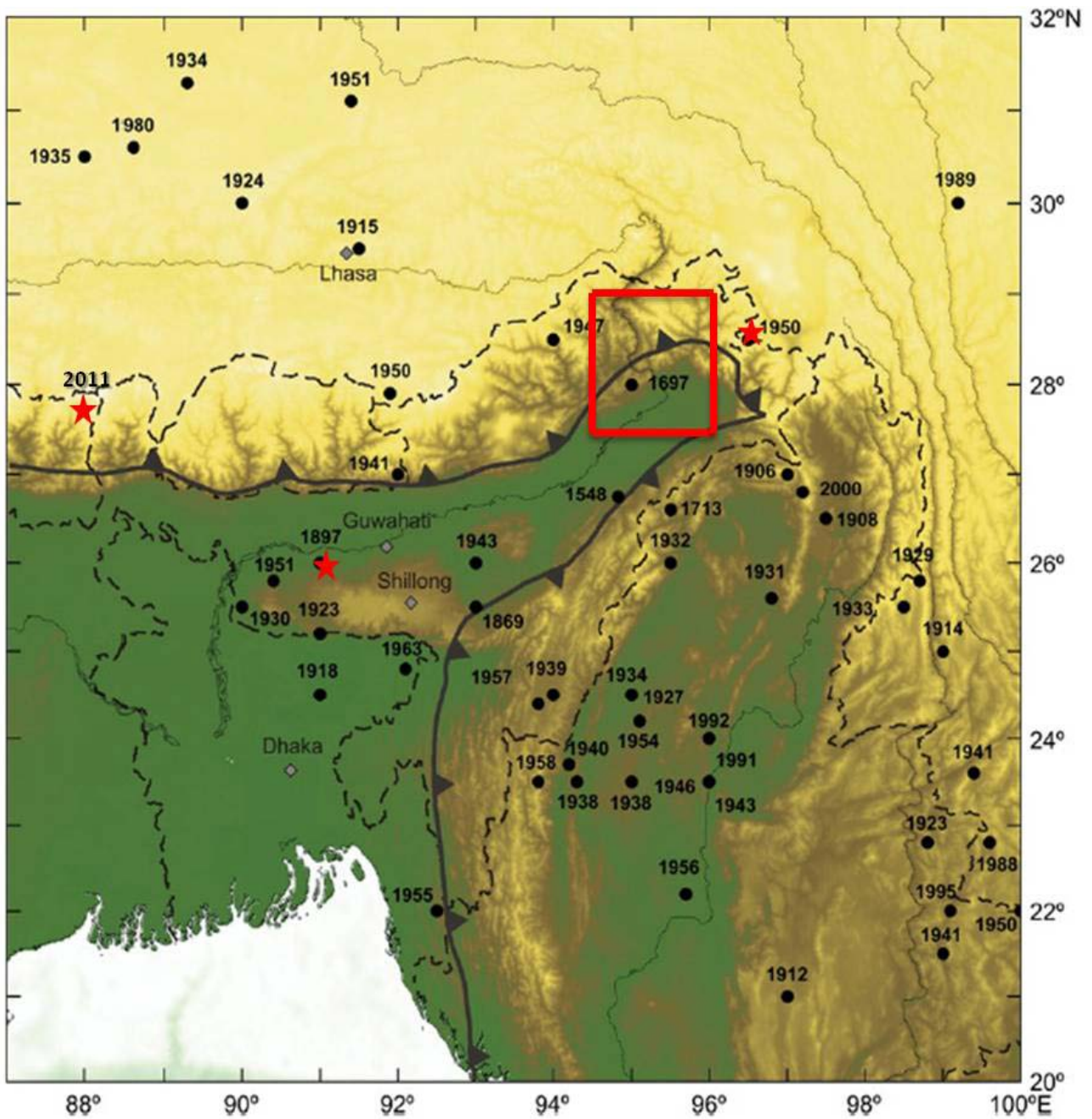


Fig 2.5 Epicenters of historical significant earthquakes occurred in NE India and its adjoining area (after Rajendran and Rajendran, 2011). The area around study region is marked by box.

Recently, the Sikkim earthquake ($M_w=6.9$) of 18 September 2011 is also occurred in the close proximity of the area. Focal mechanism solution estimated by CMT Harvard and Kumar et al. (2014) suggests that transverse motion is the cause of this earthquake. More than 100 people in India and Nepal are dead due to this earthquake. Martha et al. (2014) mapped around 1196 new landslides after this earthquake using very high resolution satellite data.

A number of small moderate and large earthquakes occurred in and around study area during last sixty years from 1950 to 2010. The epicenters of these earthquakes are marked on the tectonic map of the area are shown in Fig. 2.6. The distribution of epicenters shows that events lie to the north, north-east and north-west directions about 50 km distance from the center of area. Only two events of magnitude range of 5.0 to 6.0 have occurred in 1956 and 1982 in the vicinity of MBT as well as study area. The study area lies between the isoseismal of VI and VII on MM intensity scale due to 1897 Shillong earthquake whereas, it lies between isoseismal of IX to X on MM intensity scale due to 1950 Assam earthquake. However no microearthquake study has been carried in the study area that could show the current level of seismic activity of this region

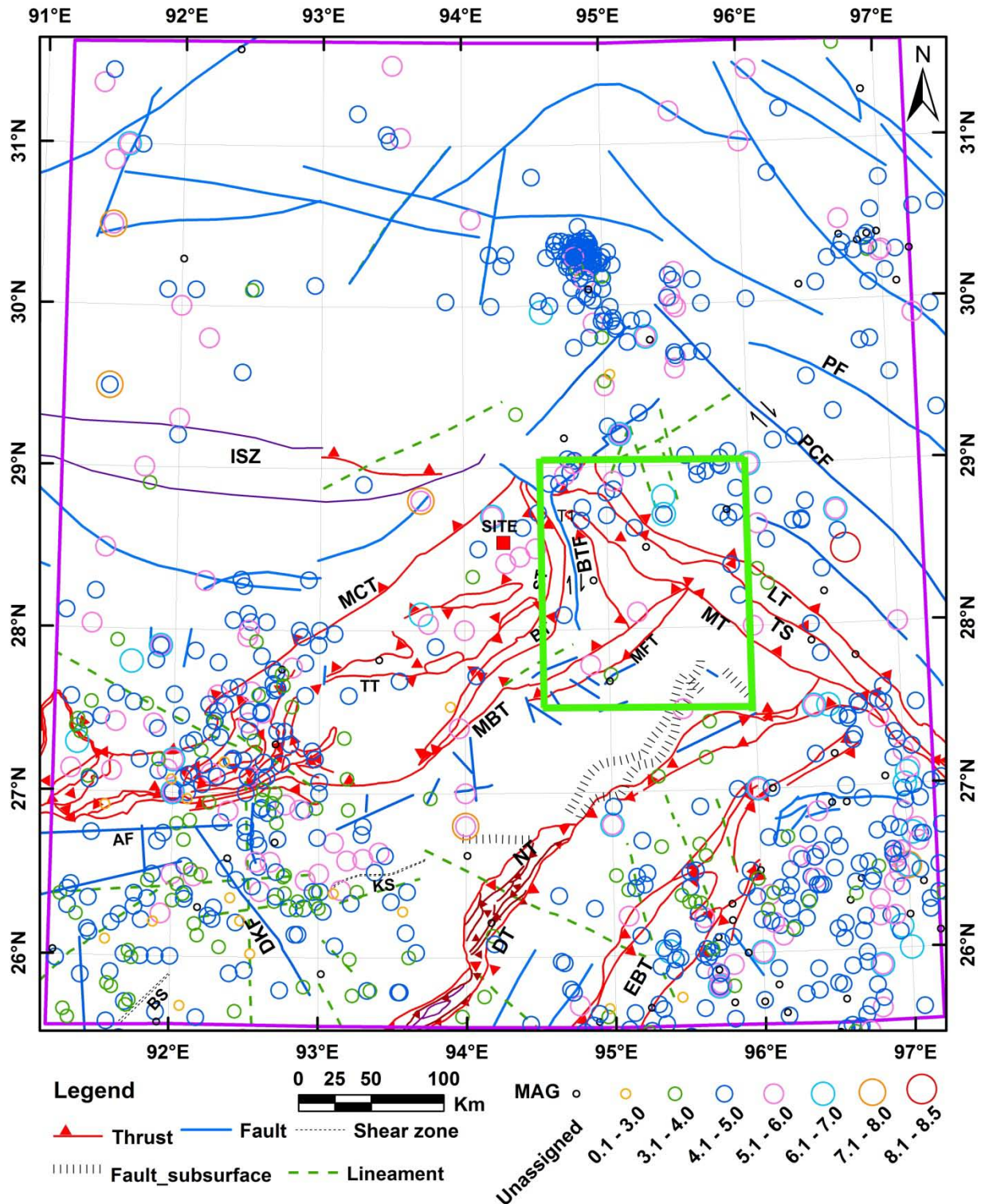


Fig. 2.6 Epicenters of earthquakes occurred within 100 km from the center of study area during 1950 to 2010. Seismotectonic setup around study area is also shown on map (Tectonics after GSI, 2000). MBT-Main Boundary Thrust, MFT- Main Frontal Thrust, BFT- Bame Tuting Fault, LT- Lohit Thrust, TS- Tidding Suture, MT- Mishmi Thrust. The study area is shown in box. (After EQ:2010-22, EQ: 2011-30)

2.5 DATA SET USED IN STUDY

Initially a seismological network consist of six stations was deployed in the region in July 2011. The detail of six stations, e.g., geographical coordinates, rock types and elevation from mean sea level are given in Table 2.1. The locations of seismological stations of the network are selected in such a way that they encompass the active seismic source zones in the region. Five stations of the network remained operative during this period, as due to some unavoidable reasons, the Yeksi station remained nonfunctional. So finally, five stations data is available for analysis. Two types of sensors have been used for carrying out the study: short-period seismometer and broad band seismometer. Out of five stations, four are short-period seismometers CMG-40 T1 (Guralp Systems Limited,UK) with sampling rate 100 sps; one is a broad band seismometer CMG-40 T (Guralp Systems Limited, UK) with sampling rate 100 sps. Each digital seismograph comprised of a 24-bit portable data acquisition system (DL-24) coupled to sensors. A Global Positioning System was used to synchronise data samples to UTC or IST.

The P-wave and S-wave arrival time data of 104 local earthquakes has been measured from the digital seismograms obtained during the period from July 2011 to May 2012 from five seismological stations. The hypocentre parameters of local earthquakes have been estimated using HYPOINVERSE computer program (Klein, 1978) integrated in SEISAN software used for the estimation of hypocentre parameters. The velocity model used for the estimation of hypocentre parameters is shown in table 2.2. The standard errors in the estimation of hypocentre parameters for these events are ≤ 0.50 sec in origin time (RMS), ≤ 5.0 km in epicentre (ERH), and ≤ 5.0 km in focal depth (ERZ). List of hypocentre parameter of local earthquakes are given in Table I.1 of appendix-I and their epicentres are plotted on the tectonic map of the area is shown in fig 2.7.

Table 2.1 stations locations along with the type of rock/soil.

Sl. No.	Name of Station	Station Code	Location		Elevation (m.)	Type of Rock/Soil
			Lat (°N)	Long. (°E)		
1.	Ayeng	AYE	28.15°	95.36°	272	Boulder Bed
2.	Rotung	ROT	28.14°	95.16°	410	Quartzite
3.	Adi-Pasi	ADI	28.36°	95.26°	997	Reddish Sandstone with Shale
4.	Yeksi	YEK	28.24°	94.98°	401	Conglomerate
5.	Ahali-Suru	AHO	28.24°	95.54°	571	Quartzite
6.	Ledum	LED	27.96°	95.13°	385	Boulder bed

Table 2.2. Velocity model used for estimation of hypocentre parameters (after Khattri et. al., 1983).

P-wave velocity	depth	Type of Soil/Rock
4.00	0.0	Sedimentary
6.00	1.0	Granitic
6.70	25.0	Basaltic
8.10	45.0	Moho

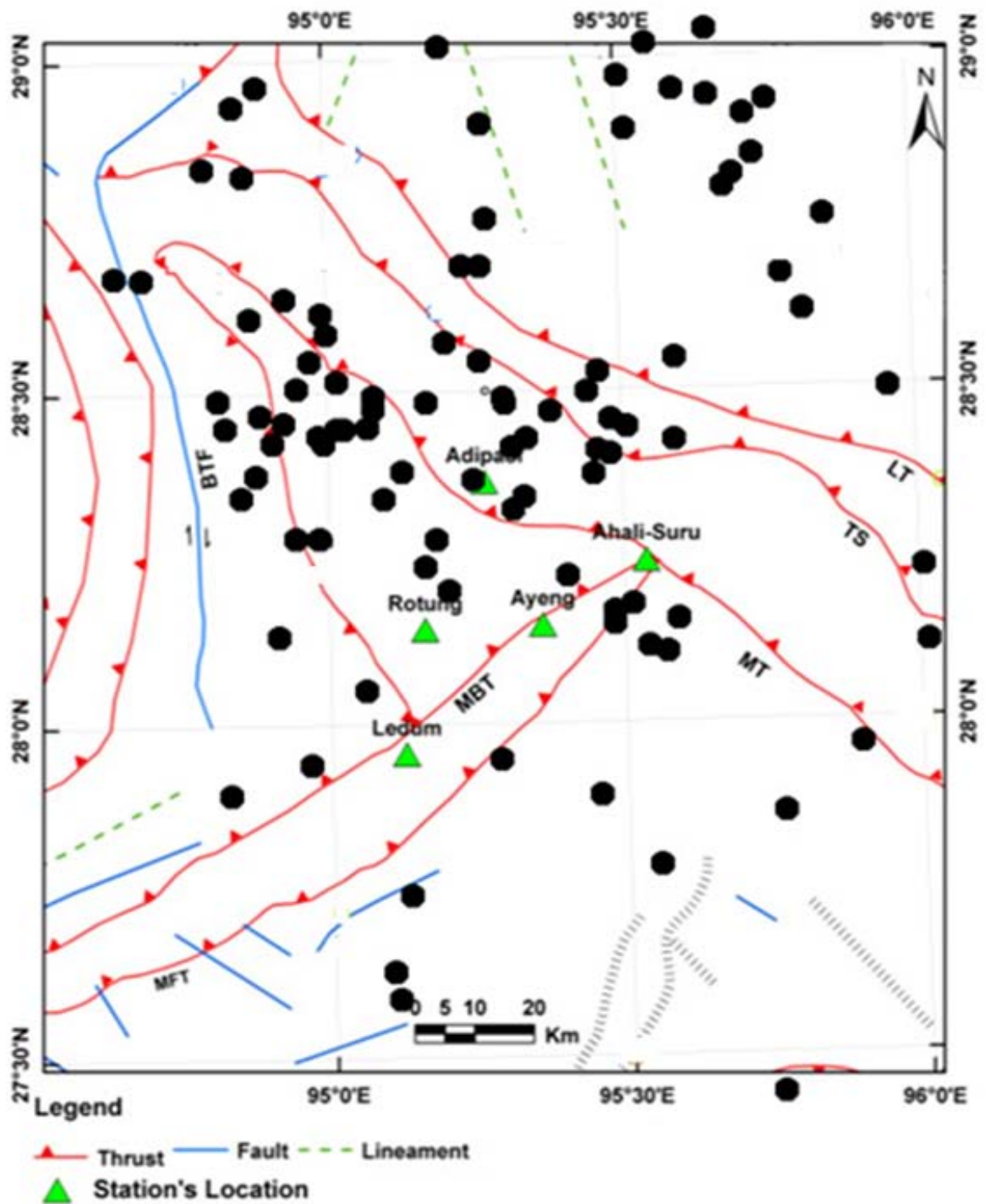


Fig. 2.7 Map showing epicenters of events recorded during July 2011 to May 2012 (solid circles). Tectonics after GSI (2000).

Estimation of Source Characteristics

3.1 INTRODUCTION

The knowledge of high frequency ground motion radiation from a moderate to large earthquake is required for engineering design of critical structure. However, this information is hindered in such cases where the strong motion events are not recorded at the site of measure damage. Also, the return period of strong motion event is very large sometime in decades. Hence, the design criteria are based on the extrapolation, simulations and scaling laws. Stress drop ($\Delta\sigma$) is a fundamental scaling parameter. It is defined as the difference between the stress state before and after the rupture (Kanamori and Anderson, 1975). Various efforts have been done to compute the scaling parameter $\Delta\sigma$ as effective stress drop, apparent stress drop, root mean square stress drop and dynamic stress drop (Hanks and Johnson, 1976; Boatwright, 1980; Snoke *et al.*, 1983; Anderson, 1997; Day *et al.*, 1998; McGarr, 1999). Some workers also argued that this parameter should not be called stress drop (Beresnev, 1997).

The scaling parameters can be estimated using near and far field data. Two independent parameters; corner frequency (f_c) and the low frequency spectral level are used to characterize earthquake's shear wave spectrum. Other source parameters such as seismic moment (M_0), stress drop ($\Delta\sigma$) source radius, are estimated using these two fundamental parameters.

In the present study source parameters of 104 local earthquakes recorded by a five station seismological network have been estimated. The MATLAB code developed Kumar *et al.*(2013) has been used for the analysis. This code is based on the Brune's Model (1971). Except a single study in the Kameng region of Arunachal Himalaya (Kumar *et al.*, 2013), no study is available till date in the region as no data or very less digital data on weak motion is available. Therefore, the present study will serve as important input for the region in various aspects such as strong ground motion simulation, stress analysis, seismicity analysis etc. A number of earthquake source models have been developed from time to time to describe basic earthquake source theory. The upcoming section

describes the development of various source models. Most of the sections are reproduced from seismic source theory (Madariaga et al., 2007) and earthquake source mechanics (Das et al., 1986) for better understanding.

3.2 EARTHQUAKE SOURCE MODELS

Reid in 1910 gives the elastic rebound theory describing the faulting processes. This concept says that during fracturing process, there is sudden release of accumulated strain energy when the material strength is overcome. In seismology, the term source mechanism consists of relating the observed seismic waveform to the parameters that defines sources. There are two ways of estimating these source parameters the direct problem and inverse problem. In the direct problems, the source models are defined in terms of mechanical models representing the physical fracture. The number of parameters which defines these source models or source representation is depending on their complexity i.e. simple the model fewer the parameter and complex the source larger the number of parameters (Madariaga, 1983; Udias and Buforn, 1991; Koyama, 1997). The derivation of source parameters from observed waveforms is called inverse problem.

There are two different ways to approach the fracturing process; kinematic and dynamic. In the kinematic source models the fracturing is described in terms of slip vector of the fault without relating the slip with the stress causing the faulting. This is the representation of slip as function of time and position on the fault plane. In these models the determination of elastic displacement field is relatively simple. The dynamic models of source relate the slip of the fault to the stress acting on fault plane. The complete dynamic model describes the fracturing from the material property of the fault plane or focal region and associated stress conditions. Dynamic models are very difficult to solve and in many cases only numerical methods able to solve them. The development of source model is the contribution of various researchers listed in the Table 3.1.

Table 3.1. Historical contribution in development of source models (After Lenhardt, 2002)

Name	Year	Contribution
Harry Fielding Reid	1910	Based on the displacement measurement of San Francisco (1906) earthquake, the Elastic rebound theory i.e Earthquake= strain accumulation near faults - release of the strain. Estimated the energy release.
A.A. Griffith	1920/24	On the basis of minimum energy theorem describe the propagating crack energy balance
Leon Knopoff & Freeman Gilbert	1959	Step source time function
Vladimir I. Keilis-Borok	1959	Stress from source radius and moment
Norman A. Haskell	1964	Haskell model, ramp source time function, at low frequency amplitude spectrum is flat
Keiiti Aki	1967	Renamed the characteristic frequency as corner frequency
James N. Brune	1970	Brune's model, introduce instantaneous radial slip, ramp source time function smoothed
Freeman Gilbert	1970	Forward modeling, moment tensor
Freeman Gilbert	1973	Moment tensor inversion
Shamita Das & Keiiti Aki	1977	Barrier-model
James D. Byerlee	1978	Friction law for normal stress less than 200 MPa, Shear stress = 0.85*normal stress
S. Hartzell, F. Wu	1978	Empirical Green functions
Keiiti Aki	1979	Barriers and asperities
Adam Dziewonski	1981	Centroid moment tensor
Thomas H. Heaton	1990	Self-healing phase, Madariaga already introduced the term healing in 1976.

3.2.1 SEISMIC WAVE RADIATION FROM A POINT FORCE

The dynamics of earthquake source is the key parameter to understand the physics of earthquake. It is required for the prediction of the ground motion and understanding the wave propagation. A point source in an elastic half space is the simplest model of an earthquake. The development of source model took more than 50 years. The first effort was made by Nakano et al. (1923) in Japan. Initially, the source models are treated as simple explosion which as a result of strains inside a sphere the displacement is conical surface. In early 1950s, the source was modeled as the single couple but latter the problem of explaining the radiation pattern of S-waves was aroused (Honda, 1962). So the next level of complexity was introduced as double couple i.e. a source with net resultant moment. The physical origin of double couple is the contribution of numerous seismologists. Maruyama (1963) and Burridge and Knopoff (1964) showed that double couple is equivalent to an elastic model of the fault.

As already described, the simplest source model is a point source it is a homogeneous isotropic half space having density ρ and elastic constants λ and μ . Let P and S wave velocity are $\alpha = \sqrt{(\lambda + 2\mu)/\rho}$ and $\beta = \sqrt{\mu/\rho}$. So we need to find the solution of elastodynamic wave equation:

$$\rho \frac{\partial^2}{\partial t^2} u(x, t) = (\lambda + \mu)\nabla(\nabla \cdot u(x, t)) + \mu\nabla^2 u(x, t) + f(x, t) \quad 3.1$$

The initial condition is $u(x, 0) = \dot{u}(x, t)$. 'f' and $\dot{u}(x, t)$ are the force density distribution and displacement due to which f is a function of time and position. The body force for an arbitrary position X_0 is:

$$f(x, t) = f s(t) \delta(x - x_0) \quad 3.2$$

where s(t) is the source time function. Equation (3.1) can be written in frequency domain using Fourier transform as;

$$\bar{u}(x, \omega) = \int_{-\infty}^{\infty} u(x, t) e^{-i\omega t} dt \quad 3.3$$

$$u(x, t) = \frac{1}{2\pi} \int_{-\infty}^{\infty} \bar{u}(x, \omega) e^{i\omega t} d\omega \quad 3.4$$

Achenbach (1975) in the frequency domain gives the solution using above equations as:

$$\bar{u}(R, \omega) = \frac{1}{4\pi\rho} \left[f \cdot \nabla \nabla \left(\frac{1}{R} \right) \right] \frac{s(\omega)}{\omega^2} \times \left[- \left(1 + \frac{i\omega R}{\alpha} \right) e^{-\frac{i\omega R}{\alpha}} + \left(1 + \frac{i\omega R}{\alpha} \right) e^{\frac{i\omega R}{\beta}} \right] + \frac{1}{4\pi\rho\alpha^2 R} (f \cdot \nabla R) \nabla R(\omega) e^{-\frac{i\omega R}{\alpha}} + \frac{1}{4\pi\rho\alpha^2 R} (f \cdot \nabla R) \nabla R(\omega) e^{-\frac{i\omega R}{\beta}} \quad 3.5$$

where R is the distance between source and point of observation. Using Fourier transform we get

$$-\frac{1}{\omega^2} \left[1 + \frac{i\omega R}{\alpha} \right] e^{-\frac{i\omega R}{\alpha}} \leftrightarrow tH\left(t - \frac{R}{\alpha}\right) \quad 3.6$$

Equation 3.5 can be transform in the time domain as:

$$u(R, t) = \frac{1}{4\pi\rho} \left[f \cdot \nabla \nabla \left(\frac{1}{R} \right) \right] \int_{R/\alpha}^{\min(t, \frac{R}{\beta})} \tau s(t - \tau) d\tau + \frac{1}{4\pi\rho\alpha^2} (f \cdot \nabla R) \nabla R s\left(t - \frac{R}{\alpha}\right) + \frac{1}{4\pi\rho\alpha\beta^2} (f \cdot \nabla R) \nabla R s\left(t - \frac{R}{\beta}\right) \quad 3.7$$

This expression contains two terms. First term decay with distance faster than R^{-1} known as near field and last two terms decay at rate R^{-1} called far field.

3.2.2 FAR FIELD BODY WAVES DUE TO A POINT SOURCE

In the seismology most of the work of practical use is done assuming the distances greater than several wavelengths from the source known as the far field. Last two terms in eqn (3.7) are important when R is very large. The term far field is very confusing. There is no exact distance at which one can define the near field and far field, and the terminology became more complicated for point source. In equation 3.5 the condition at which we can neglect the first two terms with respect to last two term defines the far field. The condition is $\omega R/\alpha \gg 1$ or $R/\lambda \gg 1$, where λ and ω are the wavelength and frequency of P waves. Hence the term far field is totally dependent on the wavelength of signal. Hence depending on the frequency content, one can be in the near field for a low frequency and in far field for high frequency. For a zero frequency signal every point on the earth is in near field while for higher frequency greater than 1 Hz every point beyond 10 km is in far field. So from a point source the far field can be written as:

$$u_{FF}^P(R, t) = \frac{1}{4\pi\rho\alpha^2 R} R^P s\left(t - \frac{R}{\alpha}\right) \quad 3.8$$

$$u_{FF}^S(R, t) = \frac{1}{4\pi\rho\alpha\beta^2 R} R^S s\left(t - \frac{R}{\beta}\right) \quad 3.9$$

where R^P and R^S are P and S waves radiation patterns. In the far field P and S waves propagates the radial and transverse component of point source respectively. The radiation patterns can be written in simpler form by using amplitudes as a function of azimuth θ of ray with respect to applied force as:

$$R^P = \cos\theta e_R, R^S = \sin\theta e_T$$

Where e_R and e_T is unit vector in radial and transverse direction respectively. The radiation pattern about the point source force are symmetrical. The P and S waves generated from a point source shows dipolar and toroidal distribution of amplitudes respectively.

3.2.3 NEAR FIELD OF A POINT SOURCE FIELD

Near field of a point source can also defined in terms of frequency or wavelength of waves generated from the source. When $\omega R/\alpha$ is not large then all terms in the eqn (3.5) are of equal importance. In such case near field and far field have same order of amplitude. The first brackets term in eqn (3.5) tends to zero as R approaches to zero. The behavior of near field can be understood by expanding the exponential of order of R^2

$$\text{i.e. } e^{-j\omega R/\alpha} = 1 - \frac{j\omega R}{\alpha} - \frac{\omega^2 R^2}{\alpha^2} + O(\omega^3 R^3)$$

The expression can be derived for S wave as:

$$\bar{u}(R, \omega) = \frac{1}{8\pi\rho R} [f \cdot \nabla R) \nabla R \left(\frac{1}{\beta^2} - \frac{1}{\alpha^2} \right) + f \left(\frac{1}{\beta^2} + \frac{1}{\alpha^2} \right)] s(\omega) \quad 3.10$$

The above equation is the product of static displacement and source time function $S(\omega)$. The displacement is produced in the direction of 'f'. Transforming the above equation in time domain, the displacement produced by point source is given by.

$$u(R) = \frac{1}{8\pi\rho R} [f \cdot \nabla R) \nabla R \left(\frac{1}{\beta^2} - \frac{1}{\alpha^2} \right) + f \left(\frac{1}{\beta^2} + \frac{1}{\alpha^2} \right)] \quad 3.11$$

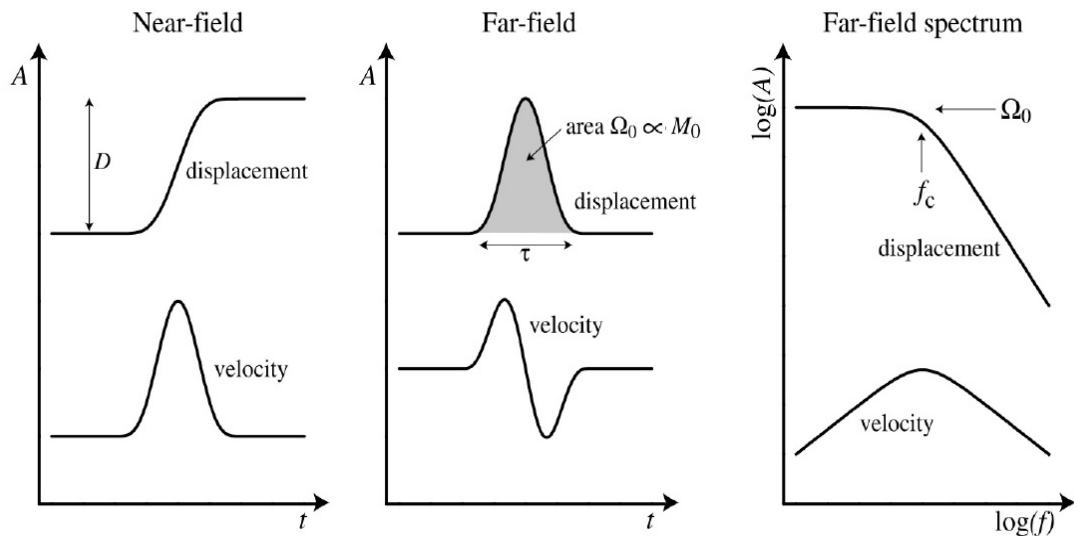


Fig. 3.1 Far field and near field displacement relation on left two panels and far field displacement and velocity spectrum on right panel.

3.2.4. KINEMATIC MODEL OF FAULT RUPTURE

In previous section, we discussed about the displacement due to a point source. The complete representation without source dimension is not possible. So a source must have dimensions and it must consider the wave radiation. The first such assumption is the cavity at focus and consists of uniformly distributed stress on its surface (Jeffrey, 1929; Nishimura, 1937; Scholte, 1962).

The kinematic model is the first extended source model of shear fracturing. It assumes that slip with propagates over a finite surface area with constant velocity. The extended source in terms of single and double couples distributed over a rectangular surface is described by Ben Menaham (1961, 62). He determined the body and surface wave displacement corresponding to single and double couple. The finite radius circular fracture that propagates from the center is studied by Berckhemer (1962). Fracture rectangular model is proposed by Haskell (1964, 1966). Elliptical fault was proposed by Savage (1966). He studied the body and surface waves. A circular fault in which the stress is suddenly applied is proposed by Brune (1970). The elastic displacement produced by circular model is studied by him in both near field and far field. The recent development in kinematic models includes the propagation of shear fracture on a finite fault with variable rise time, slip and rupture velocity (Hartzell, 1989)

3.2.5 RECTANGULAR FAULT: HASKELL'S MODEL

The simple finite dimension kinematic model is the Haskell model. This dislocation model introduced by Haskell (1964, 1966) is most widely used source model. In this model a uniform displacement discontinuity spreads inside a rectangular shaped fault at constant rupture velocity (Fig. 3.2). This model is a suitable approximation for simple rupture propagation along a strike slip fault at low frequencies or wavelength longer than the size of fault. At time $t=0$ a line of length W appear on rectangular fault plane and start moving till the length L of the fault plane approached living behind the slip dislocation D . The slip function can be obtained by assuming that fault plane is in the coordinate system (x_1, x_2) as:

$$\Delta u_1(x_1, x_2, t) = D \dot{s}(t - x_1/v_r) H(x_1) H(L - x_1) \text{ for } -w/2 < x_2 < W/2 \quad 3.12$$

Where v_r is the speed at which the rupture front propagates in x_1 direction i.e. ruptures velocity. $\dot{s}(t)$ is the time function of slip rate and remains inherent with the position of the fault in the Haskell's model.

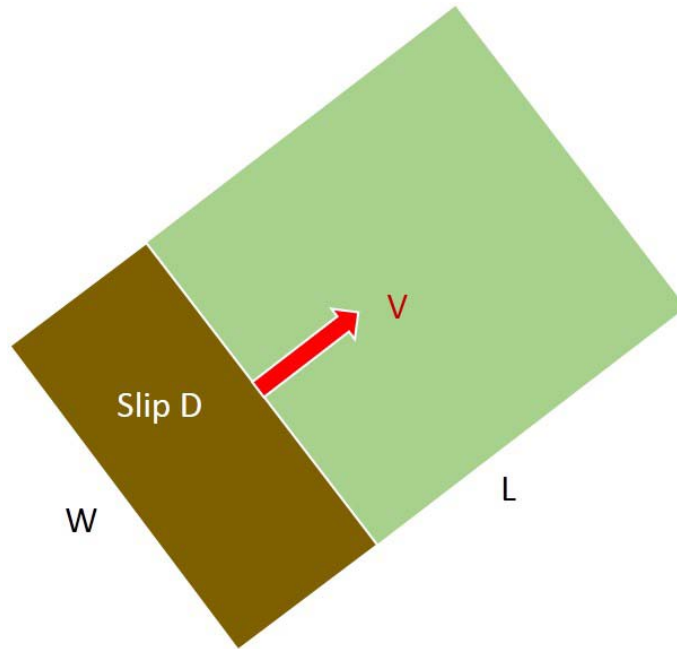


Fig 3.2. The Haskell's model is a rectangular fault with length L and width W. It ruptured with uniform velocity v living behind the slip dislocation D.

The rupture propagation is hidden in the rupture time decay x_1/v_r which is the most important feature of this model. The rupture suddenly appears in the x_2 direction which is physically not possible. The another unacceptable feature of this model is at the edges the average slip suddenly drops to zero which is a sudden break in the continuity. Hence the wave equation is not applicable at the edges. In spite of this shortcoming the Haskell's model covers important features of earthquakes and extensively used for the estimation of earthquake source parameters estimation both in near and far field.

3.2.6 CIRCULAR FAULT: BRUNE'S MODEL

Another fundamental extended seismic source model is the circular fault (Brune, 1970). It consists of finite radius circular fault plane on which instantaneous shear stress pulse is applied (Fig 3.3). This is not exactly a kinematic model because it is specific to the applied stress. There is no propagation of fracture because the shear stress pulse is applied instantaneously to the fault plane and the shear wave is generated due to shear stress pulse normal to the fault plane. The stress pulse at time t and distance x is given by:

$$\Delta\sigma(x, t) = \nabla\sigma\left(t - \frac{x}{\beta}\right) \quad 3.13$$

where β is the shear wave velocity. Since $\sigma = \mu\partial u/\partial x$, so the shear displacement for $x=0$ is given by:

$$\Delta u = H(t) \frac{\Delta \sigma}{\mu} \beta t \quad 3.14$$

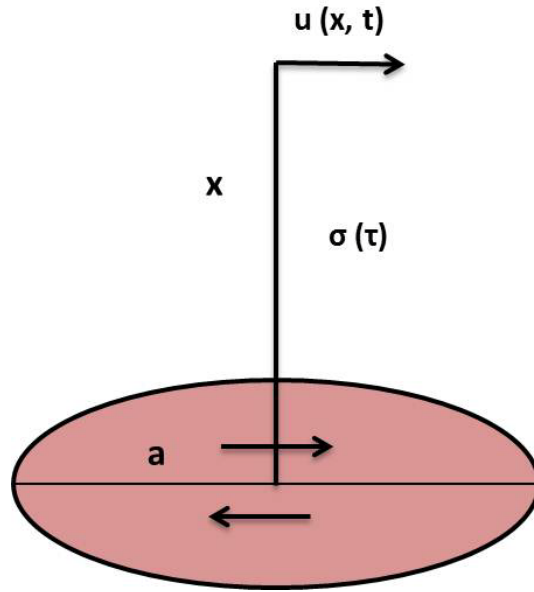


Fig 3.3 Brune's model of circular fault.

The Fourier transform of equation (3.14) is

$$\Delta U = -\frac{\Delta \sigma \beta}{\mu \omega^2} \quad 3.15$$

The difference between the tectonic stress σ_0 and friction stress σ_f ($\Delta \sigma = \sigma_0 - \sigma_f = \epsilon \sigma_0$) is known as static stress drop. For a complete stress drop ($\epsilon=1$) the displacement of S waves in the far field at distance r , not including the effect of radiation pattern is given as

$$u(t) = f(r/R) \frac{\sigma \beta}{\mu} \left(t - \frac{r}{\beta} \right) \exp \left[-b \left(t - \frac{r}{\beta} \right) \right] \quad 3.16$$

Its spectrum is

$$U(\omega) = f(r/R) \frac{\sigma \beta}{\mu} \frac{1}{\omega^2 + b^2} \quad 3.17$$

$$b = \frac{2.34 \beta}{a} \quad 3.18$$

where, a is the radius of the fault.

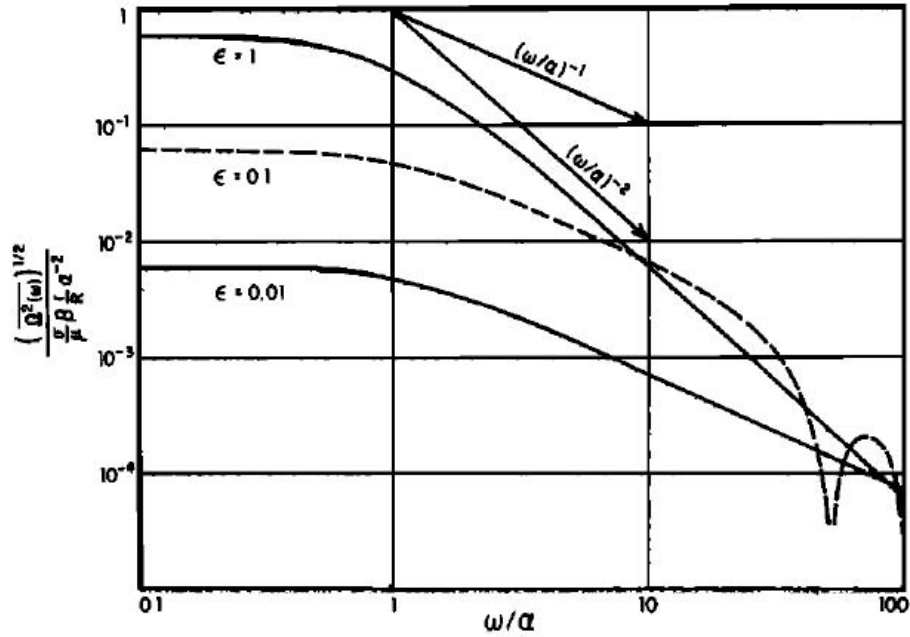


Fig 3.4 Far field average spectral density curve (after Brune, 1970)

The spectrum in Fig 3.4 has a flat part at low frequencies so approaches to M_0 . When ω/α near to unity then it decays at the as ω^{-1} which is represents that stress drop is not complete, then, for small ϵ ($\epsilon \sim 0.01$) and if ω/α greater than unity the curve falls as ω^{-2} starting at the corner frequency. Using corner frequency of S waves, the fault radius can be estimated as:

$$a = \frac{2.34\beta}{\omega_c} \quad (3.19)$$

Earthquakes are occurred in brittle crust of the earth. For the fault plane inside a seismogenic layer having dimensions less than 20 km ($M < 6$), the fractures starts from a point and grow in all directions ($L \approx W$) so in such cases Brune's model is applicable. However, in case of larger earthquakes fault plane length is greater than its width. Therefore, in such cases Haskell model is more suitable. In the present study local earthquakes of low magnitude are used for analysis. So, Brune's model has been adopted to compute the source parameters of local earthquakes.

3.2.7 DYNAMIC MODEL OF FAULT RUPTURE

The models discussed in above sections are called kinematic models which are the natural simplification of the real faults. Other types of models are known dynamic models of seismic source. These consider the dynamic problem in which the slip is considered as result of strength of the material and stress condition in focal region. These are based on the theory of fracture generation and propagation in stressed media. The earthquake mechanism is considered as shear faulting a result of stress drop. Fracture initiates at a point and expand radial in all directions with certain velocity. Hence dynamic model must include all the phases of faulting from initiation to propagation and finally arrested. The fracture dynamic studies include Keylis-Borok (1959), Kostrov (1964, 1966), Burridge (1969), Freund (1972, 1979) and Madariaga (1977). The basis of these studies is the studies carried out between 1920 to 1950 on fracture of crystal and metals by Griffith, Starr and Irwin. The dynamic models are more complicated than the kinematic models.

3.3 SOURCE PARAMETERS

The parameters which describe the property of the source are known as source parameters. These include seismic moment (M_0), Stress Drop ($\Delta\sigma$), source radius (r) and source dislocation. Seismic moment is introduced by Aki (1966) and is a measure of earthquake size. The basic assumption is that the shear faulting produced the earthquake inside the Earth's crust and is defined as:

$$M_0 = \mu \bar{D} A \quad 3.20$$

where μ is the shear modulus or modulus of rigidity, \bar{D} is the dislocation on the fault surface of area A . The moment expressed in Nm in SI system and in dyn cm in CGS. As the seismic moment includes material strength, fault area and slip so it is a good physical measure of earthquake size. The dislocation can be estimated from the fault surface of earthquake. The slip dislocation is the relative on either side of fault plane. The aftershocks relocation gives the total rupture area with the assumption that these small events collectively represent the total fault area. Quantitatively the total area and source dislocation are impossible to measure. For the displacement amplitude spectrum of seismogram corrected for geometrical spreading, the seismic moment is proportional to the zero frequency spectral level (Ω_0). Hence, the seismic moment can be computed using the Fourier transform of observed seismogram using the Ω_0 . The seismogram recorded by three mutually perpendicular components in far field was used to estimate zero frequency spectral level using L^2 -norm.

$$M_0 = \frac{4\pi\rho R\beta^3\sqrt{\Omega_0(Z)^2+\Omega_0(H_1)^2+\Omega_0(H_2)^2}}{R_{\theta\phi}} \quad 3.21$$

For S-wave horizontal component the above relation can be written as:

$$M_0 = \frac{4\pi\rho R\beta^3\Omega_0}{R_{\theta\phi}S_a} \quad 3.22$$

where, R– hypocentral distance from the earthquake source to the seismic station; ρ - average density of the medium around the source; β is the S-wave velocity of the medium around the source; $R_{\theta\phi}$ - a correction to be applied for radiation pattern; Ω_0 - S wave spectral amplitude at the low frequencies; S_a – a correction for amplification due to free surface effect.

The dislocation or relative displacement on a fault plane is due to acting shear stress which exceeds the material strength. Let σ_0 and σ_f are the stress before and after faulting. Then the two parameters σ_m and $\Delta\sigma$ called mean value of stress acting before and after earthquake and stress respectively are given by:

$$\sigma_m = \frac{1}{2}(\sigma_0 + \sigma_f) \quad 3.23$$

$$\Delta\sigma = \sigma_0 - \sigma_f \quad 3.24$$

The stress drop represents the loss of stress due to faulting. If $\sigma_f=0$, then total stress drop is $\Delta\sigma = 2 \sigma_m$. It represents the case when there is no friction of the fault surface. But there is always a friction so some residual stress σ_f is present. The tectonic stress which is responsible for the strain in the focal region is the initial stress. So the total energy release during the earthquake process in simplified form is given by:

$$E = \sigma_m \bar{D} A \quad 3.25$$

Using equation 3.20 and 3.25, the energy released in terms of seismic moment is given by:

$$E = \frac{\sigma_m}{\mu} M_0 \quad 3.26$$

If the stress drop is the total stress drop then equation 3.26 can be written as:

$$E = \frac{\Delta\sigma}{2\mu} M_0 \quad 3.27$$

This expression relates the total energy released during fracturing with the total stress drop and seismic moment. In case of shear faulting the stress drop is proportional to the dislocation, i.e., $\Delta\sigma = \bar{D}/L$, where L is the length dimension of fault. For circular fault $L'=a$ and for rectangular $L'=W$, where a is radius and w is the width. So the stress drop can be estimated using Hook's law:

$$\Delta\sigma = C\mu \frac{\bar{D}}{L'} \quad 3.28$$

where C is dimensionless factor and depends on the shape of the fracture i.e. for circular fracture $C= 7\pi/16$. Using equation 3.20 and 2.28, we obtained a relation for a circular fault,

$$M_0 = \frac{16}{7}r^3\Delta\sigma \quad 3.29$$

So the stress drop can be determined if seismic moment and dimension of fracture are known. Rearranging equation 3.29 we have:

$$\Delta\sigma = \frac{7}{16r^3}M_0 \quad 3.30$$

As in above equation r is having power three, so small error in r will introduce a large error in the determination of stress drop. The area of circular fracture is $A=\pi r^2$. Using this expression in equation 3.30 we have:

$$M_0 = \frac{16\Delta\sigma}{7\pi^{3/2}}A^{3/2} \quad 3.31$$

Taking logarithms,

$$\log M_0 = \frac{3}{2}\log A + \log\left(\frac{16\Delta\sigma}{7\pi^{3/2}}\right) \quad 3.32$$

In above equation it is clear that if the stress drop is constant then log A is proportional to the $2/3 \log M_0$. Kanamori and Anderson (1975) shows that for a large earthquakes ($m>5$), the stress drop is almost constant and within 1-10 Mpa with mean value 6 Mpa or 60 bars. They suggested that interplate earthquakes have lower stress drop (about 3 Mpa or 30 bars) than the intraplate events (about 10 Mpa or 100 bars). Tsuboi (1956) also observed the same amount of stress drop (6 Mpa) for same order of magnitude as suggested by Kanamori and Anderson (1975). Hanks and Kanamori (1979) proposed a magnitude scale which is estimated using the seismic moment known as moment magnitude (M_w). This is free from the problems associated with the other magnitude scales such as magnitude saturation. The expression used for magnitude determination is:

$$M_w = \frac{2}{3}\log(M_0) - 10.73 \quad 3.33$$

where M_0 is in dyn-cm. In equation 3.30, r is the fracture radius. It is determined by using the expression given by Brune (1970, 1971):

$$r = \frac{2.34\beta}{2\pi f_c} \quad 3.34$$

Where β is the shear wave velocity and f_c is the corner frequency which can be directly determined from the earthquake spectrum.

Along with the above parameters, Brune (1970) induced a cut off frequency in the acceleration spectrum. This high cut off frequency was interpreted as the source effect by Ida (1973). Hanks (1982) called this cut off frequency as maximum cut-off frequency f_{max} , above which acceleration spectral amplitudes diminish abruptly. Papageorgiou and Aki (1983a, b) attribute f_{max} as source effect and relates with size of cohesive zone or break down zone. Anderson and Hough (1984) called the high cut off decay parameter as kappa (κ) later the researchers such as Li et al. (1994), Castro et al. (2000) uses the κ and f_{max} in same context. Anderson and Hough (1984) said that the kappa in high frequency spectra is due to the shallow depth attenuation effect below receiver. They recognized the kappa as a site effect because they observed that the κ is higher for hard rocks and lower for soft sediments. On the other hand, Su et al. (1992) analyze the data set of 132 seismometers and found that the site amplification factor increases monotonically with geologic age of the site rocks up to 12 Hz and concluded that there is no site contribution of κ upto 12 Hz. Both f_{max} and κ are estimated using high cut filter given by Boore (1983) and Anderson and Hough (1984) respectively.

$$P(f) = \frac{1}{1+(\frac{f}{f_{max}})^p} \quad 3.35$$

$$P(f) = e^{-\pi f \kappa} \quad 3.36$$

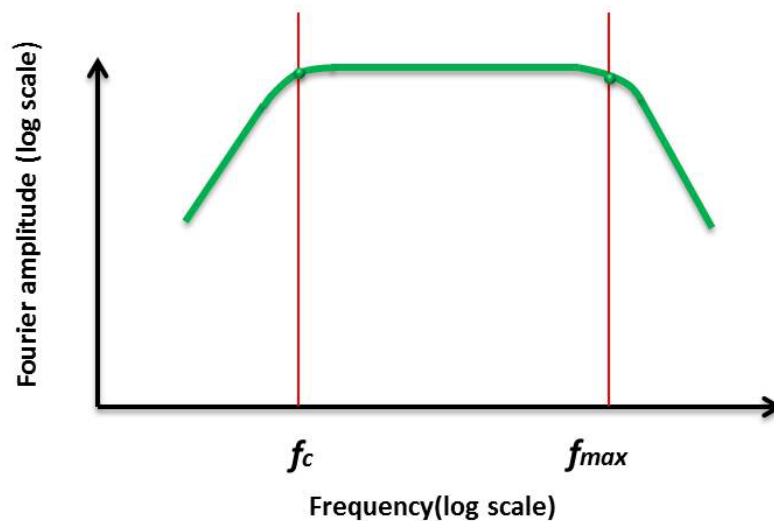


Fig 3.5 Idealized shape of Fourier amplitude spectrum of acceleration time history showing the corner frequency, f_c , and cutoff frequency, f_{max} .

3.4 ESTIMATION OF EARTHQUAKE SOURCE PARAMETERS:

PROCEDURES

A data set 104 local earthquakes recorded around the Lower Siang region of Arunachal Himalaya employing five station seismological network has been used to estimate the source parameters of the region. These events recorded by short period and broad band seismometers at 100 samples per second sampling rate during July 2011 to May 2012 in the form of digital time series. The procedure for the estimation of source parameters includes the correction of baseline, rotation of data and instrument response before the Fourier transform (FFT) of S-wave of Seismogram. The following are the details of these corrections and also other part of procedure.

3.4.1 Baseline Correction

The process of correcting the recorded signal for a bias in zero velocity or acceleration value and any drift from zero level which may be due to environmental and instrumental effect is called baseline correction. It is the procedure to correct the certain types of long period disturbance both in analog and digital data. The simplest procedure of instrument correction is the subtraction of average recorded acceleration or velocity value. Alternately, the baseline correction is done by subtracting a straight line from recorded time series. The line is either obtained by linear least square fitting of time series or time series mean value. The determination of mean value involves the calculation of mean value from a suitable portion of seismogram. Generally the mean value is calculated using the part of seismogram prior to the first P-wave. In case pre event record is absent, the entire time history is used (Fig 3.6).

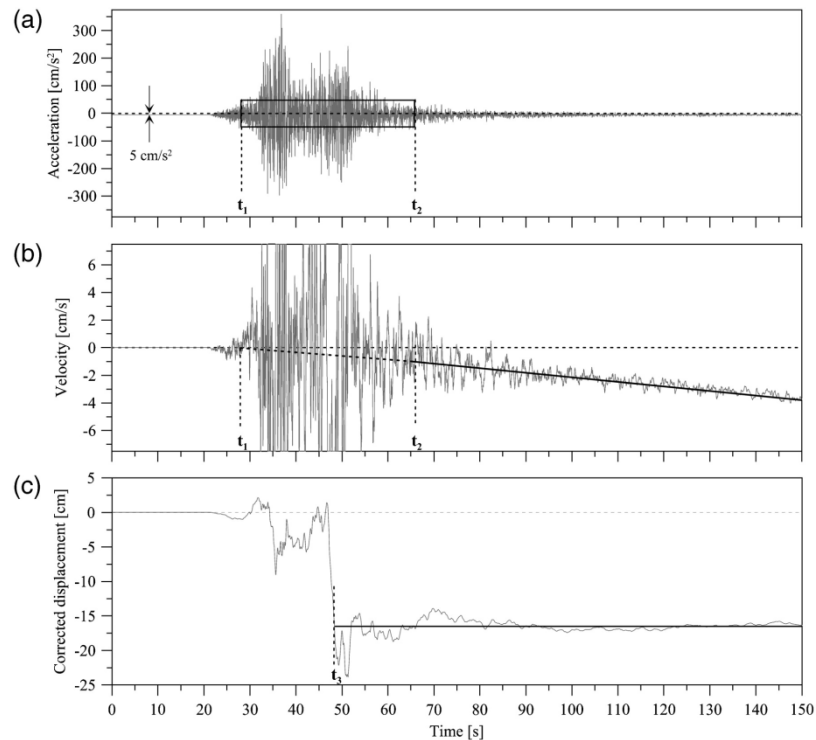


Fig. 3.6 The effect of baseline error (a) original acceleration record (b) velocity record obtained after integration of acceleration record (c) displacement record obtained by integrating the velocity record (after wang et al., 2011)

3.4.2 Seismogram rotation

Different types of seismic waves have different directions of particle motion (Fig. 3.7). Analysis of the particle motion can thus be used to identify the different wave types. Particle motion or polarization of the waves is best looked at in a coordinate system that points from the earthquake source to the seismic station (Fig. 3.7). Through a simple rotation we can change the two horizontal components into the radial (R) and transverse (T) components. The radial direction is along the line from the station to the event and the transverse direction is in the horizontal plane at a right angle to the radial direction. For example, the P wave is polarized in the direction from source to receiver, and particle motion is in the vertical-radial plane. The wave motions of the different kinds of waves are P-waves: Linear in radial and vertical plane, SH waves: Linear in the transverse direction, SV waves: Linear in the radial and vertical plane, Rayleigh waves: Elliptical in the radial and vertical plane and Love waves: Linear in the transverse direction. Thus the radial component of seismogram comprises of P, SV and Rayleigh waves whereas the transverse component of seismogram comprises of SH and Love waves.

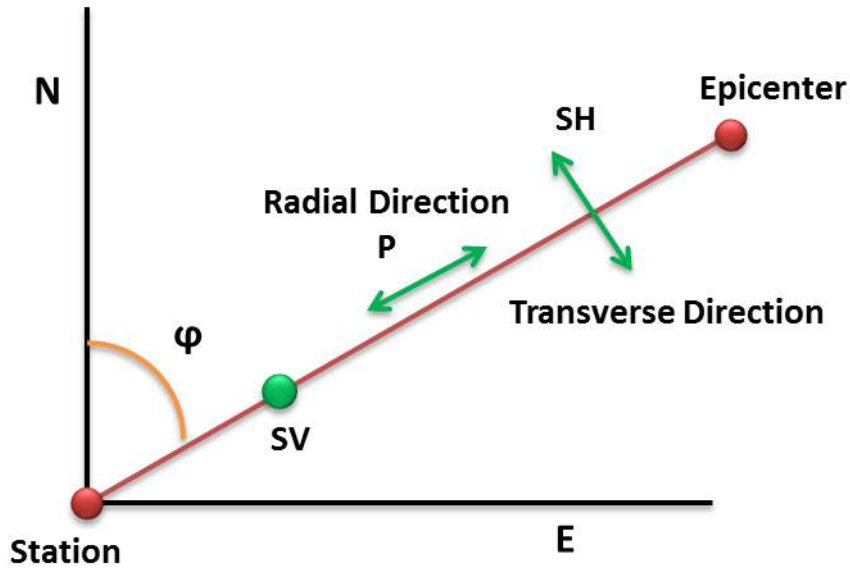


Fig 3.7 Representation of the radial and transverse directions of seismic waves.

For the purpose of computing the observed spectrum from the recorded three components of the ground motion, NS and EW components of the recorded ground motion have been rotated in the directions of azimuth to allow computing the SH component of the ground motion (Fig. 3.8). Rotation of seismogram can be performed mathematically by matrix multiplication of a vector consisting of the North-South (NS) and East-West (EW) components with a rotation matrix given below:

$$A = \begin{bmatrix} \cos\phi & \sin\phi \\ -\sin\phi & \cos\phi \end{bmatrix}$$

$$\begin{bmatrix} R \\ T \end{bmatrix} = A \cdot \begin{bmatrix} NS \\ EW \end{bmatrix}$$

Hence

$$SV = NS\cos\phi + EW \sin\phi$$

$$SH = -NS\sin\phi + EW \cos\phi$$

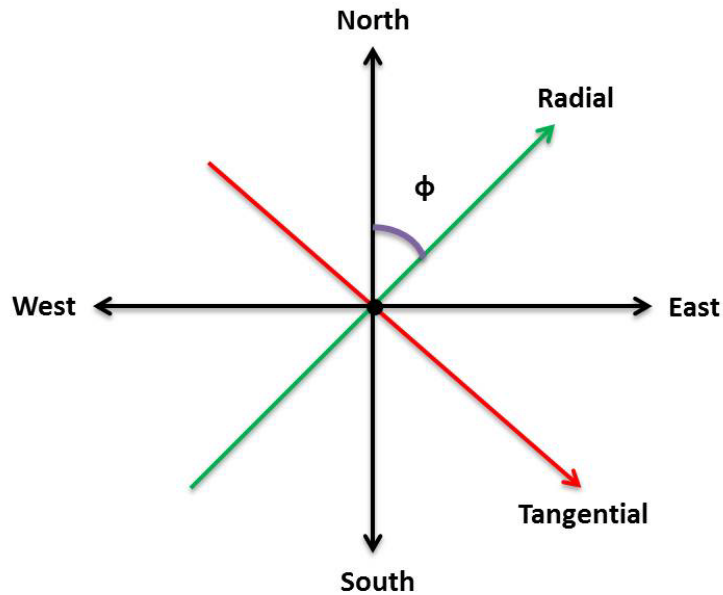


Figure 3.8 Rotation of North-South and East-West components of Seismogram towards the direction of epicentre of an earthquake by angle (ϕ).

A typical example of the observed three components of ground motion and rotated components representing SH, SV and longitudinal ground motion is shown in Fig. 3.9.

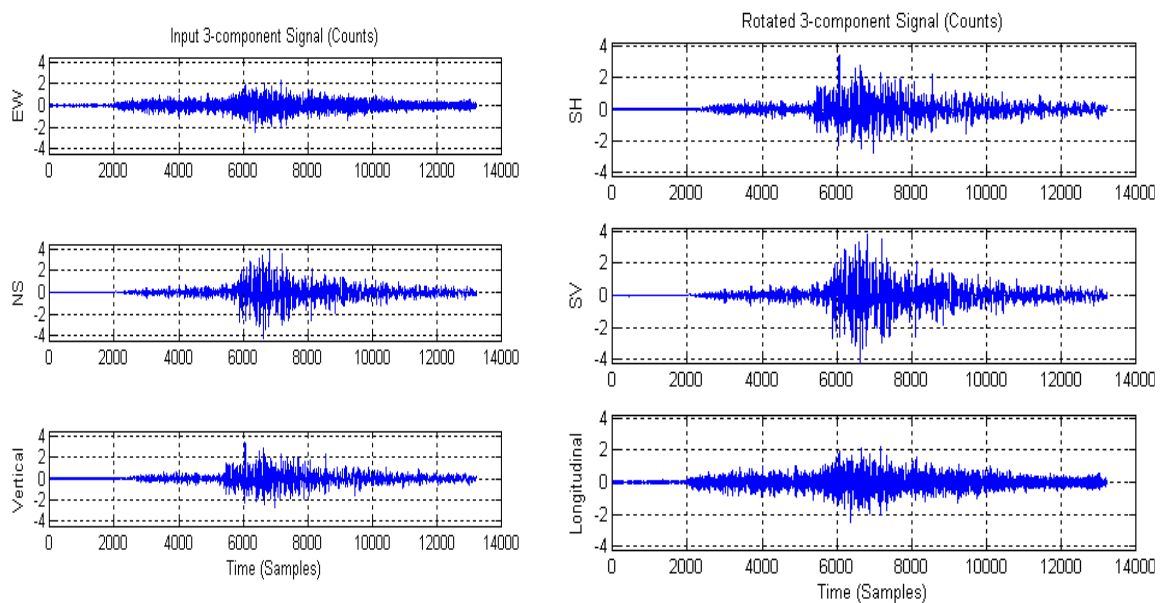


Figure 3.9 An example of 3-component vertical, NS, ES and rotated SH, SV, longitudinal components of ground motion obtained after rotation.

3.4.3 Instrument corrections

The signals recorded by the seismograms are not the true ground motion. They record some signal proportional to some characteristics of the ground motion i.e. the output of a velocity sensor is proportional to the ground velocity. But such relation follows after the natural frequency of the instrument. Below the natural frequency no such relationship followed by the sensor. Furthermore, a seismologist interested in recovering of the ground displacement. In order to get the actual ground displacement below the natural frequency of sensor the effect of the instrument filter is required to remove. This is known as the instrument correction. The detail contains how the instrument correction is applied on the data is given in Appendix-II.

3.4.4 Correction for Path Effect

Decrease of seismic wave amplitudes due to the increase in area of the wavefront with increasing distance R from the source is called geometrical spreading; this phenomenon is similar to amplitudes of water ripples decreases as they expand from the source. For local earthquakes, the decrease of amplitudes for body wave in a homogeneous space can be considered as

$$G(R) = \frac{1}{R} \quad (3.35)$$

where R is distance from earthquake source to receiver. The seismic waves when travel through the inelastic Earth dissipates some energy in form of heat due to internal friction. This inelastic or viscoelastic attenuation leads to a decrease of wave amplitudes with distance and time. The mechanisms of internal friction are complex and depend on different factors, such as on the atomic and molecular structure of crystals in minerals, as well as on the existence of cracks, fractures and inclusions in rocks (Vallina, 1999). In addition to this, attenuation also occurs due to scattering of seismic waves and redistribution of energy at boundaries due to refraction, reflection and diffraction of seismic waves.

It is a common observation that longer the seismic wave travels in the medium the greater the heterogeneity they encounter. A great variety of paths traveled by the coda waves that appear in the later part of the seismogram have been used to provide information

concerning the average properties of the medium instead of just the characteristics of a particular path. Attenuation estimated from the decay of coda waves by several investigators is a combination of scattering and intrinsic attenuation (e.g., Aki and Chouet, 1975; Singh and Herrmann, 1983; Sato and Fehler, 1998; Gupta et al. 1995; Gupta and Kumar, 2002).

Correcting waveforms or their spectra for propagation effects is an essential requirement for precise determination of the earthquake source spectrum. Correction of the propagation effects can introduce during the computation of displacement spectra multiplying the spectra by quality factor 'Q' at various frequencies. For this purpose generally frequency dependent relationship in the form of $Q=Q_0f^n$ estimated for the region is used. However, no such relation is available for the Lower Siang region. Therefore, as part of this thesis work in the chapter 5 & 6 the seismic wave attenuation for characteristics have been estimated for the P, S and Coda p[art of seismogram. Frequency dependent attenuation relation $Q_\beta = (58\pm 1)f^{(1.16\pm 0.04)}$ obtained from S-waves of local earthquakes has been used for path correction for precise determination of source parameters of the region using direct S-wave data.

3.5 Data Analysis

After applying the above mentioned corrections in the data set of 104 local earthquakes, the source parameters; seismic moment (M_0), source radius (r) and stress drop ($\Delta\sigma$) have been estimated by developing software DEQ_EQK_SRC_PARA. This software is the modified version of the software EQK_SRC_PARA developed by Kumar et al. (2012) which automatically compute both the source and spectral parameters i.e. low frequency spectral level (Ω_0) and corner frequency. The flowchart of DEQ_EQK_SRC_PARA is given in Fig. 3.10. Examples of some of the seismograms displaying the analysis procedures for computation of source parameters are shown in Fig. 3.11 a&b.

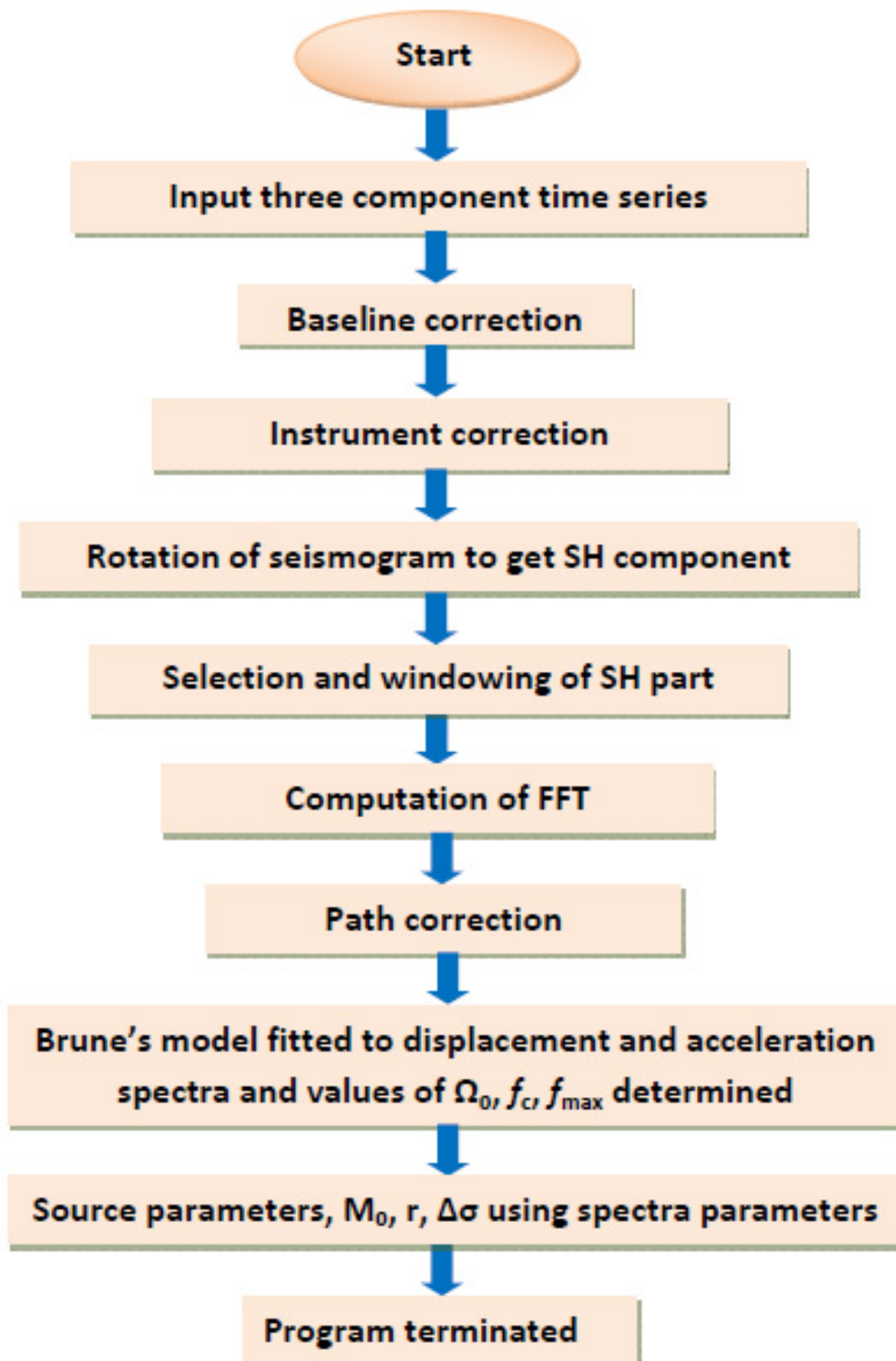


Fig . 3.10 Flow chart for estimation of source parameters using DEQ_EQK_SRC_PARA.

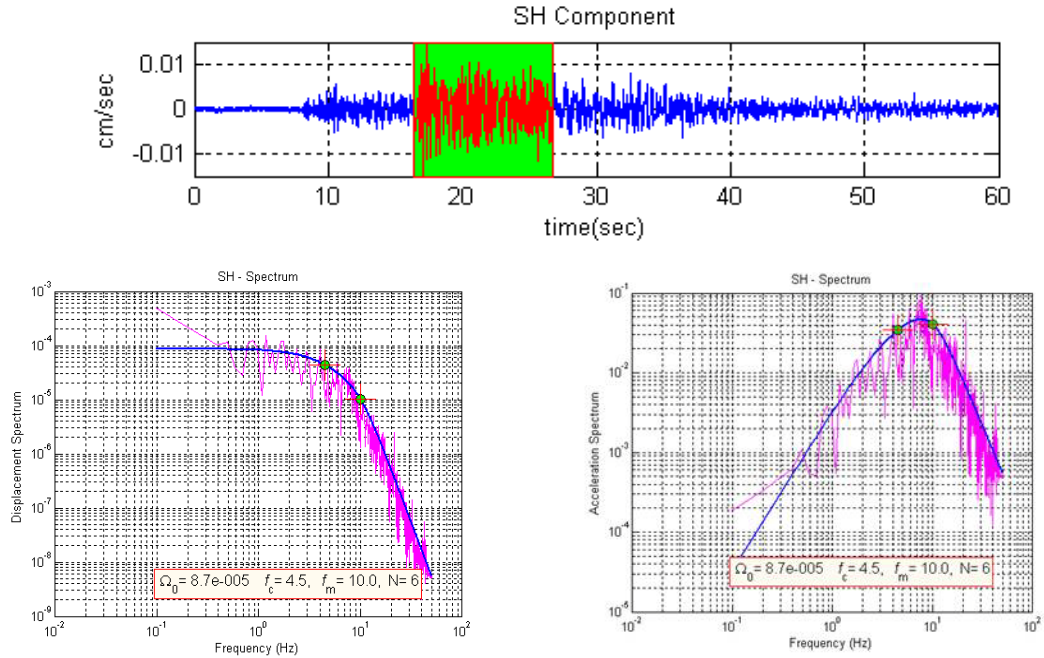


Fig. 3.11 a. An example of SH component of a seismogram of local earthquake (M_w 3.1) recorded at ADIPASI station on 29/09/2011. Showing the above displacement (left) and acceleration (right). The source model fitted for both spectra is shown in each spectrum.

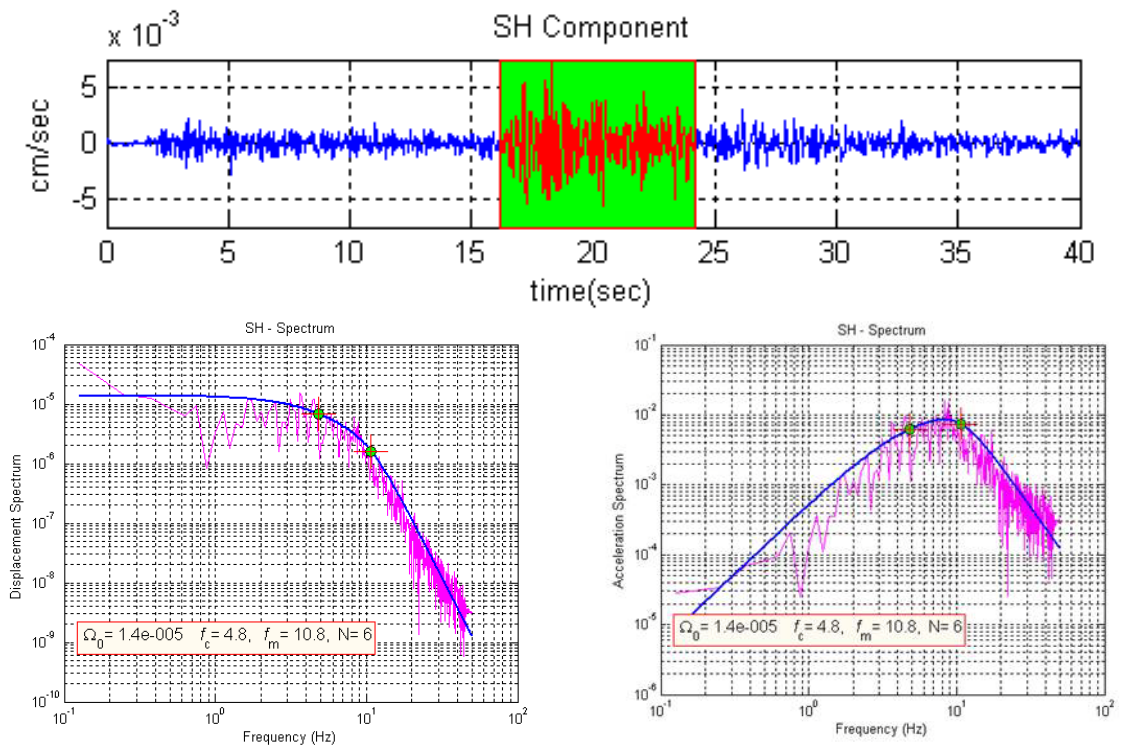


Fig. 3.11 b. An example of SH component of a seismogram of local earthquake (M_w 3.1) recorded at ADIPASI station on 29/09/2011. Showing the above displacement (left) and acceleration (right). The source model fitted for both spectra is shown in each spectrum.

3.6 Results and Discussion

The analysis of 104 local earthquakes using the above analysis procedures and software has resulted the estimation of source parameters viz, seismic moment (M_0), source radius (r) and stress drop ($\Delta\sigma$) for Lower Siang region of Arunachal Himalaya. Results of these parameters are shown in Table III.1 in appendix-III. Seismic moment (M_0), source radius (r) stress drop ($\Delta\sigma$) and Moment magnitude, vary from 1.6×10^{18} to 3.1×10^{23} dyne-cm, 157.8 to 417.1 m, 0.1 to 74 bars and 1.4 to 5.0, respectively.

To study the characteristics of computed source parameters and their relationships various plots have been prepared. The relations of some source parameters are discussed below:

The variation of source radius versus seismic moment for the 104 events is shown in Fig. 3.12. The linear curves corresponding to static stress drops of 0.1 bar, 1 bar, 10 bars and 100 bars are also plotted. Fig 3.12 shows that the seismic moment varies from 1.6×10^{18} to 3.1×10^{23} dyne-cm and the source dimensions in terms of radius of the circular fault vary from about 175 m to 357 m. The source radius of all considered events is estimated using the equation 3.34. For the estimation of source radius the corner frequency obtained from the displacement spectra is used and this source radius along with seismic moment is then used to estimate the stress drop. The stress drops computed for all such a way for all the events vary from 0.1 bars to 74 bars and shows large scatter. However there only few events which showed the high stress drop. If we exclude these events then the stress drop for most of the events the stress drop varies from 0.1 to 22.4 bars. In many studies such as, Archuleta et al., 1982; Dysart et al. 1988; Abercrombie, 1995; Garcia et al. 1996; Wu et al., 1999; Jin et al., 2000; Tusa and Gresta, 2008; Kumar et al., 2006; Sule, 2010; Kumar et al., 2012, the range from 0.1 to 26 bars is found to be constant. The low value of stress drop suggests that some earthquakes in this region may be associated with a brittle shear failure mechanism on the fault segment and/or a presence of weakened zones where the earthquake may be triggered by low stress regimes. Some exceptionally high stress drop may be due to the presence of some intruded high straight rocks or may be some other errors during computation. However, a best fit line shown in Fig. 3.12 (red colour line) shows a constant stress drop nearly 2 or 3 bars. Hence stress drop does not change with seismic moment. These results confirm the results of some researchers such as, Hanks (1982); Anderson and Hough (1984); Anderson (1986), Abercrombie (1995), who concluded that the breakdown in the stress drop scaling and minimum source dimension reported by some researchers is due to some

artifacts induced by the loss of high frequencies due to wave propagation. Fig 3.13 shows the distribution of stress drop with focal depth. Baring a few shallow focus events, the stress drop remains constant and not varies with focal depth. Hence there no dependency of stress drops with depth. It indicates that the stress drop is only the function seismic moment and fracture radius.

The scaling relations between M_0 and f_c have been established by various researchers. For the small magnitude earthquakes the measurement of stress drop is very difficult because it is hindered by high frequency loss due to attenuation. Abercrombie (1995) observed the corner frequency using the borehole data. These results are considered as most reliable (Fig.14). Abercrombie (1995) along with some other researchers such as Hanks and Wyss, 1972; Abercrombie and Leary, 1993; Boatwright, 1994; Kinoshita and Ohike, 2002, agreed with the Brune's model as:

$$M_0 \propto f_c^{-3} \quad 3.36$$

Kanamori and Rivera (2004) modified the scaling relation. They argued that although the scaling relation is $M_0 \propto f_c^{-3}$ but in real data is scattered so this is modified as:

$$M_0 \propto f_c^{-3+\varepsilon} \quad 3.37$$

where $\varepsilon \leq 1$. The scaling law estimated in present study as shown in Fig 3.15 is:

$$M_0 \propto f_c^{-3.27} \quad 3.38$$

Hence our study agreed with Kanamori and Rivera (2004).

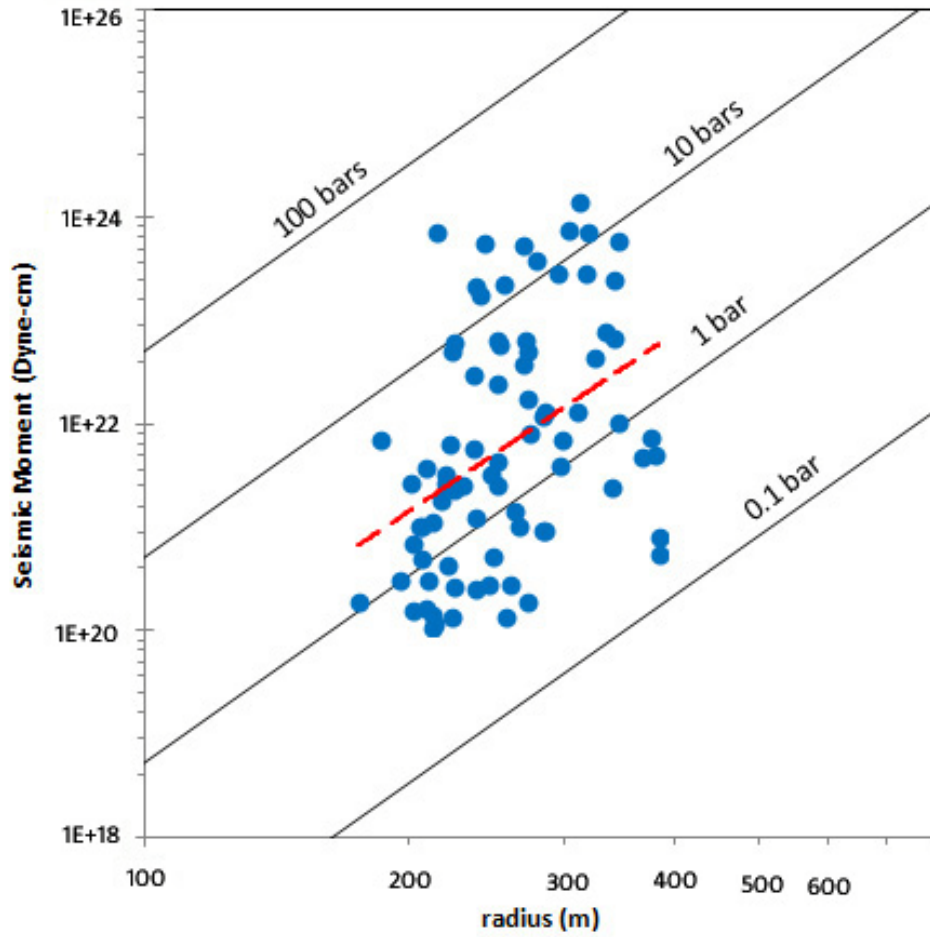


Fig. 3.12. Plot between source radius and seismic moment

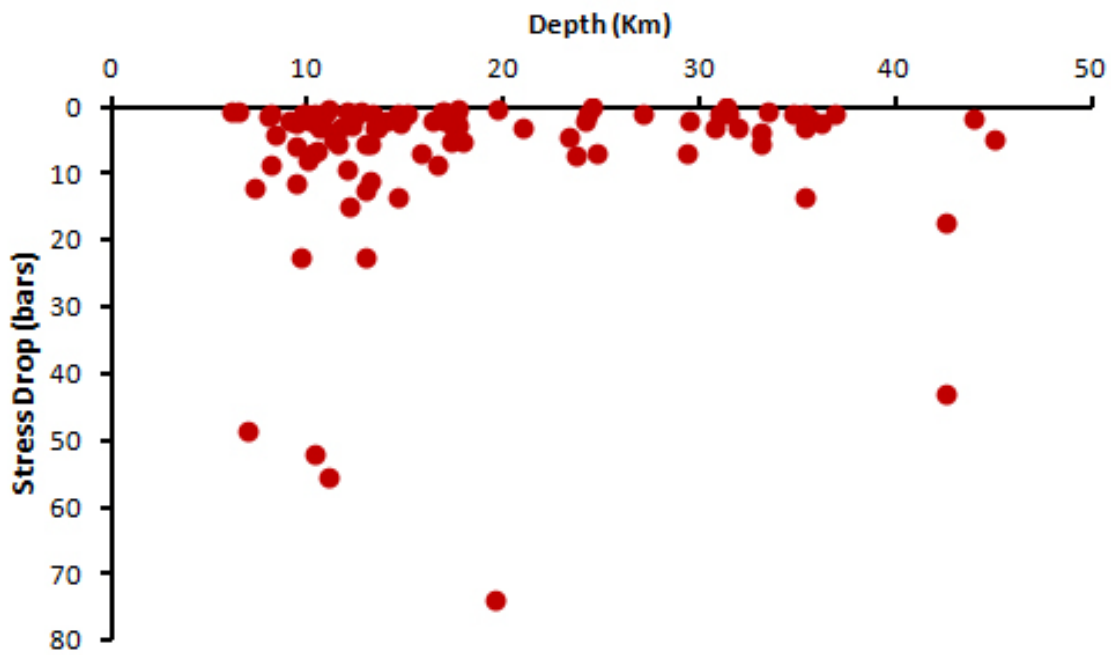


Fig. 3.13. Plot between stress drop and focal depth.

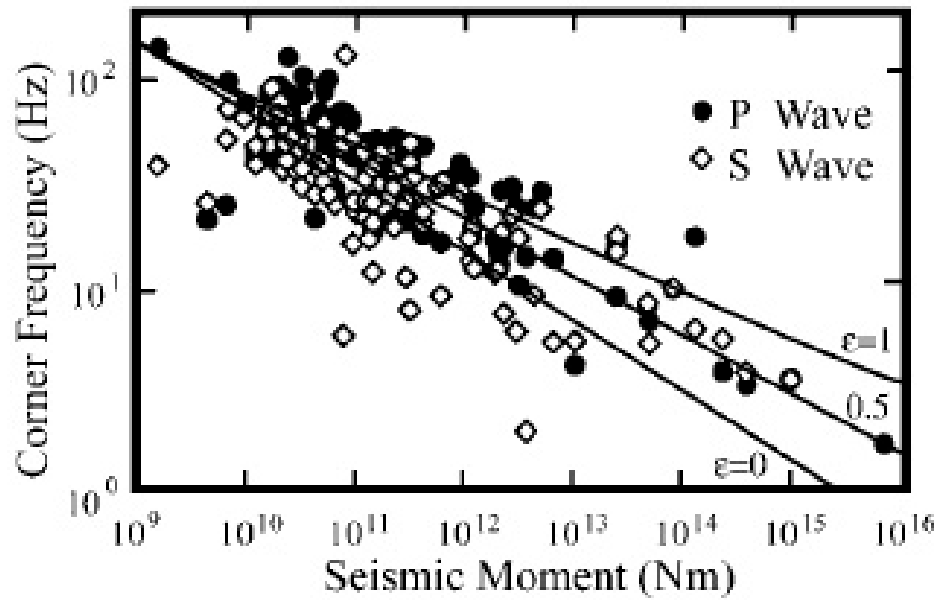


Fig 3.14 The relationship between seismic moment and corner frequency. The middle line corresponding to $\epsilon = 0.5$ shows $M_0 \propto f_c^{-3}$. (After Kanamori and Rivera, 2004)

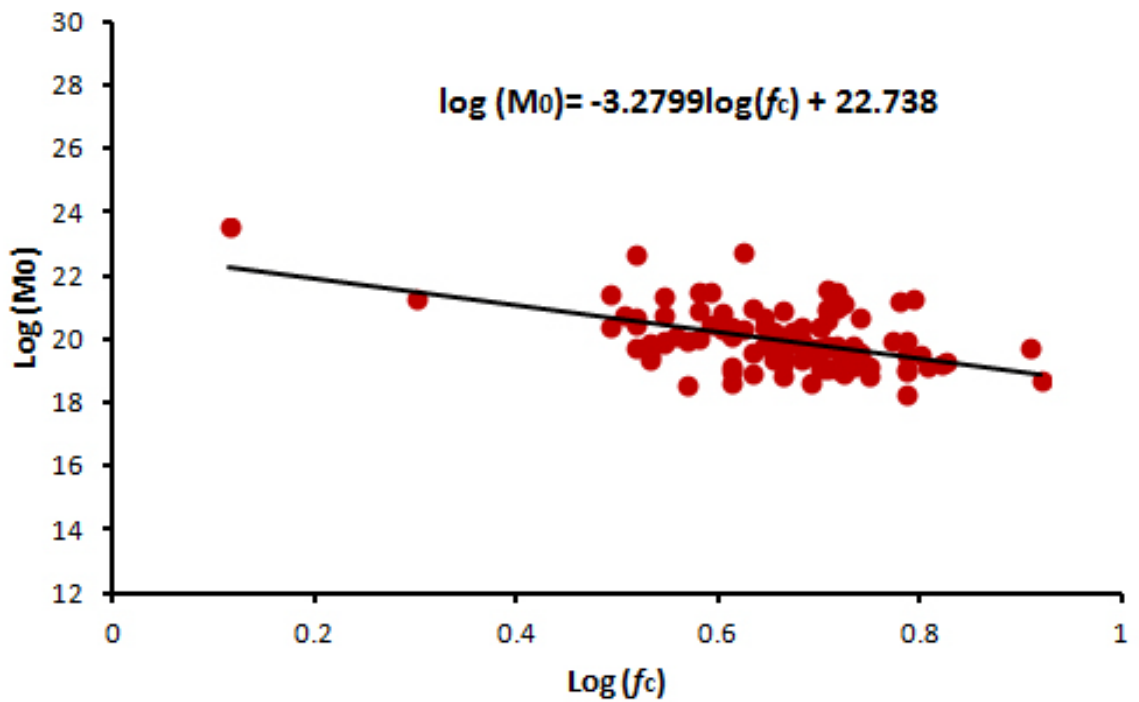


Fig. 3.15. Plot between seismic moment and corner frequency

The variations of f_c and f_{max} with seismic moment have been drawn to study the relationship to seismic source and shown in Fig 3.16. Although the dataset shows large scatter but it seems from the plot that there is a similar decreasing trend for both f_c and f_{max} with increasing seismic moment or source size. Hence, it is brought out that f_{max} has similar dependence seismic source as that of f_c on. Fig. 3.17 and Fig. 3.18 depict plots of f_c and f_{max} to focal depth and epicentral distance. In both plots a large scatter in data that follows a parallel trend to focal depth and epicentral distance has been observed. The behaviour of f_{max} with respect to focal depth and epicentral distance of earthquakes is found to be same as that of f_c . Both f_c and f_{max} are constant with epicentral distance which indicates that these are independent of it.

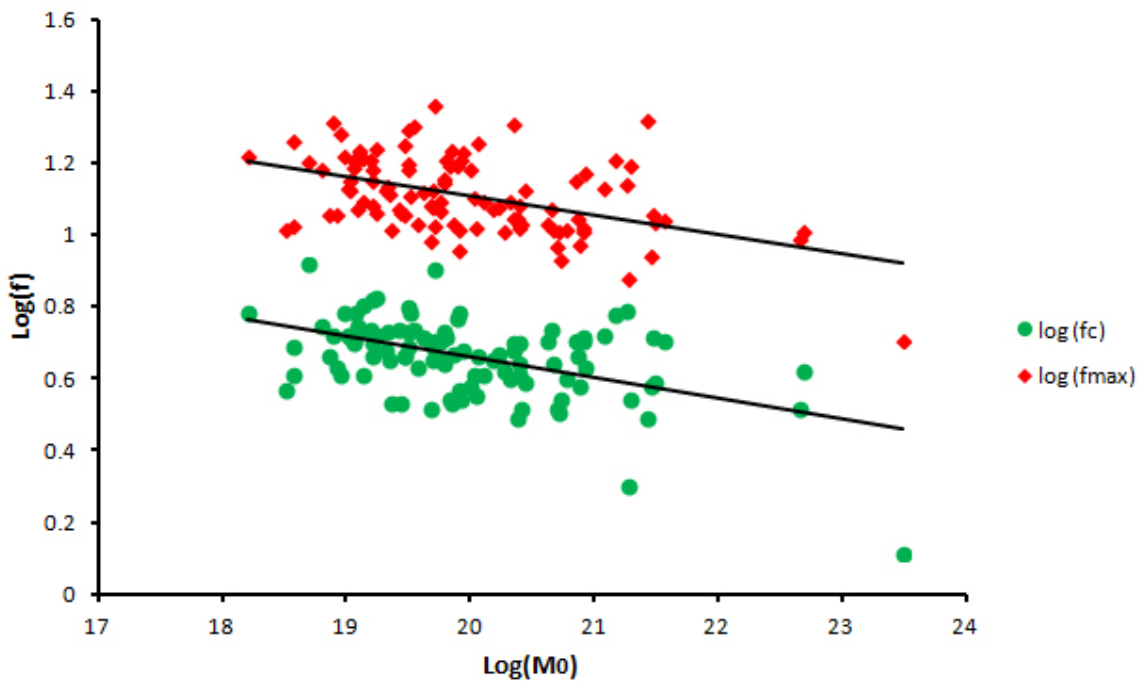


Fig. 3.16. Plot showing variation of average values of f_c and f_{max} with seismic moment.

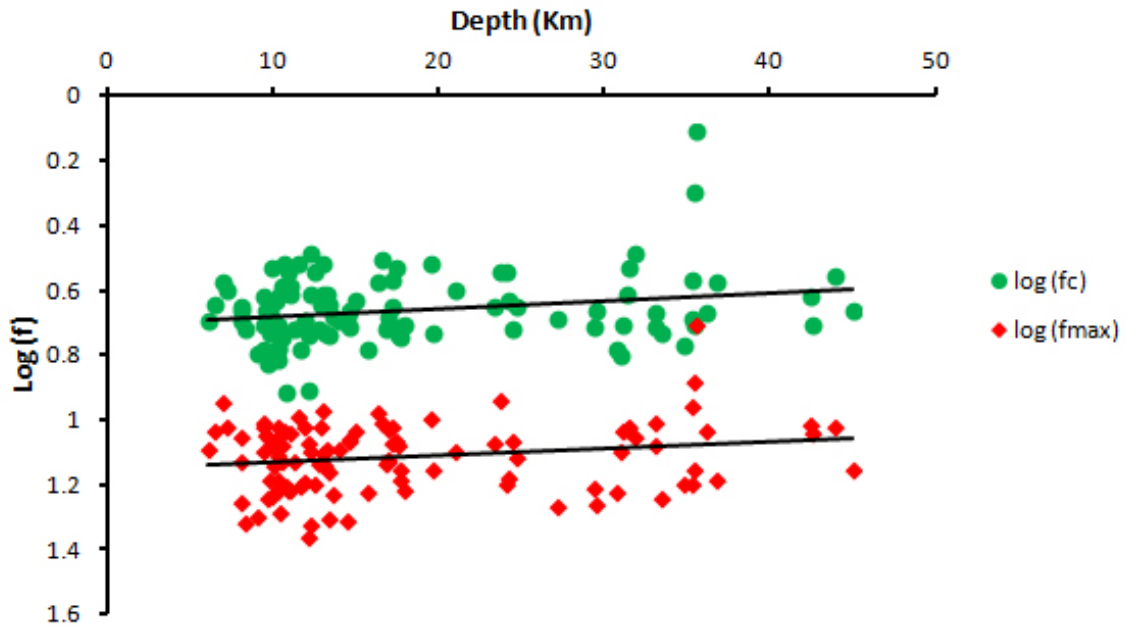


Fig. 3.17. Plot between focal depth and f_c and f_{max} .

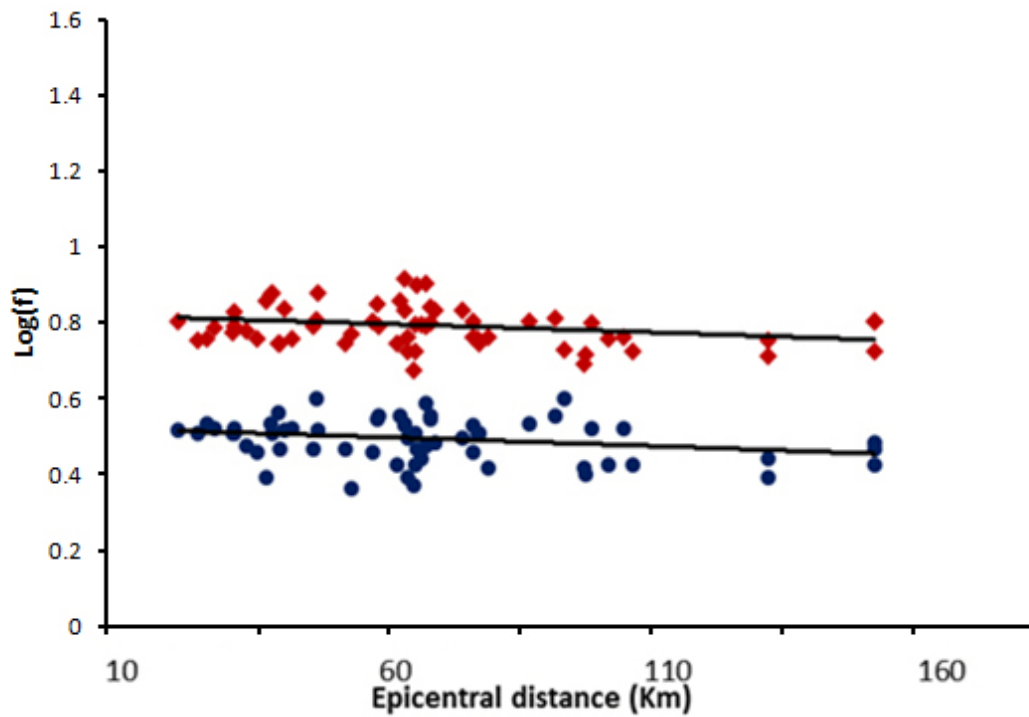


Fig. 3.18 Plot between epicentral distance (DEPI) and f_c and f_{max} .

In order to study the dependence of f_{max} , with the site characteristics, values of f_c and f_{max} are plotted between seismic moments for each site. The plots shown in Fig. 3.19a, b, c, d indicate similar scatter and almost parallel trends between f_c and f_{max} with increasing seismic moment. This indicates that f_{max} has similar behavior as for f_c to seismic moment

on each site and if f_{\max} is affected by site affects it is in similar manners as f_c . Since f_c is independent of site and is considered the source property so, f_{\max} is interoperated as caused by source process. Similar results have been presented by Kumar et al. (2013a, b) for local events occurred in Kameng region of Arunachal Lesser Himalaya and Bilaspur region of Himachal Lesser Himalaya. A similar study by Tsai and Chen (2000), they fitted a regression model in terms of distance, earthquake magnitude, and site and showed that the high-cut process is controlled by both the site and source effects. They also inferred that distance is the least significant parameter controlling the high-cut process. Relationships of f_{\max} with seismic moment and stress drop from the local earthquakes occurred in this region has been obtained and compared with other studies. f_{\max} relationships with M_0 and $\Delta\sigma$ are obtained for the study region are:

$$\log(f_{\max}) = -0.0534 \log(M_0) + 2.18 \quad 3.39$$

$$\log(f_{\max}) = -0.0699 \log(\Delta\sigma) + 1.14 \quad 3.40$$

Faccioli (1986) obtained relationship using the data of Italy and Yugoslavia as:

$$\log(f_{\max}) = -0.12 \log(M_0) + 3.864 \quad 3.41$$

Satoh et al. (1997) gives a relationship for Eastern Tohoku District, Japan as:

$$\log(f_{\max}) = -0.018 \log(M_0) + 1.58 \quad 3.42$$

The values of f_{\max} and seismic moment are plotted in Fig. 3.20 to allow comparison with the worldwide values of f_{\max} compiled by Aki (1988). The observed values of f_{\max} agree with worldwide observations. $\Delta\sigma$ relationships with M_0 , is also obtained for the study region as:

$$\log(\Delta\sigma) = 0.1804 \log(M_0) - 2.945 \quad 3.43$$

Satoh et al. (2000) obtained a relationship using deep borehole data of Japan as:

$$\log(\Delta\sigma) = -2.91 \log(M_0) + 5.8 \quad 3.44$$

The results obtained in present study are seems to be more realistic than Satoh et al. (2000). Satoh et al. (2000) relationship suggests stress drop increases as the seismic moment decreases. But in real scenario it is not possible because lower magnitude event can never have stress drop greater than high magnitude event.

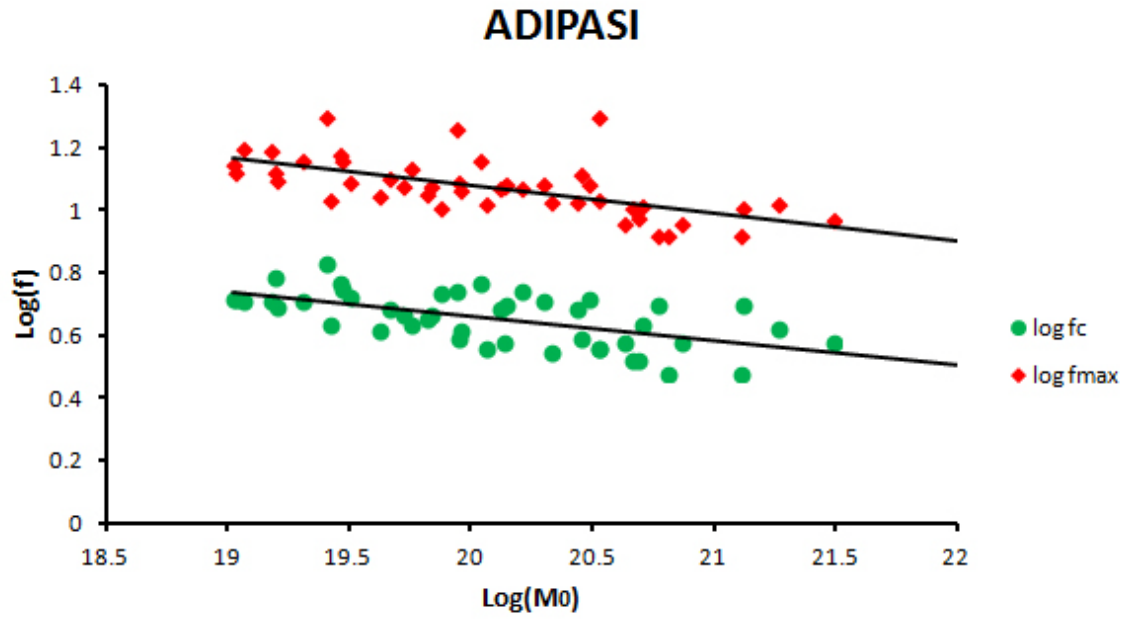


Fig. 3.19a. Plot of f_c and f_{max} with seismic moment at ADIPASI station

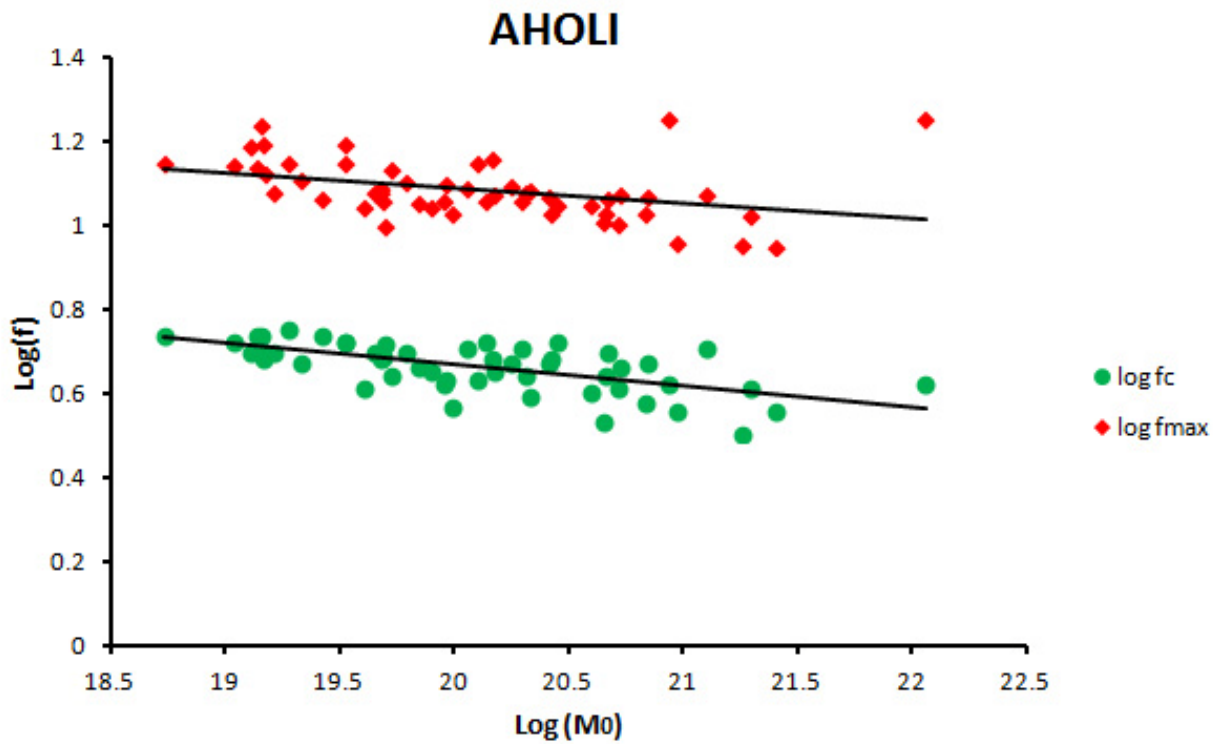


Fig. 3.19b. Plot of f_c and f_{max} with seismic moment at AHOLI station

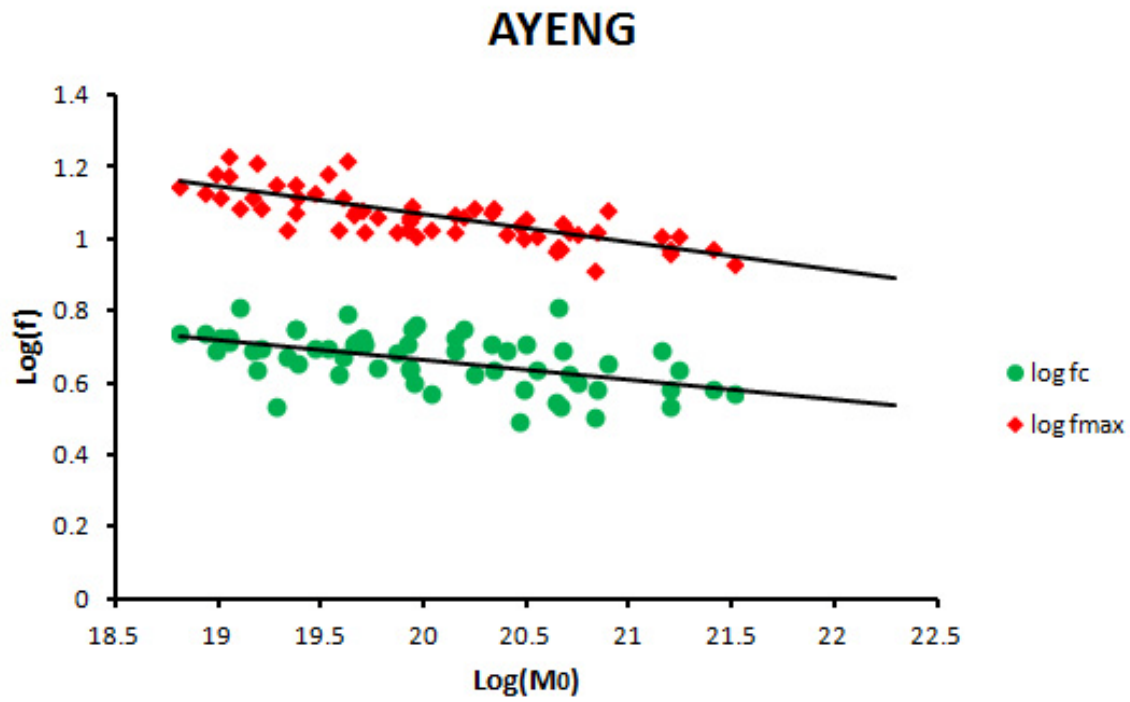


Fig. 3.19c. Plot of f_c and f_{\max} with seismic moment at AYENG station

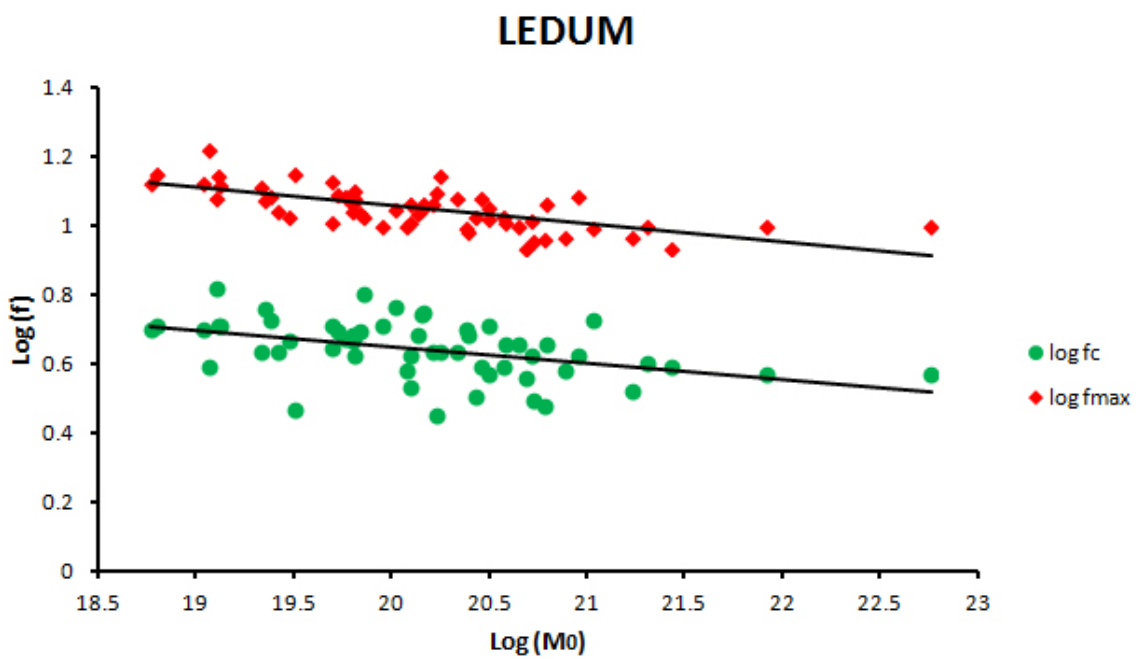


Fig. 3.19 d. Plot of f_c and f_{\max} with seismic moment at LEDUM station

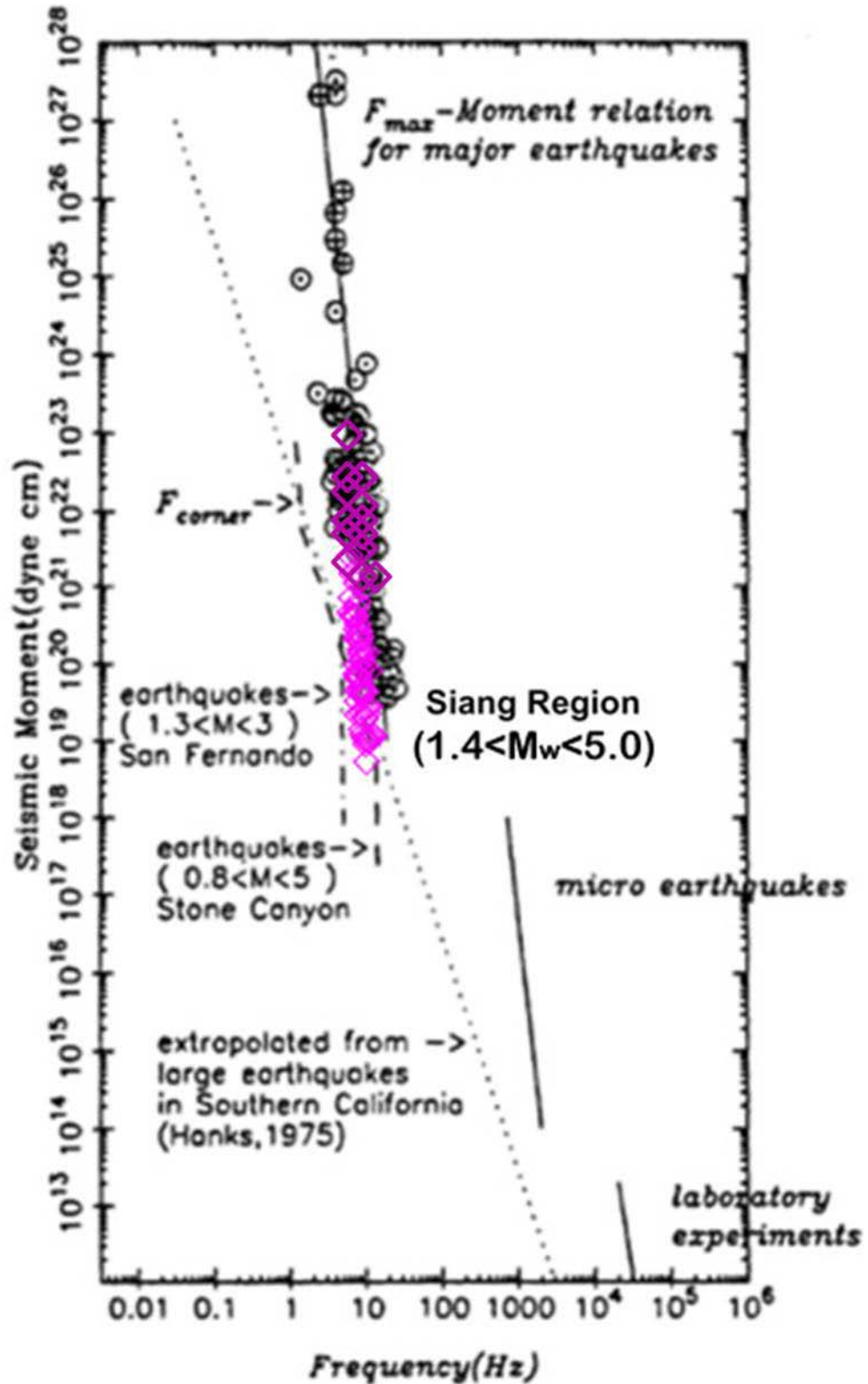


Fig. 3.20. Plot between f_{\max} and seismic moment, M_0 . The values of f_{\max} obtained from Lower Siang region of Arunachal Pradesh (NE India) (open diamonds) are overlain on results of f_{\max} from worldwide values compiled by Aki (1988).

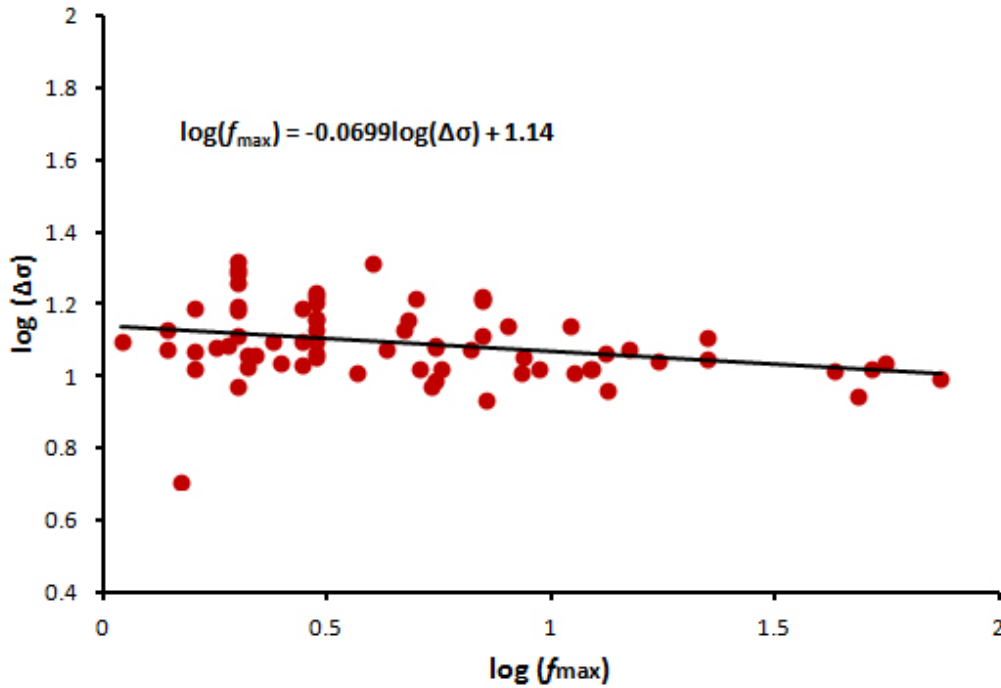


Fig 3.21 Relationship between stress drop and f_{\max}

In this chapter, the results on the source parameters and f_{\max} have been obtained for the Lower Siang region of Arunachal Himalaya from the analysis of 104 local earthquakes. The results showed that the values of seismic moment, Moment magnitude, the source radii and stress drops varies from 1.6×10^{18} to 3.1×10^{23} dyn-cm, 1.4 to 5.0, 157.8 to 417.1 m and 0.1 to 74 bars respectively. Except a few events, the stress drop remains constant and does not vary with focal depth. Based on results on seismic moment and corner frequency, the scaling relation $M_0 \propto f_c^{-3.27}$ has been obtained for the study region. The summary of results on source parameters and f_{\max} are given in chapter 8.

Moment Tensor Solutions

4.1 INTRODUCTION

A great progress in understanding the earthquake source processes has achieved due to developments of various techniques in last decade. One among these techniques is the determination of focal mechanism and identification of fault planes. Both of these parameters are very important in understating the tectonic processes and for the assessment of expected deformation and damage pattern in an area (Delouis and Legrand, 1999). The inversion of first motion polarity is well known for focal mechanism determination. This method provides very good solution for earthquakes occurred inside the network having well coverage of seismic stations. However this method is very much constrained as it requires a good azimuthal coverage of earthquake records. Hence, does not work properly when the stations recording data are unevenly distributed or the source lies outside the network. For most of Himalayan earthquakes those occurs northern side of main central thrust (MCT), seismological networks in that areas are either very sparse or not instrumented at all. And it is almost impossible to estimate the focal mechanism solution for these earthquakes. In such cases the researchers are left only with the alternatives which make possible to obtain the solutions with available recorded waveform data. One among these alternatives is the moment tensor solution.

Initially, only teleseismic data of large magnitudes was used for the estimation of moment tensor solutions. However, in the routine waveform inversion of teleseismic events, the earthquake was considered to be originated from a point source. Hence fault plane was not specified. It gives the seismic moment tensor but decomposition of moment tensor (MT) is not possible (Dziewonski et al., 1981; Sipkin, 1982; Kawakatsu, 1995; Delouis & Legrand, 1999). The only source of determination of focal mechanisms of low magnitude earthquakes is the data recorded at small epicentral distances. So workers with time require a method which can be applied on regional as well as local seismic waveform data.

Kanamori et al (1990) and Singh et al (1997) argued that the source parameters can be estimated using near field local earthquake data and the results remain constrained even by using single station data. During nineties many researchers computed the moment tensor solutions using single station data (Dreger and Helmberger, 1991; Fan and Wallace, 1991; Kim and Kraeva, 1998). Dreger and Helmberger (1991) observed that long period body waves changes slowly with distance. Hence these waves can be modeled by assuming simple layered crustal model. However the modeling of surface waves is complicated as they are very sensitive to crustal velocity gradient. Hence a precise knowledge of crustal velocity model and quality factor (Q) is needed, especially in case of single station data (Walter, 1993; Kim and Kraeva, 1999).

Kikuchi and Kanamori (1991) and Singh et al. (1997) performed waveform inversion with local event data and found that the source parameters can be well constrained by using near-field waves, even with a single station waveform data. The inversion scheme proposed by Singh et al. (2000) based on point source approximation for near field data can be used for small to moderate earthquakes. Legrand and Delouis (1999) explained the locations of point sources and gave a sharp constraint on the orientation of the fault plane when a finite-dimension-source model has been used. Later, it has been found that the single station three component displacement data is enough for waveform inversion to obtain moment tensor solutions provided a good knowledge of 1D crustal velocity structure of study region is available (Fan and Wallace, 1991; Walter, 1993; Dreger and Helmberger, 1993; Kim and Kraeva, 1999).

In the upcoming section we discussed the basic formulation of moment tensor and there decomposition including an inversion scheme of Kikuchi and Kanamori (1991). The most of the part basic theory described below of these sections is reproduced from IASPEI NMSOP volume-1 (Bormann, 2002)

4.2 METHODOLOGY

4.2.1. MOMENT TENSOR SOURCE

For a point source, a fundamental solution of the elastodynamics wave equation is the Green function. Most of seismic sources are caused by fast internal deformation. These internal sources are having Zero net force (f) and moment. These sources should satisfy two conditions:

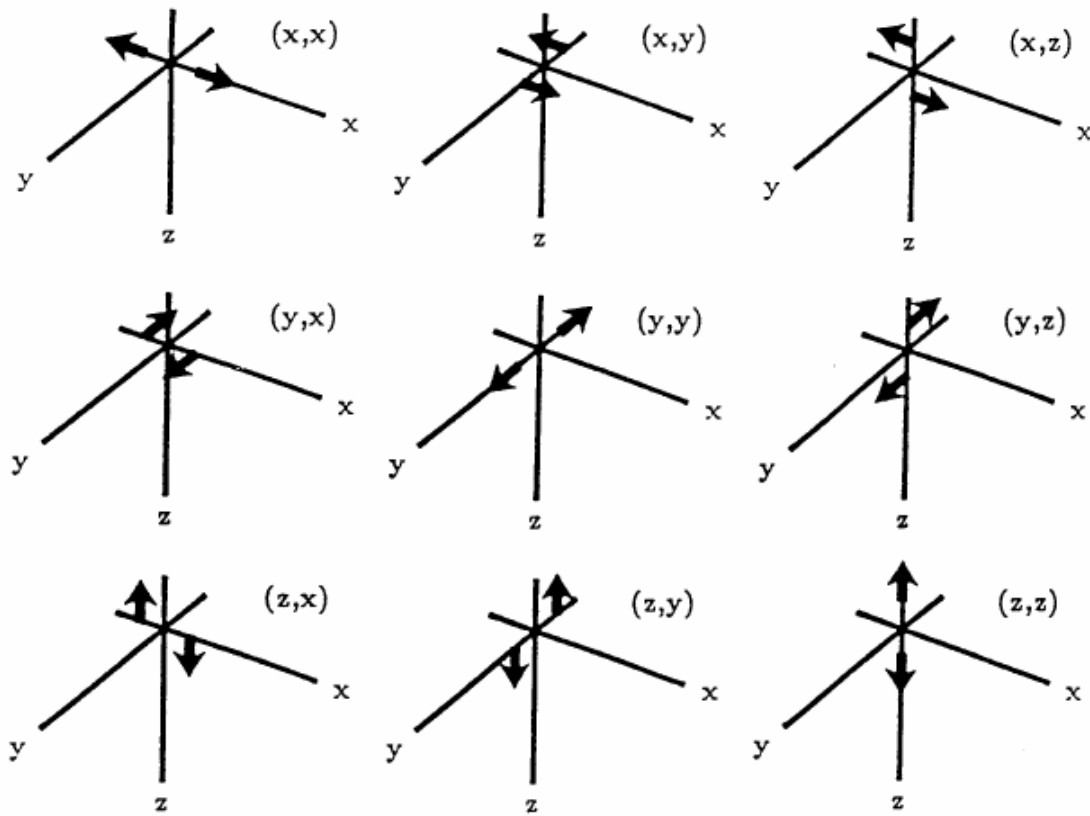
$$\sum f = 0 \tag{4.1}$$

$$\sum f \times r = 0 \quad 4.2$$

where 'r' is the distance between two forces of straight 'f'. Dipole and quadrupoles are the simplest source which satisfies the above equations. The linear dipole is consisting of two point source separated by small distance 'b' which act in opposite direction. The seismic moment of linear dipole is $M=fb$. It has been observed by experiments that such sources are not the good source model. The three orthogonal linear dipoles can be combined to generalize the source. Also the strength any of these three dipoles can be adjusted. It can be shown that the principle directions of these dipoles represent a symmetric tensor of rank 2 known as seismic moment tensor:

$$M = \begin{matrix} M_{xx} & M_{xy} & M_{xz} \\ M_{xy} & M_{yy} & M_{yz} \\ M_{xz} & M_{yz} & M_{zz} \end{matrix} \quad 4.3$$

The structure of moment tensor is identical to stress tensor but the moment tensor is not of elastic origin. If except M_{xy} all the off diagonal elements are zero. Hence a double couple is represented by this tensor whose forces acting in opposite direction. For example, M_{xy} represents the tensor in which two forces acting in x-direction separated by small distance b in y-direction. The second couple of M_{xy} consists of two forces acting oppositely in y-direction separated in x-direction (Fig 4.1). Hence the moment in first case is positive and is negative in second as per sign convention. So the condition of conservation of moment and force are satisfied. Burridge and Knopoff (1964) showed that the natural representation of an earthquake source is the double couple such that the direction of the force is in slip direction and the arm is along the fault thickness.



* **Fig 4.1** A mathematical representation of the movement on a fault during an earthquake, comprising of nine generalized couples, or nine sets of two vectors. The tensor depends of the source strength and fault orientation (After Aki and Richards, 1980).

4.2.2 BASIC FORMULATIONS

Jost and Herrmann (1989) showed that for point source, the displacement at a point on the earth is the time dependent linear combination of moment tensor elements. The convolution of moment tensor (M_{kj}) with the derivative of the Green's function gives the displacement at time 't' and position x as:

$$u(x, t) = M_{kj} * G_{sk,j} \quad 4.4$$

In frequency domain equation 4.4 can be written as:

$$u(x, f) = M_{kj} G_{sk,j} \quad 4.5$$

Or simple in matrix form as :

$$u = G M \quad 4.6$$

The M is having nine components but only six independent elements which follow the equation 4.1 and 4.2. The set five components of M for which the trace elements vanish i.e no volume change is known as the deviatoric moment tensor. If the determinant of deviatoric moment tensor is zero than it is known as the double couple source. Generally, M consist of two part called as isotropic and daviatoric:

$$M = M^{\text{isotropic}} + M^{\text{deviatoric}} \quad 4.7$$

Further, the deviatoric part can also be decomposed into two parts known as double couple (DC) and compensated linear vector dipole (CLVD):

$$M^{\text{deviatoric}} = M^{\text{DC}} + M^{\text{CLVD}} \quad 4.8$$

Using equation 4.8 in equation 4.7 we have

$$M = M^{\text{isotropic}} + M^{\text{DC}} + M^{\text{CLVD}} \quad 4.9$$

Hence moment tensor consists of three components. These three components in form of real source model along-with their equivalent force and beach ball are shown in Fig 4.2

Aki and Richards (1980) showed that in cartesian co-ordinate system for shear fault dislocation, the double couple can be expressed in terms of strike (φ), dip (δ), rake (λ) and scalar seismic moment (M_0).

$$\begin{aligned} M_{xx} &= -M_0(\sin\delta \cos\lambda \sin 2\varphi + \sin 2\delta \sin\lambda \sin^2\varphi) \\ M_{xy} &= M_0(\sin\delta \cos\lambda \cos 2\varphi + 0.5 \sin 2\delta \sin\lambda \sin 2\varphi) \\ M_{xz} &= -M_0(\cos\delta \cos\lambda \cos\varphi + \cos 2\delta \sin\lambda \sin\varphi) \\ M_{yy} &= M_0(\sin\delta \cos\lambda \sin 2\varphi - \sin 2\delta \sin\lambda \cos^2\varphi) \\ M_{yz} &= -M_0(\cos\delta \cos\lambda \sin\varphi - \cos 2\delta \sin\lambda \cos\varphi) \\ M_{xy} &= M_0 \sin 2\delta \sin\lambda \end{aligned} \quad 4.10$$

The diagonal elements of M are the eigenvalues and the principle directions associated with them are the eigenvectors. For example, in case of double couple source M is having two eigenvalues M_0 and $-M_0$ whose principle directions or eigenvectors are tensional (T) and compressional (P) axis respectively. To estimate these parameters we need to solve equation 4.6

The Greens function estimation is the most important part of Moment Tensor Inversion. There are various methods of calculation of synthetic seismogram. But the basic behind

every method is inversion of moment tensor and then the decomposition of it in DC and non-DC parts.


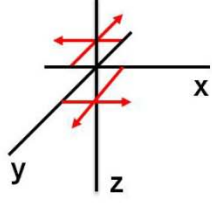
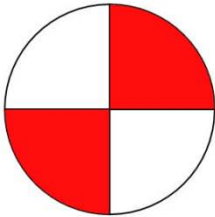

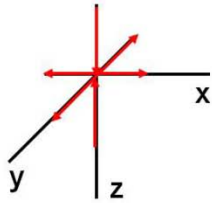
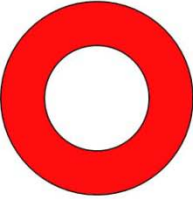

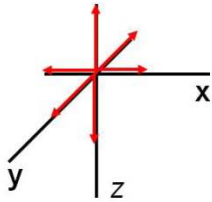
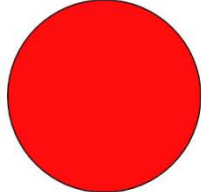
Model	Source	M	Couples	Focal Mechanism
 Strike-slip	Double-couple (DC)	$\begin{vmatrix} 0 & 1 & 0 \\ 1 & 0 & 0 \\ 0 & 0 & 0 \end{vmatrix}$		
 Ring Fault	Compensated linear vector dipole (CLVD)	$\begin{vmatrix} 1/2 & 0 & 0 \\ 0 & 1/2 & 0 \\ 0 & 0 & -1 \end{vmatrix}$		
 Explosion	isotropic	$\begin{vmatrix} 1 & 0 & 0 \\ 0 & 1 & 0 \\ 0 & 0 & 1 \end{vmatrix}$		

Fig 4.2 Representation of isotropic, DC and CLVD components in form of real source model along-with their equivalent force and beach ball (modified after Aki and Richards, 1980).

4.2.3 INVERSION OF MOMENT TENSOR

Kikuchi and Kanamori (1991) give a moment tensor inversion algorithm. In this algorithm, the moment tensor (MT) is decomposed into an explosive and double couple sources. Kikuchi and Kanamori expressed the MT as the combination of six elementary matrices as:

$$\begin{aligned}
 M_1 &= \begin{vmatrix} 0 & 1 & 0 \\ 1 & 0 & 0 \\ 0 & 0 & 0 \end{vmatrix}; & M_2 &= \begin{vmatrix} 0 & 0 & 0 \\ 1 & -1 & 0 \\ 0 & 0 & 0 \end{vmatrix}; & M_3 &= \begin{vmatrix} 0 & 0 & 0 \\ 0 & 0 & 1 \\ 0 & 1 & 0 \end{vmatrix}; \\
 M_4 &= \begin{vmatrix} 0 & 0 & 1 \\ 0 & 0 & 0 \\ 1 & 0 & 0 \end{vmatrix}; & M_5 &= \begin{vmatrix} -1 & 1 & 0 \\ 0 & 0 & 0 \\ 0 & 0 & 1 \end{vmatrix}; & M_6 &= \begin{vmatrix} 1 & 0 & 0 \\ 0 & 1 & 0 \\ 0 & 0 & 6 \end{vmatrix}
 \end{aligned}$$

These matrices basically represent the different fault types. For example pure strike slip fault are represented by M_1 and M_2 , pure dip slip striking N-S and E-W are represented by M_3 and M_4 respectively, a dip slip fault striking 45 degree is represented by M_5 and an explosive source is represented by M_6 (Fig.4.3).

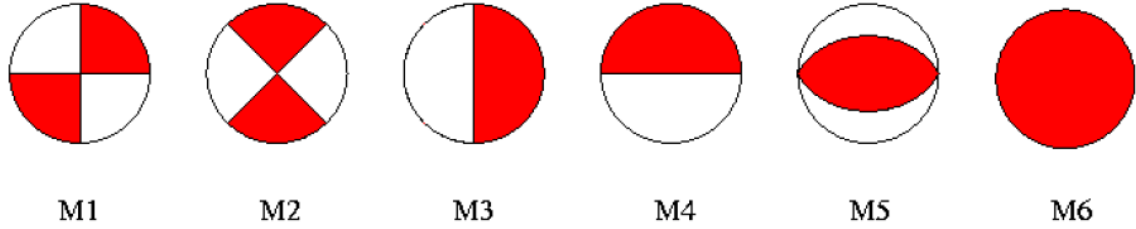


Fig.4.3 Beach balls corresponding to basic elementary matrices given by Kikuchi and Kanamori (1991).

The first five matrices represent the deviatoric source. Kikuchi and Kanamori (1991) performed inversion in time domain which can easily transferred into frequency domain by replacing the time series by its spectra. Let $x(t)$ be the observed ground displacement at station 's'. Let $w_{sn}(t)$ be the derivative of Green's function and M_n be the moment tensor. The moment tensor in terms of elementary matrices can be written as:

$$M_{kj} = \sum_{n=1}^6 a_n M_n \quad 4.11$$

where n is the number of seismogram used in inversion. a_n is coefficient and its value is obtained by minimizing the difference between observed and synthetic seismogram as:

$$\Delta d = \sum_{s=1}^{n_s} \int [x_s(t) - \sum_{n=1}^6 a_n w_{sn}(t)]^2 dt$$

$$\Delta d = R_x - \sum_{n=1}^6 a_n G_n + \sum_{n=1}^6 \sum_{m=1}^6 R_{mn} a_n a_m = \text{minimum} \quad 4.12$$

.The terms R_x and R_{mn} can be represented as:

$$R_x = \sum_{s=1}^{n_s} \int x_s(t)^2 dt \quad 4.13$$

$$R_{mn} = \sum_{s=1}^{n_s} \int [w_{sm}(t)w_{sn}(t)] dt \quad 4.14$$

$$G_n = \sum_{s=1}^{n_s} \int [w_{sn}(t)w_{sn}(t)] dt \quad 4.15$$

Hence,

$$\sum_m^6 R_{mn} a_m = G_n \quad 4.16$$

So the solution for coefficient a_n is given by using above equations as:

$$a_n = \sum_{m=1}^6 R^{-1}_{mn} G_m \quad 4.17$$

Assuming that the data is statistically independent, the variance in the coefficient a_n can be calculated as:

$$\text{variance}(a_n) = \sum_{m=1}^6 (R^{-1}_{mn})^2 \sigma_m^2 \quad 4.18$$

where σ_m^2 represents the variance in the data. There are the cases when variance in the data not known then $\sum_{m=1}^6 (R^{-1}_{mn})^2$ is used to calculate the variance.

4.2.4. DECOMPOSITION OF MOMENT TENSOR

The decomposition of MT is unique only for the deviatoric and volumetric parts. The decomposition involves a step by step process. In first step MT is decomposed into eigenvalues and associated principle direction called eigenvectors. It is basically the rotation of MT in the principle axis system. The directions of P (compressional) and T (tensional) axis are given smallest eigenvalue and largest eigenvector respectively. The direction of null axis is given by other remaining intermediate eigenvectors. The MT rotated in such way is the diagonal matrix as:

$$M = \begin{matrix} m_1 & 0 & 0 \\ 0 & m_2 & 0 \\ 0 & 0 & m_3 \end{matrix} \quad 4.19$$

The sum of the diagonal elements is known as the trace of the matrix and is expressed as Trace (M) = $m_1 + m_2 + m_3$. Now the matrix M is further decomposed into the deviatoric and volumetric components as:

$$M = \begin{matrix} \text{trace}(M) & 0 & 0 \\ 0 & \text{trace}(M) & 0 \\ 0 & 0 & \text{trace}(M) \end{matrix} + \begin{matrix} m_1^1 & 0 & 0 \\ 0 & m_2^1 & 0 \\ 0 & 0 & m_3^1 \end{matrix} \quad 4.20$$

The change in the volume at the source is shown by the isotropic part of M but it very difficult to resolve it. Hence the significance of isotropic part is not considered if it is less than 10%. The most useful part is the deviatoric part which can be further decomposed in various ways such as three double couples, one best double couple and CLVD (used by USGS and Harvard), Three CLVD, a minor and major double couple etc. When the MT is resolved in a best double couple and CLVD, the relative contribution of double couple and CLVD is described by parameter ϵ which is given by:

$$\varepsilon = \frac{m_{min}}{m_{max}} \quad 4.21$$

The m_{min} is the smallest and m_{max} is the maximum absolute values of deviatoric part. $\varepsilon=0$ for the pure double couple (DC) and $\varepsilon=0.5$ for pure CLVD. Generally the contribution of DC and CLVD is expressed in percentage. The double couple percentage contribution is $(1-2\varepsilon)*100$.

4.3 GENERAL STEPS OF MOMENT TENSOR INVERSION

In general, there is a number of factors effecting the quality of moment tensor inversion such as data quality, number of data available and their azimuthal recording. The effect of azimuthal coverage is shown by Dufumier (1996). He also showed the effects of considering only P waves, P and SH waves, together P, SH and SV waves. Sileny (1992, 1996) and Kravanja et al. (1999) showed the effects of wrong velocity model and wrong hypocenter location on the MT estimation. Following are the general steps of moment tensor inversion. Basic steps remains almost same for the inversion performed either in time or frequency domain.

1. Pre-processing of the data
 - a. Input data of good signal to noise ratio
 - b. Instrument response correction
 - c. Converting the records into displacement time series
 - d. For the point source approximation and to remove the high frequency noise, low pass filtering the data.
2. Synthetic Green's function calculation
 - a. Define the each model in terms of velocity structure
 - b. Define the position of source and receiver
3. Inversion
 - a. Selection of P, SH waves or Full seismogram for inversion
 - b. Matching the synthetic and observed seismograms.
 - c. Equation 3.33 and 3.35 evaluation

- d. Decomposition of MT into a best double couple and CLVD parts.

The Various researchers developed the different computer coda to perform the above described steps. ISOLated Asperity batter known as ISOLA is one among them which provide better platform for estimation of MT and most widely used. The computed code ISOLA is used for the estimation of moment tensor in the present study. The brief description of ISOLA code is given below.

4.4 ISOLA

The Kikuchi and Kanamori (1991) algorithm described in above section is the basis of iterative deconvolution for teleseismic data. Zahradnik et al. (2005) modified this method for regional events. The modification basically is the involvement of the full Green's functions which is calculated by discrete wavenumber method of Bouchon (1981). This modified version of iterative deconvolution and multiple point-source representation is the basis of the code ISOLA which is developed by Sokos and Zahradník (2008). These multiple point-source may represent the isolated asperity hence the name of the code is ISOLA. It is written in MATLAB with an inversion engine written in FORTRAN. This tool is closer to the robust methods which represents the source effect with minimum number of parameters such as in the patch method of Vallee and Bouchon (2004) whose advantage is good stability.

The MTs are computed by minimizing the difference between the observed and synthetic displacement in the least square sense. ISOLA computes the MT at a set of predefined trial source positions and trial origin times. The grid search (Adamova et al., 2009) provides the best time and centroid position in terms of the absolute value of the correlation coefficient between the data and synthetics. The match between the observed and best-fitting synthetic data is characterized by the overall variance reduction (VR): $VR = 1 - E/O$, where $E = \sum (O_i - S_i)^2$, $O = \sum (O_i)^2$, with O and S are the abbreviation used for the observed and synthetic data respectively, along with summation over all samples, components and stations. These characterises the match between the observed and best-fitting synthetic data (Zahradnik and Sokos, 2008). The VR is the parameters which qualify the overall match between observed and synthetic seismogram. The ISOLA code also allows complex rupture histories described by multiple point-source sub events, each one represented by a delta function (Zahradnik et al., 2005).

The recorded seismograms are the velocity records. The ISOLA code uses the displacement data for MT so the seismograms recorded as velocity data or acceleration data are first converted into the displacement. The events recorded at a small distances are also separately analyzed. The events which are recorded at small distances are less affected by the medium complexities. A low cut filter with corner frequency 0.2 Hz is applied to remove offset and microseisms. Then the instrument correction is done by correlating the record with transfer function of the seismometer. The corrected data is resembled with sampling frequency 25 Hz. In order to extract the low frequency content S-wave and surface waves, the record is further band passed with corner frequencies 0.5 Hz and 1.5 Hz. The deviatoric MT can be decomposed into DC and CLVD (non-DC) components. The relative size of each of them is $(1-2f)$ and $(2f)$ respectively. Here 1, $-f$ and $f-1$ are the normalized eigenvalues. The DC% is calculated by $100 * (1-2f)$. For subevents the MT is repeated and first subevent is searched. The synthetic seismograms of first subevent are subtracted from observed events. The residual seismograms are processed as the original one (Adamova et al., 2008). In this way DC and CLVD are computed for the using the local earthquake data. Some of the analysis procedure is describe in the following section.

4.5 ANALYSIS PROCEDURE

Before proceeding for the use ISOLA software, we need to make different files. First is the station location file which needs to be placed installation folder. Another file contains the velocity structure of the region. This crustal is to be used for the estimation of green's function. The velocity model given by Khattri et al. (1983) (Table 2.3) has been used. Some softwares are also required to run the ISOLA. There softwares are Matlab, Generic Mapping Tools (Wessel and Smith, 1991), GsView, Ghosscript and imagemagick. The information of hypocenters parameters i.e latitude, longitude, depth and origin time of the event must be available. The hypocenter parameters of 104 events considered for analysis are given in appendix-I Table I.1. The depth representing the true source depth is known as optimal depth. This depth is determined by keeping horizontal source position i.e. epicenter location fixed and performing the repeated waveform inversion for a set of trial depth. The Green's function is estimated at each depth. The correlation between the observed and synthetic seismogram is the function of depth. This process is known as the grid search. Because the grid search is performed in a vertical plane it is called vertical grid search. Vertical grid search gives single depth at which

correlation as well as DC% is high (Fig 4.4). In this way each optimal depth for each event is determined.

Now keeping this optimal depth fixed, the optimal epicenter location is determined for each event. For this purpose 49 point stencils are defined in a horizontal plane. The total horizontal plane dimension is 14 km NS and 14 Km EW with each grid size 2 km x 2 km. The waveform inversion performed for the horizontally defined source. The best epicentral position is corresponding to the maximum correlation value in the horizontal plane (Fig 4.5). Now we have best centroid position at which the final inversion is performed to have source parameters. So the final the comparison between observed and synthetic waveforms is shown in fig.4.6.

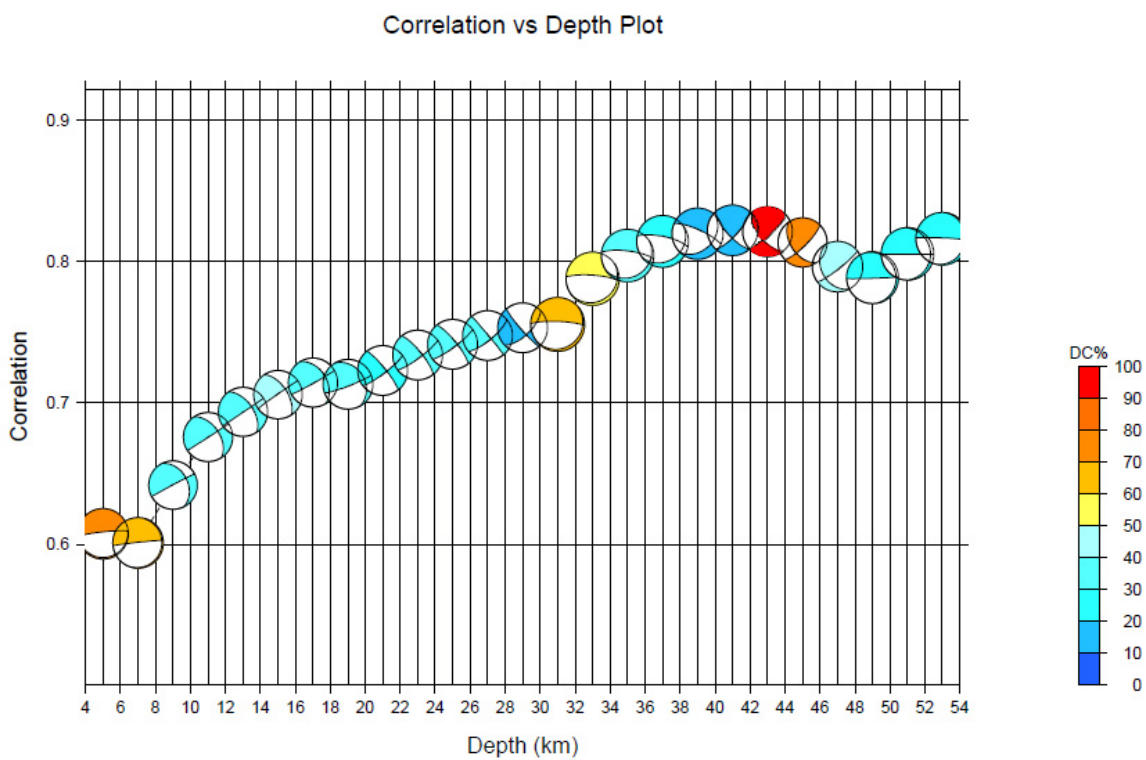


Fig. 4.4 The correlation between observed and synthetic waveforms as a function of the trial source depth. Colors represent the DC%. (a) 18/08/2011.

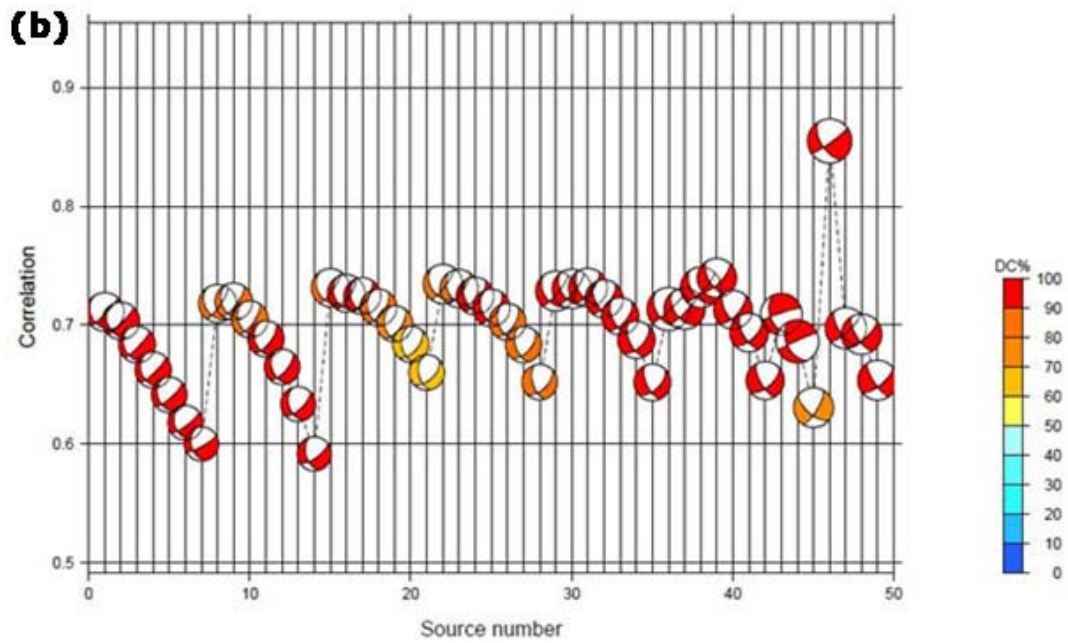
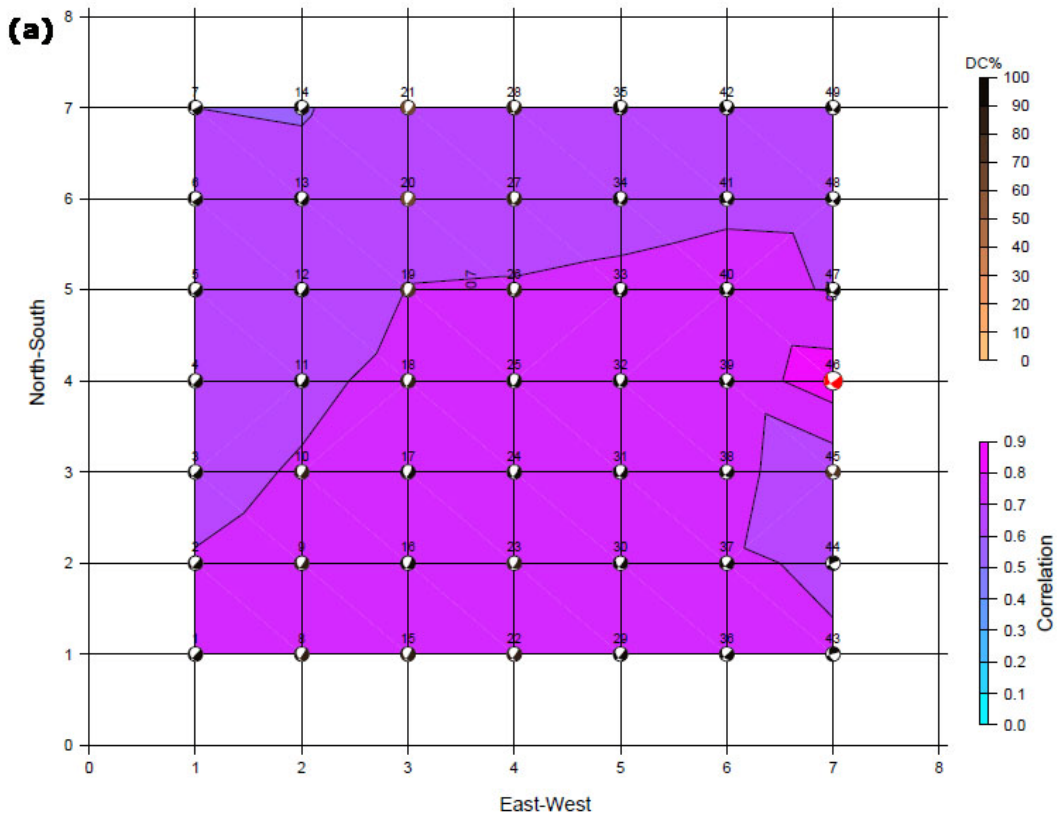
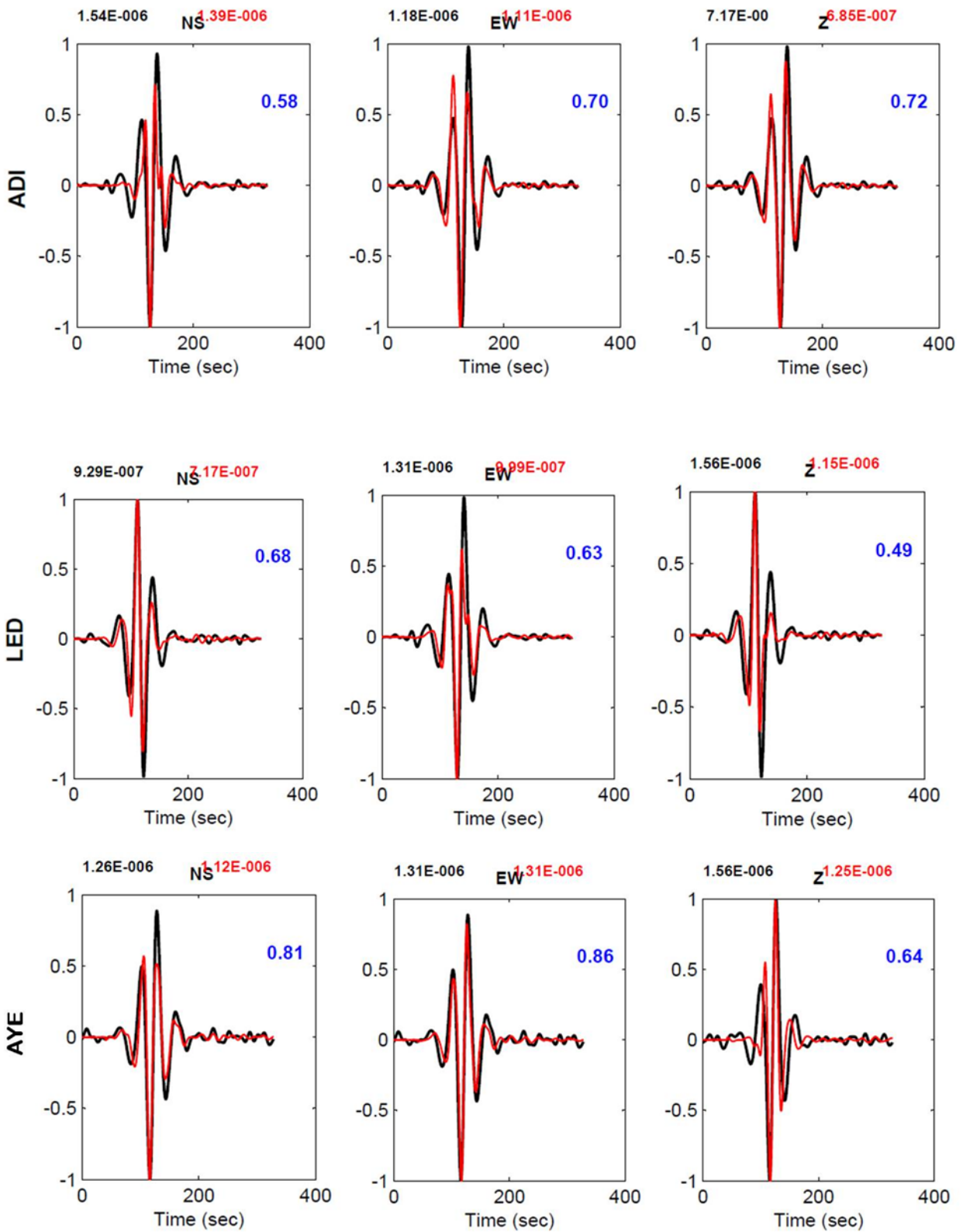


Fig. 4.5 The correlation between observed and synthetic waveforms of 18/08/2011 at various trials on 2 km x 2 km grid along NS and EW directions. The colours of beach balls represent the DC%. (a) Represent the planer view of the grid. (b) Represent the side view standing EW and looking towards NS.



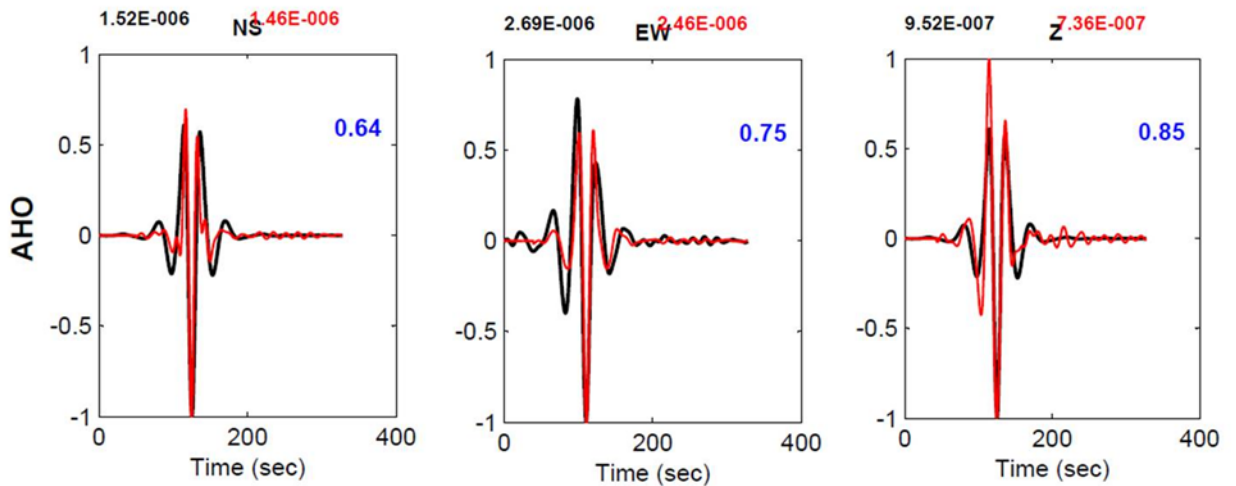


Fig. 4.6 Plot showing comparisons between observed (black) and synthetic waveforms (red) for four stations which are used in inversion. Variance reduction is shown in blue letters.

4.6 DISCUSSION OF RESULTS

The source parameters viz strike; dip and slip of the fault planes of 104 earthquakes along with the azimuth and plunge of both P and T axis are estimated using ISOLA software and shown in Table IV.1 of appendix-IV. These earthquakes are observed at local distances in the Lower Siang region. To avoid the spurious content a criteria is applied. According to these criteria only those events having magnitude greater than 2.5, signal to noise ratio (SNR) is greater than 6 and epicentral distance confined within 50 km of the network, are analyzed separately. There is only 41 such events which fulfil this criteria. The signal to noise ratio (SNR) for all 104 earthquakes is computed using a Matlab program. The parts of seismogram before the arrival of P-wave (noise) and after the P-wave arrival (signal) have been transformed to frequency domain. The ratio of their root mean square (rms) amplitude (SNR) has been estimated for considered frequency band. As the deviatoric moment tensor inversion is performed so moment tensor composed into two components knows as double couple (DC) and compensated linear vector dipole (CLVD). The CLVD is also knows as non double couple component of moment tensor and its origin is attributed to different factors. According to Vavrycuk et al. (2008) this component is due to errors in the data such as moment tent inversion is not accurate, wrong hypocenter location. Sipkin (1986) and Frohlich (1994) attributed the origin of CLVD to the different orientation of subfaults on the fault plane. Shimizu et al.(1988), Julian et al. (1998) Miller et al.(1998) and Vavrycuk (2001, 2007, 2011, 2012,

2014) said that the CLVD component is originate due to tensile stress regime. Vavrycuk (2003) showed that deep focus earthquakes have low non-DC as compared with the shallow depth events. Síleny and Vavrycuk (2000, 2002) showed that CLVD component is due to seismic anisotropy. They also said that that CLVD may be due to the lack of good azimuthal data Kravanja et al (1999) and Síleny (2009) attributed this component to the noise present in the data. Kuge and Lay argued that high magnitude events have low non-DC component as compared with low magnitude events. Since there is such a wide explanation of origination of CLVD, so in present study we try inspect the effect of some factors such as noise in the data, depth the event and magnitude of the event. The plots between CLVD and source depth are shown in Fig. 4.7a and 4.7b. Fig. 4.7a contains full data set of 104 earthquakes whereas Fig. 4.7b contains the 41 events which follow the above described criteria. It is very difficult to interpret fig. 4.7a which is highly affected by noise present in low magnitude data and structural complexity. Fig 4.7b shows large CLVD% for shallow event as compared to competitively deep events. Hence CLVD% is highly affected by the depth of the source. Here we can interpret that the depth effect in fig 4.7a may be masked by the noise and structural complexity. The plots between SNR and CLVD% are shown in Figs. 4.8a,b. From Fig. 4.8a containing all 104 events, it can be noted that randomness in the CLVD% is high when the SNR is less than 25. However, the randomness reduces when 41 good events are used (Fig. 4.8b). Also, the CLVD component is quite low for SNR greater than 25 in both cases. It means that noise plays an important role in the origination of non-DC component.

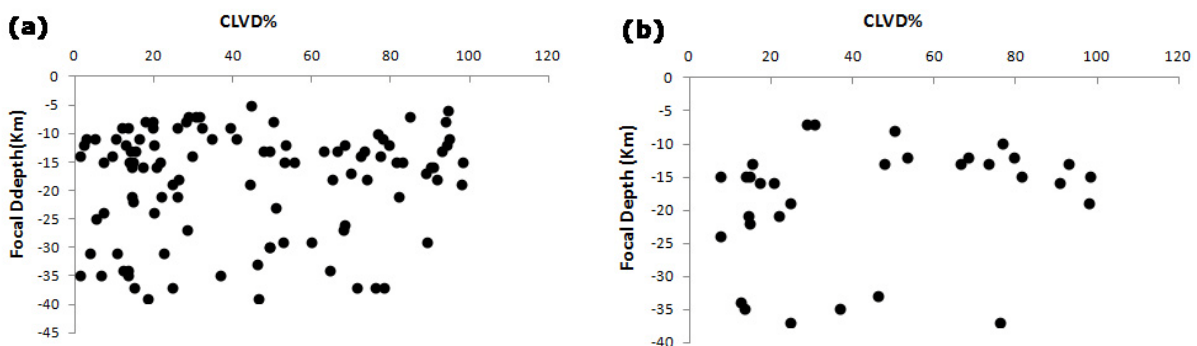


Fig. 4.7.The plot between CLVD and source depth. (a) All 104 events, (b) selected 41 good events

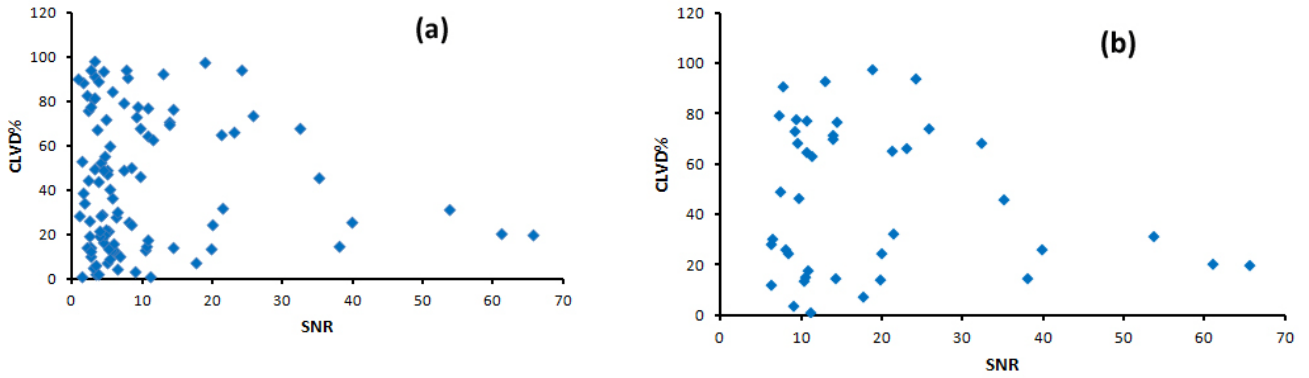


Fig. 4.8.Plot between SNR and CLVD%.(a) All 104 events, (b) selected 41 good events

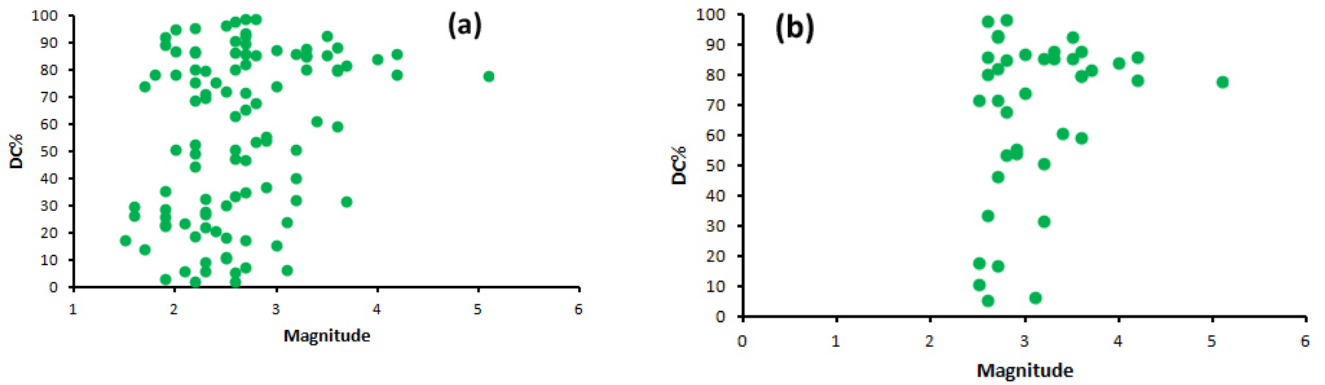


Fig. 4.9.The variation of DC% with magnitude.(a) All 104 events, (b) selected 41 good events

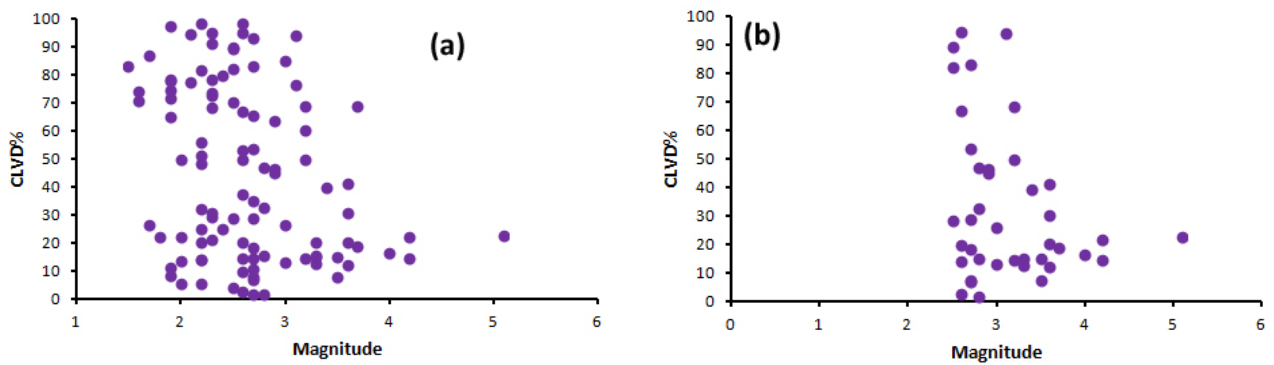


Fig. 4.10.The variation CLVD% with magnitude.(a) All 104 events, (b) selected 41 good events

The magnitude range of the earthquakes used is between 1.5 (M_w) to 5.1 (M_w) and 2.5 (M_w) to 5.1 (M_w) for 104 and 41 earthquakes respectively. The variation of DC% and CLVD% with magnitude has been studied (Fig. 4.9a,b and Fig 4.10a,b). Fig. 4.9a and 4.10a contains the all 104 events whereas Fig. 4.9b and 4.10b contains only those events sorted by applying the SNR, epicenter distance and magnitude criteria. From 4.9a and 4.10a it can be observed that in the magnitude range below 3.5 both CLVD and DC

components can be observed and their distribution is highly random. In magnitude range greater than 3.5, the DC component is prominent shown in Fig 4.9a and CLVD component is very low shown in Fig 4.9a. Fig. 4.9b and 4.10b shows the effect of magnitude on DC and CLVD with more clarity. Below magnitude 3.5 a cluster of events showing a high DC as shown in Fig. 4.9b and relatively low CLVD as shown in Fig. 4.10b. the events having magnitude greater than 3.5 shows high DC (Fig. 4.9b) and low CLVD (Fig. 4.10b). Thus magnitude of events also affects the CLVD.

For the events recorded at larger epicentral distances total network act as single station. Hence the more CLVD at higher may also be attributed to azimuthal coverage. The CLVD component may also be of physical origin but there should be positive correlation between the isotropic (ISO) and non-DC (CLVD) components (Vavrycuk, 2001; Fojtíkova et al., 2010). In the present work, the deviatoric MT has been done as ISO component is not available. Further good data available for such correlation is very less. Hence, the present study attributes the CLVD to the numerical errors of the inversion and depth of the event. These numerical errors are due to structural complexity, noise of the data and azimuthal coverage of the data. However, the possibility of this error for 41 events in Fig. 4.9 and Fig. 4.10 is quite low. So this study also agrees with the double couple theory of source mechanism for high magnitude events. So large magnitude events are of

In this chapter efforts have been made to manifest the source of non-DC (CLVD) component of MTs. from the moment tensor analysis of 104 local earthquakes. The moment tensor analysis of 41 earthquakes out of 104 earthquakes having magnitude greater than 2.5 and signal to noise ratio (SNR) greater than 6 with small epicentral distances brought out more clarity in the identification of cause of CLVD. The summery results on moment tensor obtained in the present study are given in chapter 8.

Seismic Wave Attenuation Characteristics using Body waves

5.1 INTRODUCTION

The basic physical mechanisms which are responsible for the loss of energy of propagating seismic waves are intrinsic absorption from inelasticity of rocks and scattering under distributed heterogeneities. The seismic energy is converted into heat by intrinsic absorption and redistributed due to the internal friction of medium's particle and heterogeneity of the medium through which the seismic wave passes. The higher frequency component of seismic waves attenuates more rapidly than the low frequency components resulting in resolution loss in seismograms. Therefore, the attenuation of seismic waves in the lithosphere is an important property for studying the regional earth structure in relation to seismicity (Mandal et al, 2004). On the earthquake ground motion the effect of travel path is mainly due to the wave attenuation of propagation wave.

The seismic wave attenuation characteristics of a region can be studied using different parts of the seismogram e.g. P-wave, S-wave, Surface waves and Coda waves (Aki, 1969; Aki and Chouet, 1975; Hermann, 1980; Mitchell, 1995). The P-wave and S-wave part of Seismogram provides the seismic wave attenuation of direct path from source to receiver of local earthquakes whereas the seismic wave attenuation using the information of the surface waves provide the regional structure of the medium, whereas the attenuation of Coda waves provides the average attenuation picture of the local region. The efficiency of seismic energy propagation through a medium is commonly expressed by the inverse of dimensionless quantity called quality factor Q (Knopoff, 1964).

$$Q^{-1} = -\Delta E / 2\pi E \quad (5.1)$$

Where ΔE is the energy loss per cycle and E is the total energy available in a harmonic wave.

Aki (1980) proposed the coda normalization method to estimate the frequency-dependent relation for Q_β . Yoshimoto et al. (1993) extended this method for simultaneous measurement of Q_α and Q_β which is successfully applied in the various regions of India as

well as world. For example, for Indian regions, Koyna (Sharma et al.2007); Bhuj (Padhy, 2009); Chamoli region of Garhwal Himalaya (Sharma et al., 2009). Similarly, for World region some studies are Kanto, Japan (Yoshimoto et al. 1993); Western Nagano, Japan (Yoshimoto et al. 1998); South-Eastern Korea (Chung and Sato, 2001); central South Korea (Kim et al., 2004); East-Central Iran (Mahood et al., 2009) and Cairo metropolitan area (Abdel-Fattah, 2009) and many more.

In the present study seismic wave attenuation characteristics have been determined using P-wave (Q_α) S-wave (Q_β) and Coda waves (Q_c), part of seismogram. This chapter discusses the estimation of frequency dependent quality factor of P-wave (Q_α) and S-wave (Q_β). Both Q_α and Q_β are estimated using the extended coda normalization method given by Yoshimoto et al. (1993). Also frequency dependent Q_α and Q_β relations have been developed for the study region. P and S waveforms of 104 local earthquakes recorded by the seismological network as discussed in chapter 2.0 have been used for the analysis. The investigation of Q_α/Q_β ratio and its probable significance has also been discussed. The results obtained Q_α and Q_β are compared with that obtained for other regions of the India and World.

5.2 BASIC MATHEMATICAL FORMULATION FOR WAVE ATTENUATION

The mathematical form of the energy recorded in the form of amplitudes at a distance, x , is represented as follow:

$$A(x) = A(0) * \frac{1}{x} * \exp^{-ax} \quad (5.2)$$

Where, $A(0)$ denotes amplitude of seismic wave at $x=0$, $E(x)$ amplitude of seismic wave at x , and $\frac{1}{x}$ represents geometrical spreading factor. 'a' is absorption coefficient or attenuation coefficient and given by:

$$a = \frac{\pi f x}{v Q} \quad (5.3)$$

Here 'f' represents frequency and 'v' is the velocity of propagation. Q is the quality factor. So amplitude of seismic wave can be expressed as:

$$A(x) = A(0) * \frac{1}{x} * \exp\left(\frac{-\pi f x}{v Q}\right) \quad (5.4)$$

The above equation represents the elastic energy recorded in the form of amplitude of seismic waves at a distance x in real media. The term $\exp\left(\frac{-\pi fx}{vQ}\right)$ is a measure of seismic wave attenuation. The non dimensional parameter Q , known as quality factor represents the physical properties of the medium such as internal friction due to anelasticity and heterogeneities of the medium. The reciprocal of quality factor $\left(\frac{1}{Q}\right)$ is a measure of attenuation in the medium. Attenuation of seismic waves is measured by the non dimensional parameter, Q , called the quality factor which is directly related to the decay of seismic energy when it spread through medium. Q is the representation of physical properties of the material present in the medium and its state. Therefore, the seismic wave attenuation can be determined by estimating the quality factor (Q).

5.3 METHOD FOR ESTIMATION OF Q_α AND Q_β

Aki (1980) proposed the coda normalization method based on the empirical observation for the frequency dependent relationship of Q_β . This method was extended Yoshimoto et al. (1993) for simultaneous measurement of Q_α and Q_β . For the local earthquakes recorded at distances less than 100 km, the spectral amplitude of the coda at lapse times greater than twice the S wave travel time is proportional to the source spectral amplitude of the S waves (Yoshimoto et al., 1993; Kim et al., 2004). Therefore, the normalization of S wave spectra to coda is able to remove the effects of source, site and instrument observation. The Q is estimated under the assumption that P- to S-wave radiation have same spectral ratio within some magnitude range within narrow frequency range (Yoshimoto et al., 1993). Here we briefly describe the method which is reproduced here after Aki (1980) and Yoshimoto et al. (1993). The basic assumption of the coda normalisation method is that the coda waves are consists of scattered S-waves (Aki, 1969, Aki and Chouet, 1975, Sato 1977). In this method the amplitude of the earthquake source is normalised by the coda amplitude at a fixed lapse time. It enables the estimation of Q_α and Q_β or Q_T using single station data. For lapse time (t_c) greater than the travel time of direct S-waves (t_s), spectral amplitude of coda $A_c(f, t_c)$ is independent of hypocentral distance 'r'. hence the spectral amplitude of direct S-wave can be written as (Aki, 1980) :

$$A_c(f, t_c) = S(f)P(f, t_c)G(f)I(f) \quad (5.5)$$

where $S(f)$, f , $P(f, t_c)$, $G(f)$ and $I(f)$ represents the frequency, source spectral amplitude, the coda excitation factor, site amplification factor and instrument response respectively. The coda excitation factor shows the decay of coda amplitude with lapse time. The spectral amplitude of direct S-wave $A_s(f, r)$, can be expressed as:

$$A_s(f, r) = R_{\theta\psi} S(f) r^{-\gamma} \exp\left(-\frac{\pi f r}{Q_\beta(f) V_s}\right) G(f, \psi) I(f) \quad (5.6)$$

where $R_{\theta\psi}$ is the ratio pattern, γ is the geometrical spreading exponent and is taken as unity for body waves, V_s is the average S-wave velocity, $Q_\beta(f)$ is the S wave quality factor and Ψ is the S-wave incidence angle. Dividing equation (5.6) by equation (5.5) we get:

$$\left(R_{\theta\psi}^{-1} \frac{A_s(f, r)}{A_c(f, t_c)}\right) r = \left(\frac{G(f, \psi)}{G(f)}\right) P^{-1}(f, t_c) \exp\left(-\frac{\pi f r}{Q_\beta(f) V_s}\right) \quad (5.7)$$

Taking logarithm we get:

$$\ln\left[\left(R_{\theta\psi}^{-1} \frac{A_s(f, r)}{A_c(f, t_c)}\right) r\right] = \ln\left(\frac{G(f, \psi)}{G(f)}\right) + \left\{-\frac{\pi f r}{Q_\beta(f) V_s}\right\} + \text{const}(f) \quad (5.8)$$

The term $P^{-1}(f, t_c)$ as described earlier is independent of hypocentral so for a fixed lapse time window it became constant ($\text{const}(f)$).

For favourable condition when the azimuthal distribution of the earthquakes is very wide then:

- Averaging the $R_{\theta\psi}$ over many focal planes, its effect will be zero.
- Averaging $G(f, \psi)/G(f)$ over many events, it becomes independent of ψ .

Hence the equation (5.8) get simplified as:

$$\ln\left\{\frac{A_s(f, r)r}{A_c(f, t_c)}\right\}_{r \pm \Delta r} = \frac{-\pi f r}{Q_\beta(f) V_s} + \text{const}(f) \quad (5.9)$$

The above equation is linear equation between $\ln\{A_s(f, r)r/A_c(f, t_c)\}_{r \pm \Delta r}$ and 'r'. The slope of this linear equation i.e slope $-\pi f / Q_\beta(f) V_s$ provide the quality factor of S-wave (Q_β).

The above equation was proposed by Aki (1980) to measure $Q_\beta(f)$. It represents a straight line with slope $-\pi f / Q_\beta(f)$ Vs. Hence using linear regression of $\ln\{A_s(f, r) r / A_c(f, t_c)\}_{r \pm \Delta r}$ versus r , $Q_\beta(f)$ can be estimated.

Yoshimoto et al.(1993) extended this coda normalization method. They assumed that within a small magnitude range, the ratio of spectral amplitude of P and S wave remains constant for a narrow frequency range $f \pm \Delta f$ i.e

$$\left\{ \frac{S_P(f)}{S_S(f)} \right\}_{f \pm \Delta f} = \text{const}(f) \quad (5.10)$$

Rautian et al.(1978) shows that above relation remains true even if the spectral shapes of P and S wave are different. So it can be written that:

$$A_c(f, t_c) \propto S_s(f) \propto S_P(f) \quad (5.11)$$

where $S_P(f)$ is the source spectral amplitude of P waves, $S_S(f)$ is the source spectral amplitude of S waves, f is the frequency in Hz and t_c is the reference lapse time measured from the earthquake origin time. Therefore using the equation 5.9 and 5.11, we can give

$$\ln \frac{A_P(f, r) r}{A_c(f, t_c)} = -\frac{\pi f}{Q_\alpha V_P} r + \text{const}(f) \quad (5.12)$$

Where $A_P(f, r)$ and $A_S(f, r)$ represents the amplitude spectra of the direct P and S waves at the hypocentral distance r (km) respectively. V_P is the P-wave velocity and V_S is the S-wave velocity. Q_α and Q_β can be estimated by fitting linear regression line after applying the least square method to the left hand side plot of equation (5.9) and (5.12) with respect to the hypocentral distances. The vertical (Z) components of seismograms and horizontal components (N-S) are analyzed for the estimation of Q_α and Q_β respectively. The fig.5.1 represents the seismogram recorded at. The spectral amplitude of the direct P and S waves are measured using 2.56 sec time window. The spectral amplitude of the Coda waves $A_c(f, t_c)$ is calculated using a lapse time window of 2.56 sec and the lapse time for the analyzed portion of the coda wave is taken as twice the travel time of S-wave (Aki and Chouet, 1975; Rautian and Khalturin, 1978). The geometrical spreading is r^{-1} and $\frac{1}{\sqrt{r} h_{moh}}$ for the epicentral distance of $r \leq h_{moh}$ and $r \geq h_{moh}$, respectively where h_{moh} is twice the Moh depth ((Herrmann and Kijko, 1983; Mahood et al., 2009). In the study region the Moh depth is 46 km (Khattri 1983) so h_{moh} approximately can be taken as 90 km. The hypocenters of the earthquakes considered for the analysis are less than 90 km. Therefore, r^{-1} can be considered as geometrical spreading.

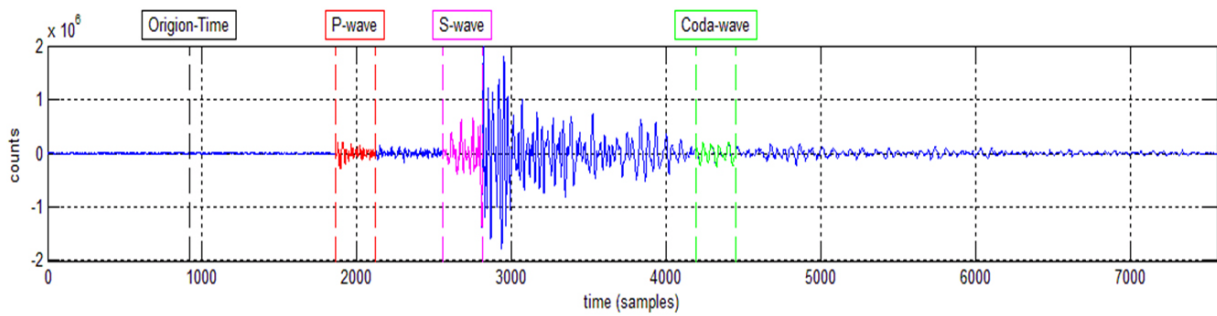


Fig 5.1 Example of a horizontal component (N–S) seismogram recorded at station LED with. The arrival time of P, S and Coda waves are marked. A time window of 2.56 sec is taken for all three waves.

5.4. ANALYSIS PROCEDURE

The basic analysis procedure of estimation of P and S-wave attenuation using extended coda normalization method is given below:

1. Consider a raw data in the form of time series for the local earthquakes.
2. Apply baseline correction before analysis.
3. Select the P –wave, S wave and coda wave part on time series.
4. Take the fast Fourier transform of the each selected portion and find the root mean square amplitude.
5. Plot the coda normalized P and S-wave spectral amplitude as a function of hypocentral distance. The slop of this linear gives the value of quality factor for P-wave (Q_α) and S wave (Q_β) using equation 5.9 and 5.12 at single frequency.
6. Average all the Q values of different station at different frequency. And fit a power law in the form $Q = Q_0 f^n$ for both P and S-waves.

The flowchart is used for developing a MATLAB code for the estimation of P and S-wave attenuation in shown below:

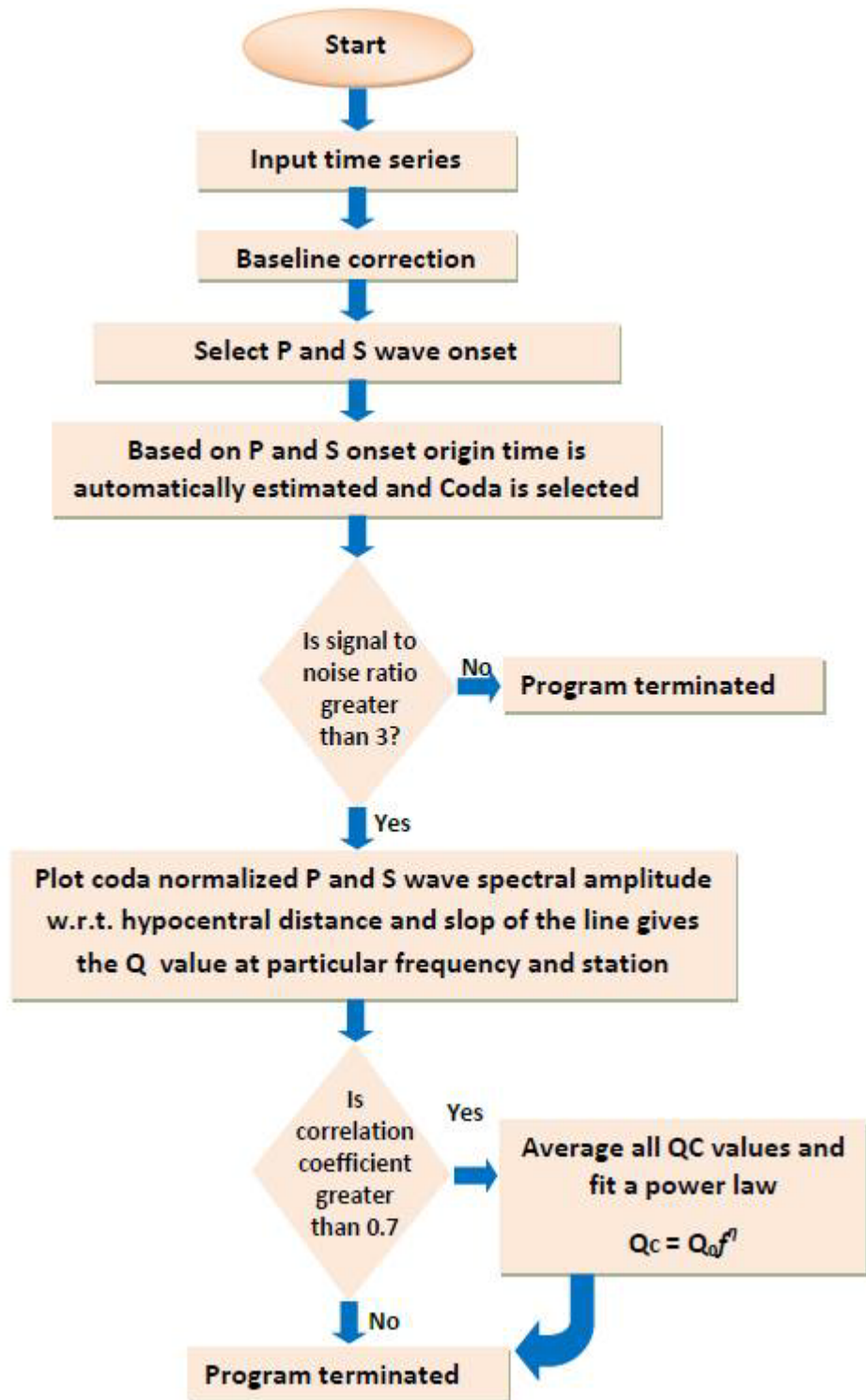


Fig 5.2 Flow chart of MATLAB code used for the estimation of P and S wave analysis.

5.5 RESULT AND DISCUSSION

Fig 5.3 and Fig 5.4 shows the Coda normalized peak amplitude decay of P and S waves with hypocentral distance for seven central frequencies at LED station and a straight line is fitted using least square technique respectively. In this way Q_α and Q_β have been determined at seven central frequencies for the Lower Siang region of Arunachal Himalaya. The variation in the quality factor at all the five stations is listed in Table 5.1 and plotted as function of frequency fig. 5.5 a and b. Both from Fig 5.5a, b it is observed that Q_α and Q_β is increases with the frequency. The average variation in Q_α value is from 49 ± 4 at 1.5 Hz to 1421 ± 6 at 24 Hz while the average value of Q_β varies from 118 ± 6 at 1.5 Hz to 2335 ± 5 at 24Hz (Table 5.2). A power law, $Q=Q_0f^\eta$ (where Q_0 is the Q value at 1 Hz and η is the frequency exponent) is obtained for each station. There frequency dependence Q_α and Q_β relations are given in Table 5.3. The average Q_α and Q_β relation $Q_\alpha = (25\pm 1)f^{(1.24\pm 0.04)}$ for P-wave and is $Q_\beta = (58\pm 1)f^{(1.16\pm 0.04)}$ are obtained for the Lower Siang region of Arunachal Himalaya. The frequency dependence Q_α and Q_β relations are found to be comparable with the other seismically active regions of India as well as world. There comparisons among the Indian and world regions are shown Fig. 5.6 and Fig. 5.7. The comparison showed that the relations of Lower Siang region are lower as compared with the other considered regions except the Chamoli region of the Garhwal Himalaya.

Q_β relations, among all Indian regions considered for the comparison, match almost similar with the kachchh region of Gujarat where a moderate earthquake occurred in January 2001 and showed aftershock activity for a longer period. Whereas Q_β is also close to the other NE region that is considered seismically active. In the comparison of World it is observed that the Q_β value in the Siang region in between of all regions.

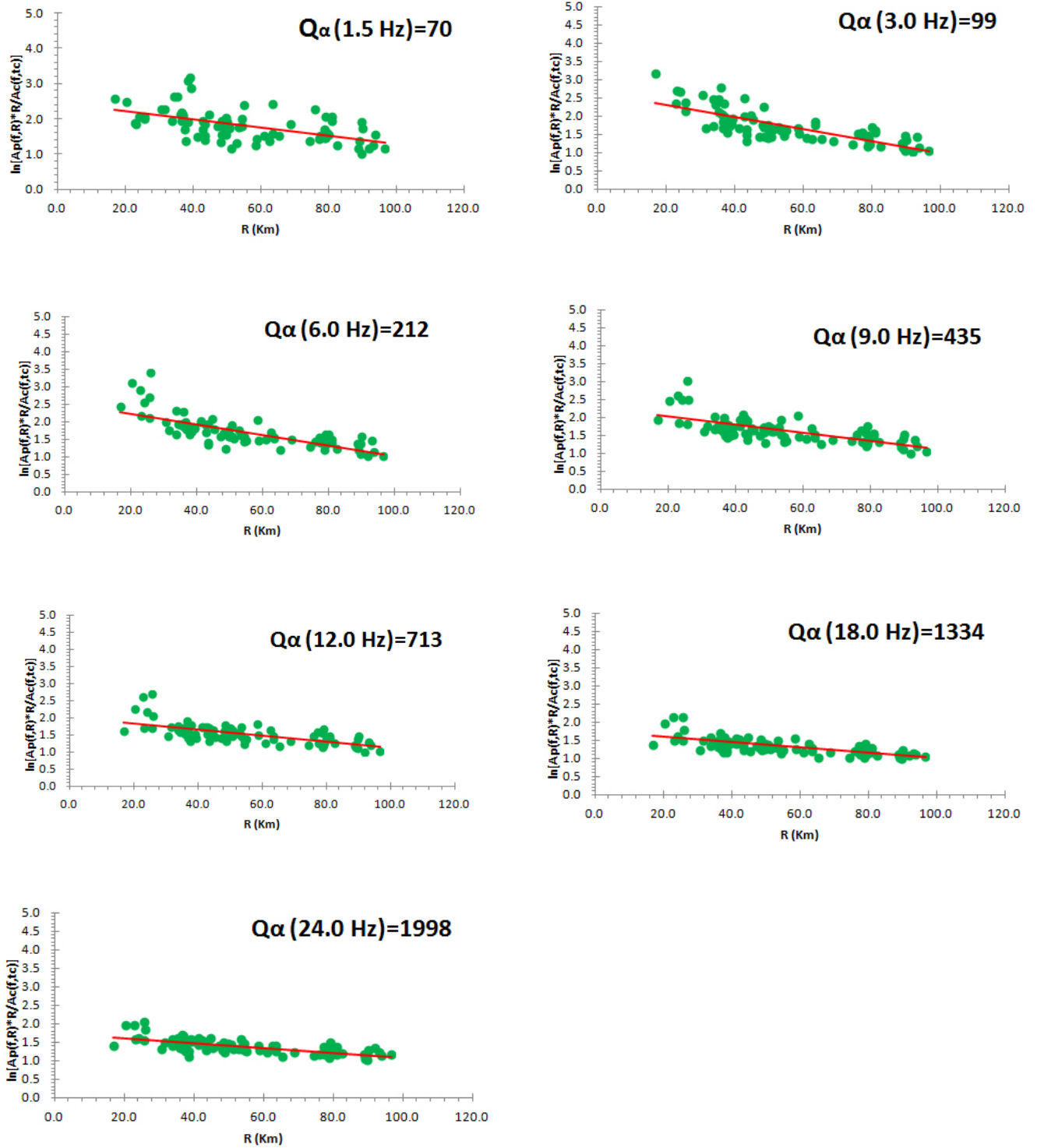


Fig 5.3 Coda normalized peak amplitude decay of P waves with hypocentral distance for five central frequencies at LED station and the regression lines from the least-squares best-fitted lines are also shown.

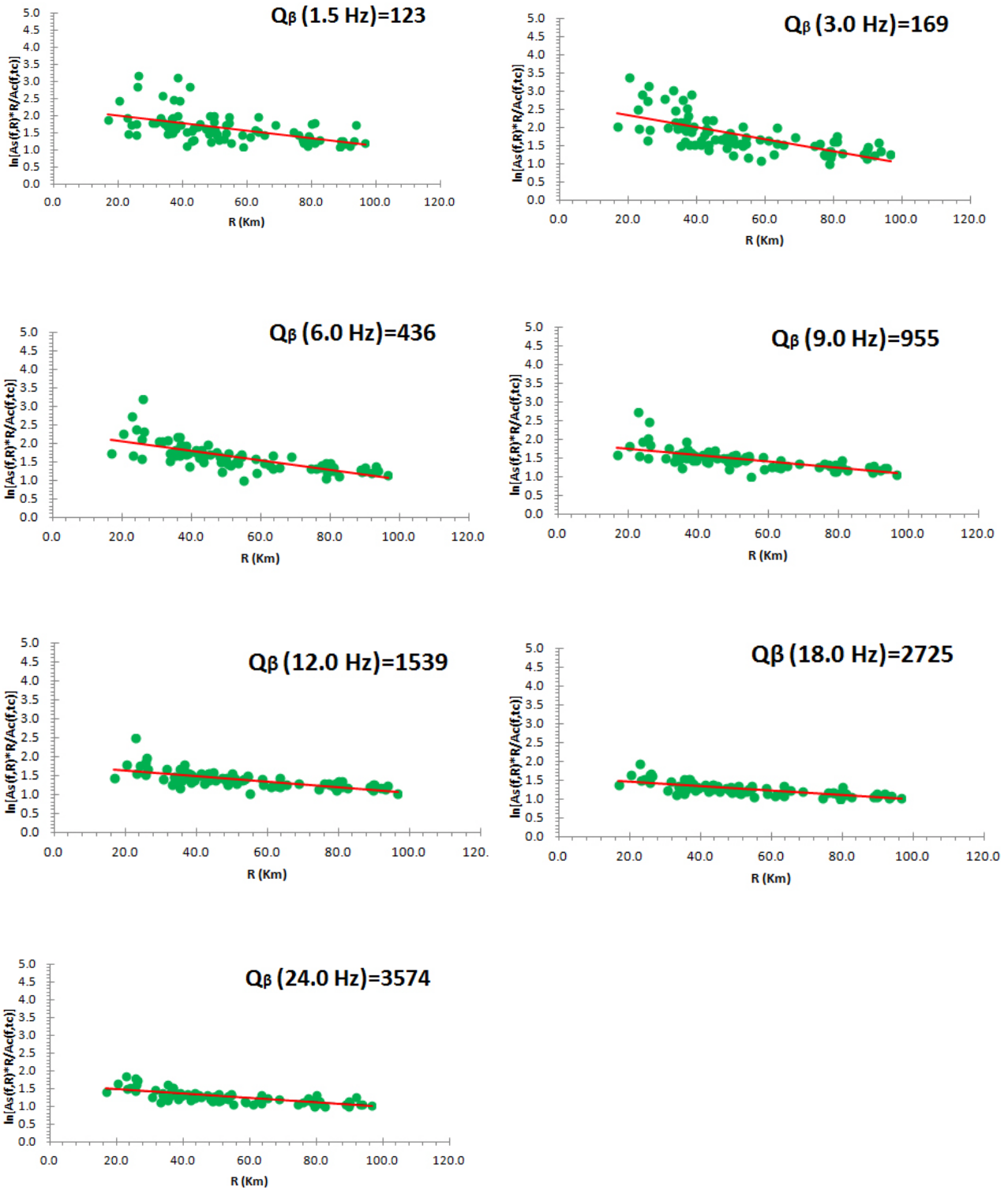


Fig 5.4 Coda normalized peak amplitude decay of S waves with hypocentral distance for five central frequencies at LED station and the regression lines from the least-squares best-fitted lines are also shown.

Table 5.1: Q_α and Q_β values along with their standard deviations at different central frequencies at five stations.

Freq. (Hz)	ADI		AHO		AYE		LED		ROT	
	(Q_α)	(Q_β)	(Q_α)	(Q_β)	(Q_α)	(Q_β)	(Q_α)	(Q_β)	(Q_α)	(Q_β)
1.5	46±4	101±5	56±4	130±6	33±4	109±5	71±6	123±7	42±4	128±7
3.0	91±4	135±3	92±3	132±4	75±3	199±4	99±3	169±3	106±3	180±4
6.0	253±6	346±5	200±4	404±5	206±4	416±4	212±3	436±4	222±3	490±5
9.0	412±6	606±4	360±4	654±5	383±4	722±4	435±5	955±6	374±3	698±4
12.0	580±6	808±3	488±4	955±4	590±5	1097±5	714±6	1939±8	585±4	1007±4
18.0	1025±7	1240±3	743±4	1471±4	1070±6	1867±6	1335±7	2725±8	937±4	1713±4
24.0	1528±9	1654±3	984±4	1996±5	1273±5	2194±5	1999±9	3574±8	1325±5	2261±4

Table 5.2: Average values of Q_α and Q_β along with their standard deviations at different central frequencies.

Freq. (Hz)	1.5	3	6	9	12	18	24
Q_α	49±4	92±3	218±4	392±4	591±5	1022±6	1421±6
Q_β	118±6	163±4	418±5	727±5	1161±5	1803±6	2335±5

Table 5.3: Frequency dependent relationships for five stations

Station code	Relation for P-wave	Relation for S-wave
ADI	$Q_\alpha = (25 \pm 1)f^{(1.28 \pm 0.03)}$	$Q_\beta = (53 \pm 1)f^{(1.07 \pm 0.05)}$
AHO	$Q_\alpha = (32 \pm 1)f^{(1.07 \pm 0.04)}$	$Q_\beta = (61 \pm 1)f^{(1.08 \pm 0.07)}$
AYE	$Q_\alpha = (18 \pm 1)f^{(1.37 \pm 0.04)}$	$Q_\beta = (61 \pm 1)f^{(1.13 \pm 0.04)}$
LED	$Q_\alpha = (30 \pm 1)f^{(1.27 \pm 0.01)}$	$Q_\beta = (52 \pm 1)f^{(1.34 \pm 0.01)}$
ROT	$Q_\alpha = (25 \pm 1)f^{(1.24 \pm 0.02)}$	$Q_\beta = (68 \pm 1)f^{(1.09 \pm 0.05)}$

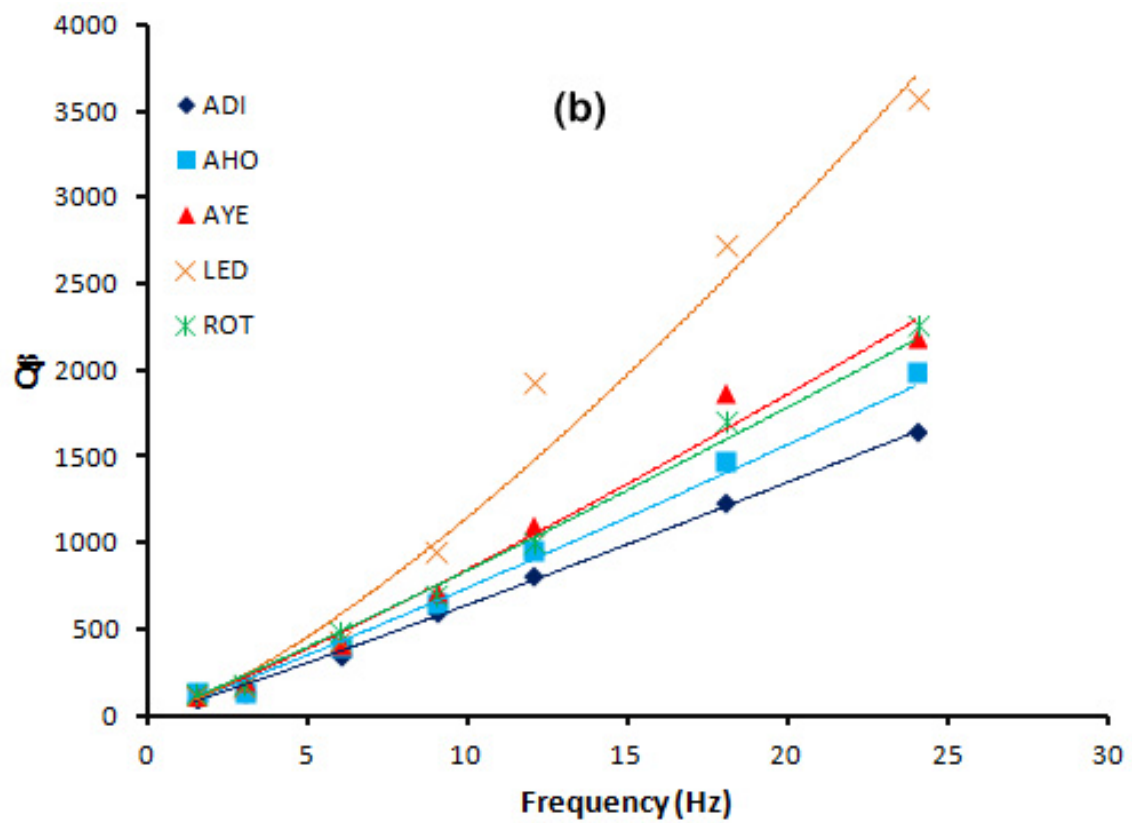
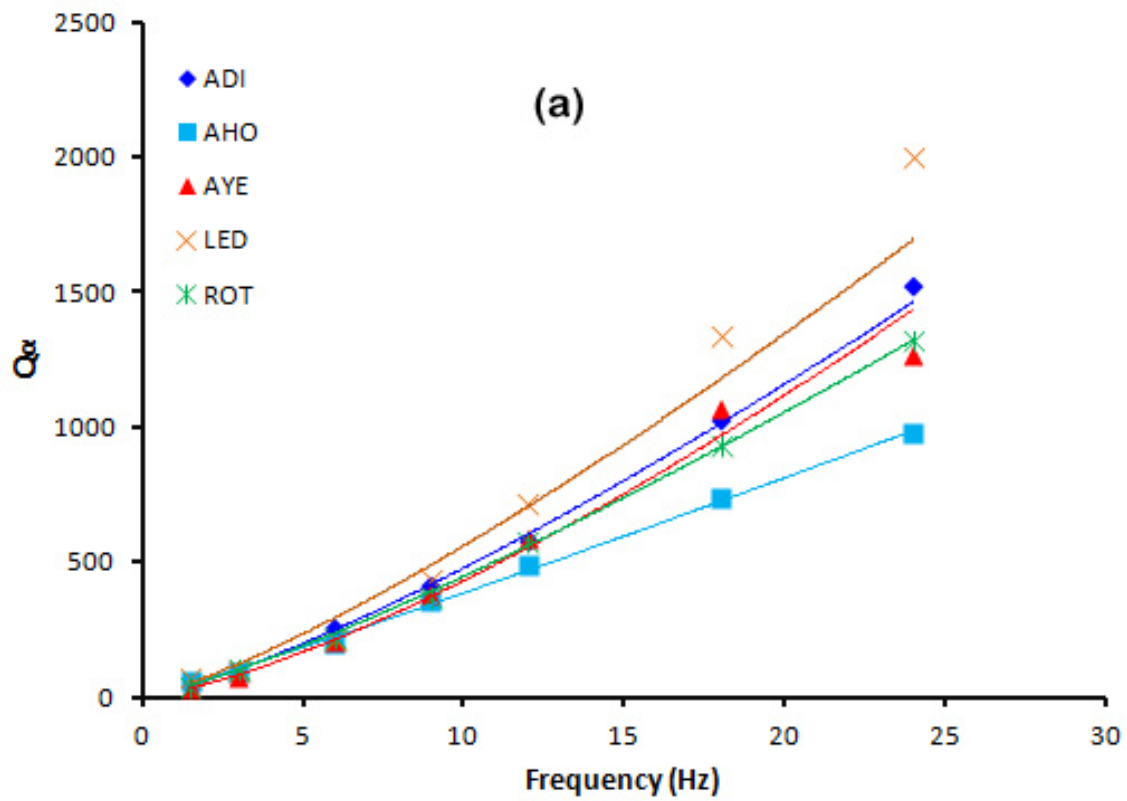


Fig. 5.5 (a). Comparison of estimated value of Q_α at all five stations, **(b)** comparison of estimated value of Q_β at all five stations

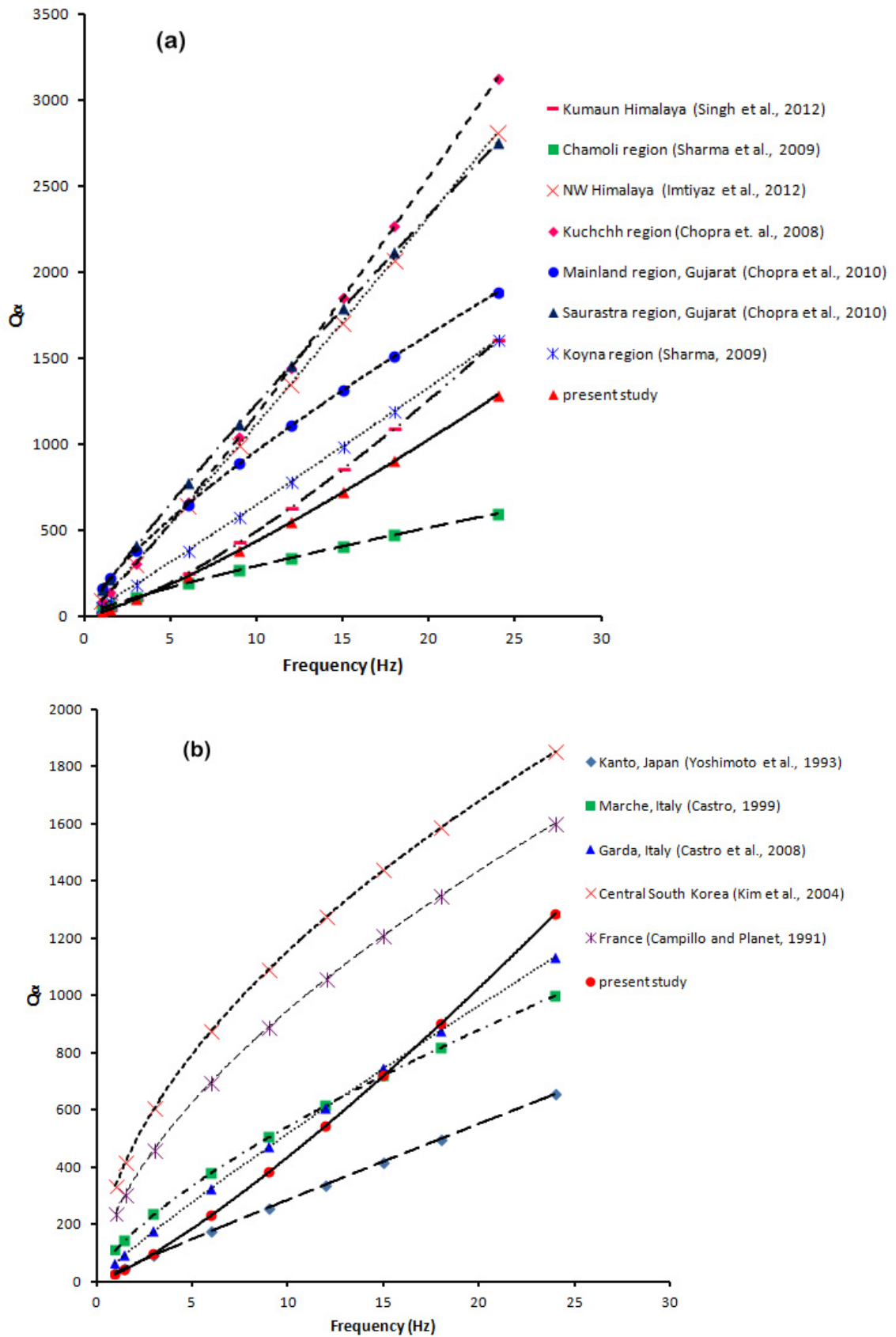


Fig 5.6. Comparison of Q_{α} (a,b) obtained in the present study with the other regions of the India and world.

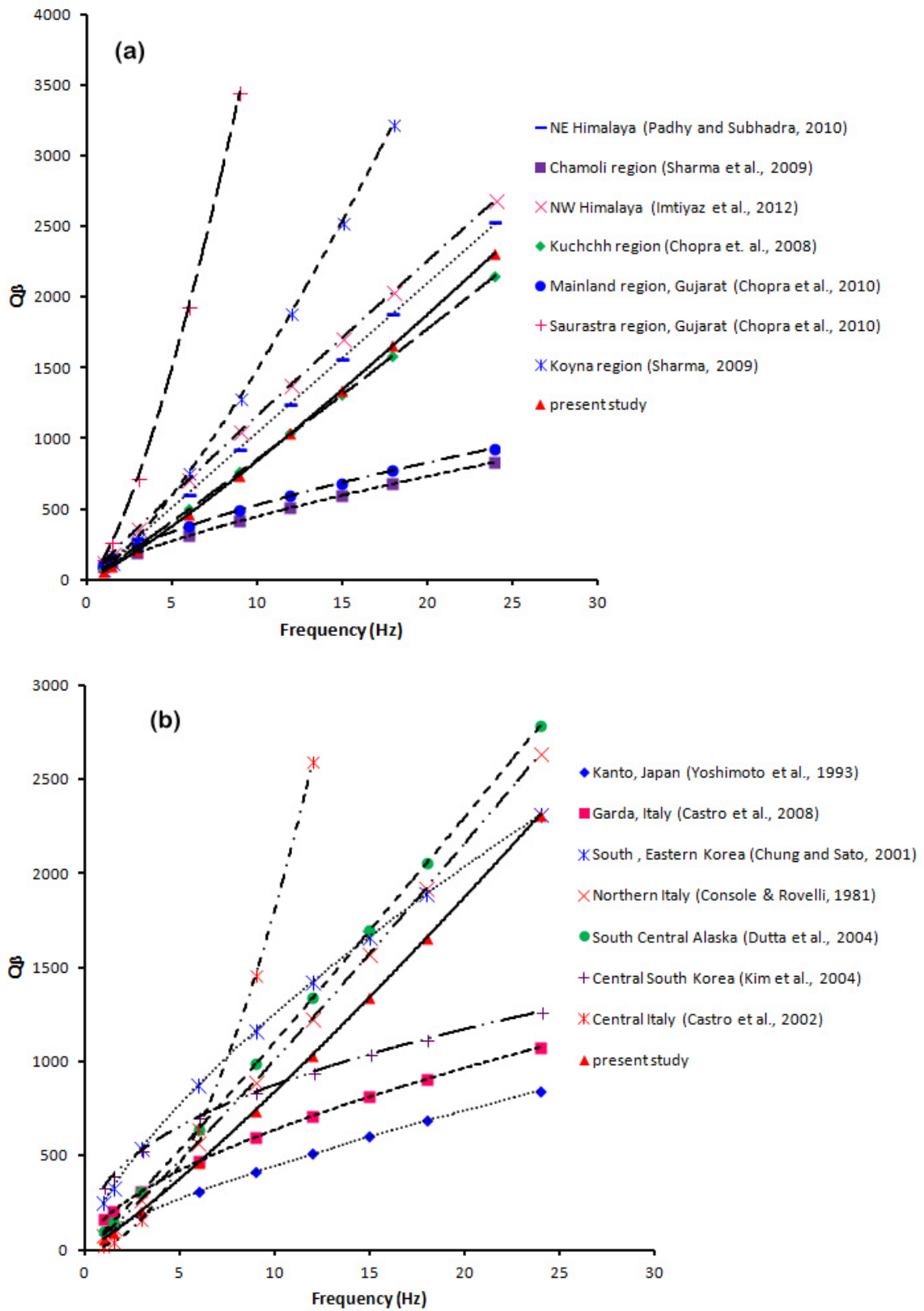


Fig 5.7. Comparison of Q_{β} (a,b) obtained in the present study with the other regions of the India and world.

A comparison of average values of Q_α and Q_β is plotted in Fig. 5.8. From the figure it has been observed that P-wave quality factor (Q_α) is lower than the S-wave quality factor (Q_β). Therefore, P waves attenuate more rapidly than the S-waves. The ratio of Q_β and Q_α is observed greater than unity ($Q_\beta/Q_\alpha > 1$) for the region. This means the region exhibits high degree of lateral heterogeneities. The similar observations are obtained by the other researchers e.g. Bianco et al.(1999) and Sato and Fehler (1998). The geology of the Lower Siang Region of Arunachal Himalaya helps in understanding the attenuation mechanism in the region. It lies within seismically active region of Eastern Syntaxial Bend. The region is considered seismically as one of the most active zone of Himalayan terrains. It comprises of alluvium of quaternary period, sedimentary and Dark green to grey amygdaloidal mafic volcanic of Miocene period, sedimentary of Permian period and metamorphic rocks of Proterozoic eon. The Sediments of the active channels, Boulders, Cobbles, Pebbles with Sand (Holocene); Boulders, cobbles, gravel, silt, clay (Pleistocene); Soft grey sandstones, silt, clay and semi-consolidated gravel-boulder beds; Miri Formation Conglomerate (Lower Permian); Quartzite and shale/slate with conglomerate lenses of Nikte Quartzite (Lower to Middle Palaeozoic) and other igneous intrusions make the regions highly heterogeneous. Hence this part of Himalaya is highly heterogeneous and similarly highly active region as the other parts of the Himalaya. The average Q_β/Q_α ratio at 1 Hz is compare with the other regions of the world (Fig. 5.9). The results obtained in this study are falling in the region where $Q_\beta > Q_\alpha$. The dash line $Q_\alpha = 2.25Q_\beta$ (i.e. $Q_\beta/Q_\alpha = 4/9$) is theoretically derived. By Sekiguchi (1991) based the 3-D wave attenuation in Kanto-Tokai area using the spectral ratio method. The theoretically derived Q_β/Q_α ratio is approximately accounts the attenuation of low frequency seismic waves having frequency less than 0.1 Hz (Anderson et. al., 1965; Yoshimoto et al., 1993). The laboratory measurements of done by Toksoz et al. (1978) shows that in water saturated rocks the Q_β/Q_α ratio is less than unity while in dry rocks it is greater than unity. Richards and Menke (1983) found that Q_β/Q_α is approximately equal to 1. Yoshimoto et al.(1993) found that this assumed ratio is not applicable for higher frequencies and observed that Q_β/Q_α is greater than unity for Kanto area, Japan for frequencies greater than 1 Hz. Yoshimoto et al. (1998) explained that Q_β/Q_α is greater than unity in frequency range about 1–30 Hz. The observed Q_β/Q_α for Oaxaca subduction zone in Mexico is 2.54 in the frequency range 1.5-24Hz (Castro and Munguia, 1993). Chung and Sato (2001), analyzing the earthquake data of Yangsan fault region of south-eastern South Korea found that in the frequency range 1.5–24 Hz, the Q_β/Q_α ratio approximately equal to the

2.25. For Koyna region (India), Sharma et al. (2007) obtained the Q_β/Q_α greater than unity for frequencies 1.5–18 Hz. for the Kanto region (Japan) the observed $Q_\beta/Q_\alpha \geq 1$ in frequency range 1–10 Hz. Padhy (2009) for Bhuj region (India) found that the Q_β/Q_α is greater than unity frequency range of 1–24 Hz. Also, for the Cairo metropolitan area the reported value of $Q_\beta/Q_\alpha > 1$ for frequencies 3-24 Hz. Recently, Singh et al (2012) reports the Q_β/Q_α for Kumaun Himalaya in the frequency range 1.5-12 Hz. Hence the present study obtained Q_β/Q_α ratio at 1 Hz is 2.32 which quite close to Yoshimoto et al. (1998) and Chung and Sato (2001). Hence our study agreed with the other worldwide reported values.

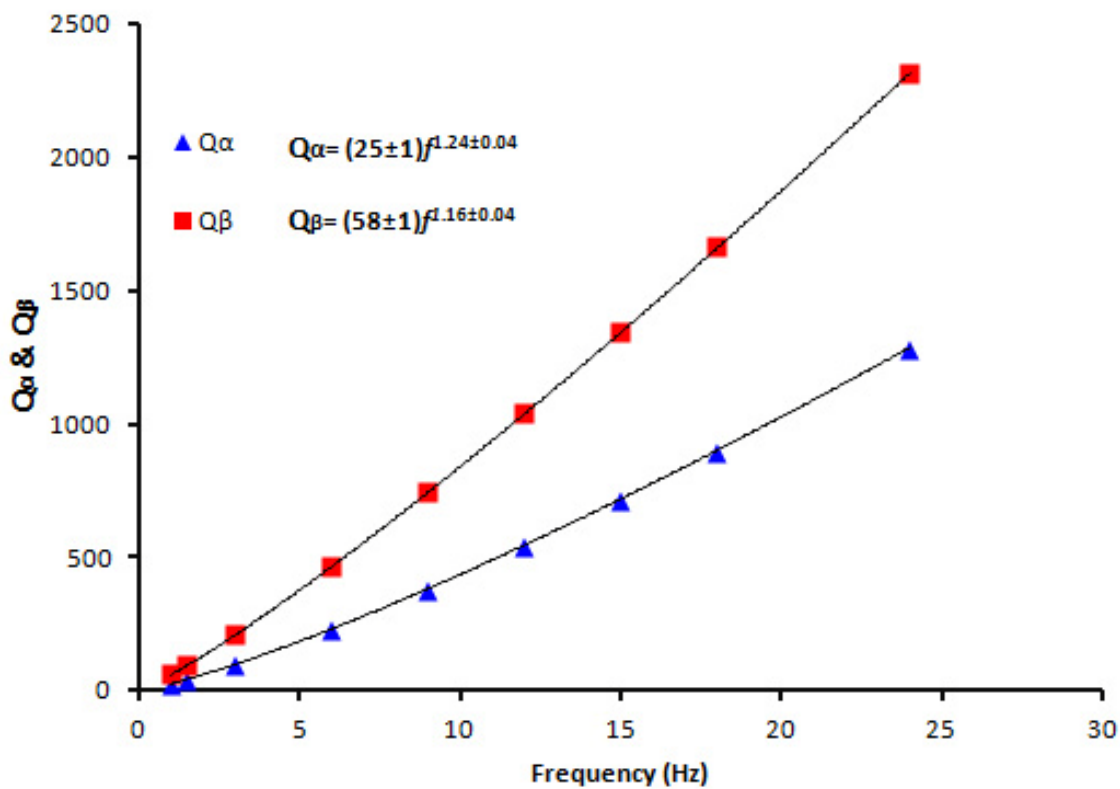


Fig. 5.8 Comparison between average Q_α and Q_β .

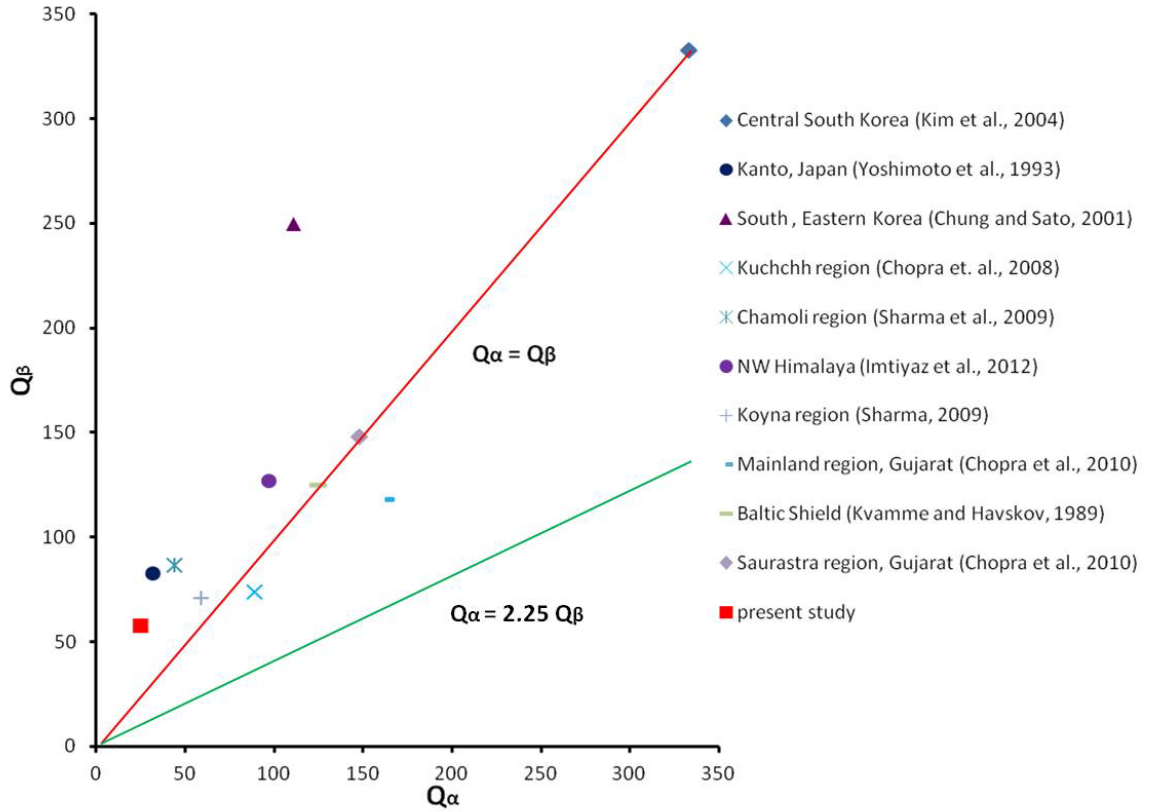


Fig 5.9. Comparison of average value of Q_β/Q_α (at 1 Hz) obtained in the present study with different regions of the world. The red line is corresponding to $Q_\beta=Q_\alpha$ and green line is theoretically derived by Sekiguchi (1991) corresponding to $Q_\alpha =2.25Q_\beta$.

In this chapter the seismic wave attenuation has been studied for Lower Siang region by estimating the quality factor of P-wave (Q_α) and S-waves (Q_β) in the frequency range 1.5 to 24 Hz adopting the extended coda normalization method. The estimated value of Q_α and Q_β are found to be strongly frequency dependence in the study region. Their mean values vary from 49 ± 4 at 1.5 Hz to 1421 ± 6 at 24 Hz for Q_α and from 118 ± 6 at 1.5 Hz to 2335 ± 5 at 24Hz for Q_β . The frequency dependence Q_α and Q_β relationships are obtained as, $Q_\alpha = (25\pm1)f^{(1.24\pm0.04)}$ for P-wave and $Q_\beta = (58\pm1)f^{(1.16\pm0.04)}$ for S-wave. The comparison of Q_α and Q_β has brought out that P wave attenuates more rapidly as compared to S-wave at all frequencies. Chapter 8 contains the summary of results obtained in this chapter.

Seismic Wave Attenuation Characteristics Using Coda Wave

6.1 INTRODUCTION

The high frequency coda is assumed to be the superposition of backscattered S-waves generated due to the heterogeneities distributed in the medium. These waves are observed on seismogram of local earthquake after the arrival of all direct waves. The seismic waves arrive at different time intervals forms coda. Therefore, in a seismogram instead of a single path connection source to station, the decay of coda waves with time represents the average attenuation characteristics of medium. These waves are generated due to various heterogeneities distributed in the medium. Hence simple deterministic method which requires a number of parameters to describe a small portion of a seismogram, are not suitable to explain these waves. However, statistical methods which require less number of parameters are capable of handling such problems. Aki (1969) and Aki and Chouet (1975) did the pioneering work in this field and proposed the single scattering model for the estimation of quality factor for coda waves (Q_c). A number of source parameters and seismic wave attenuation studies have been carried out in India as well as in World. Regarding seismic wave attenuation in India observation study has been initiated by Gupta et al. (1995) using the digital data collected in the Garhwal Himalaya. After this many such studies have been carried out by various researchers in different tectonically active as well as stable regions

In the Himalayan part some studies been carried out, for the Garhwal Himalaya by Gupta et al.(1995), Mandal et al. (2000), Sharma et al. (2008), Mukhopadhyay (2010), for the Kumaon Himalaya by Paul et al. (2003), Joshi (2006), Singh et al. (2012), for NW Himalaya by Kumar et al. (2005) and Vandana et al. (2014), for the NE Himalaya Hazarika et al. (2005) and Baruah et al. (2010). For the Kutch region of Gujarat where a moderate ($m_b=6.9$) occurred in the 2001. Several studies have been carried out of this earthquake by Mandal et al. (2004), Gupta et al. (2006), Chopra et al. (2008). In the nearby Saurashtra region of Gujarat attenuation have also been carried out e.g. Sharma et al. (2011). In the Indian shield region some studies have been done e.g. for Koyana region by Gupta et al. (1998), Mandal and Rastogi (1998) and Sharma et al. (2008). For the

tectonically stable region of Indian shield by Kumar et al. (2007), Singh et al.(2012). For the Andaman region by Padhy et al. (2011), Singh et al. (2015)

All above studies shows that no study on coda wave attenuation has been carried out in the Arunachal Himalaya. It is seismically very active and falls in the seismic zone-V as per seismic zoning map of India. In the present study seismic wave attenuation characteristics have been carried out for the Lower Siang region of Arunachal Himalaya, as no study carried out earlier in this region. For this purpose, coda waves recorded on the seismogram of 104 local earthquakes are analyzed employing the single scattering model given by Aki and Chouet (1975). In these chapter different models developed by researchers and the method which have been used for our study is discussed. The analysis procedure that includes the steps for the computation of coda-Q and results obtained are also discussed here.

6.2 MODELS AND METHODOLOGY

There is various model for the analysis of coda waves such as Surface wave model proposed by Aki(1969) and modified by Kopnichev (1975), single backscattering model proposed by Aki and Chouet (1975), Single isotropic scattering model by Sato (1977a), diffusion model by Weley (1965), Dainty et al. (1974), Kopnichev (1977b) and multiple scattering model by Kopnichev (1977b), Geo et al. (1983a, b). The basic assumptions and observations of these models are described in Table 6.1 which is reproduced after Herraiz and Eapinosa (1987).

Out of models discussed in Table 6.1, there is only two basic models; single backscattering, and multiple backscattering models, was extensively used for coda wave analysis. The single backscattering model is well established for the estimation of coda wave attenuation characteristics of local earthquakes (Aki and Chouet, 1975). It was developed to understand the behaviour of coda waves. These waves are the superposition of backscattered waves generated by various heterogeneities present in the earth's crust. Single scattering model assumes that the scattering is a weak process and waves are back scattered only once. On the other hand multiple scattering is allowed in the multiple scattering models and scattering is considered to be a strong process. In general, the single scattering model is applied for the events recorded at local epicentral distances while the multiple scattering is used for the analysis of intermediate and teleseismic events having lapse time greater than 100 sec (Geo et al., 1983).

Table 6.1 Coda wave explanation models (After Herraiz and Eapinosa, 1987)

Model	Proposed by		Assumptions			observations
		Primary wave	medium	Heterogeneity	Scattering	
Surface waves	Aki (1969)	Surface waves	Two dimensional Homogeneous, isotropic unbounded	Uniform and random distribution $l > \Delta$	Single and weak	$r = R > \Delta$
	Kopnichev (1975)	„	„	„	Single and isotropic	Extended the Aki model for intermediate distances
Single backscattering	Aki and Chouet (1975)	Surface and body waves	Two and Three dimensional Homogeneous and isotropic unbounded	„	Single and weak	Introduces the Born approximation
Single isotropic scattering	Sato (1977a)	Body waves	Three dimensional Homogeneous and isotropic unbounded	Uniform, isotropic and random distribution $l < \Delta$	Single and isotropic	Deals with energy
Diffusion	Wesley (1965), Dainty et al. (1974), Kopnichev (1977b)	Surface and body waves	Three dimensional Homogeneous and unbounded	„	Multiple and strong	Lunar and terrestrial assumption
Multiple scattering	Kopnichev (1977b)	„	Random statistical	isotropic and normal, $l > \Delta$	Double, triple strong and isotropic	Diffusion model included
	Geo et al. (1986a, b)	Body waves	Two and Three dimensional Homogeneous and isotropic unbounded	Uniform and random, $l < \Delta$	Multiple, isotropic and weak	Use of Born approximation, $r =$ $R > \Delta$

In the present study the so single scattering model is used because all the even used analysis are recorded within 100 km epicentral distance

Aki and Chouet (1975) gave the mathematical formulation of single backscattering model based on two assumptions:

1. Scattering is a weak process and only single scattering is allowed. Whenever another scatter is encountered by a seismic wave, no scattering is produced. This approximation violates the energy conservation law. But it is acceptable for various physical problems and high frequency seismic waves are successfully studied using this method.
2. The coda wave are arrives on seismogram long time after the direct S and P waves. Hence the source and receiver are considered to be placed at a same point.

The mathematical formulation of the model is described below;

Let a wavelet scattered from a scatterer located at 'r' and produces displacement. Let $\phi(\omega/r)$ be the Fourier transform of the displacement. Hence $\phi(\omega/r)$ depends on both earthquake source and scatterer. Let these scatterer producing coda wave are distributed randomly in the space. Let within radius 'r' of the station $N(r)$ be the number of scatterer present. So the numbers of scatterer bounded by zone $(r, r + \Delta r)$ will be $(dn/dr) \Delta r$.

Assuming same type (S-waves) of the primary and scattered waves travelled at same velocity, the waves backscattered in $(r, r + \Delta r)$. Let the distance Δr be such that the time Δt is greater than the individual backscattered wavelet duration. As the scatterer are randomly distributed so the energy of backscatterd wave arrives at $(t, t + \Delta t)$ is equal to the Δt times the spectral density $P(\omega, t)$ of coda waves. Here $t = 2r/v$ and $\Delta t = 2 \Delta r/v$, 'v' is the wave propagation velocity. Hence the spectral power density can be written as:

$$P(\omega, t)\Delta t = \sum_{m=r}^{m=r+\Delta r} |\phi_n(\omega)|^2 = \left(\frac{dN}{dr}\right) \Delta r |\phi_n(\omega, r)|^2 \quad (6.1)$$

The suffix 'n' represents the nth scatterer. Let body waves get scattered from scatterers having density per unit volume σ . So the number of scatterers present

within a spherical shell ($r, r + \Delta r$) is $(dn/dr) = 4\pi\sigma r^2 \Delta r$. The spectral power density can be represented as:

$$P(\omega, t)\Delta t = |\phi(\omega, r)|^2 4\pi\sigma r^2 \Delta r \quad (6.2)$$

Let r be scatterer to station and r_0 is the source to scatterer distances. Due to geometrical spreading, the amplitude spectra of scattered wave can be written as:

$$|\phi(\omega, r)| = |\phi(\omega, r_0)| \left(\frac{r_0}{r}\right)^2 \quad (6.3)$$

One more factor affecting the wave energy is the anelasticity of the medium. Due to anelasticity of the medium the wave energy get converted into heat energy by fraction of particles of wave travelling media. The energy loss per cycle due to fraction is $2\pi Q_c^{-1}$, Q_c is the quality factor. The power attenuation during time 't' is $e^{(-\omega t/Q_c)}$, ω is the angular frequency. So the intensity of secondary wave can be written as:

$$|\phi(\omega, r)| = |\phi(\omega, r_0)| \left(\frac{r_0}{r}\right)^2 e^{\left(\frac{-2\omega t}{2Q_c}\right)} \quad (6.4)$$

Using equ (6.2) and (6.4), power spectral density function can be written as:

$$P(\omega, t) = |\phi(\omega, r_0)|^2 8\pi\sigma r_0^4 v^{-1} e^{\left(\frac{-\omega t}{Q_c}\right)} \quad (6.5)$$

In general power spectral density function can be written can be written as:

$$P(\omega, t) = S t^{-m} e^{\left(\frac{-\omega t}{Q_c}\right)} \quad (6.6)$$

Where 'm' is the geometrical spreading factor and $m = 2$ for body waves. Earthquake source term 'S' represents the effects of both primary and secondary waves sources. The mean square amplitude is proportional to power spectral density and band width. Since peak to peak smoothed amplitude $A(\omega, t)$ is roughly twice the rms value of the signal. Hence we can write:

$$A(\omega, t) = 2[2P(\omega, t)\Delta t]^{\frac{1}{2}} \quad (6.7)$$

Where $\Delta f = ((\omega_1 - \omega_2)/2\pi)$ is the bandwidth of considered channel. Combining equation (6.6) and (6.7) we can write coda amplitude as:

$$A(\omega, t) = C t^{-a} e^{\left(\frac{-\omega t}{Q_c}\right)} \quad (6.8)$$

Where $\alpha = m/2 = 1$, for body waves.

Simplifying equation (6.8) we have:

$$A(f, t) = C(f)t^{-\alpha}e^{(-\frac{\pi ft}{Q_c})} \quad (6.9)$$

$A(f, t)$ represents the coda amplitude at central frequency ‘ f ’ as a function of lapse time (t). Lapse time is measured from the origin time and taken as twice the travel time of direct S-waves. Q_c is the quality factor of coda waves and represents the average attenuation properties of medium

Rearranging the terms of equ (6.9) and taking natural logarithm we have.

$$\ln(A(f, t). t) = c - bt \quad (6.10)$$

Where $c = \ln C(f)$ and $b = \pi f/Q_c$. the equation(6.10) represents a straight line whose slop gives Q_c .

6.3 ANALYSIS PROCEDURE

The selected waveform having signal to noise ratio (SNR) greater 3 are used for analysis. The effect of increase in SNR on Q_c has also been studied and found no significant variation in Q_c with the SNR and lies within the error range. The earthquake time history is band-pass filtered by Butterworth filter at different frequency bands given in table 6.2. The contamination caused by direct S-wave has been eliminated by selecting the start time of coda window from earthquake origin time as twice of travel time of S-wave (Rautian and Khalturin, 1978). Only those waveforms were considered, whose correlation coefficient during fitting a straight line between logarithmic of coda wave amplitudes and lapse time (eqn. 6.10) is greater than 0.7. In order to get stable Q_c estimates the selection of length of coda window is important. Havskov and Ottemoller (2005) suggested the minimum window length should be 20s and there is no maximum limit. In the present study, three lapse time windows i.e., 30, 40 and 50 sec are used. Following basic steps have been used for computation of Q_c :

Steps involves in computation of coda-Q.

1. Consider raw data in the form of time series (seismogram) of a local earthquake.
2. Apply baseline correction before analysis.

3. Select a long window of coda waves say 30, 40 and 50 sec. The coda window is selected from the twice the travel time of the S-wave.
4. Filtering of the time series: Butterworth filter of 8-poles is adopted for filtering of seven frequency bands (table.6.2).
5. Smoothing of filtered coda window: For applying smoothing on the filtered the time series of the coda window, root mean square (RMS) technique is adopted. In this first square then mean and then root is taken of the selected coda window of 1 sec (fig.)
6. Slope fitting for the Q_c estimation: After smoothing the coda amplitude, the amplitude is multiplied by the lapse time for correcting the geometrical spreading effect and plotted as function of lapse time in the form of linear function as given in equation 6.10. Slope of provide Q_c for particular station/event. After computing the Q_c value at number of stations and at frequencies for all local earthquakes, a power law is to fit in the form of $Q_c = Q_0 f^\eta$, Q_0 is the value of Q_c at 1 Hz and ' η ' is the frequency exponent. This power law gives the average coda-Q attenuation for the region.

Table 6.2. Various central frequencies with low-cut and high-cut frequency bands used for filtering.

Low cut-off (Hz)	Central frequency (f) (Hz)	High cut-off (Hz)
1.00	1.50	2.00
2.00	3.00	4.00
4.00	6.00	8.00
6.00	8.00	12.00
8.00	12.00	16.00
12.00	18.00	24.00
16.00	24.00	32.00

A MATLAB program CODAQ is developed for coda-Q estimation based on the eqns. (1-3) and above analysis procedures. The program follows the guidelines of CODAQ subroutine of SEISAN (Havskov and Ottemoller; 2003). The general procedure for estimation of Q_c using CODAQ program is shown in the flowchart below:

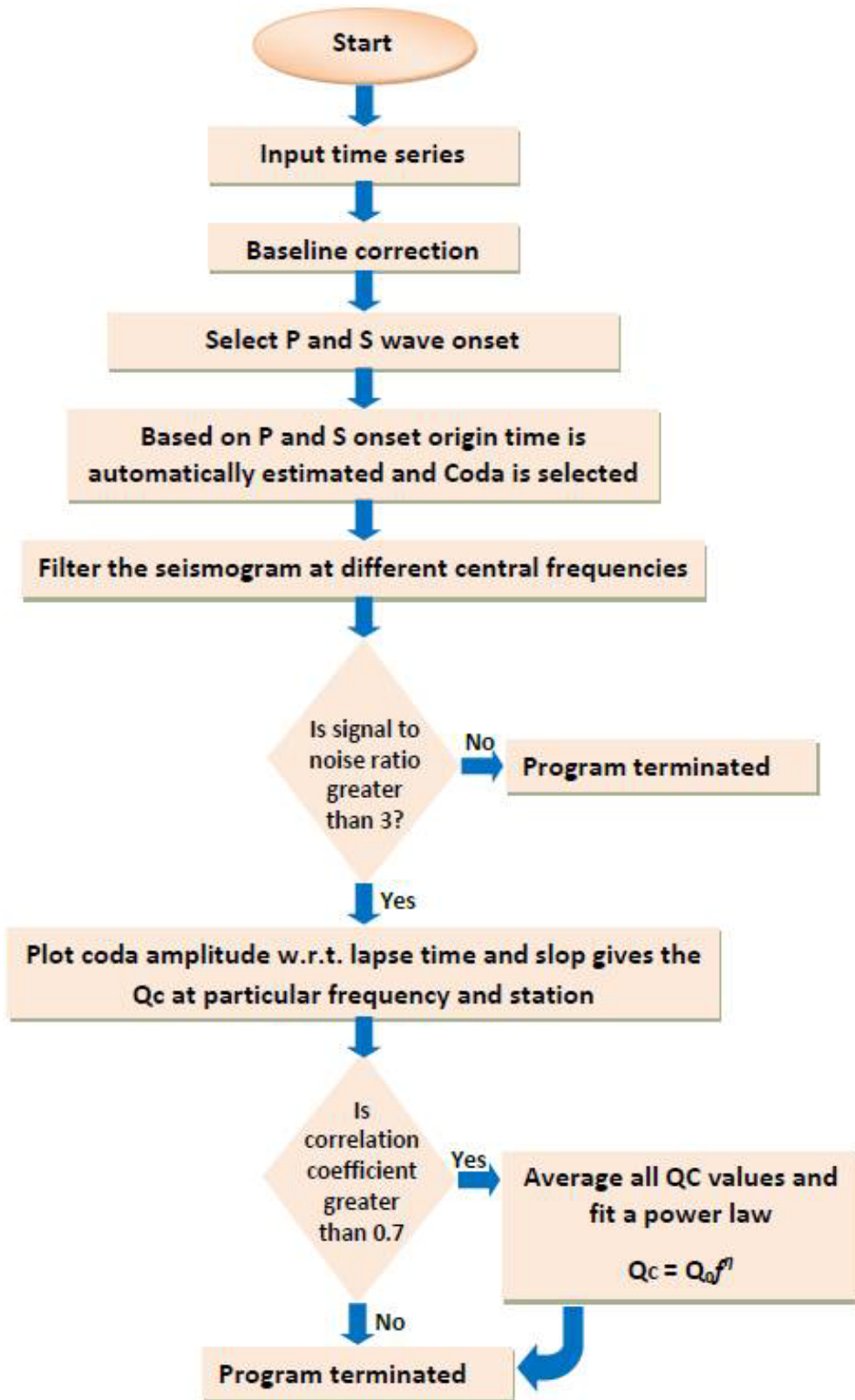


Fig. 6.1. Flow of CODAQ program used for coda wave attenuation estimation.

For applying geometrical spreading correction on the part of coda waves, the coda wave amplitudes have been multiplied by a factor $t^{-\alpha}$ where, $\alpha=1$ for body waves of local earthquakes. The envelope of considered signal is estimated from root mean square (RMS) values of coda amplitudes from a moving window of 2 seconds with stepping of 1 second. Then natural log of RMS amplitudes is taken and plotted as a function of lapse time t and a linear equation is fitted whose slope gives coda Q for considered central frequency (f_c). An example of an event occurred on August 13, 2011, recorded at LED station of the network and considered for coda Q analysis is shown in fig. 6.2. In this figure shows, a) origin time of event, arrival time of P & S-waves, b-h) band pass filtered seismogram at seven frequency bands along with the linear line fitted between $\ln [Ac(x, t)]$ and lapse time t . The correlation coefficient for each liner fitting and Q_c value at each central frequency is also mentioned.

The dependence of coda-Q on lapse time is described by various researchers (Roecker et al., 1982; Pulli, 1984; Canas et al., 1995). The lapse time is related the region of sampling (Gupta et al. 2012). According to Pulli (1984), the coda wave attenuation is average decay of amplitude of back-scattered waves on the surface of ellipsoid volume having earthquake source and station as foci. So accordingly the coda-Q represents the average attenuation of ellipsoidal volume having depth, $h = h_{av} + D2$. Where $D2 = \sqrt{D1^2 - \Delta^2}$, is the small minor axis of ellipsoid for Δ epicentral distance and h_{av} is the average focal depth of events. The large semi axis $D1$ is the surface projection of ellipsoid having hypocenter and station as foci. It can be defined as $ct/2$, where 'c' is the s-wave velocity and t is the average lapse time. The average lapse time is given by the relationship: $t = t_{st} + t_{win} / 2$, where t_{st} is the start lapse and t_{win} the window length. The depths calculated for the ellipsoidal volume for different stations of data are given in table 6.3. Therefore, the coda generating area of the surface projection of ellipsoid in circular shape having radius as depth coverage is determined for each station and given in Table 6.3.

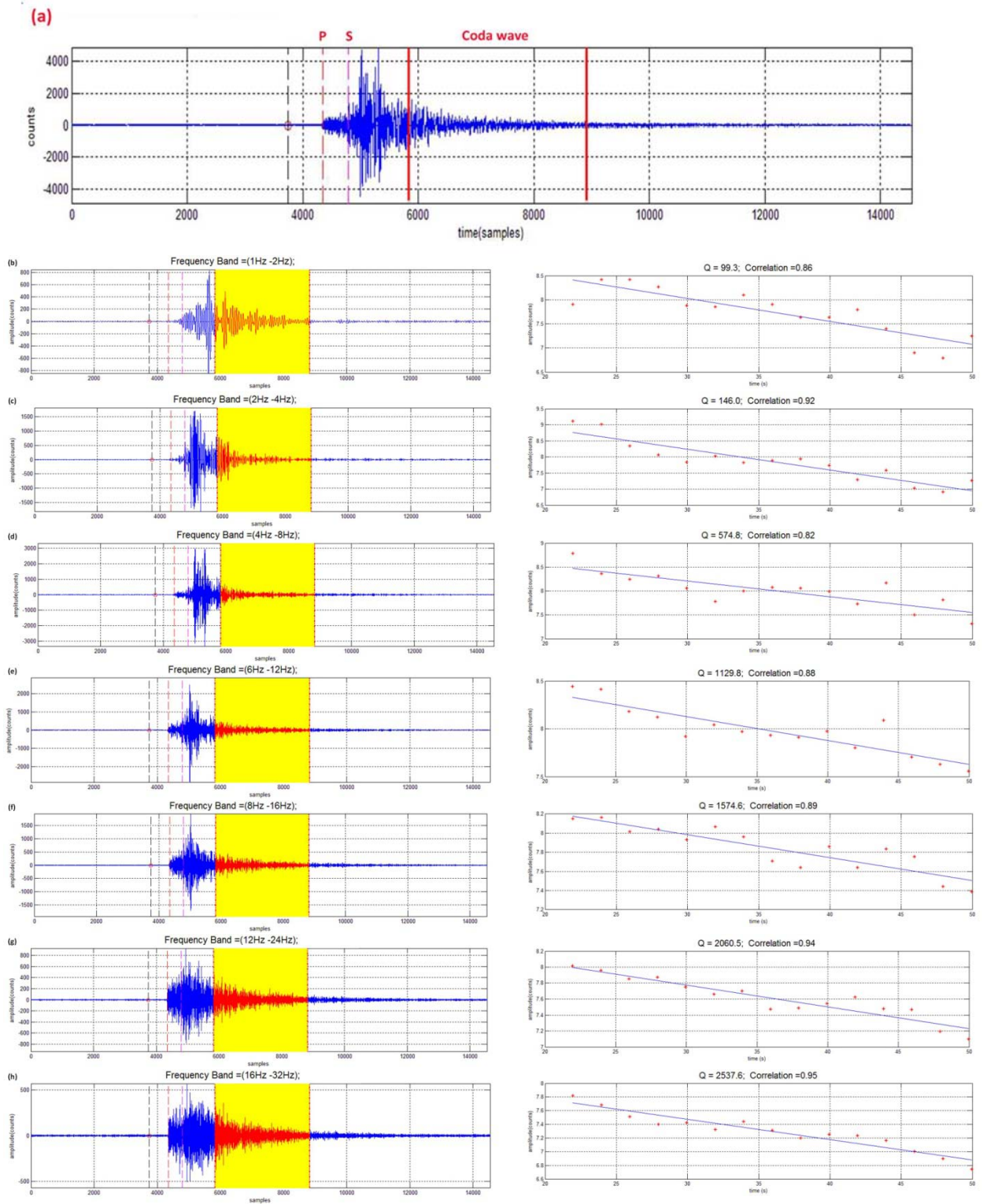


Fig. 6.2. Q_c estimate of an event recorded at LED station occurred on 13/08/2011. (a) Unfiltered data trace with coda window, (b) to (h) band pass filtered displacement amplitudes of coda window at 1-2 Hz, 2-4Hz, 4-8Hz, 6-12Hz, 8-16Hz, 12-24Hz and 16-32Hz respectively. Abbreviations are: P: P-wave arrival time; S: S-wave arrival time.

Table 6.3.Maximum depth of the ellipsoidal volume at various stations. Here ‘A’ is the average are generating coda.

Stations	Average distance (Δ)	Average focal depth (h_{av})	Average lapse time (t)	Average s-wave velocity	D1=ct/2 (km)	D2= $\sqrt{D1^2 - \Delta^2}$	Depth of ellipsoidal = $h_{av}+D2$ (Km)	Surface area (sq km)
ADI	55.20	18.18	39.68	3.56	70.62	44.05	62.24	12163.79
AHO	66.53	14.33	44.48	3.56	79.18	42.93	57.26	10265.14
AYE	62.39	17.75	45.14	3.56	80.35	50.63	68.38	14682.09
LED	71.189	17.87	46.32	3.56	82.45	41.60	59.47	11105.18
ROT	61.06	17.10	44.29	3.56	78.85	49.87	66.97	14082.84

6.4 Results and Discussions

The single back-scattering model of Aki and Chouet (1975) has been used to estimate the frequency dependent attenuation characteristics of coda waves in Siang region of Arunachal Himalaya. The seismograms have been analyzed at seven frequency bands for 30, 40 and 50 sec duration lapse time windows. The average of estimated Q_c at various stations deployed in the region for three lapse time windows at seven frequency bands is shown in Table 6.4. The average Q_c value along with standard error varies from 109 ± 33 , 138 ± 42 and 162 ± 46 at 1.5 Hz to 3149 ± 923 , 3439 ± 944 , and 3889 ± 1165 at 24 Hz for lapse time windows of 30, 40 and 50 sec, respectively (table 6.5). Therefore, the Q_c value increases with increase of frequency as well as lapse time window. A power law of the form power law, $Q_c = Q_0 f^{\eta}$, for each station and lapse time window pair is obtained from the estimated Q_c -values are plotted as a function of frequency as shown in Fig. 6.3. The table 6.6 shows the Q_0 (quality factor at 1 Hz) and frequency dependent ‘ η ’ estimated using different lapse time window at different stations. The average relationships for the region are $Q_c=(52\pm1)f^{1.22\pm0.03}$, $Q_c=(83\pm1)f^{1.18\pm0.02}$ and $Q_c=(105\pm1)f^{1.16\pm0.02}$ for lapse time windows of 30 , 40 and 50 sec, respectively (fig. 6.4 and Table 6.7).

Table 6.4. Mean value of Q_c at each station at three lapse time windows for different frequencies along with standard errors.

Freq. (Hz)	ADI	AHO	AYE	LED	ROT
Lapse time 30 s					
1.5	100±30	118±36	98±32	123±32	104±35
3	204±57	210±55	199±60	202±64	231±76
6	502±147	547±158	563±204	509±163	572±156
9	970±293	899±261	1033±325	992±386	924±300
12	1459±461	1338±341	1559±485	1449±435	1304±449
18	2200±656	2017±401	2628±714	2426±688	2004±548
24	3092±1207	2958±689	3642±859	3111±763	2940±1095
Lapse time 40 s					
1.5	130±42	147±37	130±40	145±46	138±44
3	270±72	312±87	235±54	246±74	323±78
6	693±190	711±188	678±192	615±189	787±222
9	1149±257	1105±308	1354±391	1113±337	1182±311
12	1609±416	1547±409	1807±506	1610±416	1482±299
18	2523±787	2308±524	2742±538	2534±611	2184±495
24	3326±988	3257±963	4077±1141	3494±928	3041±699
Lapse time 50 s					
1.5	156±51	174±43	168±57	153±36	161±44
3	339±92	451±105	343±105	319±85	367±83
6	874±191	1050±264	869±191	839±214	947±231
9	1403±350	1463±333	1605±349	1378±325	1421±371
12	1900±532	1961±478	2379±586	1997±589	1753±358
18	2800±787	3022±842	3803±1171	2967±689	2613±675
24	3755±1118	3610±844	4437±1651	4000±1067	3645±1146

Table 6.5. Fitted power law for each station and mean power law for the region for different lapse time 30, 40 and 50 sec.

Station	Power law $Q_c = Q_0 f^\eta$	Q_0 (Q_c at 1 Hz)	η (frequency exponent)
Lapse time 30 sec			
ADI	$Q_c = (55 \pm 1) f^{1.27 \pm 0.03}$	55	1.27
AHO	$Q_c = (66 \pm 1) f^{1.19 \pm 0.03}$	66	1.19
AYE	$Q_c = (52 \pm 1) f^{1.34 \pm 0.03}$	52	1.34
LED	$Q_c = (63 \pm 1) f^{1.23 \pm 0.05}$	63	1.23
ROT	$Q_c = (64 \pm 1) f^{1.20 \pm 0.01}$	64	1.20
Mean	$Q_c = (52 \pm 1) f^{1.22 \pm 0.03}$	52	1.22
Lapse time 40 sec			
ADI	$Q_c = (78 \pm 1) f^{1.19 \pm 0.02}$	78	1.19
AHO	$Q_c = (94 \pm 3) f^{1.11 \pm 0.01}$	94	1.11
AYE	$Q_c = (70 \pm 1) f^{1.28 \pm 0.05}$	70	1.28
LED	$Q_c = (78 \pm 1) f^{1.19 \pm 0.04}$	78	1.19
ROT	$Q_c = (96 \pm 1) f^{1.10 \pm 0.03}$	96	1.10
Mean	$Q_c = (83 \pm 1) f^{1.18 \pm 0.02}$	83	1.18
Lapse time 50 sec			
ADI	$Q_c = (100 \pm 1) f^{1.16 \pm 0.03}$	100	1.16
AHO	$Q_c = (128 \pm 1) f^{1.09 \pm 0.04}$	128	1.09
AYE	$Q_c = (97 \pm 3) f^{1.24 \pm 0.04}$	97	1.24
LED	$Q_c = (93 \pm 1) f^{1.20 \pm 0.03}$	123	1.09
ROT	$Q_c = (110 \pm 1) f^{1.11 \pm 0.03}$	110	1.11
Mean	$Q_c = (105 \pm 1) f^{1.16 \pm 0.02}$	105	1.16

Table 6.6. Mean value of Q_c at three lapse time windows for different frequencies along with standard errors.

Lapse time (sec)	1.5Hz $Q_c \pm \sigma$	3Hz $Q_c \pm \sigma$	6Hz $Q_c \pm \sigma$	9Hz $Q_c \pm \sigma$	12Hz $Q_c \pm \sigma$	18Hz $Q_c \pm \sigma$	24Hz $Q_c \pm \sigma$
30	109±33	209±63	539±166	964±313	1422±434	2255±601	3149±923
40	138±42	277±73	697±196	1181±321	1611±409	2458±591	3439±944
50	162±46	364±94	916±218	1454±346	1998±509	3041±833	3889±1165

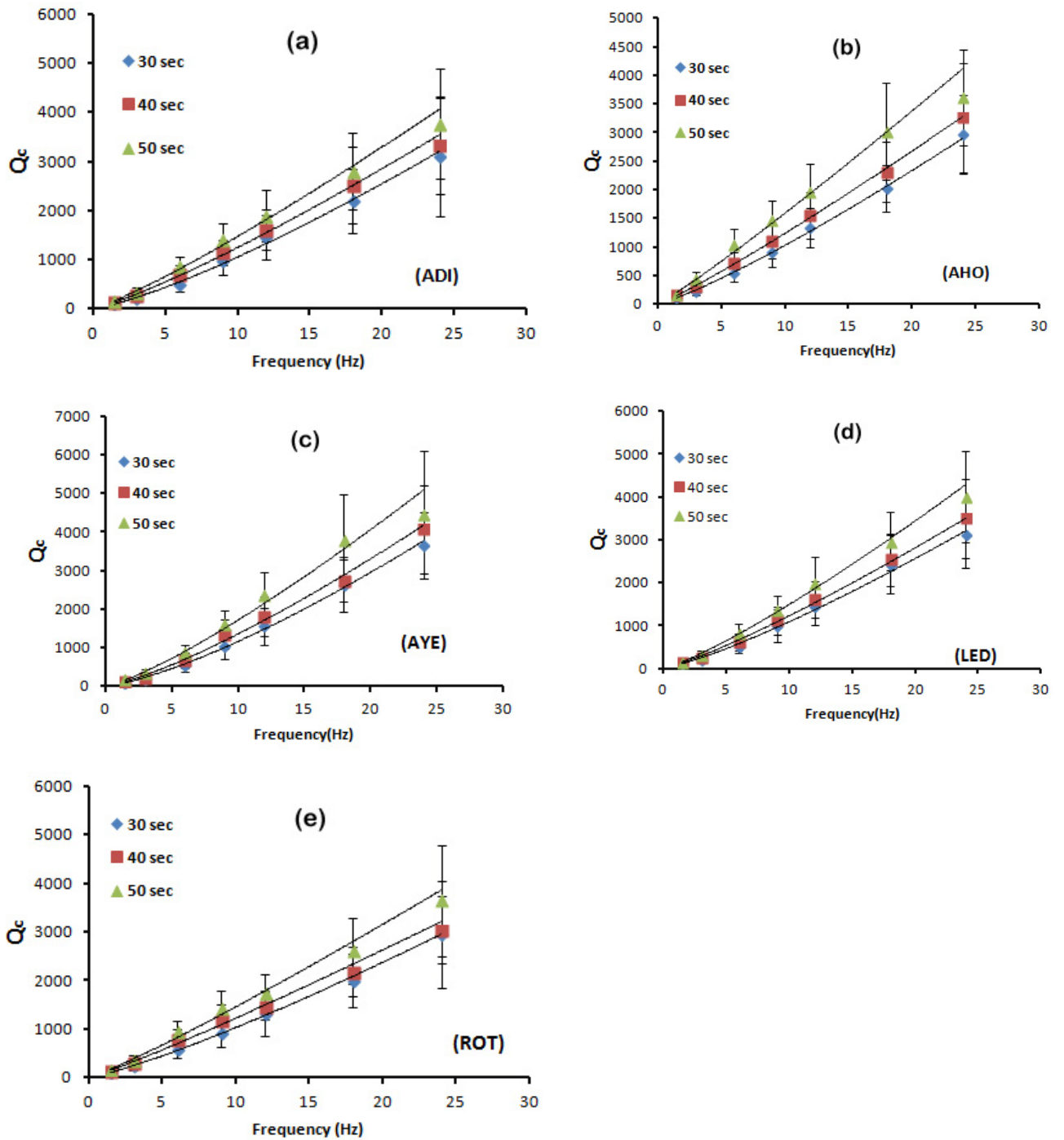


Fig.6.3. Plots of quality factors and central frequencies for all the five stations (a) to (e) and average with linear regression frequency dependent relationship (f), $Q_c = Q_0 f^n$ at different lapse time 30, 40 and 50 sec.

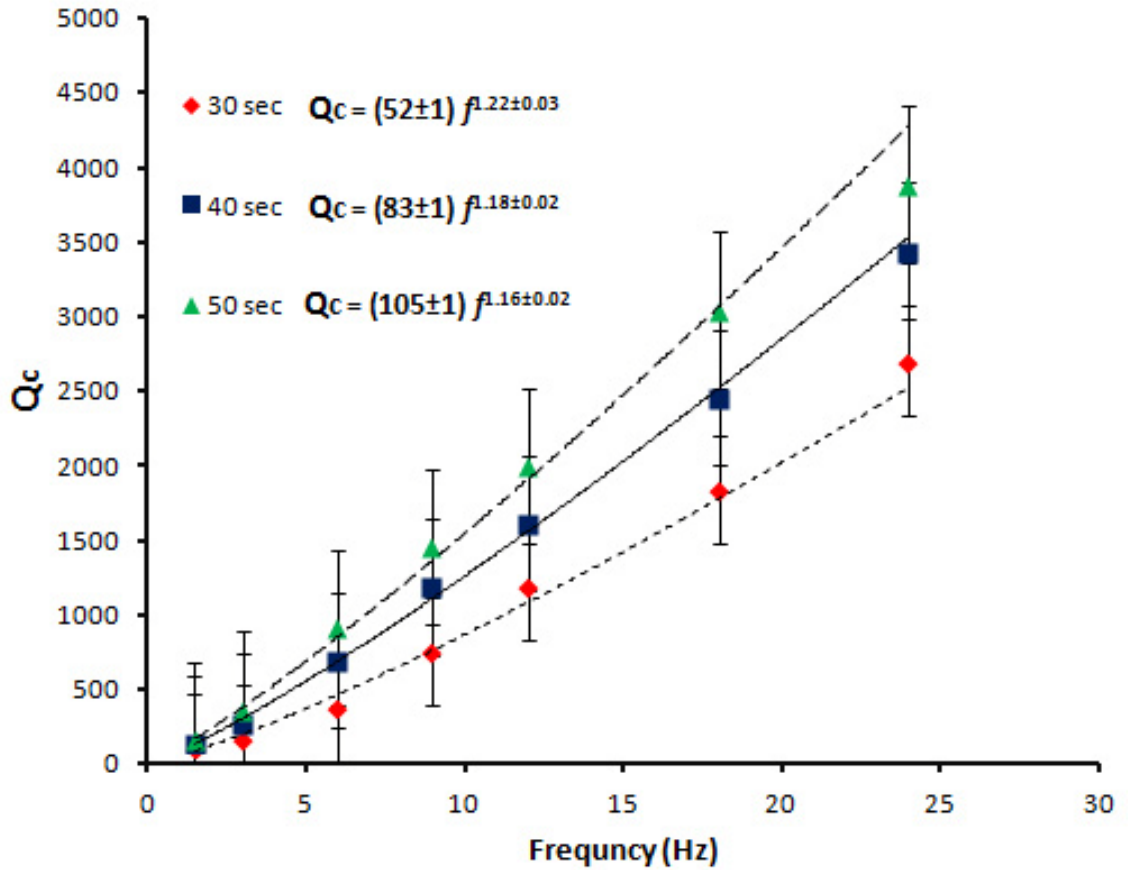


Fig.6.4. Plots of average quality factors and central frequencies with linear regression frequency dependent relationship $Q_c = Q_0 f^\eta$ at different lapse time window 30, 40 and 50 sec.

Table 6.7. Mean power law for the region for different lapse time 30, 40 and 50 sec.

Lapse time (sec)	Power law $Q_c = Q_0 f^\eta$	Q_0 (Q_c at 1 Hz)	η (frequency exponent)
30	$Q_c = (52 \pm 1) f^{1.22 \pm 0.03}$	52	1.22
40	$Q_c = (83 \pm 1) f^{1.18 \pm 0.02}$	83	1.18
50	$Q_c = (105 \pm 1) f^{1.16 \pm 0.02}$	105	1.16

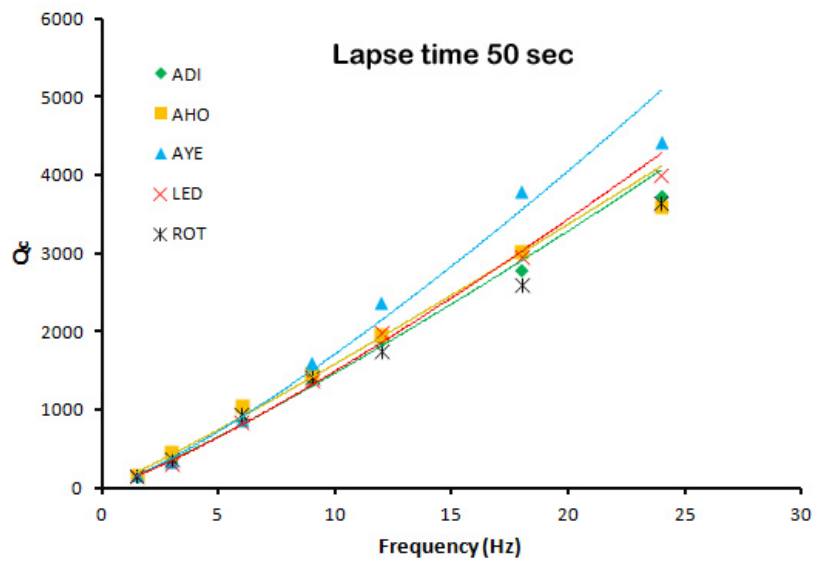
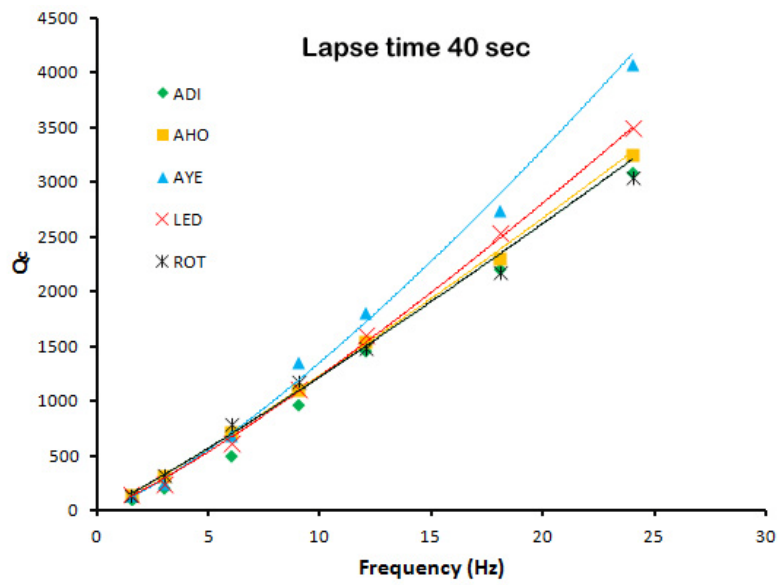
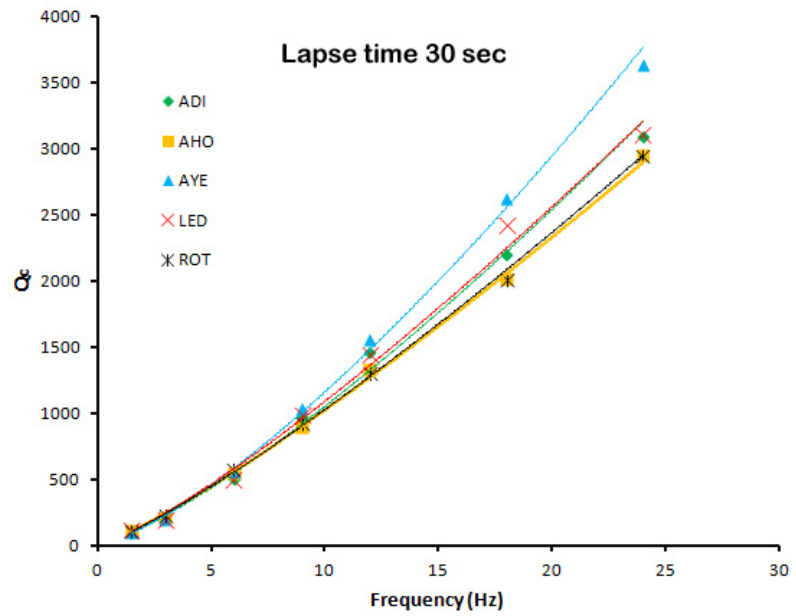


Fig. 6.5. Q_c variation with frequency at each station for lapse time window 30, 40 and 50 sec

From table 6.5, it has been observed that Q_0 values increases with lapse time for all stations. However estimated Q_c is not same for all the stations. This can be attributed to the heterogeneities present in the regions and/or difference in the distances of the events from the recording stations. Also the degree of frequency dependence is found higher in the tectonically active regions as compared with the stable regions. In most of tectonically active regions the η value are greater than 0.7 (Sharma et al., 2009), including Garhwal Himalaya (Gupta et al., 1995), Parlfeld (Hellweg et al., 1995), while in the stable regions it is 0.3 to 0.7 (Barros et. al. 2011). As per the seismic zoning map of India IS-2014, the study region is one among the highest seismic active region (zone-V). It is also indicated by high value of ' η '. It has been found that n value decrease with the lapse time window. The increase in Q_c and decrease in the value of η shows the depth dependent character as larger time window sampled the effect of deeper part of the Earth. Also, Woodgold (1994) explain the increase in Q_c with lapse time. He attributed the variation in Q_c to the factors like consideration of non-zero source receiver distance with anisotropic scattering and assumption of single scattering model instead of multiple scattering. In present study, the coda start time is twice the S-wave travel time. Hence, only back scattered waves are considered for analysis (Aki and Chouet, 1975). The multiple scattering effects are not important for local events where the lapse time less than 100 seconds (Gao et al., 1983). In the present study all the earthquakes are analyzed with lapse time window length less than 100 seconds using the single backscattering model. Hence, increase in Q_0 as well as decrease in η with increasing lapse time window in the studied region is attributed to decrease in heterogeneities with depth (Mukhopadhyay and Tyagi, 2007).

The Himalaya is tectonically active region and various seismological studies for wave attenuation were carried out for its different regions by researchers (e.g., Gupta et al., 1995; Gupta and Kumar, 2002; Paul et al., 2003, Kumar et al., 2014) as discussed earlier in the chapter. A comparison of Q_c estimated in the present study with that obtained by number of researchers the various study in various Indian regions has been shown in fig. 6.6. It is clear from the fig.6.6 that the Q_c for Lower Siang Region of Arunachal Himalaya is comparable to Garhwal Himalaya (Gupta et. al., 1995), Kumaun Himalaya (Paul et al., 2003), Koyna Region (Gupta et. al., 1998) and NE Himalaya (Hazarika et al., 2009). The Garhwal and Kumaun Himalaya are seismological highly active regions of Himalaya. Also, the Koyna is the classical example of reservoir induced seismicity. The ' η ' value in Lower Siang Region is found to be greater than the any other region and near to the NE region India (Table 6.8). It indicates that this region is the

highly seismically active in India. High ‘n’ value indicates that the study area is highly heterogeneous also. For lapse time window of 30 sec high values of ‘ η ’ found in the Kachchh region of Gujarat ($Q_c = 102f^{0.98}$ by Mandal et al., 2004; $Q_c = 106f^{1.11}$ by Gupta et al., 2006 and $Q_c = 148f^{1.01}$ by Sharma et al., 2008) because Kachchh region is also seismically active. In the study region, the value of Q_0 (Q_c at 1 Hz) is lower than any other region of India. It may also be due to the presence of many of criss-crossed fracture and dykes. In the most of Q_c studies it has been found that the regions located around the fault and composed of sedimentary rocks shows low Q_0 value. Hence the seismic wave energy rapidly attenuated when travel through such media. In the present study, it has been found that the relatively low Q_0 and high η value are corresponding to the high seismicity and heterogeneity of earth’s crust.

It has been observed that at AYE station the frequency dependence ‘ η ’ is higher than the other stations. This may be due to the AYE station is at the foothills. The Q_c estimated in the Lower Siang region of Arunachal Himalaya is comparable to other regions of the world (Fig 6.7) (Rovelli ,1982; Sherbaum and Kisslinger, 1985; Ambeh and lynch, 1993; Wilkie and Gibson, 1995; Mak et. al, 2004; Mahood and Hamzehloo, 2009; Barros et al, 2011). A comparative description of Q_0 and η obtained in present study with that obtained in different regions of the World is given in Table 6.9.

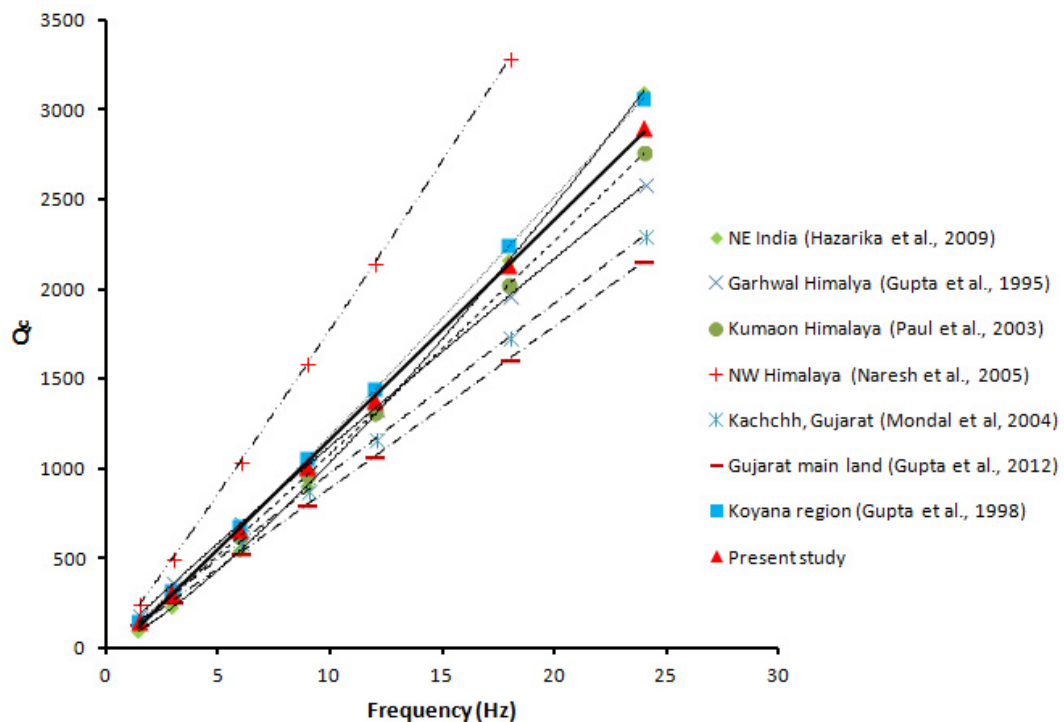


Fig.6.6 Comparison of Q_c values for Lower Siang Region of Arunachal Himalaya, India with the existing Q studies in India.

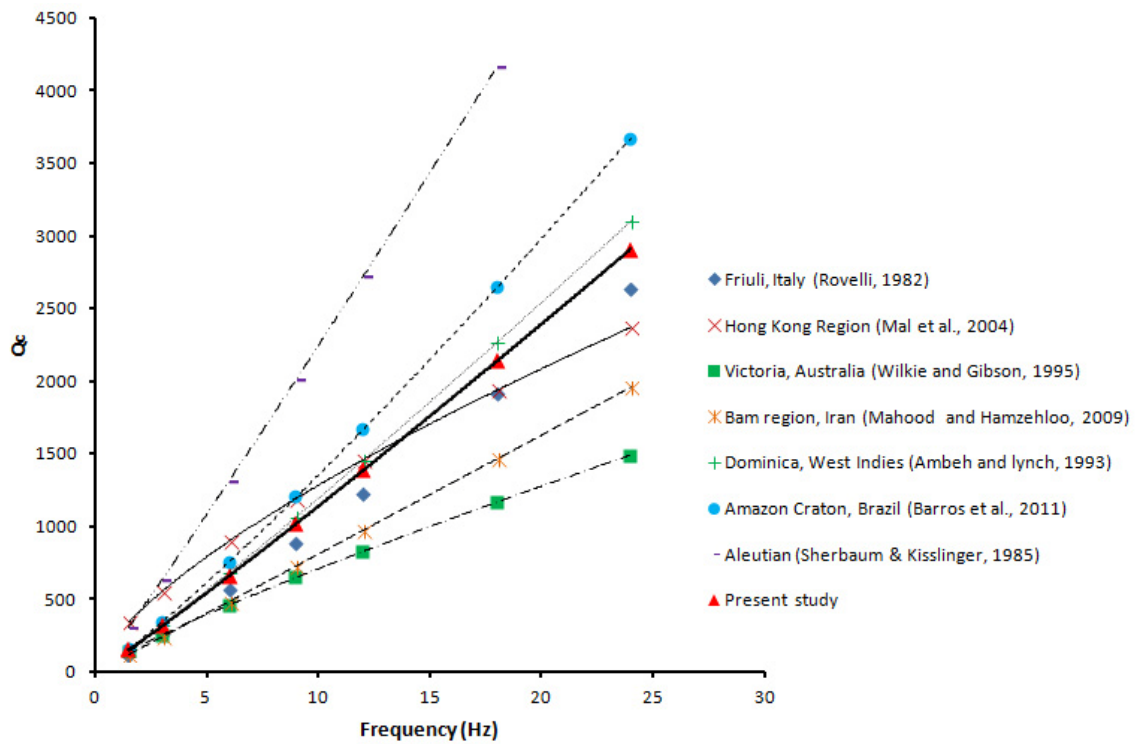


Fig.6.7. Comparison of Q_c values for Lower Siang Region of Arunachal Himalaya, India with the existing Q studies worldwide.

Table 6.8. Comparative study of observed Q_0 and n values for other regions of the India for 30 sec lapse time window.

Places	Q_0	n	source
Koyna Region	96	1.09	Gupta et. al.(1998)
Garhwal Himalaya	126	0.95	Gupta et. al.(1995)
Kumaun Himalaya	92	1.07	Paul et al. (2003)
Kachchh, Gujarat	102	0.98	Mondal et al (2004)
NW Himalayas	158	1.05	Naresh et al.(2005)
Mainland Gujarat	87	1.01	Gupta et. al. (2012)
North East region	86	1.01	Gupta and Kumar (2002)
Northeastern region	52	1.32	Hazarika et al. (2009)
Lower Siang region of Arunachal Himalaya	66 ± 8	1.2 ± 0.03	Present study

Table 6.9.Comparative study of observed Q_0 and n values for other regions of the World for 30 sec lapse time window.

Places	Q_0	n	source
Hong Kong	256	0.7	Mak et. al (2004)
Friuli, Italy	80	1.1	Rovelli (1982)
Bam region, Iran	79	1.01	Mahood and Hamzehloo (2009)
Victoria, Australia	100	0.85	(Wilkie and Gibson, 1995)
Dominica, West Indies	97	1.09	Ambeh and Lynch (1993)
Amazon Craton, Brazil	78	1.17	Barros et al (2011)
Aleutian	200	1.05	Sherbaum& Kisslinger (1985)

In this chapter the coda waves of 104 local earthquakes have been analyzed for three lapse time windows (30, 40 and 50sec) employing the single backscattering model at seven frequency bands with a central frequency in the range of 1.5 Hz to 24.0 Hz. Obtained Results show the average variation in Q_c is from 109 ± 33 , 138 ± 42 and 162 ± 46 at 1.5 Hz to 3149 ± 923 , 3439 ± 944 , and 3889 ± 1165 at 24 Hz for lapse time windows of 30, 40 and 50 sec, respectively. The frequency dependence relationships; $Q_c=(52\pm1)f^{1.22\pm0.03}$, $Q_c=(83\pm1)f^{1.18\pm0.02}$ and $Q_c=(105\pm1)f^{1.16\pm0.02}$ are obtained for lapse time windows of 30 , 40 and 50 sec respectively. The summary of results on coda wave attenuation is given in chapter 8.

Separation of Scattering and intrinsic Attenuations

7.1 INTRODUCTION

Seismic energy radiated from the source gets attenuated as it propagates through medium. This decay is partially due to distribution of energy on an expanding wavefront and partially due to medium properties. The dimensionless quantity called factor Q (Knopoff, 1964) is the efficiency of seismic energy propagation through a medium. The attenuation is expressed as the inverse of quality factor (Q^{-1}). It helps in understanding the physical mechanism of propagation of seismic wave through a medium. There are mainly two factors responsible for the absorption of seismic energy in the medium known as scattering and inelastic attenuation.

Intrinsic attenuations are the loss of energy due to anelasticity of the medium. This is basically the conversion of seismic energy in heat due to internal particles friction. Due to this elastic energy get absorbed in the medium. In an inelastic medium the seismic wave mechanical energy is withdrawn from each passing waves and get converted into another forms such as heat which is an irreversible phenomena. There are various phenomenons responsible for such loss. The collection of all is called absorption or intrinsic attenuation.

Aki (1980) describe the loss of amplitude of seismic energy due to heterogeneities distributed in the medium. Kikuchi (1981) studied scattering by distributed cracks and cavities. The best way to describe the scattering with referenced to laterally homogeneous media in which the travelling wavefronts can be tracked. In such medium the geometrical methods describes the propagation of seismic ray path. Wherever discontinuities encountered in ray the path the seismic energy get reflected and/or refracted. In case laterally close distributed obstacles or variation in elastic parameters the seismic energy get deflected known as scattering.

The scattering of seismic waves is basically the production of new secondary wave due to the heterogeneity distribution the medium. This description is applied in various areas. However this description seems to be oversimplified. In order to property

understand the scattering mechanism; it is essential to consider all the elements that take part in the process. The seismogram observed at local distance is mainly consisting of P-wave, S-wave and the converted waves. However, if high frequencies are considered the P to S and S to P conversions could be neglected (Knopoff and Hudson, 1964, 1967). The word heterogeneity means obstacles such as cracks, faults, variation in density and variation in velocity within a homogeneous media. In this case one needs to solve the inhomogeneous wave equations in a homogeneous medium where the scattering process is treated as a continuous medium. Such problem may become extremely complicated. Some researchers tried to explain the heterogeneity as discrete model with a random uniform distribution (Aki, 1969; Aki and Chouet, 1975; Dainty, 1981; Kikuchi, 1981). In such approach a space with average characteristics in which deviation in velocity, density or the Lamé parameters from their mean values produce random heterogeneities. The size of the heterogeneity (a), wavelength (λ), wave number (k) and product $P = k*a$ are main parameters on which the scattering depends. The seismic wave remains unaffected if $P \gg 1$ or $P \ll 1$. In all other cases the incident seismic wave gets scattered in various directions. In crustal studies the scattering effects are most significant (Wu and Aki, 1988). Due to inhomogeneous nature, geological media act as the scatterer for the waves traveled in the Earth medium. However in the deep interior of the Earth it is very small and is often neglected.

The attenuation is the reciprocal of quality factor (Q). The seismic wave attenuation can be estimated using P-wave (Q_α), S-wave (Q_β), coda waves (Q_c), and Lg waves (Q_{Lg}) recorded at local or regional distances. The attenuation computed using coda wave (Aki & Chouet 1975; Singh & Herrmann 1983; Sato & Fehler 1998; Gupta et al. 1998; Kumar et al. 2014) is the combined effect of scattering and intrinsic attenuation. The simultaneous knowledge of direct S-wave attenuation (Q_i) and coda wave attenuation (Q_c) is important to estimate the intrinsic attenuation (Q_i) and scattering (Q_s). The relative contribution of scattering and intrinsic attenuation is required for appropriate ground motion simulation and tectonic interpretation (Hoshihara 1993; Akinci et al. 1995; Del Pezzo et al. 1995; Bianco et al. 1999; Mukhopadhyay and Tyagi, 2008). Some researchers (Tsujiura, 1978; Aki, 1980) give more importance to scattering than intrinsic in quantification of physical properties of earth's crust while others (Frankel and Wennerberg, 1987) argued that intrinsic plays more important role. Although it is difficult to separate out the relative contribution of intrinsic attenuation and scattering attenuation from seismic wave attenuation but still efforts are being done to study the

contribution of intrinsic and scattering attenuation of the measured total attenuation. To separate these two one need to understand the total attenuation.

Aki (1969) and Aki and Chouet (1975) proposed the single back-scattering model to estimate the coda wave attenuation using local event data. Till date this method is successfully applied for coda wave attenuation estimation for local data. The basic assumption of this model is that the scattering is a weak process and that the scattering is much longer than the travel distance under consideration. The wave attenuation estimated using coda decay is the combination of both scattering and intrinsic attenuation. While Frankel and Wennerberg (1987) stated that intrinsic attenuation is dominant in coda wave attenuation while Tsujiura (1978) and Aki (1980) stated that scattering attenuation plays a more significant role than intrinsic attenuation. Wu (1985) developed a method to separate the scattering and intrinsic attenuation from the dependence of the entire *S*-wave energy on hypocentral distance. The method is based on the radiative transfer theory. He described two terms called seismic albedo $B_0 = \eta_s/(\eta_s+\eta_a)$ and medium's excitation coefficient $\eta_e = \eta_s + \eta_a$. Here η_s and η_a are the seismic absorption and scattering coefficients of the medium. In the solution of energy transfer equation the shape of seismic energy density spatial distribution depends on the seismic albedo and excitation coefficient of medium. For the perfectly scattering medium the B_0 is unity. The η_s and η_a can be calculated from B_0 and η_e for a medium having $B_0 \geq 0.5$ for isotropic or nearly isotropic scattering medium. On the other hand if there is large scale heterogeneities distributed in the medium then the separation of intrinsic and scattering becomes very difficult. Wu and Aki (1988) point out that in only two cases can the apparent attenuation be expressed as an exponential decay form. One case is corresponding to $B_0 \leq 0.5$ to known as dark medium case and another is corresponding to $B_0 \geq 0.5$ called bright medium case. In first case the absorption is dominant and the apparent attenuation (b) is given by the coherent wave scattering attenuation $b = (\eta_s+\eta_a)$. In second case when $B_0 \geq 0.5$ the scattering dominate over absorption. This is also known as diffuse scattering regime and the apparent attenuation is $b = d_0 (\eta_s+\eta_a)$. Here d_0 is known as diffusion constant and its value depends on seismic albedo. Hshiba et al. (1991) proposed another method based on Monte-Carlo simulation method. According to this method a seismogram along with direct waves consists of three parts namely: earlier, middle and latter part of coda waves. The middle and latter mainly composed of scattering. They numerically simulated the time integral of each portion's density functions based on the Monte-Carlo simulation and results are plotted against the hypocentral distance. The set of curve given by then are

very sensitive to seismic albedo and total attenuation strength. Hence enables the estimation of scattering and intrinsic attenuation by comparing the simulated curves with the time integrated energy density of observed seismogram.

Wennerberg (1993) proposed a methodology to estimate intrinsic attenuation (Q_i) and scattering (Q_s) using approximation given by Abubakirov and Gusev (1990) and scattering model developed by Zeng (1991). For this purpose Q_β and Q_c has been used. The numerical estimation of Q_i and Q_s . is based on the comparison of single backscattering model's coda shape and Zang model assuming the source and station are co-located. The approximation given by Wennerberg is also applicable for large lapse time if source and receiver are separated.

In this chapter the separation of intrinsic and scattering attenuation has been carried for the Lower Siang region of Arunachal Himalaya using Wennerberg's methodology. The mathematical expressions given by Wennerberg (1993) are reproduced here.

7.2 METHOD FOR ESTIMATION OF Q_s AND Q_i

The scattering (Q_s) and intrinsic (Q_i) attenuation can be estimated using the Wennerberg (1993) method. This method uses Q_c value estimated using the numerical correlation between the single scattering model (Aki and Chouet, 1975) and Zeng (1991). The relative contribution of Q_s and Q_i can be estimated by using the attenuation estimated using the direct S-wave (Q_β) and coda wave (Q_c) as:

$$\frac{1}{Q_\beta} = \frac{1}{Q_i} + \frac{1}{Q_s} \quad (7.1)$$

Wennerberg (1993) predicted that the observed value of Q_c can be expressed as the combination of Q_c and Q_i as:

$$\frac{1}{Q_c} = \frac{1}{Q_i} + \frac{1-2\delta t}{Q_s} \quad (7.2)$$

Here

$$\delta(\tau) = \frac{0.72}{4.44+0.738\tau} - 0.5 \quad (7.3)$$

$$\tau = \frac{\omega t}{Q_s} \quad (7.4)$$

where ω and t represents angular frequency and lapse time respectively. The Q_s and Q_i can also be express using Del Pezzo et al. (1995) expression as:

$$\frac{1}{Q_s} = \frac{1}{2\delta(\tau)} \left(\frac{1}{Q_\beta} - \frac{1}{Q_c(\tau)} \right) \quad (7.5)$$

$$\frac{1}{Q_i} = \frac{1}{2\delta(\tau)} \left(\frac{1}{Q_c} + \frac{2\delta(\tau)-1}{Q_\beta} \right) \quad (7.6)$$

Using the equations (7.2), (7.3) and (7.4), the following expression is obtained:

$$4.44 \left(\frac{1}{Q_\beta} - \frac{1}{Q_c} \right) Q_s^2 + \left[0.738 \left(\frac{1}{Q_\beta} - \frac{1}{Q_c} \right) \omega t - 5.88 \right] Q_s - 0.738 \omega t = 0 \quad (7.7)$$

Q_s is the positive root of the equation (7.7). So Q_s and Q_i can be obtained as function of lapse time for different frequencies because Q_c is measured as a function as lapse time.

7.3 RESULTS AND DISCUSSION

In order to separate the scattering and intrinsic attenuation characteristics of the crust of Lower Siang region of Arunachal Himalaya, independently estimated Q_β and Q_c have been used employing the Wennerberg method (1993). For this purpose, Q_c value estimated using at three lapse time windows 30, 40 and 50 sec have used (given in chapter 6). The term 't' in equation (7.7) is the confusing term because in most of literature it is simply described as lapse time i.e. the time measured from earthquake origin time. But corresponding to which wave type of the waveform is not given. Lorenzo et al. (2013) explained the time 't' as the lapse time window length used in the estimation of Q_c . Since Q_c is lapse time dependent so the Q_i and Q_s estimated using Q_c are also time lapse time dependent. The estimated Q_i and Q_s values obtained from Q_c and Q_β at different lapse time window are listed in Table 7.1. The average value of Q_s varies from 49, 75 and 92 at 1 Hz to 913, 1437 and 1679 at 24 Hz for lapse time window of 30, 40 and 50 sec respectively. Similarly average value of Q_i varies from 84, 205 and 244 at 1 Hz to 1499, 3739 and 3520 at 24 Hz for lapse time window of 30, 40 and 50 sec respectively. From estimated Q_s and Q_i values are plotted as a function of frequency as shown in Fig. 7.1a and 7.1 b power laws; $Q_s = Q_0 f^\eta$ and $Q_i = Q_0 f^\eta$ for each lapse time window are obtained. the Q_0 (quality factor at 1 Hz) and frequency dependent ' η ' estimated using different lapse time window is shown in table 7.2. The average scattering relationships for the region are $Q_s = (31 \pm 1) f^{1.04 \pm 0.02}$, $Q_s = (48 \pm 1) f^{1.05 \pm 0.02}$ and $Q_s = (61 \pm 1) f^{1.05 \pm 0.02}$ and the average intrinsic relationships for the region are

$Q_i=(68\pm 1)f^{0.95\pm 0.06}$, $Q_i=(134\pm 1)f^{1.01\pm 0.05}$ and $Q_i=(167\pm 1)f^{0.96\pm 0.03}$ for lapse time windows of 30, 40 and 50 sec, respectively (fig.7.1.a,b and Table 7.2).

Table 7.1. Q_c , Q_β , Q_s and Q_i values in frequency range 1.5-24 Hz for 30, 40 and 50 sec lapse time windows.

Freq. (Hz)	Q_c	Q_β	Q_s	Q_i	Q_s^{-1}	Q_i^{-1}	$B_0 = \frac{Q_s^{-1}}{Q_s^{-1} + Q_i^{-1}}$
30 sec							
1.5	109±33	118±6	49	84	0.020399	0.011924	0.63
3	209±63	163±4	101	269	0.009853	0.003718	0.73
6	539±166	418±5	189	347	0.005278	0.002886	0.65
9	964±313	727±5	320	572	0.003125	0.00175	0.64
12	1422±434	1161±5	423	666	0.002363	0.001501	0.61
18	2255±601	1803±6	632	972	0.001584	0.001029	0.61
24	3149±923	2335±5	913	1499	0.001095	0.000667	0.62
40sec							
1.5	138±42	118±6	75	205	0.013352	0.004878	0.73
3	277±73	163±4	-	-	-	-	-
6	697±196	418±5	-	-	-	-	-
9	1181±321	727±5	-	-	-	-	-
12	1611±409	1161±5	677	1624	0.001477	0.000616	0.71
18	2458±591	1803±6	986	2176	0.001014	0.00046	0.69
24	3439±944	2335±5	1437	3739	0.000696	0.000267	0.72
50 sec							
1.5	162±46	118±6	92	244	0.010859	0.004106	0.73
3	364±94	163±4	-	-	-	-	-
6	916±218	418±5	-	-	-	-	-
9	1454±346	727±5	-	-	-	-	-
12	1998±509	1161±5	891	1975	0.001122	0.000506	0.69
18	3041±833	1803±6	1246	2487	0.000803	0.000402	0.67
24	3889±1165	2335±5	1679	3520	0.000596	0.000284	0.68

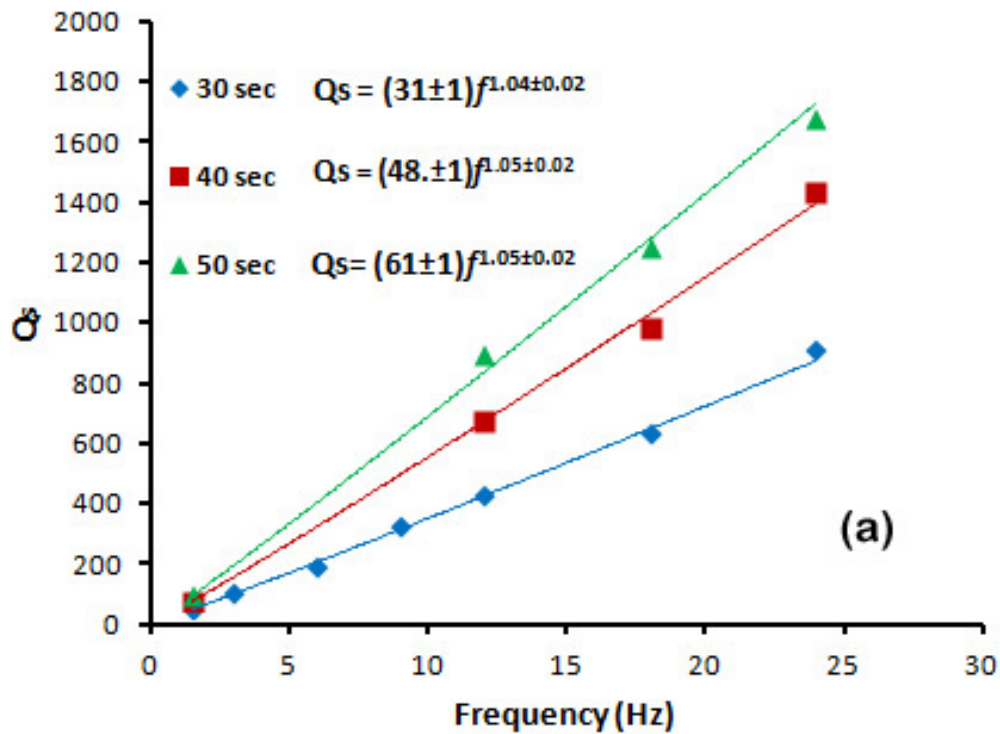
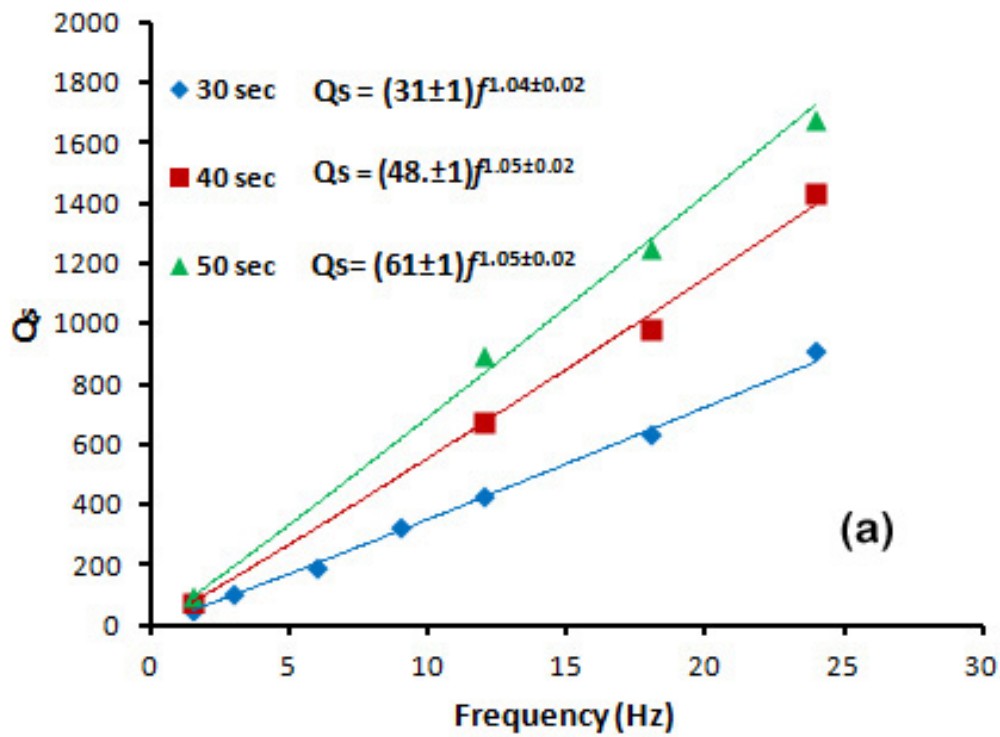


Fig 7.1 (a) Plots of average quality factors and central frequencies with linear regression frequency dependent relationship $Q_s = Q_0 f^{\beta}$ **(b)** Plots of average quality factors and central frequencies with linear regression frequency dependent relationship $Q_i = Q_0 f^{\beta}$ at various lapse time window

Table 7.2 Mean power laws for the region for different lapse time 30, 40 and 50 sec.

Lapse time (sec)	Power law $Q_s = Q_0 f^\eta$	Power law $Q_i = Q_0 f^\eta$
30	$Q_s = (31 \pm 1) f^{1.04 \pm 0.02}$,	$Q_i = (68 \pm 1) f^{0.95 \pm 0.06}$,
40	$Q_s = (48 \pm 1) f^{1.05 \pm 0.02}$	$Q_i = (134 \pm 1) f^{1.01 \pm 0.05}$
50	$Q_s = (61 \pm 1) f^{1.05 \pm 0.02}$	$Q_i = (167 \pm 1) f^{0.96 \pm 0.03}$

From Table 7.2, it can be noted that in the form of power law $Q_s = Q_0 f^\eta$ the value of Q_0 (Q_s at 1 Hz) increases with the lapse time. As in the case of coda wave attenuation larger lapse time sampled the effect of larger depth. Also, it is well known that the heterogeneities decrease with depth. So the increase in Q_0 may be attributed to the decrease in heterogeneity in the crust of Lower Siang region of Arunachal Himalaya. From the laws of intrinsic attenuation $Q_i = Q_0 f^\eta$, it is observed that Q_0 (Q_i at 1 Hz) also increase with lapse time window. Various researchers e.g., Roecker et al. (1982), Woodgold (1994), Del Pezzo et al. (1995), Mukhopadhyay and Tyagi (2008), Mahood and Hamzehloo (2011) argued that the increase in Q_0 could imply that energy loss due to dissipation is decreases with increasing depth. It may show that with increase in depth the rocks become more and more compacted which is initially due to increase in pressure. As a result relative motion of grains decreases and the inter-grain friction decreases with increasing depth. So the intrinsic attenuation decreases with increasing depth. In the chapter 6 we observed the same character of Q_c with lapse time as Q_s and Q_i . But there is a decrease in the frequency exponent ‘ η ’ with lapse time while it almost remain constant for both Q_s and Q_i .

The comparison of Q_β and Q_c with Q_i and Q_s (Fig. 7.2) shows that both Q_i and Q_s are lower than the Q_β as well as Q_c at 30 sec lapse time. As the lapse time increases both Q_i and Q_s increases in such a manner that Q_c will increase as it contains the effect of both (Wennerberg, 1993). This agrees with the theoretical as well as the laboratory measurements. Also, Q_c is higher than Q_β , it supports the model given by Zeng et al. (1991) which predict the combination of Q_i and Q_s should be such that Q_c is more than Q_β .

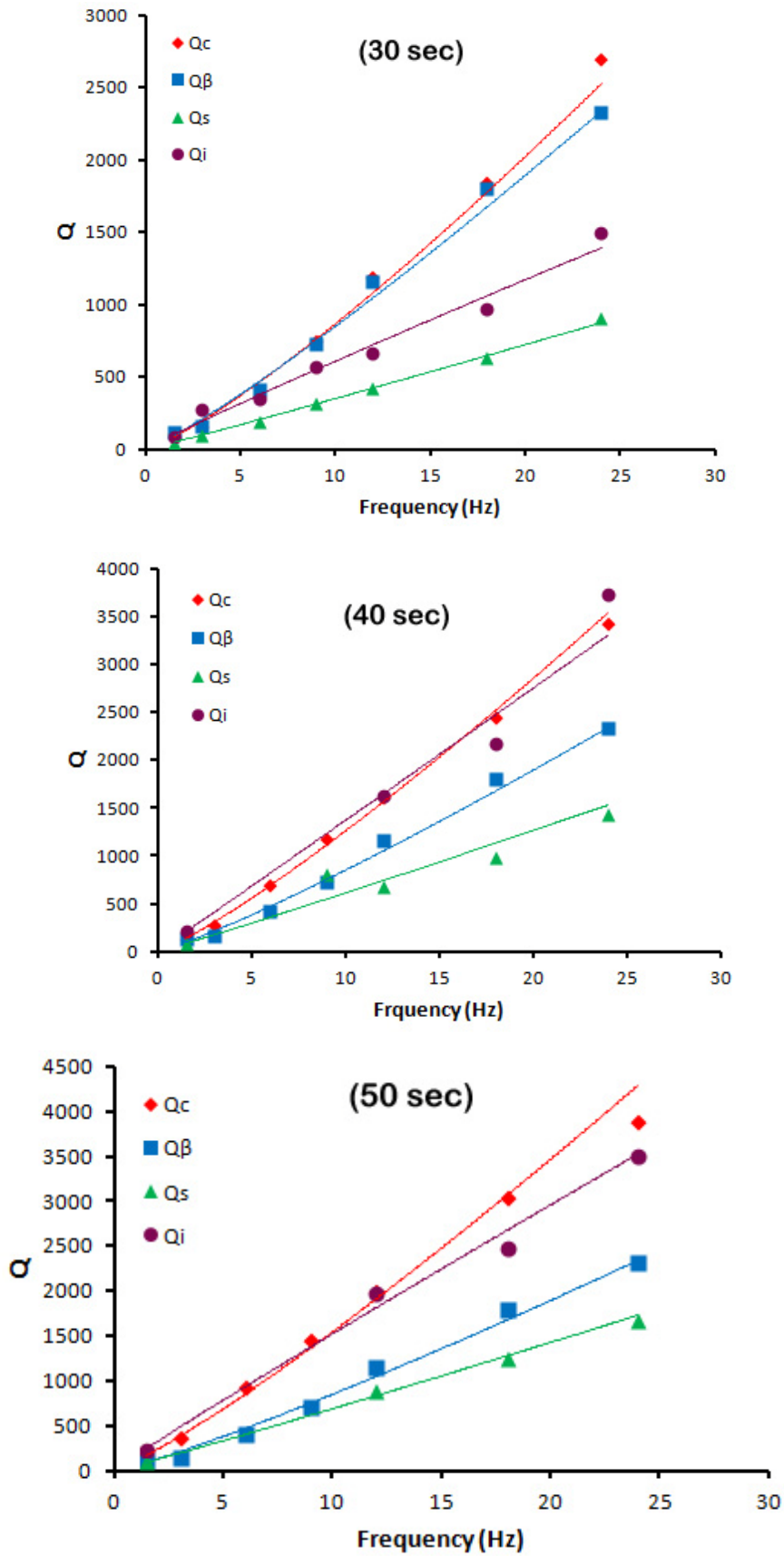


Fig. 7.2 Average values of Q_c , Q_β , Q_s and Q_i at different frequencies for the Lower Siang region along with the least-squares best-fitted lines at different lapse time window.

Another important parameter is the Seismic albedo (B_0) which is ratio of scattering attenuation to total attenuation. If seismic albedo greater than 0.5 then the scattering is dominant in the region else intrinsic attenuation dominates. In the present study, B_0 is greater than 0.5 at three lapse time windows which indicates that scattering is dominates for in the frequency range 1.5 to 24 Hz.. It is also observed that with lapse time 30 to 40 sec seismic albedo increases at all frequency which indicates that the relative attenuation contribution of scattering is greater that the intrinsic attenuation. As the lapse time increases from 40 to 50 sec then there is not a great variation in the seismic albedo indicating that the rock mass at depth sampled at two lapse times is behaving same. The region consists of conglomerates, quartzite, boulders bed, sandstone with reddish shale and various tectonic features. At 30 sec lapse time the sampled depth is low as compared with the 40 and 50 sec. so these near surface heterogeneities and particle friction in these rocks lower both intrinsic and scattering attenuation. As the depth increases the homogeneity of the medium increases and the particle friction also decreases due to increase in pressure. Hence our results also agree with the geology of area.

The comparison of obtained results has been made with Indian as well other worldwide studies. The Q_s obtained in the present study are compared with the other seismically active region of India such as Garhwal Himalaya (Simanchal Padhy, 2009), Chamoli region (Sharma, 2014), NW Himalaya (Mukhopadhyay et al., 2006), Bhuj, Gujrat (Padhy, 2007) etc. The Q_s value is close to the Chamoli region (Sharma, 2014) upto 18 Hz and close to Northwestern Himalaya 24 Hz (Fig. 7.3 a). The obtained scattering relations are found to be comparable with the other worldwide studies ((Fig. 7.3 b). The Q_i values also compared with Indian as well as other seismically active regions of the world. It is observed that the Q_i is close to the Chamoli (Sharma, 2014) and NW Himalaya (Mukhopadhyay and Tyagi, 2008). Hence both Q_i and Q_s are close to the Chamoli and NW Himalaya which may be due to fact that being a part of Himalayan Mountain range there is not a great variation in the local geology of these three areas. Obtained Q_i value is also comparable with the other worldwide studies as shown in Fig. 7.4.

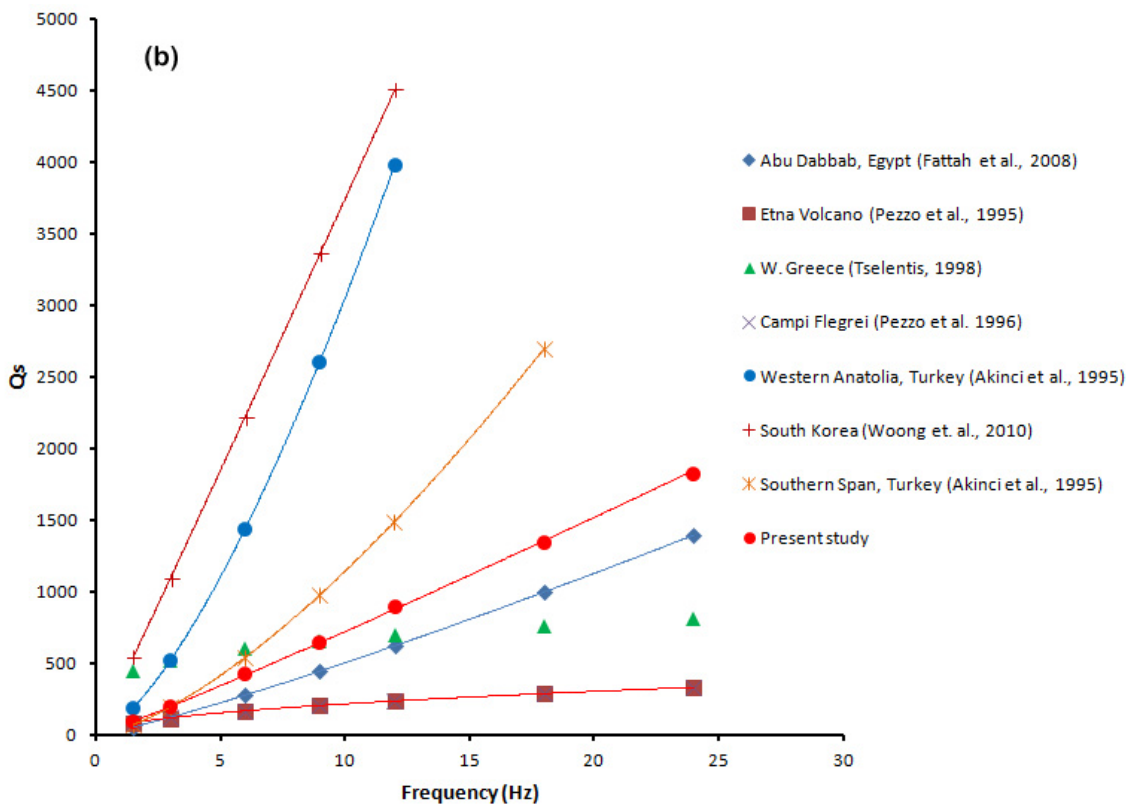
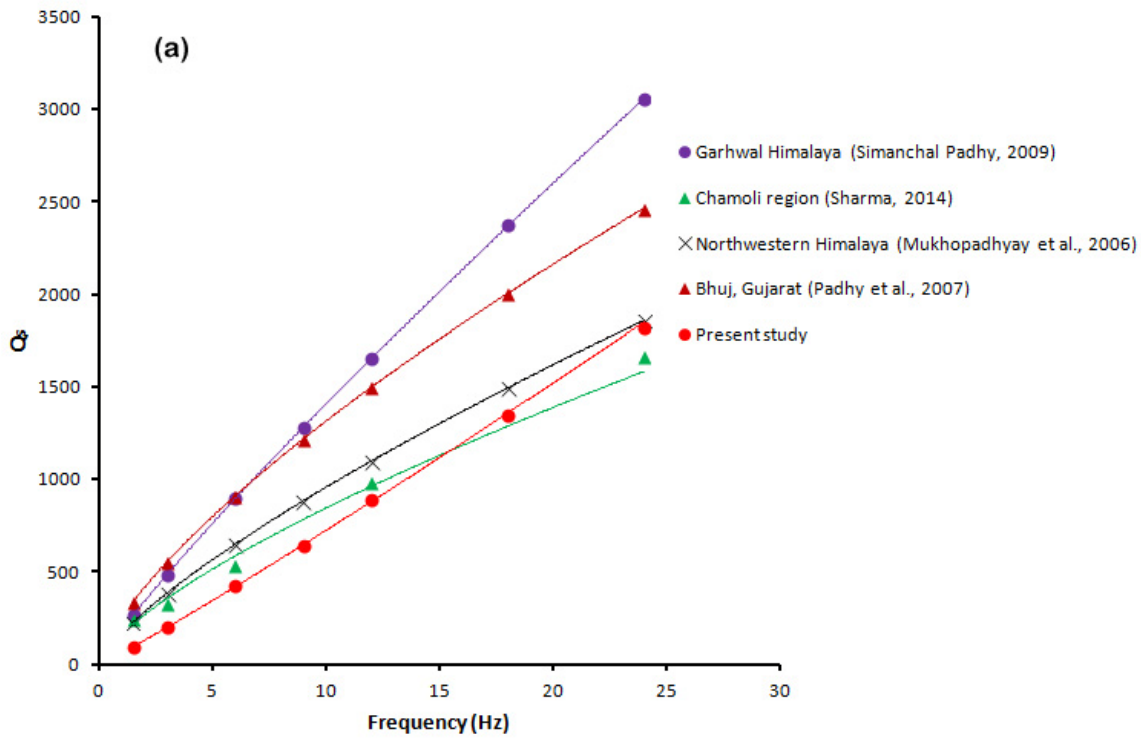


Fig. 7.3 Comparison of quality factor for scattering attenuation (Q_s) with other region of India and World.

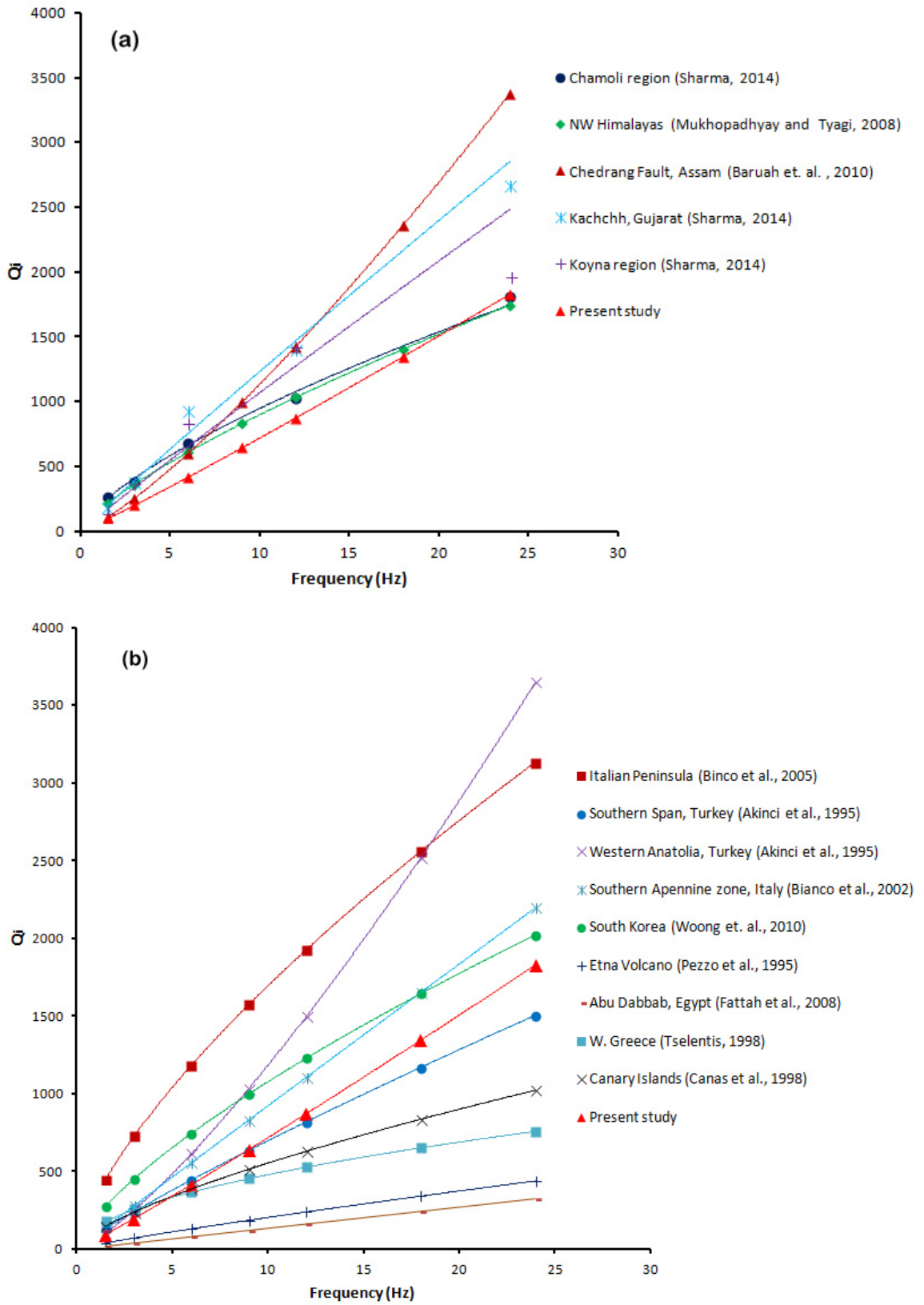


Fig. 7.4. Comparison of quality factor for intrinsic attenuation (Q_i) with other region of India and World.

In this chapter The separation of scattering (Q_s) and intrinsic (Q_i) attenuation from the S-wave attenuation (Q_β) and coda wave attenuation (Q_c) has been carried out employing the Wennerberg (1993) method and developed the frequency dependent Q_s and Q_i relations. The Q_i and Q_s show the frequency dependent character in the frequency range 1.5 to 24 Hz. The average scattering and intrinsic relationships are obtained for the region as $Q_s=(31\pm 1)f^{1.04\pm 0.02}$, $Q_s=(48\pm 1)f^{1.05\pm 0.02}$ and $Q_s=(61\pm 1)f^{1.05\pm 0.02}$ and $Q_i=(68\pm 1)f^{0.95\pm 0.06}$, $Q_i=(134\pm 1)f^{1.01\pm 0.05}$ and $Q_i=(167\pm 1)f^{0.96\pm 0.03}$ for lapse time windows of 30 , 40 and 50 sec, respectively. Both Q_c and Q_i at a given frequency increases with lapse time duration. This can be attributed to the decreases in the heterogeneities and the inter-grain fraction with increase in depth as larger the lapse time represents the characteristics of deeper depths. Q_i and Q_s comparison and values of seismic albedo shows that scattering attenuation is more prominent over intrinsic attenuation in the region over entire frequency range 1.5 to 24 Hz. The summary of results on separation of scattering (Q_s) and intrinsic (Q_i) attenuation is given in chapter 8.

Summary of Results and Conclusions

8.1 INTRODUCTION

The present work has started with objectives to estimate the source parameters and wave attenuation characteristics of the part of Arunachal Pradesh. The study has carried out using a data set of 104 local earthquakes recorded through a five station seismological station operated in Lower Siang region of Arunachal Himalaya. The source parameters source parameters; seismic moment (M_0), source radius (r) and stress drop ($\Delta\sigma$) have been estimated employing Brune's model (1970, 1971). Along-with the source parameters, moment tensor solutions of 104 earthquakes have also been estimated using the ISOLA, developed by Sokos and Zahradník (2008) and works on the basis of iterative deconvolution .

The seismic attenuation characteristics have also been estimated from the body waves and coda waves part of seismogram. The extended coda normalization method given by Yoshimoto et al. (1993) is used for simultaneous measurement of quality factor for P-wave (Q_α) and for S-wave (Q_β). The Q is estimated under the assumption that P- to S-wave radiation have same spectral ratio within some magnitude range within narrow frequency range. The frequency of Q_α and Q_β dependent relationships has developed for the study region. In addition to the estimation of Q_α and Q_β , the Coda wave attenuation characteristics are also computed. The single scattering model proposed by Aki and Chouet (1975) is used to estimate the quality factor of coda waves (Q_c) of local earthquakes in high frequency range. According to this model the coda waves are comprised of backscattered S-waves generated within an unbounded, homogeneous and isotropic medium. The scatters distributed randomly and two dimensionally in the earth's crust and upper mantle. The model assumes that scattering is a weak process and outgoing waves are scattered only once before reaching the receiver and source and receiver are co-located. The frequency dependent Q_c relation has also been also developed for the study region.

The Q_β and Q_c are considered as the combination of scattering (Q_s) and intrinsic (Q_i) attenuations. The relative contribution of scattering and intrinsic attenuations is separated using Wennerberg's (1993) method. The methodology adopted for analysis of data and results obtained on source parameters, moment tensor analysis and attenuation characteristics are presented in chapter 3, 4, 5, 6, and 7. In this chapter the results obtained on each component are summarized.

8.2 SUMMARY THE RESULTS OF SOURCE PARAMETERS

The results on the source parameters and f_{\max} have been obtained for the Lower Siang region of Arunachal Himalaya from the analysis of 104 local earthquakes. The results showed that the values of seismic moment, Moment magnitude, the source radii and stress drops varies from 1.6×10^{18} to 3.1×10^{23} dyn-cm, 1.4 to 5.0, 157.8 to 417.1 m and 0.1 to 74 bars respectively. Except a few events, the stress drop remains constant and does not vary with focal depth. Hence no dependency of stress drops with depth is obtained for the study region that indicates that the stress drop is only the function seismic moment and fracture radius. Based on results on seismic moment and corner frequency, the scaling relation $M_0 \propto f_c^{-3.27}$ has been obtained for the study region. $\Delta\sigma$ relationships with M_0 , $\log(\Delta\sigma) = 0.1804 \log(M_0) - 2.945$ is also obtained for the study region. Satoh et al. (2000) obtained a relationship $\log(\Delta\sigma) = -2.91 \log(M_0) + 5.8$ using deep borehole data of Japan. The results obtained in present study are seems to be more realistic than Satoh et al. (2000). Satoh et al. (2000) relationship suggests stress drop increases as the seismic moment decreases. But in real scenario it is not possible because lower magnitude event can never have stress drop greater than high magnitude event.

The results have been obtained based on the comparative study of f_c and f_{\max} showed that both f_c and f_{\max} behaves in a similar manner with respect to source, focal depth and epicentral distance. From the various plots of both f_c and f_{\max} with seismic moment, focal depth, epicentral distance at different recording site showed the same amount of scatters and trends in the distribution of data. From this, it is observed that f_{\max} is having almost similar behavior to seismic moment as obtained for f_c to the seismic moment. For this it is brought out that f_{\max} is due to source process because it is affected by source as well as site in similar way as f_c and it is well known that f_c is the source property so f_{\max} is also a source effect. Both f_c and f_{\max} are found to be independent of epicentral distance and

depth of occurrence. Relationship of f_{\max} with seismic moment and stress drop has also been obtained.

8.3 SUMMARY OF RESULTS ON MOMENT TENSOR SOLUTIONS

In the present study efforts have been made to manifest the source of non-DC (CLVD) component of MTs. from the moment tensor analysis of 104 local earthquakes. The moment tensor analysis of 41 earthquakes out of 104 earthquakes having magnitude greater than 2.5 and signal to noise ratio (SNR) greater than 6 with small epicentral distances brought out more clarity in the identification of cause of CLVD. It has also been observed that variation in CLVD caused by various source such as noise in the data, focal depth and magnitude of the event. Source depth acts a controlling factor of CLVD. For selected 41 events the high CLVD component confined to shallow depth. For high SNR the CLVD% is quite low. CLVD is also dependent on the magnitude of event. In the higher magnitude range greater than 3.5, DC% is greater than 60%. Hence most of high magnitude earthquakes are having double couple (DC) source mechanism. The appearance of CLVD in low magnitude may also be attributed to the directivity effect (Adamova and Siley, 2010).

8.4 SUMMARY OF SEISMIC WAVE ATTENUATION USING BODY WAVES

The seismic wave attenuation has been studied for Lower Siang region by estimating the quality factor of P-wave (Q_α) and S-waves (Q_β) in the frequency range 1.5 to 24 Hz adopting the extended coda normalization method. The estimated value of Q_α and Q_β are found to be strongly frequency dependence in the study region. Their mean values vary from 49 ± 4 at 1.5 Hz to 1421 ± 6 at 24 Hz for Q_α and from 118 ± 6 at 1.5 Hz to 2335 ± 5 at 24 Hz for Q_β . The frequency dependence Q_α and Q_β relationships are obtained as, $Q_\alpha = (25 \pm 1)f^{(1.24 \pm 0.04)}$ for P-wave and $Q_\beta = (58 \pm 1)f^{(1.16 \pm 0.04)}$ for S-wave. The comparison of Q_α and Q_β has brought out that P wave attenuates more rapidly as compared to S-wave at all frequencies.

The results obtained in the present study are found to be comparable with the other seismically active regions of the India as well as world. The comparison of Q_α and Q_β with the other seismically active regions of India showed that the region around the Lower Siang is more attenuating among almost all Indian regions except the Chamoli

region which showed higher attenuation, whereas the comparison among some regions of World showed similarly increasing pattern with increasing frequency. The higher frequency dependence of attenuation describes the region is high seismically active. Also low value of Q_α and Q_β in the Lower Siang region as compared to other Indian regions indicate the high tectonic activity. Higher Q_β than Q_α for the entire frequency range indicate the crust of the Lower Siang region of Arunachal Himalaya is highly heterogeneous.

8.5 SUMMARY OF RESULTS ON SEISMIC WAVE ATTENUATION USING CODA WAVES

The coda waves of 104 local earthquakes have been analyzed for three lapse time windows (30, 40 and 50sec) employing the single backscattering model at seven frequency bands with a central frequency in the range of 1.5 Hz to 24.0 Hz. Obtained Results show the average variation in Q_c is from 109 ± 33 , 138 ± 42 and 162 ± 46 at 1.5 Hz to 3149 ± 923 , 3439 ± 944 , and 3889 ± 1165 at 24 Hz for lapse time windows of 30, 40 and 50 sec, respectively. The frequency dependence relationships; $Q_c=(52\pm1)f^{1.22\pm0.03}$, $Q_c=(83\pm1)f^{1.18\pm0.02}$ and $Q_c=(105\pm1)f^{1.16\pm0.02}$ are obtained for lapse time windows of 30, 40 and 50 sec respectively. So in the study region Q_c is found to be function of frequency and lapse time window and Q_c increase with increase of frequency as well as lapse time window. The increase in Q_c value with the time window is attributed to the increase in Q_c with depth because heterogeneities of the medium decreases with depth. In the frequency dependent relation given above Q_0 (Q_c at 1 Hz) value increases with the lapse time window while there is a nominal decrease in the degree of frequency dependence (η) with increasing window length. This may be due to decrease in scattering effect and hence the decrease heterogeneities of the medium with depth. The comparison of Q_c value obtained in the Lower Siang region with that obtained in other part of India and World showed that Siang region is tectonically active.

8.6 SUMMARY OF RESULTS ON SEPARATION OF SCATTERING AND INTRINSIC ATTENUATIONS

The separation of scattering (Q_s) and intrinsic (Q_i) attenuation from the S-wave attenuation (Q_β) and coda wave attenuation (Q_c) has been carried out employing the Wennerberg (1993) method and developed the frequency dependent Q_s and Q_i relations.

The Q_i and Q_s show the frequency dependent character in the frequency range 1.5 to 24 Hz. The average scattering and intrinsic relationships are obtained for the region as $Q_s=(31\pm 1)f^{1.04\pm 0.02}$, $Q_s=(48\pm 1)f^{1.05\pm 0.02}$ and $Q_s=(61\pm 1)f^{1.05\pm 0.02}$ and $Q_i=(68\pm 1)f^{0.95\pm 0.06}$, $Q_i=(134\pm 1)f^{1.01\pm 0.05}$ and $Q_i=(167\pm 1)f^{0.96\pm 0.03}$ for lapse time windows of 30, 40 and 50 sec, respectively. Both Q_c and Q_i at a given frequency increases with lapse time duration. This can be attributed to the decreases in the heterogeneities and the inter-grain fraction with increase in depth as larger the lapse time represents the characteristics of deeper depths. Q_i and Q_s comparison and values of seismic albedo shows that scattering attenuation is more prominent over intrinsic attenuation in the region over entire frequency range 1.5 to 24 Hz.

Various studies of Q in various regions of the world show high Q -value in seismically stable regions and relatively low Q value in the seismically active regions. The Q -values and their frequency dependent relationships estimated in the present study are well correlate with highly seismically active and heterogeneous regions. The frequency dependent attenuation relations developed in present study would be useful in various scientific and engineering applications including earthquake hazard assessment, earthquake source parameter estimation and understanding the physical phenomenon related earthquake elastic energy propagation of Lower Siang region as well as other regions of Arunachal Himalaya and NE region as a whole.

8.7 LIMITATIONS OF THE PRESENT STUDY

As the present study on the estimation of source parameters, moment tensor solutions, seismic wave attenuation characteristics of the Lower Siang region of Arunachal Himalaya is based on the small data set of local 104 earthquakes falling in the magnitude range 1.4 to 5.0 recorded through a five station seismological network. Most of events lie outside the seismological networks and having poor azimuthal coverage. Therefore, to understand the source as well as path characteristics a larger data set with a larger stations network is needed.

8.8 SUGGESTIONS FOR THE FURTHER STUDY

Following are the suggestions for future studies:

1. In many observational studies it has been observed that corner frequency is affected by the local site characteristics. Hence examination of this fact is required using a good data set.
2. To understand the f_{\max} whether it is the property of earthquake source, path or site, a small to moderate sized earthquake data is needed.
3. To study breakdown of self-similarity high resolution broadband data, preferably from boreholes, is needed to be analyzed.
4. Dependence of non-DC component of MTs on source and site need to be quantified. So to resolve the mystery a high magnitude data set with a good azimuthal coverage is needed.
5. In low magnitude range, we suggest the further inspection as done by Fojtikov et al., 2010, Stierle et al., 2014a,b and Vavrycuk, 2001. They showed that the positive correlation between the ISO and CLVD can be an indicator of the presence of tensile faulting. In present study, the positive correlation between the ISO and CLVD could not be achieved as deviatoric MT method has been used for the analysis of the data because data set with poor azimuthal coverage is available.
6. To resolve the non-DC (CLVD) of moment tensor completely in a given region a small to moderate sized earthquake data set with good azimuthal coverage is needed.
7. The work on comparison of attenuation studies carried out using strong motion data and weak motion of local earthquakes can be done for a region.

Appendix I

Table I.1 Hypocenter parameters estimated by hypocenter location program- HYPOINVERSE.

S.N.	Date	Time	Lat.	Long.	Depth (Km)	Mag. (M _L)	RMS sec	ERH Km	ERZ Km
	DD/MM/YYYY	HR MN SS	DEG MN North	DEG MN East					
001	24/07/2011	23 11 37.14	28 49.07	95 40.49	09.42	1.9	0.07	1.21	0.62
002	26/07/2011	12 59 38.40	27 28.65	95 46.29	42.52	3.1	0.08	1.16	0.33
003	29/07/2011	10 41 41.26	28 08.26	94 54.74	24.40	1.9	0.10	1.16	1.24
004	29/07/2011	11 28 49.28	28 55.52	95 33.65	08.02	2.2	0.06	1.45	0.63
005	31/07/2011	13 45 20.47	28 56.37	95 42.60	06.00	1.9	0.09	2.50	1.90
006	02/08/2011	21 55 23.48	28 12.45	95 12.07	31.35	1.7	0.14	0.58	3.73
007	05/08/2011	20 29 42.18	28 28.80	95 17.62	11.26	2.3	0.25	2.14	2.78
008	08/08/2011	19 25 02.30	28 40.61	95 45.46	43.88	2.2	0.18	2.63	0.51
009	09/08/2011	19 14 42.54	27 54.23	94 49.99	17.60	1.7	0.11	1.57	3.22
010	10/08/2011	21 52 35.07	28 25.18	94 59.34	23.30	2.1	0.26	3.12	3.66
011	13/08/2011	14 46 27.22	28 39.62	94 38.01	07.23	3.1	0.11	1.12	0.64
012	15/08/2011	11 05 41.36	28 25.07	95 18.30	10.12	2.4	0.41	2.77	2.85
013	18/08/2011	14 45 51.23	28 39.35	94 40.82	06.91	3.5	0.12	1.11	0.94
014	20/08/2011	12 26 18.20	28 32.51	95 15.00	14.61	2	0.34	2.88	1.92
015	30/08/2011	20 57 54.13	28 24.87	95 26.96	30.98	2.1	0.22	3.37	2.28
016	06/09/2011	20 19 50.65	28 26.98	94 55.26	13.19	2.8	0.13	1.44	1.50
017	11/09/2011	21 16 37.04	28 22.23	94 52.35	17.21	1.9	0.03	0.41	2.58
018	12/09/2011	22 04 00.99	28 25.80	94 58.62	33.04	3.1	0.13	2.00	2.27
019	14/09/2011	06 25 26.17	28 32.39	94 57.76	06.39	2.7	0.16	1.54	0.65

020	14/09/2011	06 40 47.65	28 26.56	95 03.62	23.67	3.1	0.26	3.47	3.95
021	22/09/2011	20 45 55.01	28 19.61	95 18.53	10.62	2.9	0.23	1.24	1.97
022	26/09/2011	20 54 52.52	28 20.65	95 19.56	12.95	2.6	0.46	2.87	3.75
023	29/09/2011	13 49 01.88	28 22.81	95 26.66	14.56	3	0.18	2.51	1.35
024	01/10/2011	17 49 03.65	28 29.14	95 17.42	10.48	1.8	0.13	0.92	1.37
025	05/10/2011	01 43 38.29	28 30.59	95 00.54	12.85	3	0.18	1.38	0.93
026	08/10/2011	12 34 57.62	28 28.77	96 36.60	35.50	3.2	0.23	3.76	3.38
027	08/10/2011	17 36 11.98	28 26.42	95 00.80	35.27	1.9	0.08	1.08	1.81
028	08/10/2011	17 43 44.83	28 26.26	95 01.15	33.40	1.9	0.14	1.13	1.58
029	14/10/2011	15 06 25.00	25 09.91	95 31.40	35.40	3.6	0.14	3.50	2.96
030	15/10/2011	16 40 06.68	27 59.42	95 54.02	16.88	2.3	0.25	1.95	2.77
031	16/10/2011	22 58 43.16	28 40.63	95 12.95	11.02	1.6	0.28	1.16	0.93
032	18/10/2011	21 27 26.85	28 28.02	95 22.00	11.91	1.6	0.10	0.92	1.23
033	21/10/2011	10 21 36.03	29 10.40	94 49.36	09.41	4.1	0.19	4.02	3.26
034	21/10/2011	23 45 58.69	28 50.89	95 42.86	09.33	2.8	0.11	1.52	0.72
035	28/10/2011	19 56 42.95	27 21.55	94 45.89	09.90	2.2	0.22	2.12	1.19
036	29/10/2011	18 08 46.17	27 26.86	95 31.37	13.97	2.6	0.36	2.43	4.14
037	02/11/2011	14 29 20.92	27 13.81	95 51.15	10.28	3.7	0.28	3.14	4.18
038	04/11/2011	00 36 15.19	28 37.82	96 05.00	12.70	3	0.09	3.16	3.68
039	07/11/2011	01 11 33.15	28 27.41	95 28.46	12.94	2.6	0.11	1.16	0.62
040	09/11/2011	18 40 22.18	28 10.29	95 35.40	16.93	1.8	0.10	0.92	0.87
041	10/11/2011	18 13 36.62	28 08.29	96 00.71	17.55	2.1	0.43	3.15	2.06
042	14/11/2011	00 30 16.54	28 36.09	94 51.38	11.01	3.4	0.09	0.99	0.59
043	15/11/2011	07 21 19.12	28 09.92	95 35.59	16.57	3	0.09	0.85	0.77
044	15/11/2011	21 51 03.40	28 09.98	95 35.25	16.76	2	0.12	0.98	0.96
045	18/11/2011	21 54 17.20	28 07.85	95 32.49	36.12	2.4	0.08	0.82	1.18
046	21/11/2011	20 28 28.87	27 36.83	95 03.30	09.70	2.3	0.44	4.00	3.69

047	21/11/2011	20 19 09.00	27 36.77	95 06.93	11.90	2.3	0.10	1.60	0.58
048	23/11/2011	20 35 05.72	28 31.90	95 27.00	14.99	1.9	0.17	1.06	0.48
049	23/11/2011	20 47 03.23	28 06.60	95 30.89	33.08	2.5	0.64	2.85	3.27
050	03/12/2011	18 30 23.10	27 51.66	94 51.70	17.59	1.7	0.03	1.47	3.54
051	07/12/2011	22 35 33.36	28 48.90	94 46.61	12.19	2.5	0.17	3.83	3.11
052	09/12/2011	18 49 43.50	28 56.23	94 51.92	08.00	2.2	0.21	2.46	1.71
053	14/12/2011	19 14 32.01	28 09.60	95 29.04	19.57	2.6	0.09	1.21	0.93
054	16/12/2011	23 41 10.89	28 37.95	94 55.30	17.11	2	0.18	1.39	1.53
055	17/12/2011	20 25 25.70	27 25.70	95 11.60	45.00	2.2	0.28	2.97	3.90
056	18/12/2011	03 25 43.77	28 35.01	94 59.18	09.56	2.6	0.07	0.87	3.63
057	18/12/2011	16 29 13.19	28 03.81	95 03.49	11.49	2.4	0.18	1.00	1.26
058	27/12/2011	02 52 04.38	27 45.87	95 08.61	42.47	2.5	0.10	1.61	0.99
059	01/01/2012	00 27 57.11	28 28.60	94 48.44	13.14	2.3	0.08	0.84	0.48
060	03/01/2012	15 27 52.94	27 54.81	95 27.84	24.66	2.7	0.14	0.93	1.82
061	05/01/2012	18 47 53.44	28 28.09	95 03.91	30.74	1.4	0.12	0.94	1.34
062	19/01/2012	19 34 39.49	2837.97	94 57.50	27.10	1.9	0.23	3.30	3.90
063	01/02/2012	20 20 28.43	28 11.30	95 30.63	29.42	2.7	0.07	0.86	1.19
064	01/02/2012	1651 01.49	28 29.02	95 09.84	24.21	3.1	0.16	1.25	1.34
065	13/02/2012	1750 32.90	28 54.35	94 49.56	10.01	3.4	0.20	1.91	0.99
066	21/02/2012	1710 47.08	28 23.08	95 07.38	35.35	3.2	0.15	1.47	1.23
067	24/02/2012	1652 50.99	28 25.53	95 34.66	12.15	2.4	0.14	1.07	0.60
068	01/03/2012	0824 40.97	28 40.91	95 14.79	10.21	2	0.16	1.18	0.90
069	11/03/2012	19 52 21.66	28 16.78	95 10.99	35.32	2.2	0.07	0.78	0.85
070	12/03/2012	04 44 47.57	28 29.40	95 04.38	24.11	3.6	0.14	1.14	2.89
071	14/03/2012	14 49 11.09	28 30.73	94 56.12	12.04	2.9	0.19	1.57	1.42
072	16/03/2012	14 44 50.41	28 06.97	95 34.21	31.46	2.1	0.08	1.45	0.94
073	23/03/2012	13 54 28.83	28 25.56	95 19.95	10.25	2.7	0.12	0.74	1.00

074	27/03/2012	12 48 55.80	27 44.92	95 15.40	36.79	2.4	0.12	1.29	1.70
075	27/03/2012	21 13 21.72	28 45.57	95 49.68	10.28	2	0.19	1.78	0.85
076	28/03/2012	18 58 52.15	28 13.57	95 24.17	29.33	2.4	0.08	0.69	1.12
077	03/04/2012	07 13 13.15	28 33.90	95 11.20	15.69	1.9	0.33	3.74	1.01
078	03/04/2012	16 27 38.83	27 48.77	95 33.76	10.81	2.4	0.64	5.89	2.99
079	03/04/2012	21 51 39.21	28 33.17	95 34.86	13.39	2	0.39	2.05	1.15
080	04/04/2012	20 02 13.54	27 57.67	94 17.36	09.83	2.3	0.33	4.19	3.39
081	07/04/2012	18 19 18.01	28 53.40	95 14.99	11.63	1.9	0.19	1.76	0.85
082	07/04/2012	21 27 13.06	28 14.49	95 09.36	10.41	2	0.11	0.78	1.83
083	07/04/2012	21 29 43.19	28 14.54	95 09.17	08.96	2.3	0.08	0.64	1.19
084	10/04/2012	10 12 19.88	28 27.22	95 30.22	08.27	2.1	0.21	1.24	3.57
085	10/04/2012	21 21 29.34	29 01.65	95 37.75	09.68	2.2	0.19	4.07	1.52
086	11/04/2012	16 30 41.34	28 30.11	94 56.36	13.54	2.5	0.07	1.14	0.57
087	18/04/2012	23 19 59.67	28 30.29	95 25.65	17.85	2.2	0.21	1.49	1.90
088	21/04/2012	15 46 19.63	28 22.38	95 14.25	31.03	2.8	0.13	0.96	1.11
089	22/04/2012	11 28 37.93	27 56.78	94 58.27	16.94	2	0.18	1.71	2.15
090	23/04/2012	06 11 36.59	28 27.35	94 52.94	16.30	3.3	0.23	1.80	2.03
091	26/04/2012	09 13 33.33	28 19.93	94 51.28	31.85	2.7	0.09	1.14	2.27
092	02/05/2012	06 48 46.03	28 13.07	94 57.74	34.72	2.5	0.23	1.90	1.32
093	02/05/2012	17 00 10.35	28 20.72	94 16.84	09.75	2.6	0.26	3.89	2.23
094	02/05/2012	19 57 43.40	28 19.65	94 17.38	19.52	4	0.37	3.24	2.17
095	04/05/2012	20 09 28.90	27 39.24	95 06.62	20.97	3.3	0.10	2.99	1.48
096	08/05/2012	08 05 26.29	28 25.28	94 53.78	08.01	2.5	0.16	2.46	4.13
097	11/05/2012	15 40 57.68	28 26.28	94 49.21	13.30	2.6	0.11	1.16	0.80
098	12/05/2012	14 38 50.96	27 52.68	94 09.20	10.55	2.8	0.23	4.12	4.04
099	13/05/2012	17 57 09.85	28 48.45	94 50.75	12.24	3.3	0.10	4.20	2.47
100	14/05/2012	23 18 45.04	28 16.57	94 56.68	12.47	2.7	0.54	3.42	3.65

101	15/05/2012	18 48 42.37	28 16.81	94 58.62	10.72	1.7	0.32	1.65	3.47
102	16/05/2012	03 30 08.21	28 55.50	95 43.87	10.20	3.5	0.50	2.15	3.34
103	24/05/2012	21 59 55.87	28 15.27	96 00.12	17.44	2.5	0.25	2.31	2.30
104	25/05/2012	10 47 20.41	29 00.07	95 10.96	14.50	2.8	0.19	4.28	3.18

Appendix II

II.1 Instrument correction

It is well known that the output of a sensor $Y(\omega)$ is the multiplication of system response $A(\omega)$ with input ground motion $X(\omega)$ as:

$$Y(\omega) = X(\omega) A(\omega) \quad \text{II.1}$$

From a digital system the $Y(\omega)$ is in counts or voltage from an amplifier. The $A(\omega)$ is the displacement amplitude response of ground displacement sensor and velocity response in case of ground velocity sensor. The ground motions can be recovered from above equation:

$$X(\omega) = Y(\omega)/A(\omega) \quad \text{II.2}$$

This represents the single frequency instrument correction which is widely used for earthquake magnitude determination. For a various frequencies, the system is seems to be RC low pas filter as shown in Fig.II.1. To have amplitude response, both the input and output frequencies varied. There is not only the change in the amplitude of the output signal but also delays little with respect to input signal. In other words, we can say a phase sifts. Hence the equation II.1 can be written as:

$$Y(\omega) = X(\omega) A(\omega) + \Phi(\omega) \quad \text{II.3}$$

Where $\Phi(\omega)$ represents the phase shift relative to input $X(\omega)$. Hence the complete response function of a filter or system consists of both the amplitude response function and phase response function which are known as Bode Diagram. The bode diagram of the short period and broadband seismogram are shown in fig II.2.

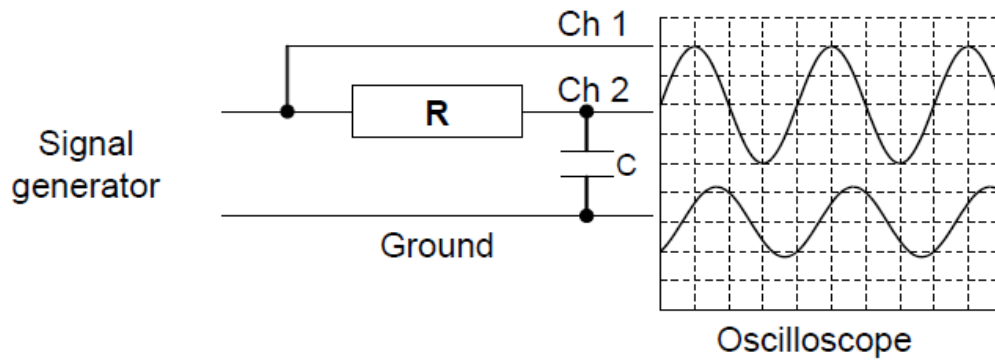


Fig.II.1 Measurement of amplitude response of RC filter. In ch 1, the signal directly observed from generator and the output signal is analyzed in ch.2.

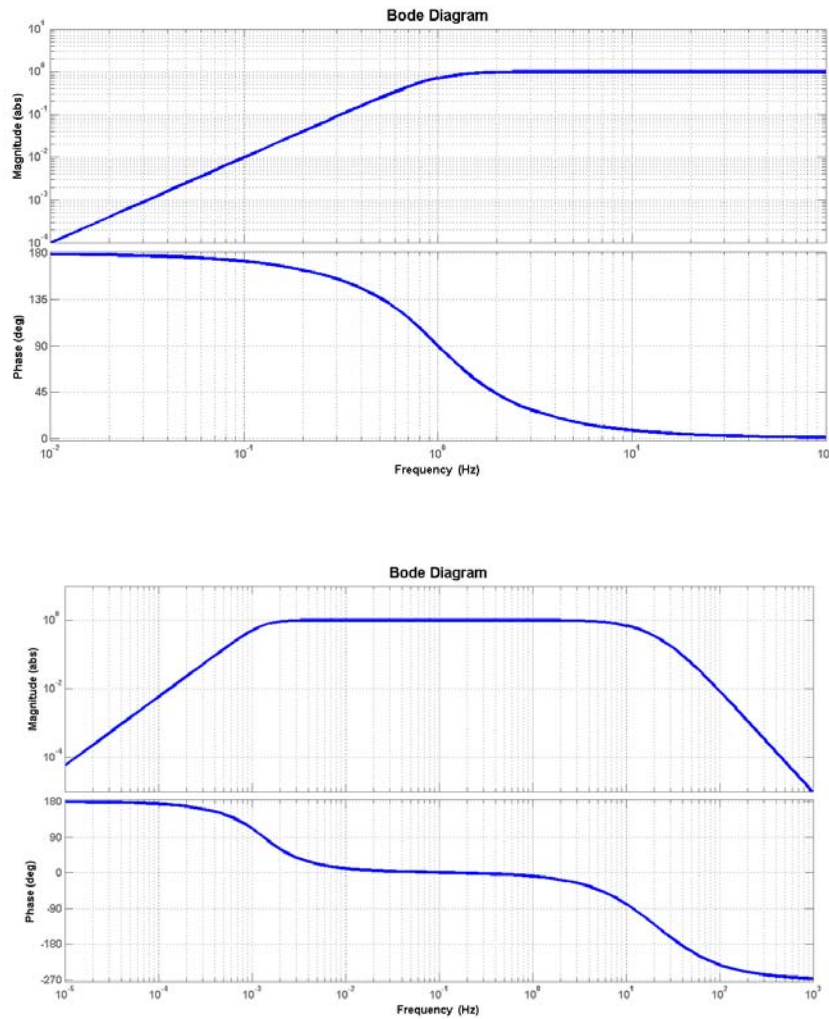


Fig. II.2 Amplitude and phase response of Seismometer (a) short period seismometer (b) broad band seismometer

The response function defined in equation b.3 is simple single frequency response function. As we know that seismic input signal $X(\omega)$ is the complex signal, so the response function of such system a complex one function $T(\omega)$. So the output $Y(\omega)$ of such filter is given by:

$$Y(\omega) = X(\omega) T(\omega) \quad \text{II.4}$$

Where $A(\omega) = \sqrt{re(T(\omega))^2 + im(T(\omega))^2}$ is the amplitude spectrum and $\Phi(\omega) = \tan^{-1} \frac{Im(T(\omega))}{re(T(\omega))}$, is the phase response spectrum.

Thus practically, the ground displacement is calculated by dividing the output Fourier spectrum with complex displacement response function. The above described response function can be written for a RC filter as:

$$T_{RC}(\omega) = \frac{1}{1+j\omega RC} \quad \text{II.5}$$

The above equation after a complex mathematics can be written in terms of amplitude response function of seismometer as:

$$T_d(\omega) = \frac{\omega^2}{\omega_0^2 - \omega^2 + i\omega\omega_0 h} \quad \text{II.6}$$

Equation b.6 can be rewritten in terms of response function of a mechanical seismometer:

$$T_d(\omega) = \frac{-(i\omega)^2}{\omega_0^2 + i\omega\omega_0 h + (i\omega)^2} \quad \text{II.5}$$

The response function T_d could be any complex function. Generally, it contains all the mechanical or electrical components such as resistors, coils, capacitors, semiconductors, springs and masses etc. these electrical and mechanical components can be represented as a function of $i\omega$ as:

$$T(\omega) = \frac{a_0 + a_1(j\omega) + a_2(j\omega) + \dots}{b_0 + b_1(j\omega) + b_2(j\omega) + \dots} \quad \text{II.8}$$

Where a_i and b_i are the constants. The complexity of the system decided the number of polynomials. The above equation can be simplified by factorizing the polynomials as:

$$T(\omega) = c \frac{(i\omega - z_1)(i\omega - z_2)(i\omega - z_3)\dots}{(i\omega - p_1)(i\omega - p_2)(i\omega - p_3)\dots} \quad \text{II.9}$$

Where c is the normalization factor, z and P represents the zero (or roots) of nominator and poles of denominator respectively. Equation II.9 is the standard presentation of response function, also known as the poles and zeros representation of $T(\omega)$. In the presents study two types of sensor namely; short period (CMG-40 T1), and broad band (CMG 40T) are used the pole zeros and normalizing factors of theses seismometers are given in table below.

Table II.1. Poles, zeros and normalizing factors of short period (CMG-40 T1), and broad band (CMG 40T) seismometers

CMG 40T		
Poles	Zeros	Normalization factor at 1 Hz
-80.0	0	2 304 000
-160.0	0	
-180.0		
$-0.02356 + 0.02356j$		
$-0.02356 - 0.02356j$		

CMG 40T-1		
Poles	Zeros	Normalization factor at 1 Hz
$-4.44 + 4.44j$	0	625000

-4.44 - 4.44j	0	
---------------	---	--

A Matlab function **zp2tf** has been adopted to convert the values of zeros and poles in the polynomial form as:

$$H(s) = \frac{N(s)}{D(s)} \quad \text{II.10}$$

As mentioned in the Matlab manual, following function form the transfer function:

$$[N(s), D(s)] = \text{zp2tf}(Z,P,K) \quad \text{II.11}$$

In the above expression, Z vector contains values of zeros, P vector contains values of poles and K is a scalar gain. Vectors N(s) and D(s) are returned with numerator and denominator coefficients in descending powers of s. A filter has been designed with coefficients N(s) and D(s) and applied on input data to obtain the corrected data as given below:

$$\text{CORRECTED_DATA} = \text{filter}(N(s), D(s), \text{INPUT_DATA}) \quad \text{(II.12)}$$

A typical example of the input data available in counts and corrected data in cm/sec after applying instrument response correction is shown in the Fig. II 3. SH part of data selected for analysis is shown in Fig. II.4 as shown below:

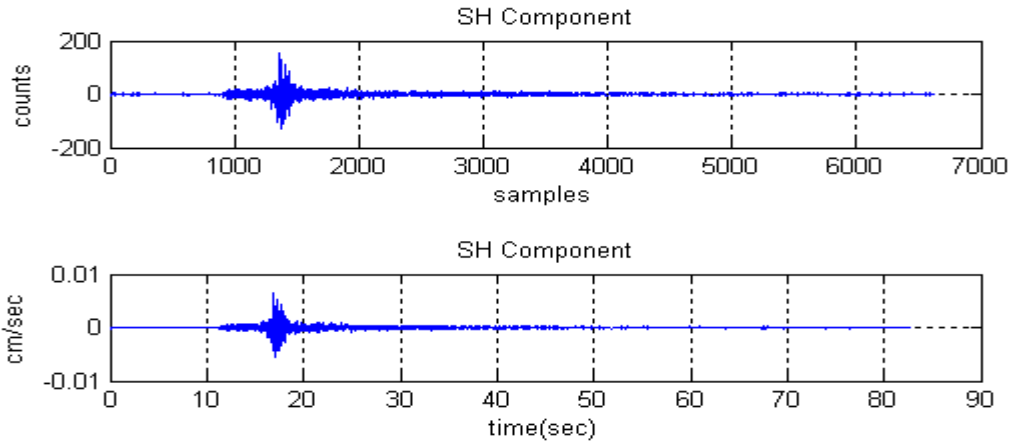


Fig. II.3 An example of input data in counts and its corrected output in cm/sec.

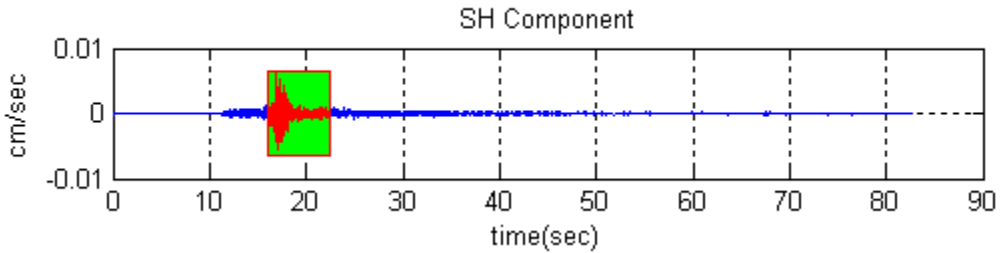


Fig. II.4 An example of SH part of data selected for analysis.

Similar procedure has been applied to other data sets wherever applicable.

II.2 Computation of Fourier Transform

For the purpose of computing the SH spectra, the prominent pulse/ground motion representing the shear waves was selected from the time series corrected for instrument response. The choice of time window used in the study is based on the fact that it includes scattered coda part of shear wave that minimizes the effect of radiation pattern and also the variance of the amplitude measure (Mayeda et al., 2003).

In seismology, the recorded time histories are generally used to read various seismic phases to infer locations of earthquakes, structure of the earth etc. These time histories represent

arrivals of different phases and variations of amplitudes of various phases w.r.t. time. However, many properties like other sciences need the presentation of time history according to frequency or wave numbers. The frequency domain refers to the presentation of earthquake time history with respect to frequency, rather than time i.e. a time-domain graph shows how a signal changes over time, whereas a frequency-domain graph shows how much of the signal lies within each given frequency band over a range of frequencies. A frequency-domain representation can also include information on the phase shift that must be applied to each sinusoid in order to be able to recombine the frequency components to recover the original earthquake time history.

Earthquake time histories can be converted between the time and frequency domains with a pair of mathematical operators called a transform. Usually Fast Fourier transform, is used for the conversion, which decomposes a given time history into the sum of a number of sine wave frequency components. The 'spectrum' of frequency components is the frequency domain representation of the signal. The inverse Fast Fourier transform converts the frequency domain earthquake time history back to an earthquake time history

Before computing the Fourier transformation, the selected signals were tapered using a Matlab Kaiser Window function. During signal processing, like Fast Fourier Transform of band limited time history of earthquakes, ringing artefacts appear as spurious signals near sharp transitions in the output signal in frequency domain. The term "ringing" is because the output signal in frequency domain oscillates at a fading rate around a sharp transition in the input, similar to a bell after being struck. Mathematically, this effect is known as Gibbs phenomenon. In order to minimise this artefact a window function has been applied to input band limited time series before transforming it to frequency domain. Various types of window functions have been designed to remove this effect (e.g., Hamming window, Kaiser window, Cosine Tapered window

etc.). The windowing process introduces a loss in spectral resolution and removes the effect of spectral leakage. Thus, the choice of window function involves a trade-off between these two effects. That is, a window with better frequency resolution capabilities usually fails to stop the spectral leakage and vice-versa. In order to process the earthquake time histories various window functions have been tested with a sine wave and Kaiser window has been selected to perform the windowing of earthquake time histories.

This window function was developed by James Kaiser at Bell Laboratories and is known as Kaiser window or Kaiser-Bessel window (fig. II.5). The mathematical form of this window function is given below:

$$w(n) = \begin{cases} \frac{I_0(\pi\alpha\sqrt{1-(\frac{2n}{N-1}-1)^2})}{I_0(\pi\alpha)}, & \leq n \leq N - 1 \\ 0 & \textit{otherwise} \end{cases} \quad (\text{II.13})$$

Here, N is the number of samples, I_0 zeroth order Modified Bessel function of the first kind, α is a non-negative arbitrary real number. The shape of the window is determined by it. The main decision in window designing is the trade-off between the side and main lobes. This trade-off is also determined by α . The peak value of the window are $w[(N-1)/2] = 1$ and $w[N/2-1] = w[N/2] < 1$ corresponding to N is odd and even respectively.

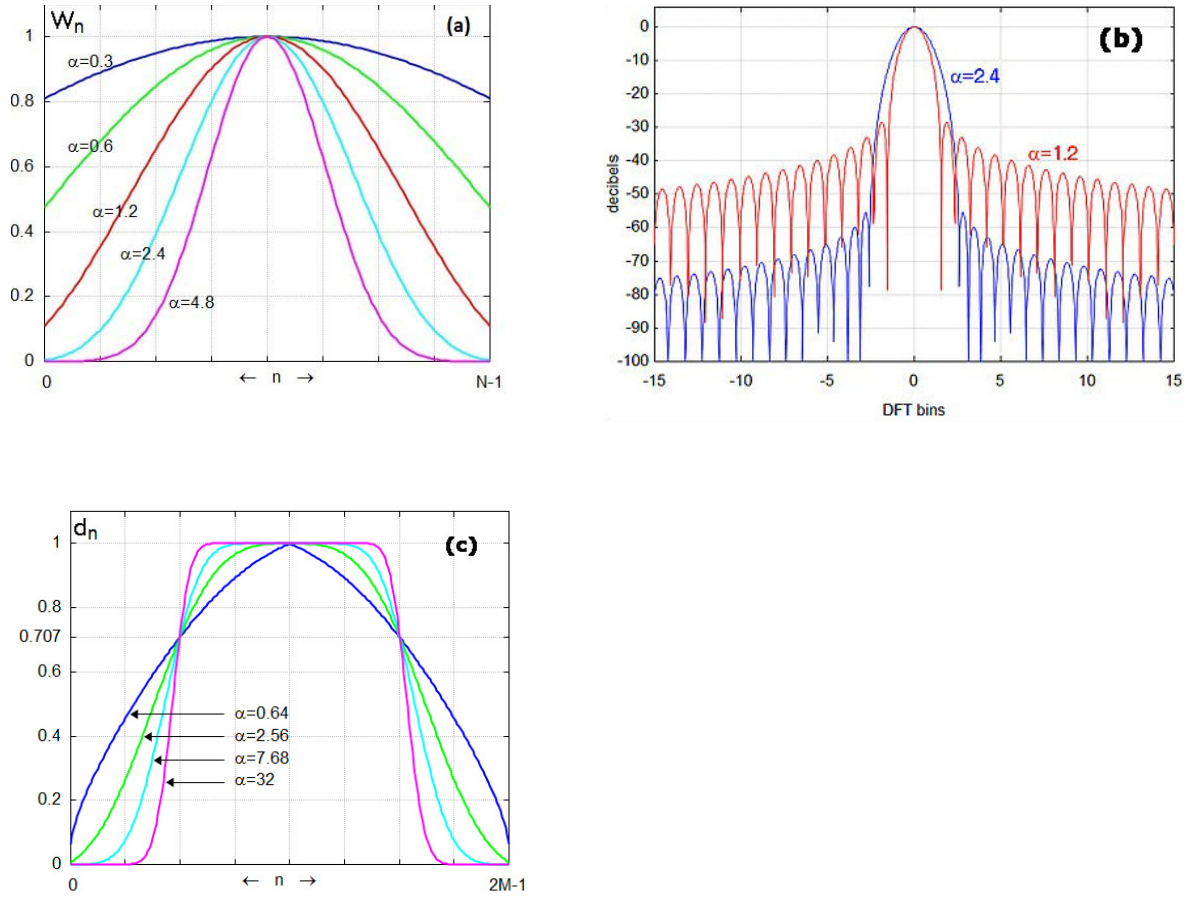


Figure II.5 (a). Parametric family of Kaiser Windows. (b). for a typical value of parameter, Fourier transforms of Kaiser Windows. (c) Window functions derived by Kaiser Bessel.

The windowed time series is Fourier transformed adopting the standard methodology using the FFT function in Matlab. The brief description of the procedure adopted is described below:

The earthquake time history $s(t)$ can be transformed to frequency domain $S(f)$ and vice-versa given below:

$$S(f) = \int_{-\infty}^{\infty} s(t) \cdot e^{-i2\pi ft} dt. \quad (\text{II.14})$$

$$s(t) = \int_{-\infty}^{\infty} S(f) \cdot e^{i2\pi ft} df, \quad (\text{II.15})$$

FFT Discrete Fourier transforms. $\text{FFT}(X)$ is the discrete Fourier transform (DFT) of vector X . For matrices, the FFT operation is applied to each column. For N-D arrays, the FFT operation operates on the first non-singleton dimension. $\text{FFT}(X,N)$ is the N-point FFT, padded with zeros if X has less than N points and truncated if it has more. $\text{FFT}(X, N, \text{DIM})$ applies the FFT operation across the dimension DIM .

For length N input vector x , the DFT is a length N vector X , with elements N

$$X(k) = \sum_{n=1}^N x(n) \exp(-j \cdot 2 \cdot \pi \cdot (k-1) \cdot (n-1) / N), \quad 1 \leq k \leq N, n=1 \quad (\text{II.16})$$

The inverse DFT (computed by IFFT) is given by N

$$x(n) = (1/N) \sum_{k=1}^N X(k) \exp(j \cdot 2 \cdot \pi \cdot (k-1) \cdot (n-1) / N), \quad 1 \leq n \leq N, k=1 \quad (\text{II.17})$$

Table III.1. Source parameters of earthquakes occurred in Siang region of Arunachal Lesser Himalaya.

S. N.	Date (yymmdd)	Lat. Deg Mn North	Long. Deg Mn East	Depth (km)	f_c (Hz)	f_{max} (Hz)	M_0 (dyn- cm)	Mag. M_w	r (m)	$\Delta\sigma$ (bars)
001	24/07/2011	28 49.07	95 40.49	09.42	5.1	12.4	5.72×10^{19}	2.5	219.4	2.4
002	26/07/2011	27 28.65	95 46.29	42.52	5.1	11.0	3.71×10^{21}	3.4	231.1	17.3
003	29/07/2011	28 08.26	94 54.74	24.40	5.3	11.6	1.75×10^{19}	2.2	210.1	0.1
004	29/07/2011	28 55.52	95 33.65	08.02	5.0	11.2	2.22×10^{20}	2.5	223.1	8.7
005	31/07/2011	28 56.37	95 42.60	06.00	5.0	12.2	1.62×10^{19}	2.1	224.9	0.6
006	02/08/2011	28 12.45	95 12.07	31.35	4.1	10.6	3.77×10^{18}	1.8	275.1	0.1
007	05/08/2011	28 28.80	95 17.62	11.26	5.3	13.4	1.07×10^{19}	2.2	213.5	4.7
008	08/08/2011	28 40.61	95 45.46	43.88	3.6	10.5	1.13×10^{20}	2.3	310.6	1.6
009	09/08/2011	27 54.23	94 49.99	17.60	5.6	15.3	6.46×10^{18}	2	232.8	2.8
010	10/08/2011	28 25.18	94 59.34	23.30	4.5	11.8	1.56×10^{20}	2.8	251.6	4.3
011	13/08/2011	28 39.62	94 38.01	07.23	4.0	10.4	6.07×10^{20}	3.2	278.4	12.2
012	15/08/2011	28 25.07	95 18.30	10.12	4.3	11.4	8.31×10^{18}	2.1	258.7	2.1
013	18/08/2011	28 39.35	94 40.82	06.91	3.8	8.8	2.92×10^{21}	3.6	298.1	48.6
014	20/08/2011	28 32.51	95 15.00	14.61	4.6	11.4	7.22×10^{18}	2	244.5	2.2
015	30/08/2011	28 24.87	95 26.96	30.98	6.4	12.5	1.38×10^{19}	2.1	174.7	1.1
016	06/09/2011	28 26.98	94 55.26	13.19	4.1	12.2	2.52×10^{20}	2.9	271.6	5.5
017	11/09/2011	28 22.23	94 52.35	17.21	3.7	10.4	3.23×10^{18}	2.2	302.0	5.1
018	12/09/2011	28 25.80	94 58.62	33.04	5.2	10.2	8.34×10^{20}	3.2	214.9	3.7
019	14/09/2011	28 32.39	94 57.76	06.39	4.4	10.8	2.49×10^{20}	2.8	252.4	0.7
020	14/09/2011	28 26.56	95 03.62	23.67	3.5	8.6	5.33×10^{20}	3.1	317.7	7.2

021	22/09/2011	28 19.61	95 18.53	10.62	3.3	10.7	2.60x10 ²⁰	2.9	342.8	2.8
022	26/09/2011	28 20.65	95 19.56	12.95	3.3	9.3	4.98x10 ²⁰	3.1	342.4	5.4
023	29/09/2011	28 22.81	95 26.66	14.56	5.2	11.5	3.05x10 ²¹	3.1	215.9	13.3
024	01/10/2011	28 29.14	95 17.42	10.48	5.6	11.9	1.24x10 ¹⁹	2.3	201.6	6.6
025	05/10/2011	28 30.59	95 00.54	12.85	4.4	10.4	4.76x10 ²⁰	3.1	256.0	12.4
026	08/10/2011	28 28.77	96 36.60	35.50	1.3	5.1	3.10x10 ²³	5	211.2	1.5
027	08/10/2011	28 26.42	95 00.80	35.27	3.7	9.1	8.25x10 ¹⁹	2.3	299.3	13.4
028	08/10/2011	28 26.26	95 01.15	33.40	5.4	17.3	1.28x10 ¹⁹	2.1	208.9	0.6
029	14/10/2011	25 09.91	95 31.40	35.40	2.0	7.6	1.90x10 ²¹	3.5	279.8	2.0
030	15/10/2011	27 59.42	95 54.02	16.88	5.2	13.2	4.24x10 ¹⁹	2.4	217.0	0.5
031	16/10/2011	28 40.63	95 12.95	11.02	4.1	16.5	1.36x10 ¹⁹	2.1	273.0	0.3
032	18/10/2011	28 28.02	95 22.00	11.91	5.0	15.4	1.15x10 ¹⁹	2	223.4	0.5
033	21/10/2011	29 10.40	94 49.36	09.41	4.2	10.2	4.93x10 ²²	4.2	266.6	11.3
034	21/10/2011	28 50.89	95 42.86	09.33	6.1	10.4	8.29x10 ¹⁹	3.9	184.9	5.7
035	28/10/2011	27 21.55	94 45.89	09.90	4.9	12.0	5.05x10 ¹⁹	2.5	229.8	1.8
036	29/10/2011	27 26.86	95 31.37	13.97	5.0	12.2	4.80x10 ¹⁹	2.5	224.7	1.9
037	02/11/2011	27 13.81	95 51.15	10.28	5.1	10.5	8.38x10 ²⁰	3.9	320.2	52.1
038	04/11/2011	28 37.82	96 05.00	12.70	5.3	13.6	1.19x10 ²¹	3.1	312.8	0.5
039	07/11/2011	28 27.41	95 28.46	12.94	4.1	12.7	1.09x10 ²⁰	2.7	283.0	22.4
040	09/11/2011	28 10.29	95 35.40	16.93	5.1	10.6	5.18x10 ¹⁹	2.5	220.1	2.1
041	10/11/2011	28 08.29	96 00.71	17.55	5.5	11.9	2.63x10 ¹⁹	2.3	202.3	1.4
042	14/11/2011	28 36.09	94 51.38	11.01	3.9	10.9	3.15x10 ²¹	3.4	291.1	55.5
043	15/11/2011	28 09.92	95 35.59	16.57	3.2	10.2	5.31x10 ²⁰	3.2	295.5	8.6
044	15/11/2011	28 09.98	95 35.25	16.76	5.3	13.6	1.03x10 ¹⁹	2	212.4	0.5
045	18/11/2011	28 07.85	95 32.49	36.12	4.7	10.8	7.50x10 ¹⁹	2.6	236.3	2.5

046	21/11/2011	27 36.83	95 03.30	09.70	5.4	15.3	3.18x10 ¹⁹	2.3	206.5	1.6
047	21/11/2011	27 36.77	95 06.93	11.90	5.0	10.5	2.48x10 ²⁰	2.9	225.5	9.4
048	23/11/2011	28 31.90	95 27.00	14.99	4.3	10.8	3.78x10 ¹⁹	2.4	263.4	0.9
049	23/11/2011	28 06.60	95 30.89	33.08	4.7	12.0	1.70x10 ²⁰	2.8	237.2	5.5
050	03/12/2011	27 51.66	94 51.70	17.59	5.2	14.2	1.08x10 ¹⁹	2	356.8	0.2
051	07/12/2011	28 48.90	94 46.61	12.19	4.1	12.5	1.31x10 ²⁰	2.7	273.2	2.8
052	09/12/2011	28 56.23	94 51.92	08.00	4.5	13.4	5.04x10 ¹⁹	2.5	251.2	1.4
053	14/12/2011	28 09.60	95 29.04	19.57	5.4	14.1	6.13x10 ¹⁹	2.5	208.4	0.3
054	16/12/2011	28 37.95	94 55.30	17.11	4.5	11.7	5.70x10 ¹⁹	2.1	247.6	1.6
055	17/12/2011	27 25.70	95 11.60	45.00	4.6	14.2	1.64x10 ¹⁹	2.1	246.2	4.8
056	18/12/2011	28 35.01	94 59.18	09.56	4.6	11.1	7.46x10 ²⁰	3.2	243.8	22.4
057	18/12/2011	28 03.81	95 03.49	11.49	3.3	9.7	4.90x10 ¹⁹	2.5	339.6	5.5
058	27/12/2011	27 45.87	95 08.61	42.47	4.2	10.3	1.92x10 ²⁰	2.9	269.3	43.0
059	01/01/2012	28 28.60	94 48.44	13.14	5.4	13.7	2.20x10 ¹⁹	2.2	206.3	1.1
060	03/01/2012	27 54.81	95 27.84	24.66	4.5	13.0	2.26x10 ¹⁹	2.2	248.5	0.7
061	05/01/2012	28 28.09	95 03.91	30.74	6.1	16.6	1.60x10 ¹⁸	1.4	212.4	0.3
062	19/01/2012	28 37.97	94 57.50	27.10	4.9	18.4	3.71x10 ¹⁸	1.7	267.0	0.1
063	01/02/2012	28 11.30	95 30.63	29.42	4.6	18.1	1.15x10 ²⁰	2.7	285.8	0.2
064	01/02/2012	28 29.02	95 09.84	24.21	4.3	15.0	8.60x10 ²⁰	3.3	304.6	0.1
065	13/02/2012	28 54.35	94 49.56	10.01	6.2	13.8	1.82x10 ²¹	3.5	281.9	0.8
066	21/02/2012	28 23.08	95 07.38	35.35	5.1	14.2	7.18x10 ²⁰	3.3	269.1	0.3
067	24/02/2012	28 25.53	95 34.66	12.15	8.1	22.9	5.20x10 ¹⁹	2.5	201.2	0.1
068	01/03/2012	28 40.91	95 14.79	10.21	6.6	15.2	1.64x10 ¹⁹	2.1	261.2	0.2
069	11/03/2012	28 16.78	95 10.99	35.32	4.9	15.8	3.16x10 ¹⁹	2.3	267.0	0.1
070	12/03/2012	28 29.40	95 04.38	24.11	3.5	15.6	2.0x10 ²¹	3.5	368.7	0.2

071	14/03/2012	28 30.73	94 56.12	12.04	5.5	11.8	4.57x10 ²⁰	3.1	238.4	1.5
072	16/03/2012	28 06.97	95 34.21	31.46	3.4	10.4	2.31x10 ¹⁹	2.2	384.7	0.1
073	23/03/2012	28 25.56	95 19.95	10.25	6.1	12.9	3.32x10 ¹⁹	2.3	212.4	0.2
074	27/03/2012	27 44.92	95 15.40	36.79	3.8	15.3	1.00x10 ²⁰	2.6	346.0	0.1
075	27/03/2012	28 45.57	95 49.68	10.28	5.5	16.3	1.58x10 ¹⁹	2.1	238.4	0.1
076	28/03/2012	28 13.57	95 24.17	29.33	5.2	16.2	6.52x10 ¹⁹	2.5	251.8	0.7
077	03/04/2012	28 33.90	95 11.20	15.69	6.1	16.6	9.73x10 ¹⁸	2	212.4	0.7
078	03/04/2012	27 48.77	95 33.76	10.81	3.5	16.3	8.44x10 ¹⁹	2.6	376.6	0.1
079	03/04/2012	28 33.17	95 34.86	13.39	4.4	14.4	6.29x10 ¹⁹	2.5	296.6	0.3
080	04/04/2012	27 57.67	94 17.36	09.83	3.4	17.2	7.03x10 ¹⁹	2.6	381.4	0.1
081	07/04/2012	28 53.40	95 14.99	11.63	6.1	16.0	1.80x10 ¹⁹	2.2	212.4	0.3
082	07/04/2012	28 14.49	95 09.36	10.41	4.1	19.3	9.08x10 ¹⁸	1.9	317.8	0.2
083	07/04/2012	28 14.54	95 09.17	08.96	6.3	19.7	3.15x10 ¹⁹	2.3	205.3	0.2
084	10/04/2012	28 27.22	95 30.22	08.27	5.3	20.6	7.84x10 ¹⁸	1.9	246.4	0.4
085	10/04/2012	29 01.65	95 37.75	09.68	6.7	17.4	1.76x10 ¹⁹	2.1	195.1	0.1
086	11/04/2012	28 30.11	94 56.36	13.54	4.8	17.0	8.90x10 ¹⁹	2.6	274.0	0.3
087	18/04/2012	28 30.29	95 25.65	17.85	5.1	16.3	1.15x10 ¹⁹	2	257.1	0.5
088	21/04/2012	28 22.38	95 14.25	31.03	5.1	10.8	4.17x10 ²⁰	3.1	241.4	0.1
089	22/04/2012	27 56.78	94 58.27	16.94	4.8	13.4	2.06x10 ¹⁹	2.2	221.5	0.1
090	23/04/2012	28 27.35	94 52.94	16.30	3.8	9.4	7.64x10 ²⁰	3.3	346.0	0.2
091	26/04/2012	28 19.93	94 51.28	31.85	3.1	11.2	2.42x10 ²⁰	2.9	253.8	0.3
092	02/05/2012	28 13.07	94 57.74	34.72	5.9	15.7	8.01x10 ¹⁹	2.6	222.5	0.1
093	02/05/2012	28 20.72	94 16.84	09.75	4.6	11.4	3.00x10 ¹⁹	2.3	285.8	0.1
094	02/05/2012	28 19.65	94 17.38	19.52	3.3	9.8	4.65x10 ²²	4.2	393.0	7.4
095	04/05/2012	27 39.24	95 06.62	20.97	4.0	12.4	2.10x10 ²⁰	3.3	324.7	0.3

096	08/05/2012	28 25.28	94 53.78	08.01	4.6	17.8	3.00×10^{19}	2.3	284.0	0.1
097	11/05/2012	28 26.28	94 49.21	13.30	5.5	20.2	3.50×10^{19}	2.4	238.4	0.1
098	12/05/2012	27 52.68	94 09.20	10.55	3.9	13.4	2.80×10^{20}	3	333.7	0.3
099	13/05/2012	28 48.45	94 50.75	12.24	3.1	20.9	2.69×10^{21}	3.6	417.1	0.2
100	14/05/2012	28 16.57	94 56.68	12.47	3.5	15.6	6.91×10^{19}	2.5	368.7	0.1
101	15/05/2012	28 16.81	94 58.62	10.72	8.3	16.0	5.03×10^{18}	1.8	157.8	0.1
102	16/05/2012	28 55.50	95 43.87	10.20	6.0	16.3	1.51×10^{21}	3.5	216.9	0.7
103	24/05/2012	28 15.27	96 00.12	17.44	3.4	11.6	2.81×10^{19}	2.3	384.7	0.3
104	25/05/2012	29 00.07	95 10.96	14.50	4.8	20.5	2.23×10^{20}	2.9	272.4	0.1

Annexure IV

TableIV.1 Waveform Inversion results of 104 earthquakes occurred in Lower Siang region of Arunachal Himalaya

Num.	DATE (YYMMDD)	Depth (km)	NP1 strike	NP1 Dip	NP1 slip	NP2 stri e	NP2 dip	NP2 slip	mag (Mw)	DC%	CLVD %	T-axis azimuth	P-axis azimuth	T-axis plunge	P-axis plunge	VR
001	24/07/2011	11.00	212	32	-100	44	59	-84	1.9	8.2	91.8	309	152	13	76	0.71
002	26/07/2011	37.00	321	35	-73	121	57	-102	3.1	63	37	39	177	11	75	0.81
003	29/07/2011	21.00	192	20	152	309	81	72	2.2	73.7	26.3	18	234	51	33	0.62
004	29/07/2011	07.00	161	73	-163	66	74	-18	2.2	1.7	98.3	294	203	1	24	0.69
005	31/07/2011	09.00	60	69	-36	165	57	-155	1.9	20.3	79.7	115	198	8	40	0.57
006	02/08/2011	34.00	71	51	-39	188	61	-134	1.7	34.7	65.3	127	225	6	52	0.63
007	05/08/2011	15.00	164	74	-157	67	68	-17	2.2	5.7	94.3	295	207	4	27	0.49
008	08/08/2011	37.00	218	61	92	34	29	86	2.4	21.8	78.2	313	307	74	16	0.58
009	09/08/2011	14.00	71	51	-39	188	61	-134	1.9	65.3	34.7	127	225	6	52	0.53
010	10/08/2011	17.00	303	29	-135	172	70	-69	2.5	52.2	47.8	66	292	22	59	0.71
011	13/08/2011	07.00	181	23	123	326	71	77	3	53.4	46.6	36	246	62	25	0.65
012	15/08/2011	23.00	137	12	-153	21	85	-79	2.2	27.5	72.5	281	122	39	49	0.59
013	18/08/2011	09.00	11	87	25	280	65	177	3.6	92.6	7.4	58	143	20	15	0.71
014	20/08/2011	21.00	14	85	132	110	42	7	2	89.2	10.8	140	72	36	28	0.74
015	30/08/2011	35.00	197	80	34	100	57	168	2.2	32.1	67.9	244	324	31	15	0.42
016	06/09/2011	14.00	146	89	-138	55	48	-1	2.8	47.1	52.9	273	27	29	42	0.71
017	11/09/2011	19.00	28	11	149	149	84	81	2.2	79.9	20.1	48	247	50	39	0.72
018	12/09/2011	29.00	69	3	-24	183	89	-93	3.2	87.6	12.4	276	90	44	46	0.77
019	14/09/2011	09.00	84	46	-164	343	78	-45	2.8	90.6	9.4	221	113	21	40	0.71
020	14/09/2011	25.00	116	62	18	17	74	151	2	23.1	76.9	154	248	32	8	0.64
021	22/09/2011	15.00	268	3	-24	22	89	-93	2.7	96.3	3.7	295	109	44	46	0.79

022	26/09/2011	11.00	19	68	-88	194	22	-95	2.7	31.5	68.5	108	113	23	67	0.61
023	29/09/2011	08.00	332	49	-66	118	46	-115	3.1	92.6	7.4	45	131	1	72	0.73
024	01/10/2011	11.00	358	44	-126	224	56	-60	1.9	10.6	89.4	113	9	6	65	0.66
025	05/10/2011	13.00	182	82	-12	78	31	-16	2.9	82	18	296	242	31	45	0.61
026	08/10/2011	31.00	65	44	56	288	55	118	5.1	85.2	14.8	93	117	49	39	0.65
027	08/10/2011	34.00	314	44	-138	191	62	-54	2	95	5	76	330	10	57	0.65
028	08/10/2011	37.00	284	11	-151	165	85	-80	1.9	50.6	49.4	67	266	39	49	0.67
029	14/10/2011	39.00	23	78	125	130	37	20	3.7	25.9	74.1	148	86	46	25	0.74
030	15/10/2011	17.00	263	20	-113	107	72	-82	2.5	46.5	53.5	11	210	26	63	0.69
031	16/10/2011	16.00	51	90	-121	321	31	-1	1.5	71.7	28.3	168	114	37	37	0.65
032	18/10/2011	14.00	278	30	-10	17	85	-120	1.6	80.2	19.8	311	78	33	42	0.68
033	21/10/2011	08.00	296	72	0	206	90	-162	4.2	86.3	13.7	340	72	13	13	0.73
034	21/10/2011	09.00	164	86	-178	74	88	-4	3	9.1	90.9	299	209	1	4	0.72
035	28/10/2011	37.00	344	20	-147	223	79	-73	2.8	69.4	30.6	118	333	32	53	0.63
036	29/10/2011	16.00	9	38	-74	169	54	-102	2.7	5.5	94.5	88	216	8	77	0.62
037	02/11/2011	11.00	279	10	-156	165	86	-81	4	80.2	19.8	67	265	40	48	0.53
038	04/11/2011	15.00	290	88	-177	199	87	-2	3.5	86	14	65	335	1	4	0.51
039	07/11/2011	13.00	261	68	-1	351	89	-158	2.6	79.3	20.7	304	38	15	16	0.51
040	09/11/2011	13.00	342	45	-39	102	64	-128	2.3	50.5	49.5	38	103	11	55	0.62
041	10/11/2011	19.00	249	66	-118	122	36	-44	2.2	44.4	55.6	359	299	16	59	0.72
042	14/11/2011	13.00	21	27	-50	158	70	-108	3.3	31.7	68.3	82	221	23	61	0.63
043	15/11/2011	21.00	238	10	-104	72	80	-88	3.2	53.8	46.2	340	165	-35	-55	0.74
044	15/11/2011	13.00	188	17	34	65	81	104	2	71.4	28.6	172	323	52	34	0.52
045	18/11/2011	35.00	346	88	112	81	22	5	2.7	59.1	40.9	97	56	43	39	0.55
046	21/11/2011	07.00	30	42	-70	183	51	-107	2.3	55.7	44.3	106	215	5	76	0.85
047	21/11/2011	13.00	314	6	-72	116	84	-92	2.7	85.3	14.7	28	204	39	51	0.58
048	23/11/2011	18.00	174	88	22	83	68	178	1.9	5.3	94.7	221	306	17	14	0.51
049	23/11/2011	35.00	63	84	77	309	14	155	2.6	97.6	2.4	139	165	49	38	0.77
050	03/12/2011	18.00	149	18	165	253	85	73	1.7	87	13	325	179	47	38	0.73
051	07/12/2011	15.00	206	56	146	316	62	39	2.6	9.7	90.3	354	2602	46	4	0.82
052	09/12/2011	12.00	344	43	-77	146	48	-101	2.4	55.2	44.8	65	172	3	81	0.67

053	14/12/2011	18.00	240	84	123	339	33	11	2.7	60.7	39.3	1	303	42	31	0.52
054	16/12/2011	12.00	339	43	-16	193	52	-68	2.1	17.9	82.1	87	342	5	72	0.71
055	17/12/2011	37.00	235	78	179	325	89	12	2.3	47	53	11	279	9	8	0.61
056	18/12/2011	11.00	278	64	38	169	56	148	2.7	98.7	1.3	317	42	45	5	0.73
057	18/12/2011	13.00	259	16	-78	67	74	-93	2.2	61	39	339	152	29	61	0.59
058	27/12/2011	39.00	295	44	-101	130	47	-80	2.8	29.4	70.6	33	292	2	82	0.53
059	01/01/2012	14.00	70	4	-171	331	89	-86	2.3	97.2	2.8	237	65	44	45	0.79
060	03/01/2012	24.00	30	37	150	145	72	57	2.7	23.8	76.2	197	79	51	21	0.62
061	05/01/2012	31.00	180	66	114	312	33	48	1.5	73.9	26.1	307	252	61	18	0.42
062	19/01/2012	27.00	98	19	43	327	77	104	2.3	68.4	31.6	74	225	56	31	0.54
063	01/02/2012	29.00	178	55	122	311	46	53	2.6	35.4	64.6	326	178	53	122	0.68
064	01/02/2012	24.00	313	68	-122	192	38	-37	3.3	18.7	81.3	66	2	17	55	0.63
065	13/02/2012	12.00	175	69	107	315	27	53	3.6	75.4	24.6	291	252	62	22	0.81
066	21/02/2012	34.00	16	90	164	106	74	0	3.3	22.6	77.4	150	62	11	11	0.71
067	24/02/2012	14.00	320	47	-166	220	80	-44	2.6	11	89	97	350	21	37	0.68
068	01/03/2012	10.00	289	72	179	19	89	18	2.1	15.1	84.9	66	333	13	12	0.65
069	11/03/2012	31.00	188	47	133	314	58	54	2.5	49.2	50.8	349	249	59	6	0.75
070	12/03/2012	26.00	353	76	-91	177	14	-86	3.7	88	12	84	82	31	59	0.56
071	14/03/2012	15.00	301	52	-139	183	59	-46	3.5	78.2	21.8	63	328	4	53	0.63
072	16/03/2012	29.00	41	54	58	268	47	126	2.5	86.5	13.5	71	153	64	4	0.69
073	23/03/2012	08.00	112	10	2	20	90	100	2.7	98.5	1.5	120	280	44	44	0.73
074	27/03/2012	35.00	32	64	-13	128	78	-153	2.7	75.4	24.6	78	173	10	27	0.73
075	27/03/2012	11.00	354	26	-143	230	75	-69	2.2	40	60	123	347	27	55	0.62
076	28/03/2012	30.00	16	58	40	262	57	141	2.6	67.7	32.3	50	139	50	1	0.71
077	03/04/2012	18.00	271	25	-167	169	85	-66	1.9	94.7	5.3	58	284	35	45	0.62
078	03/04/2012	12.00	321	47	-105	162	45	-74	2.7	17	83	62	337	1	79	0.69
079	03/04/2012	08.00	191	12	64	38	79	95	2.5	89.5	10.5	134	303	56	34	0.49
080	04/04/2012	09.00	251	43	-128	118	57	-60	2.6	6.1	93.9	7	261	8	64	0.71
081	07/04/2012	15.00	14	62	-63	147	38	-130	2.2	22.1	77.9	85	148	13	63	0.66
082	07/04/2012	16.00	189	72	124	304	38	30	2.3	36.8	63.2	318	254	51	20	0.53
083	07/04/2012	07.00	197	61	116	332	38	52	2.3	77.6	22.4	332	269	64	12	0.64

084	10/04/2012	06.00	32	88	-74	129	16	-173	2.3	86.6	13.4	107	137	41	45	0.62
085	10/04/2012	08.00	29	77	122	139	34	24	2.2	28.6	71.4	153	95	48	25	0.56
086	11/04/2012	13.00	320	60	-118	187	40	-51	2.6	81.5	18.5	70	2	11	63	0.62
087	18/04/2012	16.00	15	80	-121	269	32	-19	2.3	30.1	69.9	129	73	28	46	0.53
088	21/04/2012	30.00	218	66	134	331	49	33	3.2	82.9	17.1	356	278	49	10	0.52
089	22/04/2012	15.00	116	57	142	229	59	40	2.2	70.4	29.6	263	172	49	1	0.81
090	23/04/2012	12.00	323	34	-122	213	34	-34	3.2	49.8	50.2	77	19	25	48	0.62
091	26/04/2012	33.00	256	32	-162	151	81	-59	2.9	74	26	36	272	29	46	0.51
092	02/05/2012	27.00	287	50	-140	169	61	-48	2.7	85	15	50	312	6	53	0.42
093	02/05/2012	11.00	152	57	-37	264	60	-141	3.6	85.7	14.3	208	299	2	48	0.73
094	02/05/2012	19.00	287	69	-113	157	31	-44	4.2	83.8	16.2	34	344	21	59	0.58
095	04/05/2012	22.00	16	85	78	264	13	157	3.3	93.2	6.8	75	178	66	6	0.84
096	08/05/2012	11.00	151	77	81	6	16	124	2.6	33.4	66.6	229	248	57	31	0.56
097	11/05/2012	12.00	205	89	74	112	16	176	2.6	26.7	73.3	279	310	44	42	0.62
098	12/05/2012	12.00	21	71	-166	286	77	-20	3	2	98	154	63	4	23	0.67
099	13/05/2012	16.00	311	76	-169	218	79	-14	3.6	84.7	15.3	85	354	2	18	0.71
100	14/05/2012	13.00	249	36	-170	151	84	-55	2.9	85.6	14.4	33	273	30	40	0.75
101	15/05/2012	15.00	248	49	-10	245	82	-139	1.8	50.5	49.5	289	35	22	34	0.61
102	16/05/2012	09.00	329	81	-168	237	78	-9	3.4	98.8	1.2	103	13	2	15	0.72
103	24/05/2012	21.00	281	84	-126	183	36	-10	2.5	71.1	28.9	40	338	30	40	0.73
104	25/05/2012	15.00	177	45	99	344	46	81	2.9	7	93	356	261	84	0	0.73

LIST OF PUBLICATIONS

1. **Rohtash Kumar, S.C. Gupta**, Arjun Kumar and Himanshu Mittal (2013). Source parameters and f_{\max} in lower Siang region of Arunachal Lesser Himalaya. *Arabian Journal of Geosciences*. DOI: 10.1007/s12517-013-1223-8.
2. **Rohtash Kumar, S.C. Gupta** and Arjun Kumar (2014). Attenuation characteristics of seismic body waves for the crust of Lower Siang region of Arunachal Himalaya. *International Journal of Advanced Research*, 2(6), 742-755.
3. **Rohtash Kumar, S.C. Gupta** and Arjun Kumar (2015). Non-double-couple mechanism of moderate earthquakes occurred in Lower Siang region of Arunachal Himalaya: Evidence of factors affecting non-DC. *Journal of Asian Earth Sciences*, 98, 105-115.
4. **Rohtash Kumar, S.C. Gupta** and Arjun Kumar (2015). Moment tensor inversion: An application of single station data for focal mechanism estimation. *Journal of seismology*. (under review)
5. **Rohtash Kumar, S.C. Gupta** and Arjun Kumar (2015). Coda waves attenuation characteristics for Lower Siang region of Arunachal Himalaya. *Tectonophysics*. (communicated)

References

1. Abercrombie, R. E. (1995). Earthquake source scaling relationships from 1 to 5 *ML* using seismograms recorded at 2.5 km depth, *J. Geophys. Res.* **100**, 24,015–24,036.
2. Abercrombie, R. E. (1997). Near-surface attenuation and site effects from comparison of surface and deep boreholes recordings, *Bull. Seism. Soc. Am.* **87**, 731–744.
3. Abdel-Fattah, A. K. (2009). Attenuation of body waves in the crust beneath the vicinity of Cairo Metropolitan area Egypt using coda normalization method, *Geophys. J. Int.* **1761**, 126-134.
4. Adamova, P., E. Sokos and Zahradnik (2009). Problematic non-double couple mechanism of the 2002 Amfilochia Mw 5 earthquake. Western Greece, *Journal of Seism.* **13**, 1–12.
5. Aki, K. (1966). Generation and propagation of G waves from the Niigata earthquake of June 16, 1964, Part 2: Estimation of earthquake moment, released energy, and stress-strain drop from the G wave spectrum, *Bull. Earthq. Res. Inst.* **44**, 73–88.
6. Aki, K. (1967). Scaling relation of seismic spectrum, *J. Geophys. Res.* **72**, 1217-1231.
7. Aki, K. (1969). Analysis of seismic coda of local earthquakes as scattered waves, *J. Geophys. Res.* **74**, 615–631.
8. Aki, K. (1972). Earthquake mechanism, *Tectonophysics* **13**, 423–446.
9. Aki, K. and B. Chouet (1975). Origin of coda waves; source, attenuation and scattering effects, *J. Geophys. Res.* **80**, 3322-3342.
10. Aki, K.. and B. Chouet (1975). Origin of coda waves: Source, attenuation and scattering effects, *J. Geophys. Res.* **80**, 3322–3342.
11. Aki, K.. (1980). Attenuation of shear waves in the lithosphere for frequencies from 0.05 to 25 Hz, *Phys. Earth Planet. Interiors* **21**, 50–60.

12. Aki, K., & Richards, P. G. (1980). Quantitative seismology: Theory and methods. *San Francisco*.
13. Aki, K. (1987). Magnitude-frequency relation for small earthquakes: A clue to the origin of f_{\max} of large earthquakes, *J. Geophys. Res.* **92**, 1349-1355.
14. Aki, K. (1988). Physical theory of earthquakes. In J. Bonnin, M. Cara, A. Cisternas and R. Fantechi (eds.) *Sesmic Hazard in Mediterranean Region*, 3-33.
15. Aki, K. and A. S. Papageorgiou (1988). Separation of source and site effects in acceleration power spectral of major California earthquakes, *Proc. 9th WCEE* 8 163-167.
16. Akinci, A., Del Pezzo, E., & Ibanez, J. M. (1995). Separation of scattering and intrinsic attenuation in southern Spain and western Anatolia (Turkey). *Geophys. J. Int.* **121(2)**, 337-353.
17. Ambeh, W.B. and J.D. Fairhead, (1989). Coda- Q estimates in the Mount Cameroon volcanic region, West Africa, *Bull. Seism. Soc. Am.* **79**, 1589–1600.
18. Ambeh, W.B. and L.L. Lynch (1993). Coda Q in the eastern Caribbean, West Indies, *Geophys. J. Int.* **112(3)**, 507-516.
19. Anderson, D. L., A. Ben-Menahem and C. B. Archambeau (1965). Attenuation of seismic energy in the upper mantle, *J. Geophys. Res* **70**, 1441-1448.
20. Anderson, J. G. and S. E. Hough (1984). A model for the shape of the Fourier amplitude spectrum of acceleration at high frequencies, *Bull. Seism. Soc. Am.* **74**, 1969-1993.
21. Anderson, J. G. (1986). Implication of attenuation for studies of the earthquake source, in *Earthquake Source Mechanics, Maurice Ewing Series 6*, S. Das, J. Boatwright, and C. H. Scholz (Editors), American Geophysical Union, Washington, D.C., 311-318.

22. Anderson, J. G. (1991). A preliminary descriptive model for the distance dependence of the spectral decay parameter in southern California, *Bull. Seism. Soc. Am.* **81**, 2186–2193.
23. Anderson, J. G., Y. Lee, Y. Zeng and S. Day (1996). Control of strong motion by the upper 30 meters, *Bull. Seism. Soc. Am.* **86**, 1749–1759.
24. Anon (1974). Geology and mineral resources of the states of India-Assam and adjoining states, *Geol Surv India Misc Publ* **20**, 1–24.
25. Archuleta, R.J., E. Cranswick, Ch. Mueller and P. Spudich (1982). Source parameters of the 1980 Mammoth lakes, California, earthquakes sequence, *J. Geophys. Res.* **87(B6)**, 4595-4607.
26. Backus, G., and M. Mulcahy (1976). Moment tensors and other phenomenological descriptions of seismic sources—I. Continuous displacements, *Geophys. J. Int.* **46(2)**, 341-361.
27. Banghar, A. R. (1972). Focal mechanisms of Indian earthquakes, *Bull. Seism. Soc. Am.* **62(2)**, 603-608.
28. Bansal, B. K., S. K. Singh, R. Dharmaraju, J. F. Pacheco, M. Ordaz, R. S. Dattatrayam and G. Suresh (2009). Source study of two small earthquakes of Delhi, India, and estimation of ground motion from future moderate, local events, *J. Seism.* **13(1)**, 89-105.
29. Barros, L.V., M. Assumpção, R. Quintero and V.M. Ferreira (2011). Coda wave attenuation in the Parecis Basin Amazon craton – Brazil – Sensitivity to basement depth, *J. Seism.* **15**, 391-409.
30. Baruah, S., D. Hazarika, A. Kalita and S. Goswami (2010). Intrinsic and scattering attenuation in Chedrang Fault and its vicinity-the rupture area of great Assam earthquake of 12 June 1897 (M= 8.7) *Current Science*, **99(6)**, 775-784.

31. Beresnev, I. A., K. L. Wen and Y. T. Yeh (1995). Seismological evidence for nonlinear elastic ground behavior during large earthquakes, *Soil Dynamics and Earthquake Engineering* **14(2)**, 103-114.
32. Beresnev, I. A. and K. L. Wen (1996). The possibility of observing nonlinear path effect in earthquake-induced seismic wave propagation. *Bull. Seism. Soc. Am.* **86(4)**, 1028-1041.
33. Berckhemer, H. (1962). Die Ausdehnung der Bruchfläche im Erdbebenherd und ihr Einfluss auf das seismische Wellenspektrum. *Gerlands Beitr. Geophys.*, **71**, 5-26.
34. Bormann, P. History, Aim and Scope of the 1st and 2nd Edition of the IASPEI New Manual of Seismological Observatory Practice.
35. Huang, M. W., J. H. Wang, K. F. Ma, C. Y. Wang, J. H. Hung and K. L. Wen (2007). Frequency-dependent site amplifications with $f \geq 0.01$ Hz evaluated from velocity and density models in central Taiwan, *Bull. Seism. Soc. Am.* **97(2)**, 624-637.
36. Bhattacharya, S. N. (2007). Moment tensor solutions and triggering environment for earthquakes in Koyna-Warna water reservoirs region, India, *Pure and Applied Geophys.* **164(5)**, 909-928.
37. Bianco, F., M. Castellano, E. Del Pezzo and J.M. Ibañez, 1999. Attenuation of short-period seismic waves at Mt. Vesuvius, Italy, *Geophys. J. Int.* **138**, 67–76.
38. Bilham, R. and P. England (2001). Plateau ‘pop-up’ in the great 1897 Assam earthquake, *Nature* **410(6830)**, 806-809.
39. Boore, D. M. (1983). Stochastic simulation of high-frequency ground motion based on seismological models of the radiated spectra, *Bull. Seism. Soc. Am.* **73**, 1865-1894.
40. Bora, D. K., S. Baruah, R. Biswas and N. K. Gogoi (2013). Estimation of Source Parameters of Local Earthquakes Originated in Shillong–Mikir Plateau and its Adjoining Region of Northeastern India. *Bull. of Seism. Soc. Am.* **103(1)**, 437-446.

41. Bormann P (2002) IASPEI: New Manual of Seismological Observatory Practice (NMSOP). Geo Forschungs Zentrum.
42. Bouchon, M. (1981). A simple method to calculate Green's functions for elastic layered media, *Bull. of Seism. Soc. Am.* **71**, 959–971.
43. Bouchon, M. (2003). A review of the discrete wavenumber method, *Pure and Applied Geophysics* **160**, 445–465.
44. Brune, J. N. (1970). Tectonic stress and the spectra of seismic shear waves from earthquake, *J. Geophys. Res.* **75**, 4997-5009.
45. Brune, J. N. (1971). Correction to tectonic stress and the spectra of seismic shear waves from earthquakes, *J. Geophys. Res.* **76**, 5002.
46. Burridge, R. and L. Knopoff (1964). Body force equivalents for seismic dislocations, *Bull. Seism. Soc. Am.* **54**, 1875–1878.
47. Campillo, M. (1983). Numerical evaluation of near-field, high-frequency radiation from quasi-dynamic circular faults, *Bull. Seism. Soc. Am.* **73**, 723-734.
48. Campillo, M. and J. L. Planet (1991). Frequency dependence and spatial distribution of seismic attenuation in France: experimental results and possible interpretations, *Phys. Earth Planet. Inter.* **67**, 48–64.
49. Canas, J.A., L. Pujades, M.J. Blanco, V. Soler and J.C. Carracedo (1995). Coda-Q distribution in the Canary Islands, *Tectonophysics* **246**, 245–261.
50. Castro, R. R., G. Monachesi, M. Mucciarelli, L. Trojani and F. Pacor, 1999. P-and S-wave attenuation in the region of Marche, Italy, *Tectonophysics* **3021**, 123-132.
51. Castro, R. R., L. Trojani, G. Monachesi, M. Mucciarelli, and M. Cattaneo (2000). The spectral decay parameter κ in the region of UmbriaMarche, Italy, *J. Geoph. Res.* **105**, 23,811–23,823.

52. Castro, R.R., M. Monachesi, L. Trojani, M. Mucciarelli and M. Frapiccini (2002). An attenuation study using earthquakes from the 1997 Umbria-Marche sequence, *J. Seism.* **6**, 43–59.
53. Castro, R. R., M. Massa, P. Augliera and F. Pacor (2008). Body-wave attenuation in the region of Garda, Italy, *Pure Appl. Geophys.* **1657**, 1351-1366.
54. Catherine, R.D.W. (1990). Estimation of Q in Eastern Canada using coda waves, *Bull. Seism. Soc. Am.* **80**, 411-429.
55. Chandra, U. (1977). Earthquakes of peninsular India—a seismotectonic study, *Bull. Seism. Soc. Am.* **67(5)**, 1387-1413.
56. Chang, K., W.C. Chi, Y. Gung, D. Dreger, W.H. Lee and H.C. Chiu (2011). Moment tensor inversions using strong motion waveforms of Taiwan TSMIP data, 1993–2009. *Tectonophysics* **511(1)**, 53-66.
57. Chaudhtjry, H. and H. N. Srivastava (1976). Seismicity and focal mechanism of some recent earthquakes in North-east India and neighborhood, *Annals of Geophysics* **29(1-2)**, 41-57.
58. Chen, W. P. and P. Molnar (1990). Source parameters of earthquakes and intraplate deformation beneath the Shillong plateau and the northern Indoburman ranges, *J. Geophys. Res.: Solid Earth (1978–2012)* **95(B8)**, 12527-12552.
59. Chlieh, M., J.P. Avouac, V. Hjorleifsdottir, T.R.A. Song, C. Ji, K. Sieh and J. Galetzka (2007). Coseismic slip and afterslip of the great Mw 9.15 Sumatra–Andaman earthquake of 2004, *Bull. Seism. Soc. Am.* **97(1A)**, S152-S173.
60. Chopra, S., D. Kumar and K. M. Rao (2008). Attenuation of P and S waves in the Kachchh Region, *J. Ind. Geophys. Union* **121**, 11-22.
61. Chopra, S., Dinesh Kumar and B.K. Rastogi (2010). Attenuation of High Frequency P and S Waves in the Gujarat Region, India, *Pure Appl. Geophys.* **168(5)**, 797-813.

62. Chopra, S., J. Sharma, A. Sutar and B. K. Bansal (2013). Estimation of Source Parameters of Mw 6.9 Sikkim Earthquake and Modeling of Ground Motions to Determine Causative Fault, *Pure and Applied Geophysics*, 1-18.
63. Chung, T.W. and H. Sato (2001). Attenuation of high-frequency P and S waves in the crust of southeastern South Korea, *Bull. Seism. Soc. Am.* **91**, 1867–1874.
64. Chung, J. K., Y. L. Chen and T. C. Shin (2009). Spatial distribution of coda Q estimated from local earthquakes in Taiwan area, *Earth Planets and Space (EPS)* **61(9)**, 1077.
65. Chouhan, R. K. S. and V. K. Srivastava (1975). Focal mechanisms in northeastern India and their tectonic implications, *pure and applied geophysics* **113(1)**, 467-482.
66. CISMHE (2011). Environmental Feasibility Report of Hironag H.E. project on Siyom River in Arunachal Pradesh for Jaypee Associates, New Delhi.
67. Console, R. and A. Rovelli (1981). Attenuation parameters for Friuli region from strong-motion accelerogram spectra, *Bull. Seism. Soc. Am.* **71(6)**.
68. Curran J.R., D.G. Moore, L.A. Lawver, F.J. Emmel, R.W. Raitt, M. Henry, and R. Kieckhefer (1979). Tectonics of the Andaman Sea and Burma: Convergent Margins 189-198.
69. Das, S., Boatwright, J. and Scholz, C. H. (Eds.). (1986). *Earthquake source mechanics* (No. 37). American Geophysical Union.
70. Day, S. M., Yu, G., & Wald, D. J. (1998). Dynamic stress changes during earthquake rupture. *Bull. Seism. Soc. Am.*, **88(2)**, 512-522.
71. Deng Q, Zhang P, Ran Y, Yang X, Min W, Chu Q (2003) Basic characteristics of active tectonics of China, *Science in China Series D: Earth Sciences* 46(4): 356-372.

72. Del Pezzo, E., F. Ferulano, A. Giarrusso and M. Martini (1983). Seismic coda Q and scaling law of the source spectra at the Aeolian Islands, southern Italy. *Bull. Seism. Soc. Am* **73(1)**, 97-108.
73. Del Pezzo, E., J. Ibanez, J. Morales, A. Akinci and R. Maresca (1995). Measurements of intrinsic and scattering seismic attenuation in the crust. *Bull. Seism. Soc. Am* **85(5)**, 1373-1380.
74. Delouis., B. and D. Legrand (1999). Focal mechanism determination and identification of the fault plane of earthquakes using only one or two near-source seismic recordings, *Bull. Seism. Soc. Am.* **89(6)**, 1558-1574.
75. Der, Z.A. (1998). High frequency P and S wave attenuation in the Earth, *Pure Appl. Geophys.* **153**, 273–310.
76. Doglioni, C. and G. Flores (1997). An introduction to Italian geology, universita degli Studi Basilicata, Lamisco.
77. Dreger D.S. and D.V. Helmberger (1991). Complex faulting deduced from broadband modeling of the 28 February 1990 Upland earthquake (ML=5.2). *Bull. Seism. Soc. Am.* **81**,1129–1144.
78. Dreger D.S. (1992). Modeling earthquakes with local and regional broadband data, ph.d. thesis, Calif Inst of Tectnol, Pasadena
79. Dreger D.S. and D.V. Helmberger (1993). Determination of source parameters at regional distances with three-component sparse network data, *J. Geophys. Res.* **98(B5)**, 8107-8125.
80. Dreger D.S. (2002). TDMT_INV: time-domain seismic moment tensor inversion. In: Lee, Lee, Jennings H, Kisslinger PC, Kanamori H (Eds.) (2002) International Handbook of Earthquake and Engineering Seism. , Part B. Academic Press, Amsterdam 1627 and files on attached CD-ROM.

81. Duda, S. J. (1978). Physical significance of the earthquake magnitude the present state of interpretation of the concept, *Tectonophysics* **49**, 119-130
82. Dutta, U., N.N. Biswas, D.A. Adams and A. Papageorgiou (2004). Analysis of S-wave attenuation in South-Central Alaska, *Bull. Seism. Soc. Am.* **94**, 16–28.
83. Dysart, P. S., J. A. Snoke, and I. S. Sacks (1988). Source parameters and scaling relations for small earthquakes in the Matsushiro region, southwest Honshu, Japan, *Bull. Seism. Soc. Am.* **78**, 571–589
84. Dziewonski, A.M., T.A. Chou and J.H. Woodhouse (1981). Determination of earthquake source parameters from waveform data for studies of global and regional seismicity, *J. Geophys. Res.* **86**, 2825–2852.
85. Dziewonski, A.M. and J.H. Woodhouse (1983b). An experiment in systematic study of global seismicity: centroid-moment tensor solutions for 201 moderate and large earthquakes of 1981, *J. Geophys. Res.* **88**, 3247-3271.
86. EQ: 2006-02. Report on source parameters and attenuation characteristics in the environs of Bichom and Tenga dam sites, Kameng hydroelectric project, Arunachal Pradesh. *Department of Earthquake Engineering, IIT Roorkee.*
87. Ewing, W. M., W. S. Jardentzky and F. Press (1957). *Elastic Waves in Layered Media* (McGraw-Hill, New York).
88. Faccioli, E. (1986). A study of spectra and peak values of strong motion accelerograms from Italy and Yugoslavia in terms of gross source properties, in *Earthquake Source Mechanics*, Geophysical Monograph 37, Maurice Ewing Series, vol. 6, S. Das, J. Boatwright, and C. H. Scholz, Editors, American Geophysical Union, Washington, D.C., 297-310.

89. Fan, G. and T.C. Wallace (1991). The determination of source parameters for small earthquakes from a single very broadband seismic station, *Geophys. Res. Lett.* **18**, 1385-1388.
90. Fedotov, S.A. and S.A. Boldyrev (1969). Frequency dependence of the body wave absorption in the crust and the upper mantle of the Kuril Island chain, *Izv. Acad. Sci. USSR. Solid Earth* **11**, 553–562.
91. Feignier, B. and R.P., Young (1992). Moment tensor inversion of induced microseismic events: evidence of non-shear failures in the $-4 < M < -2$ moment magnitude range, *Geophys. Res. Lett.* **19**, 1503–1506.
92. Fitch, T.J. (1972). Plate convergence, transcurrent faults, and internal deformation adjacent to Southeast Asia and the western Pacific, *J. Geophys Res* **77(23)**, 4432-4460.
93. Frankel, A. and L. Wennerberg (1987). Energy flux model of the seismic coda: separation of scattering and intrinsic attenuation, *Bull. Seism. Soc. Am.* **77**, 1223–1251.
94. Freund, L. B. (1979). The mechanics of dynamic shear crack propagation, *J. Geophys. Res.: Solid Earth (1978–2012)* **84(B5)**, 2199-2209.
95. Freund, L. B. (1972). Energy flux into the tip of an extending crack in an elastic solid. *Journal of Elasticity* **2(4)**, 341-349.
96. Fujiwara, H. and K. Irikura (1991). High-frequency seismic wave radiation from antiplane cohesive zone model and f_{max} as source effect, *Bull. Seism. Soc. Am.* **81(4)**, 1115-1128.
97. Fojtíkova, L., V. Vavryčuk, A. Cipciar and J. Madaras (2010). Focal mechanisms of micro-earthquakes in the Dobrá Voda seismoactive area in the Malé Karpaty Mts.(Little Carpathians), Slovakia, *Tectonophysics* **492(1)**, 213-229.

98. Frohlich, C. (1994). Earthquakes with non-double-couple mechanisms, *Science* **264**, 804–809.
99. Julian, B.R., A.D. Miller and G.R. Foulger (1998). Non-double-couple earthquakes 1: Theory, *Reviews of Geophysics* **36**, 525–549.
100. Gansser, A. (1964). Geology of the Himalayas. Interscience Publishers, London, 286p.
101. Gao, L.S., N.N. Biswas, L.C. Lee and K. Aki (1983). Effects of multiple scattering on coda waves in three dimensional medium, *Pure Appl. Geophys.* **121**, 3–15.
102. Garcia-Garcia, J. M., F. Vidal, M. D. Romacho, J. M. Martin-Marfil , A. Posadas and F. Luzon (1996). Seismic source parameters for microearthquakes of the Granada basin (southern Spain), *Tectonophysics* **261**, 51-66.
103. Ghimire, S. and M. Kasahara (2007). Source process of the Ms= 6.6, Udayapur earthquake of Nepal–India border and its tectonic implication, *Journal of Asian Earth Sciences* **31(2)**, 128-138.
104. Giardini, D. (1984). Systematic analysis of deep seismicity: 200 centroid-moment tensor solutions for earthquakes between 1977 and 1980, *Geophys. J. Int.* **77(3)**, 883-914.
105. Gilbert, F. and A.M. Dziewonski (1975). An application of normal mode theory to the retrieval of structural parameters and source mechanisms from Seismic spectra. *Philosophical Transactions for the Royal Society of London. Series A, Mathematical and Physical Sciences* **278**, 187-269.
106. GSI (2000). Seismotectonic Atlas of India and its Environs. *Geol. Surv. India*, Sp. Pub., P. L. Narula, S. K. Acharya and J. Banerjee (eds.).

107. GSI (2000) Case Study of Tehri Dam Project, District Tehri Garhwal, Uttarakhand.
108. Gupta, S.C., A. Kumar, V.N. Singh and S. Basu (1996). Lapse- time dependence of Q_c in the Garhwal Himalaya, *Bull. Indian. Soc. Earthquake Technol.* **33**, 147–159.
109. Gupta, I. D. and V. Rambabu, (1993). Source parameters of some significant earthquakes near Koyna dam, India, *pure and applied geophysics* **140(3)**, 403-413.
110. Gupta, S.C., V.N. Singh and A. Kumar (1995). Attenuation of coda waves in the Garhwal Himalaya, India, *Phys. Earth Planet. Inter.* **87**, 247–253.
111. Gupta, S. C., S. S. Teotia, S. S. Rai and N. Gautam (1998). Coda Q estimates in the Koyna region, India, *Pure Appl. Geophys.* **153**, 713–731.
112. Gupta, S.C. and A. Kumar (2002). Seismic wave attenuation characteristics of three Indian regions-A comparative study. *Curr. Sci.* **82**, 407–413.
113. Gupta, S. C., A. Kumar, A. K. Shukla, G. Suresh and P. R Baidya, (2006). CodaQ in the Kachchh Basin, Western India using aftershocks of the Bhuj earthquake of January 26, 2001, *Pure Appl. Geophys.* **163(8)**, 1583–1595.
114. Gupta, A. K., A. K. Sutar, S. Chopra, S. Kumar and B. K., Rastogi (2012). Attenuation characteristics of coda waves in Mainland Gujarat (India). *Tectonophysics* **530**, 264-271.
115. Hanks, T. C. and Johnson, D. A. (1976). Geophysical assessment of peak accelerations. *Bull. Seism. Soc. Am.* **66(3)**, 959-968.
116. Hanks, T. C. and H. Kanamori (1979). A moment magnitude scale, *J. Geophys. Res.* **84**, 2348–2350.
117. Hanks, T. C. (1982). f_{max} , *Bull. Seism. Soc. Am.* **72**, 1867-1879.

118. Hannay, S. T. (1851). Brief notice of the Sil-sako or stone bridge in Zillah Kamrup, *J. Asiat. Soc. Bengal* 20, 291-294.
119. Hasegawa, H.S. and H. Kanamori (1987). Source mechanism of the magnitude 7.2 Grand Banks earthquake of November 1929: double couple or submarine landslide?. *Bull. Seism. Soc. Am.* **77**, 1984–2004.
120. Havskov, J. and L. Ottemoller (2003). SEISAN: The Earthquake Analysis Softwares for Windows, Solaris and Linux, Version 8.0. Institute of Solid Earth Physics, University of Bergen, Norway.
121. Havskov, J. and L. Ottemoller (2005). SEISAN (version 8.1): the earthquake analysis software for Windows, Solaris, Linux, and Mac OSX Version 8.0. pp 254.
- Hazarika, D., S. Baruah, and N. K. Gogoi (2009). Attenuation of coda waves in the Northeastern Region of India, *J. Seism.* **13(1)**, 141-160.
122. Hazarika, P., M. R. Kumar, G. Srijayanthi, P. S. Raju, N. P. Rao, and D. Srinagesh, (2010). Transverse tectonics in the Sikkim Himalaya: evidence from seismicity and focal-mechanism data, *Bull. Seism. Soc. Am.* **100(4)**, 1816-1822.
123. Hazarika, P., M. R. Kumar and D. Kumar (2013). Attenuation character of seismic waves in Sikkim Himalaya, *Geophys. J. Int.* **gg241**.
124. Herrmann, R. (1980). Q estimates using coda of local earthquakes, *Bull. Seism. Soc. Am.* **70**, 447–468.
125. Herrmann, R.B. and A. Kijko (1983). Modelling some empirical vertical component Lg relations, *Bull. Seism. Soc. Am.* **73**, 157–171
126. Herrmann, R.B. and C.Y. Wang (1985). A comparison of synthetic seismograms. *Bull. Seism. Soc. Am.* **75**, 41–56.
127. Herraiz, M. and A.F. Espinosa (1987). Coda waves: a review. *Pure Appl. Geophys.* **125**, 499–577.

128. Hellweg, M., P. Spandich, J.B. Fletcher and L.M. Baker (1995). Stability of coda Q in the region of Parkfield, California: view from the U.S. Geological Survey Parkfield Dense Seismograph Array, *J. Geophys. Res.* **100**, 2089–2102.
129. Hoshiya, M. (1993). Separation of scattering attenuation and intrinsic absorption in Japan using the multiple lapse time window analysis of full seismogram envelope. *J. Geophys. Res.: Solid Earth (1978–2012)* **98(B9)**, 15809-15824.
130. Ho-Liu and Phyllis Hang-Yin (1988). Attenuation tomography. Modelling regional love waves: Imperial Valley to Pasadena. Dissertation (Ph.D.), California Institute of Technology.
131. Honda, H. (1962). Earthquake mechanism and seismic waves, *Journal of Physics of the Earth* **10**, 1–98.
132. Hough, S.E. and J.G. Anderson (1988). High-frequency spectra observed at Anza, California: implications for Q structure. *Bull. Seism. Soc. Am.* **78**, 692–707.
133. Ida, Y. (1973). The maximum acceleration of seismic ground motion. *Bull. Seism. Soc. Am* **63(3)**, 959-968.
134. Ide, S., G. C. Beroza, S. G. Prejean and W. L. Ellsworth (2003). Apparent break in earthquake scaling due to path and site effects on deep borehole recordings, *J. Geophys. Res.: Solid Earth (1978–2012)*, 108(B5).
135. India Meteorological Department, 2014. Seismicity map of Indian region with events of magnitude 5 and above (up to June 2011). <http://www.imd.gov.in/>
136. IS 1893 (Part-1): 2002 Indian standard criteria for earthquake resistant design of structures Part 1 – General Provisions and Buildings. Bureau of Indian Standards, New Delhi.
137. Iyengar, R. N., D. Sharma and J. M. Siddiqui (1999). Earthquake history of India in medieval times, *Indian Journal of History of Science* **34**, 181-238.

138. Jain, R., B. K. Rastogi and C. S. P. Sarma, (2004). Precursory changes in source parameters for the Koyna–Warna (India) earthquakes, *Geophys. J. Int.* **158(3)**, 915–921.
139. Jeffreys, H. (1929), (1959). *The Earth, its origin, history and physical constitution* (Cambridge University Press), 2nd edition, 1929, 4th edition, 1959.
140. Jin, A. and K. Aki (1988). Spatial and Temporal Correlation between Coda Q and Seismicity in China, *Bull. Seism. Soc. Am.* **78**, 741–769.
141. Jin, A. and K. Aki (2005). High-resolution maps of coda Q in Japan and their interpretation by the brittle-ductile interaction hypothesis. *Earth Planets Space* **57**, 403–409.
142. Jost, M. U. and R. B. Herrmann (1989). A student's guide to and review of moment tensors, *Seism. Res. Lett.* **60(2)**, 37-57.
143. Joshi, A. (2006). Use of acceleration spectra for determining the frequency dependent attenuation coefficient and source parameters. *Bull. Seism. Soc. Am.* **96**, 2,165–2,180.
144. Jost, M.U. and R.B. Herrmann (1989). A student's guide to and review of moment tensors, *Seism Res Lett.* **60(2)**, 37-57.
145. Kanamori, H., & Anderson, D. L. (1975). Amplitude of the Earth's free oscillations and long-period characteristics of the earthquake source. *J. Geophys. Res.* **80(8)**, 1075-1078.
146. Kanamori, H. and J.W. Given (1981). Use of long-period surface waves for rapid determination of earthquake-source parameters, *Physics of the Earth and Planetary Interiors* **27**, 8-31.
147. Kanamori, H. and J.W. Given (1982). Use of long-period surface waves for rapid determination of earthquake source parameters: 2. Preliminary determination of

- source mechanisms of large earthquakes ($M_s > 6.5$) in 1080, *Physics of the Earth and Planetary Interiors* **30**,260-268
148. Kawakatsu, H. (1995). Automated near-realtime CMT inversion. *J. Geophys. Lett.* **22(19)**, 2569-2572.
149. Kawasaki, I. and T. Tanimoto (1981). Radiation patterns of body waves due to the seismic dislocation occurring in an anisotropic source medium, *Bull. Seism. Soc. Am.* **71**, 37–50.
150. Kayal, J.R. (1987). Microseismicity and source mechanism study: Shillong Plateau, Northeast India, *Bull. Seism. Soc. Am.* **77**, 184–194.
151. Kayal, J. R., V. K. Srivastava, S. N. Bhattacharya, P. K. Khan and Rima Chatterjee (2009). Source parameters and focal mechanisms of local earthquakes: single broadband observatory at ISM Dhanbad, *Journal. Geological Society of India* **74**,413-419.
152. Keiles-Borok, V. (1959). An estimation of the displacement in an earthquake source and of source dimensions, *Ann. Geofis. (Rome)* **12**, 205 214.
153. Kesari, G.K., G. Das Gupta, H.S.M. Prakash, B.K. Mohanty, S. Lahiri and J.N. Ray (2010). Geology and mineral resources of Arunachal Pradesh, *Geological Survey of India*, 1-60.
154. Khan, P. K., S. Chakraborty, V. K. Srivastava and R. Prasad (2009). Seismicity, source parameters and scaling relationships for the eastern part of Eastern Indian Shield region, *Indian Minerals* **61**, 65-74
155. Khattri, K., M. Wyss, V. K. Gaur, S. N. Saha and V. K. Bansal (1983). Local seismic activity in the region of the Assam gap, northeast India, *Bull. Seism. Soc. Am.* **73(2)**, 459-469.

156. Kikuchi, M. and H. Kanamori (1991). Inversion of complex body waves—III, *Bull. Seism. Soc. Am.* **81**, 2335–2350.
157. Kim, S.G. and N. Kraeva (1998). Seismic source study of local and regional earthquakes in and near Korea using moment tensor inversion, *J. Kor. Earth. Sc.* **19(3)**, 283-293.
158. Kim, S.G. and N. Kraeva (1999). Source parameter determination of local earthquakes in Korea using moment tensor inversion of single station data, *Bull. Seism. Soc. Am.* **89**, 1077–1082.
159. Kim, S.G. and N. Kraeva and Y.T. Chen (2000). Source parameter determination of regional earthquakes in the Far East using moment tensor inversion of single-station data, *Tectonophysics* **317(1)**, 125-136.
160. Kim, K.D., T.W. Chung and J.B. Kyung (2004). Attenuation of high-frequency P and S waves in the crust of Choongchung provinces, Central South Korea, *Bull. Seism. Soc. Am.* **94**, 1070–1078.
161. Klein, F.W. (1978). Hypocenter location program: HYPOINVERSE. *US Department of the Interior, Geological Survey, Open-File Rep.* **78-694**, pp 113.
162. Knopoff, L. (1964). *Q*, *Rev. Geophys.* **2**, 625–660.
163. Knopoff, L. and M. J. Randall (1970). The compensated linear vector dipole: a possible mechanism for deep earthquakes, *J. Geophys. Res.* **75**, 4957–4963.
164. Köhler, N., G. Cua, F. Wenzel and M. Bose (2009). Rapid source parameter estimations of southern California earthquakes using PreSEIS. *Seism. Res. Let.* **80(5)**, 748-754.
165. Kopynichev, Y. F. (1977). The role of multiple scattering in the formation of seismogram's tail, *Izvestiya, Phys. Solid Earth* **13**, 394–398.

166. Kostiov B. V. , (1964). Self-similar problems of propagation of shear cracks, *J. appl. Math. Mech.* **28**, 1077–1087.
167. Kostrov B. V. (1966). Unsteady propagation of longitudinal shear cracks, *J. appl. Math. Mech.* **30**, 1241–1248
168. Koyama, J. (1997). *The complex faulting process of earthquakes* **16**. Springer.
169. Kravanja, S., Panza, G. F. and Šílený, J. (1999). Robust retrieval of a seismic point-source time function. *Geophys. J. Int.* **136(2)**, 385-394.
170. Kuhn, D. and V. Vavrycuk (2013). Determination of full moment tensors of microseismic events in a very heterogeneous mining environment. *Tectonophysics* **589**, 33-43.
171. Kuge, K. and T. Lay (1994). Data-dependent non-double-couple components of shallow earthquake source mechanisms: effects of waveform inversion instability, *Geophys. Res. Lett.* **21**, 9–12.
172. Kumar, A., A. D. Pandey, M. L. Sharma, S. C. Gupta, A. K. Verma, and B. K. Gupta (1994). Processing and Preliminary Interpretation of Digital Data Obtained from Digital Telemetered Seismic Array in the Garhwal Himalaya, *Xth Symposium on Earthquake Engineering, University of Roorkee*.
173. Kumar, G., 1997. Geology of Arunachal Pradesh, *Geological Society of India, Bangalore*, pp.1-217.
174. Kumar, A., A.D. Pandey, M.L. Sharma, S.C. Gupta, A.K. Verma and B. K. Gupta (1997). Processing and preliminary interpretation of digital data obtained from telemetered seismic array in the Garhwal Himalaya, *10th Symp. of Earthquake Engineering, University of Roorkee, Roorkee*, 141–152.
175. Kumar, N, A. Parvez Imtiyaz and H.S. Virk (2005). Estimation of coda wave attenuation for NW Himalayan region using local earthquakes, *Phys. of the Earth and Planet. Int.* **151**, 243–258.

176. Kumar, D., I. Sarkar, V. Sriram, and K. N. Khattri (2005). Estimation of the source parameters of the Himalaya earthquake of October 19, 1991, average effective shear wave attenuation parameter and local site effects from accelerograms, *Tectonophysics* **407**, 1–24.
177. Kumar, N., I. A. Parvez, and H. S. Virk (2005). Estimation of coda wave attenuation for NW Himalayan region using local earthquakes, *Physics of the Earth and Planetary Interiors* **151(3)**, 243-258.
178. Kumar, A., S. C. Gupta, A. Kumar, A. Sen, A. K. Jindal and S. Jain (2006). Estimation of source parameters from local earthquakes in Western part of the Arunachal Lesser Himalaya, *13SEE*, 9-17.
179. Kumar, D., V. S. Ram and K. N. Khattri (2006). A study of source parameters, site amplification functions and average effective shear wave quality factor Q_{seff} from analysis of accelerograms of the 1999 Chamoli earthquake, Himalaya, *pure and applied geophysics* **163(7)**, 1369-1398.
180. Kumar, D., V. Sriram, I. Sarkar and S. S. Teotia (2008). An Estimate of a Scaling Law of Seismic Spectrum for Earthquakes in Himalaya, *Indian Minerals* 61(3-4) and 62 (1-4), 83-92.
181. Kumar, A., A. D. Pandey and M. L. Sharma, EQ: 2009-33 (2009). “ Seismological Network Around Tehri Region” Report on processing and Interpretation of seismological Data Collected (from January 2008 to December +2008) Department of Earthquake Engineering, IIT Roorkee.
182. Kumar, Arjun (2011). Study of earthquake source parameters using microearthquakes and strong motion data. Indian Institute of Technology, Roorkee.
183. Kumar, A., A. Kumar, H. Mittal, A. Kumar and R. Bhardwaj (2012). Software to estimate earthquake spectral and source parameters, *Int. J. Geosciences* **3**, 1142.
184. Kumar, A., A. Kumar, A. Kumar, S.C. Gupta, A.K. Jindal and H. Mittal (2012). Source parameters of Uttarkashi earthquake of 21st Sept 2009, *15 WCEE Lisbon*.

185. Kumar, A., A. Kumar, S. C. Gupta, H. Mittal, and R. Kumar (2013). Source parameters and f_{\max} in Kameng region of Arunachal Lesser Himalaya. *J. Asian Earth Sciences* **70**, 35-44.
186. Kumar, R., S.C. Gupta, A. Kumar and H. Mittal (2013). Source parameters and f_{\max} in lower Siang region of Arunachal lesser Himalaya, *Arabian Journal of Geosciences*, 1-11, DOI 10.1007/s12517-013-1223-8
187. Kumar, R., S. C. Gupta and A. Kumar (2014). Attenuation characteristics of seismic body waves for the crust of Lower Siang region of Arunachal Himalaya. *International Journal of Advanced Research* **2(6)**, 742-755.
188. Kumar, R., S. C. Gupta and A. Kumar (2014). Coda waves attenuation characteristics for Lower Siang region of Arunachal Himalaya. *Tectonophysics*. (under review)
189. Kumar, R., S. C. Gupta and A. Kumar (2014). Non-double-couple mechanism of moderate earthquakes occurred in Lower Siang region of Arunachal Himalaya: evidence of factors affecting non-DC. *Journal of Asian Earth sciences*. . (accepted)
190. Kumar, R., S. C. Gupta and A. Kumar (2014). Effect of azimuth coverage of an earthquake on Moment Tensor solutions estimated by waveform inversion. *Arabian Journal of Geosciences*. DOI 10.1007/s12517-014-1666-6.
191. Kvamme L.B. and J. Havskov (1989). Q in Southern Norway, *Bull. Seism. Soc. Am.* **79**, 1575–1588.
192. Langston, C.A. (1981). Source inversion of seismic waveforms: The Koyna, India, earthquakes of 13 September 1967, *Bull. Seism. Soc. Am.* **71(1)**, 1-24.
193. Legrand D., and B. Delouis (1999). Automatic determination of the fault plane using a single near field seismic station with a finite dimension source model, *Geophy. J. Int.* **138**, 801-808.

194. Le Fort, P. (1975). Himalaya, the collided range: present knowledge of the continental arc, *American Journal of Science* **275a**, 1-44.
195. Li, Y. and C. H. Thurber (1988). Source properties of two microearthquakes at Kilauea volcano, Hawaii, *Bull. Seism Soc. Am.* **78 (3)**, 1123-1132.
196. Lindholm, C. D., H. Bungum, E. Hicks and M. Villagran (2000). Crustal stress and tectonics in Norwegian regions determined from earthquake focal mechanisms, *Geological Society, London, Special Publications* **167(1)**, 429-439.
197. Lenhardt, W. A. (2002). Seismicity in Tyrol in relation to the TRANSALP transect. *Mem. Sci. Geol* **54**, 49-52.
198. Hartzell, S. (1989). Comparison of seismic waveform inversion results for the rupture history of a finite fault: application to the 1986 North Palm Springs, California, earthquake. *J. Geophys. Res.: Solid Earth (1978–2012)* **94(B6)**, 7515-7534.
199. Hicks, E. C., H. Bungum and C. D. Lindholm, (2000). Stress inversion of earthquake focal mechanism solutions from onshore and offshore Norway, *Norsk Geologisk Tidsskrift* **80(4)**, 235-250.
200. Hicks, E. C., H. Bungum, and C. D. Lindholm (2000). Seismic activity, inferred crustal stresses and seismotectonics in the Rana region, Northern Norway, *Quaternary Science Reviews* **19(14)**, 1423-1436.
201. Lindsay, J. M., R. B. Trumbull and W. Siebel (2005). Geochemistry and petrogenesis of late Pleistocene to Recent volcanism in southern Dominica, Lesser Antilles, *Journal of volcanology and geothermal research* **148(3)**, 253-294.
202. Liu, H. P., D. L. Anderson and H. Kanamori (1976). Velocity Dispersion due to Anelasticity; Implications for Seism. and Mantle Composition, *Geophys. J. R. Astr. Soc.* **47**, 41–58.

203. Maercklin, N., A. Zollo, A. Orefice, G. Festa, A. Emolo, R. De Matteis and A. Bobbio (2011). The effectiveness of a distant accelerometer array to compute seismic source parameters: the April 2009 L'Aquila earthquake case history. *Bull. Seism. Soc. Am.* **101(1)**, 354-365.
204. Mahajan, A. K. and S. Kumar (2004). Macro seismic field observations of January 26th, 2001 Kachchh earthquake and its seismotectonics, *J. Asian Earth Sciences* **23(1)**, 17-23.
205. Mahajan, A. K., V. Gupta and V. C. Thakur (2012). Macro seismic field observations of 18 September 2011 Sikkim earthquake, *Natural hazards* **63(2)**, 589-603.
206. Mahood, M. and H. Hamzehloo (2009). Estimation of coda wave attenuation in East Central Iran, *J. Seism.* **13**, 125–139. DOI 10.1007/s10950-008-9130-2.
207. Mak, S., L. S. Chan, A. M. Chandler and R. C. H. Koo (2004). Coda Q_c estimates in the Hong Kong Region, *Journal of Asian Earth Sciences* **24(1)**, 127-136.
208. Mandal, P. and B.K. Rastogi (1998). A frequency-dependent relation of coda Q_c for Koyna-Warna region, India, *Pure Appl. Geophys.* **153**, 163–177.
209. Mandal, P., S. Padhy, B.K. Rastogi, H.V.S. Satyanarayana, M. Kousalaya R. Vijayraghavan and A. Srinivasan (2001). Aftershock activity and frequency-dependent low coda Q_c in the epicentral region of the 1999 Chamoli earthquake of magnitude M_w 6.4, *Pure. Appl. Geophys.* **158**, 1719–1735.
210. Mandal, P., Jainendra, S. Joshi, S. Kumar, R. Bhunia and B.K. Rastogi (2004). Low coda- Q_c in the epicentral region of the 2001 Bhuj Earthquake of M_w 7.7, *Pure Appl. Geophys.* **161**, 1635–1654.
211. Mandal, P. and A. Johnston (2006). Estimation of source parameters for the aftershocks of the 2001 M_w 7.7 Bhuj Earthquake, India, *Pure Appl. Geophys.* **163**, 1537–1560.
212. Mandal, P. and S. Horton (2007). Relocation of aftershocks, focal mechanisms and stress inversion: implications toward the seismo-tectonics of the causative fault zone

- of Mw7.6 2001 Bhuj earthquake (India), *Tectonophysics* **429(1)**, 61-78.
213. Mandal, H. S., P. K. Khan and A. K. Shukla (2013). Shear wave attenuation characteristics over the Central India Tectonic Zone and its surroundings, *Journal of Asian Earth Sciences* **73**, 440-451.
214. Madariaga, R. (1977). High-frequency radiation from crack (stress drop) models of earthquake faulting. *Geophys. J. Int.* **51(3)**, 625-651.
215. Madariaga, R. (1983). High frequency radiation from dynamic earthquake fault models. *Ann. Geophys.* **1(1)**, 17-23.
216. Madariaga, R. (2007). Seismic source theory. *Treatise on Geophysics* **4**, 59-82.
217. Maruyama, T. (1963). On the force equivalents of dynamical elastic dislocations with reference to the earthquake mechanism, *Bull. of the Earthquake Research Institute* **41**, 467-486.
218. Martha, T. R., K. Babu Govindharaj and K. Vinod Kumar (2014). Damage and geological assessment of the 18 September 2011 (M_w 6.9) earthquake in Sikkim, India using very high resolution satellite data, *Geoscience Frontiers*.
219. Masuda, T. (1988). Corner frequencies and Q values of P waves by simultaneous inversion technique, *Sci. Rep. to Univ. Ser. 5. Geophys* **31**, 101-125.
220. Mathur, L.P. and P. Evans (1964). Oil in India, Internat. Geol. Congress, 22nd Session, 1-85.
221. Mayeda, K., A. Hofstetter, J. L. O'Boyle and W. R. Walter (2003). Stable and transportable regional magnitudes based on coda-derived moment rate spectra, *Bull. Seism. Soc. Am.* **93**, 224-239.
222. McGarr, A. (1999). On relating apparent stress to the stress causing earthquake fault slip. *J. Geophys. Res.: Solid Earth (1978-2012)* **104(B2)**, 3003-3011.
223. McCaffrey, R. (2009). The tectonic framework of the Sumatran subduction zone, *Annual Reviews of Earth and Planetary Sciences* **37**, 345-366.
224. Menahem B.A. (1961). Radiation of seismic surface-waves from finite moving sources. *Bull. Seism. Soc. Am* **51(3)**, 401-435.

225. Menahem B.A. (1962). Radiation of seismic body waves from a finite moving source in the earth. *J. Geophys.Res.* **67(1)**, 345-350.
226. Miller, A.D., Foulger, G.R., Julian, B.R., 1998. Non-double-couple earthquakes 2: Observations. *Reviews of Geophysics* **36**, 551–568.
227. Mitchell, B. J. (1995). Anelastic structure and evolution of the continental crust and upper mantle from seismic surface wave attenuation, *Reviews of Geophysics* **334**, 441-462.
228. Mitchell, B. J. and L. Cong (1998). Lg coda Q and its relation to the structure and evolution of continents: A global perspective, *Pure Appl. Geophys.* **153**, 655–663.
229. Mohanty, W. K., R. Prakash, G. Suresh, A. K. Shukla, M. Y. Walling and J. P. Srivastava (2009). Estimation of coda wave attenuation for the national capital region, Delhi, India using local earthquakes, *Pure and applied Geophysics* **166(3)**, 429-449.
230. Mori, J., McKee, C., 1987. Outward-dipping ring-fault structure at Rabaul caldera as shown by earthquake locations. *Science* **235**, 193–195.
231. Molnar, P., B. E. Tucker and J. N. Brune (1973). Corner frequencies of P and S waves and models of earthquake sources, *Bull. Seism. Soc. Am.* **63(6-1)**, 2091-2104.
232. Molnar, P. (1987). The distribution of intensity associated with the 1905 Kangra earthquake and bounds of the extent of the rupture zone; *J.Geol.Soc.India* **29**, 211–229
233. Molnar, P. (1990). A review of the seismicity and the rates of active under thrusting and deformation at the Himalaya, *J. Him. Geol.* **1**,131-154
234. Mukhopadhyay, M. (1984). Seismotectonics of transverse lineaments in the eastern Himalaya and foredeep. *Tectonophysics* **109**, 227–240.

235. Mukhopadhyay, S. (1990). Seismic velocity structure and seismotectonics of the Shillong massif, north eastern India. Unpublished Ph. D. thesis, Univ. of Roorkee, 247.
236. Mukhopadhyay, S. and C. Tyagi (2007). Lapse time and frequency-dependent attenuation characteristics of coda waves in the Northwestern Himalayas, *J. Seism.* *11(2)*, 149-158.
237. Mukhopadhyay, S., J. Sharma, R. Massey and J. R. Kayal (2008). Short Note Lapse-Time Dependence of Coda Q in the Source Region of the 1999 Chamoli Earthquake, *Bull. Seism. Soc. Am.* **98(4)**, 2080-2086.
238. Nakano, H. (1923). Notes on the nature of the forces which give rise to the earthquake motions. *Seismological Bulletin of Central METROLOGICAL Observatory of Japan* **1**, 92–120.
239. Nandy, D.R. (1976). The Assam syntaxis of the Himalayas—a reevaluation. *Semin Rec Geol Study Himal Misc Publ Geol Surv India* **24**, 363-368.
240. Narula, P.L., R. Shanker and S. Chopra (2000). Rupture mechanism of Chamoli earthquake on 29 March 1999 and its implication for seismotectonics of Garhwal Himayala, *J. Geol. Soc. of India* **55**, 493-503.
241. Nath, S. K., K. K. S. Thingbaijam and A. Raj (2008). Earthquake hazard in northeast India—a seismic microzonation approach with typical case studies from Sikkim Himalaya and Guwahati city, *Journal of earth system science* **117(2)**, 809-831.
242. Narula, P.L., R. Shanker and S. Chopra (2000). Rupture mechanism of Chamoli earthquake on 29 March 1999 and its implication for seismotectonics of Garhwal Himayala, *J. Geol. Soc. of India* **55**, 493-503.

243. Ni, J. and M. Barazangi (1984). Seismotectonics of the Himalayan collision geometry of the underthrusting Indian Plate beneath the Himalaya, *J. Geophys. Res.* **89**, 1147– 1163.
244. Nishimura, G (1937). On the Elastic Waves due to Pressure Variation on the Inner Surface of a Spherical Cavity in an Elastic Solid. *Bull. Earthquake Res. Inst.* 15, 614-635.
245. Oth, A., D. Bindi, S. Parolai and F. Wenzel (2008). S-wave attenuation characteristics beneath the Vrancea region in Romania: new insights from the inversion of ground-motion spectra, *Bull. Seism. Soc. Am* **98(5)**, 2482-2497.
246. O'Connell, D.R.H. and L.R. Johnson (1988). Second-order moment tensors of microearthquakes at the Geysers Geothermal Field, California. *Bull. Seism. Soc. Am.* **78**, 1674--1692.
247. Oldham, R. D. (1899). Report of the great earthquake of 12th June, 1897, Office of the Geological survey.
248. Padhy, S. (2009). Characteristics of body wave attenuations in the Bhuj crust, *Bull. Seism. Soc. Am.* **99**, 3300–3313.
249. Padhy, S. and N. Subhadra (2010). Attenuation of high-frequency seismic waves in northeast India, *Geophys. J. Int.* **181(1)**, 453-467.
250. Parvez, I. A., A. K. Sutar, M. Mridula, S. K. Mishra and S. S. Rai (2008). Coda Q estimates in the Andaman Islands using local earthquakes, *Pure and appl. Geophys.* **165(9-10)**, 1861-1878.
251. Papageorgiou, A. S. and K. Aki (1983a). A specific barrier model for the quantitative description of inhomogeneous faulting and the prediction of strong ground motion. I. Description of the model, *Bull. Seism. Soc. Am.* **73**, 693-722.

252. Papageorgiou, A. S. and K. Aki (1983b). A specific barrier model for the quantitative description of inhomogeneous faulting and the prediction of strong ground motion. II. Application of the model, *Bull. Seism. Soc. Am.* **73**, 953-978.
253. Parvez, I. A., P. Yadav and K. Nagaraj (2012). Attenuation of P, S and Coda Waves in the NW-Himalayas, India, *Int. J. Geosciences* **3**(1).
254. Pasyanos M.E., D.S. Dreger and B. Romanowicz (1996). Toward real time estimation of regional moment tensors, *Bull. Seism. Soc. Am.* **86**, 1255-1269.
255. Patton, H. and K. Aki (1979). Bias in the estimate of seismic moment tensor by the linear inversion method. *Geophys. J. the Royal Astronomical Soc.* **59**, 479-498.
256. Patton, H. (1980). Reference point equalization method for determining the source and path effects of surface waves, *J. Geophys. Res.: Solid Earth* **85** (B2), 821-848.
257. Paul, A., S. Gupta and C. C. Pant (2003). Coda Q estimates for Kumaun Himalaya, *Proc. Indian Acad. Sci.* **112**, 569-576.
258. Paul, A., B. Kumar, V. Rana and D. Gandhiyan (2007). Low stress drop earthquakes in the Garhwal Himalayan region, *Journal of Himalayan Geology, (Abs. Volume)* 28 (3), 29.
259. Paul, A. and N. Kumar (2010). Estimates of source parameters of M 4.9 Kharsali earthquake using waveform modeling, *J. Earth Syst. Sci.* 119 (5), 731-743.
260. Pieri, M. and L. Mattavelli (1986). Geological Framework of Italian Petroleum Resources, *Am. Ass. Petrol. Geol. Bull.* **70** (2), 103-130.
261. Pinar, A., K. Kuge and Y. Honkura (2003). Moment-tensor inversion of recent small to moderate sized earthquakes: Implications for seismic hazard and active tectonics beneath the sea of Marmara, *Geophys. J. Int.* **153**, 133-145.
262. Pradhan, R., S. K. Prajapati, S. Chopra, A. Kumar, B. K. Bansal and C. D. Reddy (2013). Causative source of Mw6.9 Sikkim-Nepal border earthquake of September 2011: GPS baseline observations and strain analysis, *J. Asian Earth Sciences* **70**, 179-192.

263. Prajapati, S. K., A. Kumar, S. Chopra and B. K. Bansal (2013). Intensity map of Mw 6.9 2011 Sikkim–Nepal border earthquake and its relationships with PGA: distance and magnitude, *Natural hazards* **69(3)**, 1781-1801.
264. Prejean, S. G. and W. L. Ellsworth (2001). Observations of earthquake source parameters at 2 km depth in the Long Valley caldera, eastern California, *Bull. Seism. Soc. Am.* **91(2)**, 165-177.
265. Pulli, J.J. (1984). Attenuation in New England, *Bull. Seism. Soc. Am.* **74**, 1149–1166.
266. Pujades, L., J.A. Canas, J.J. Egozcue, M.A. Puigvi, J. Pous, J. Gallart, , X. Lana, and A. Casas (1991). Coda Q distribution in the Iberian Peninsula, *Geophys. J. Int.* **100**, 285–301.
267. Rajendran, C. P. and K. Rajendran, (2005). The status of central seismic gap: A perspective based on the spatial and temporal aspects of the large Himalayan earthquakes, *Tectonophysics* **395(1)**, 19-39.
268. Rao, A. R. (1983). Geology and hydrocarbon potential of a part of Assam–Arakan basin and its adjacent region. Petroliferous Basins of India, *Petroleum Asia J.* 127-158.
269. Rao, N. P. and M. R. Kumar (1999). Evidences for cessation of Indian plate subduction in the Burmese arc region. *Geophysical research letters*, 26(20), 3149-3152.
270. Rao, C. N., N. P. Rao and B. K. Rastogi (2013). Evidence for right-lateral strike-slip environment in the Kutch basin of northwestern India from moment tensor inversion studies, *Journal of Asian Earth Sciences* **64**, 158-167.
271. Rastogi, B. K. Singh, J. Verma, R. K. (1973). Earthquake mechanism and tectonics in the Asia-Burma region, *Tectonophysics* **18**, 355- 366.

272. Rautian, T.G. and V.I. Khalturin (1978). The use of the coda for the determination of the earthquake source spectrum, *Bull. Seism. Soc. Am.* **68**, 923–948.
273. Rautian, T.G., V.I. Khalturin, V.G. Martynov and P. Molnar (1978). Preliminary analysis of the spectral content of P and S waves from local earthquakes in the Garm, Tadjikistan region, *Bull. Seism. Soc. Am.* **68**, 949–971.
274. Reid, H. F. (1910). The mechanics of the earthquake (Vol. 2). Carnegie institution of Washington.
275. Richards, P.G. and W. Menke (1983). The apparent attenuation of a scattering medium, *Bull. Seism. Soc. Am.* **73**, 1005–1021.
276. Roecker, S.W., B. Tucker, J. King and D. Hartzfield (1982). Estimates of Q in Central Asia as a function of frequency and depth using the coda of locally recorded earthquakes, *Bull. Seism. Soc. Am.* **72**, 129–149.
277. Ross, A.G., G.R. Foulger and B.R. Julian (1996). Non-double-couple earthquake mechanisms at the Geysers geothermal area, California, *Geophys. Res. Lett.* **23**, 877–880.
278. Rovelli, A. (1982). On the frequency dependence of Q in Friuli from short period digital records, *Bull. Seism. Soc. Am.* **72**, 2369–2372.
279. Rovelli, A. (1984). Seismic Q for the lithosphere of the Montenegro region (Yugoslavia): frequency, depth, and time windowing effects, *Phys. Earth Planet. Inter.* **34**, 159–172.
280. ROY, S. S. (1976). A possible Himalayan microcontinent, 117-120.
281. Rudajev, V. and J. Sileny (1985). Seismic events with non-shear components, II, Rockbursts with implosive source component, *Pure and Appl. Geophys.* **123**, 17–25.
282. Sato, H. (1977). Energy propagation including scattering effect, *J. Phys. Earth.* **25**, 27–41.

283. Savage, J. C. (1966). Radiation from a realistic model of faulting. *Bull. Seism. Soc. Am* **56(2)**, 577-592.
284. Sato, H. (1992). Thermal Structure of the Mantle Wedge beneath Northeastern Japan: Magmatism in an Island Arc from the Combined Data of Seismic Anelasticity and Velocity and Heat Flow, *J. Volcanol. Geotherm. Res.* **51**, 237–252.
285. Sato, H. and M. Fehler (1998). Scattering and attenuation of seismic waves in heterogeneous earth, AIP press, Springer Verlag, New York.
286. Scott, D.R. and H. Kanamori (1985). On the consistency of moment tensor source mechanisms with first motion data, *Physics of the Earth and Planetary Interiors* **37**, 97-107.
287. Scholte, J. G. J., & Ritsema, A. R. (1962). Generation of earthquakes by a volume source with moment. *Bull. Seism. Soc. Am* **52(4)**, 747-765.
288. Sekiguchi, S. (1991). Three-dimensional Q structure beneath Kanto-Tokai district, Japan, *Tectonophysics* **195**, 83–104.
289. Shanker, R., Kumar, G. and Saxena, S. P. (1989). Stratigraphy and sedimentation in Himalaya: a reappraisal. In *Geology and tectonics of the Himalaya* **26**, pp. 1-60.
290. Shanker, R., V. K. Mathur, G. O. Kumar, Pendra and M. C. Srivastava (1997). Additional Ediacaran biota from the Krol Group, Lesser Himalaya, India and their significance, *Geosci. J.* **18**, 79-94.
291. Sharma, M. L. and H. R. Wason (1994), Occurrence of low stress drop earthquakes in the Garwal Himalayan region. *Physics of the Earth and Plantary Interiors* **85**, 265-272.
292. Sharma, B., S.S. Teotia and D. Kumar (2007). Attenuation of P, S and coda waves in Koyna region, India, *J. Seism.* **11**, 327–344.

293. Sharma, B., A.K. Gupta, D. K. Devi, D. Kumar, S.S. Teotia and B. K. Rastogi (2008). Attenuation of high frequency seismic waves in Kachchh region, Gujarat, India, *Bull. Seism. Soc. Am.* **98**, 2325–2340.
294. Sharma, B., S. S. Teotia, D. Kumar and P. S. Raju (2009). Attenuation of P-and S-waves in the Chamoli Region, Himalaya, India, *Pure and applied geophysics* **166(12)**, 1949-1966.
295. Sharma, B., D. Kumar, S. S. Teotia, B. K. Rastogi, Arun K. Gupta and S. Prajapati (2011). Attenuation of Coda Waves in the Saurashtra Region, Gujarat (India), *Pure Appl. Geophys.* **169(1-2)**, 89-100. DOI: 10.1007/s00024-011-0295-1.
296. Shashidhar, D., N. P. Rao and H. Gupta (2011). Waveform inversion of broad-band data of local earthquakes in the Koyna–Warna region, western India, *Geophys. J. Int.*, **185(1)**, 292-304.
297. Seeber, L. and J. G. Armbruster (1981). Great detachment earthquakes along the Himalayan arc and long-term forecasting, *Earthquake prediction* 259-277.
298. Sherbaum, F. and C. Kisslinger (1985). Coda *Q* in the Adak seismic zone, *Bull. Seism. Soc. Am.* **75**, 615–620.
299. Sieh K. and D. Natawidjaja (2000). Neotectonic of the Sumatran fault, Indonesia, *J. Geophys. Res.* **105(B12)**, 28295–28326, doi:10.1029/2000JB900120
300. Sileny, J. and V. Vavrycuk (2000). Approximate retrieval of the point source in anisotropic media: numerical modeling by indirect parameterization of the source. *Geophys. J. Int.* **143**, 700–708.
301. Sileny, J. and A. Milev (2008). Source mechanism of mining induced seismic events—resolution of double couple and non-double couple models. *Tectonophysics* **456(1)**, 3-15.

302. Síleny, J., D. P. Hill, L. Eisner and F. H. Cornet (2009). Non–double-couple mechanisms of microearthquakes induced by hydraulic fracturing, *J. Geophys. Res.: Solid Earth* **114(B8)**, 1978–2012.
303. Singh, I. B. (1996). Geological evolution of Ganga Plain – an overview, *J. Palaeont. Soc. India* **41** 99–137.
304. Singh, D. D. and H. K. Gupta (1980). Source dynamics of two great earthquakes of the Indian subcontinent, *Bull. Seism. Soc. Am.* **70 (3)**, 757-773.
305. Singh, S.K. and R.B. Herrmann (1983). Regionalization of crustal coda Q in the continental United States, *J. Geophys. Res.* **88**, 527–538.
doi:10.1029/JB088iB01p00527
306. Singh, S. and P.K. Chowdhary (1990). An outline of the geological framework of the Arunachal Himalaya, *Journal of Himalayan Geology* **1(2)**, 189–197.
307. Singh, S. (1993). Geology and tectonics of the Eastern Syntaxial Bend, Arunachal Himalaya, *J. Himalayan Geol.* **4(2)**, pp.149-163.
308. Singh, I. B. (1996). Geological evolution of Ganga Plain – an overview, *J. Palaeont. Soc. India* **41**, 99–137.
309. Singh, S.K., J. Paeheco, F. Courboux and D.A. Novelo (1997). Source parameters of the Pinotepa Nacional, Mexico, earthquake of 27 March, 1996 ($M_w = 5.4$) estimated from near-field recordings of a single station, *J. Seism.* **1**,39-45
310. Singh, S. K., R. S. Dattatrayam, N. M. Shapiro, P. Mandal, J. F. Pacheco and R. K. Midha (1999). Crustal and upper mantle structure of Peninsular India and source parameters of the 21 May 1997, Jabalpur earthquake ($M_w = 5.8$): Results from a new regional broadband network, *Bull. Seism. Soc. Am.* **89(6)**, 1631-1641.

311. Singh, S.K., M. Ordaz, J.F. Pacheco and F. Courboulex (2000). A simple source inversion scheme for displacement seismograms recorded at short distances, *J. Seism.* **4(3)**, 267-284.
312. Singh, C., A. Singh, V. K. Bharathi, A. R. Bansal, and R. K. Chadha (2012). Frequency-dependent body wave attenuation characteristics in the Kumaun Himalaya, *Tectonophysics* **524**, 37-42.
313. Singh, C., V. K. Srinivasa Bharathi and R. K. Chadha (2012). Lapse time and frequency-dependent attenuation characteristics of Kumaun Himalaya. *Journal of Asian Earth Sciences* **54**, 64-71.
314. Sipkin, S. (1982). Estimation of earthquake source parameters by the inversion of waveform data: synthetic waveforms, *Phys. Earth Planet Int.* **30**, 242-259.
315. Sipkin, S.A. (1986). Interpretation of non-double-couple earthquake mechanisms derived from moment tensor inversion, *J. Geophys. Res.: Solid Earth* **91(B1)**, 531-547.
316. Snoke, J.A., J.W. Munsey, A.G. Teague and G.A. Bollinger (1984). A program for focal mechanism determination by combined use of polarity and SV-P amplitude ratio data, *Earthquake notes* 55p.
317. Sokos, E. and J. Zahradnik (2008). ISOLA—a Fortran code and a Matlab GUI to perform multiple-point source inversion of seismic data, *Comput. Geosci.* **34**, 967–977.
318. Sonley, E. and R. E. Abercrombie (2006). Effects of methods of attenuation correction on source parameter determination. *Earthquakes: Radiated Energy and the Physics of Faulting*, 91-97.

319. Stead, R.J. (1990). Finite differences and a coupled analytic technique with applications to explosions and earthquakes (Doctoral dissertation, California Institute of Technology).
320. Sriram, V. and K. N. Khattri (1997). A study of source spectrum, site amplification functions, response spectra, Fourier spectra and peak ground accelerations from the strong ground motion data of the 1991 Uttarkahi earthquake, *Curr. Sci.* **72**, 728-740.
321. Stierle, E., V. Vavrycuk, J. Síleny and M. Bohnhoff (2014). Resolution of non-double-couple components in the seismic moment tensor using regional networks—I: a synthetic case study, *Geophys. J. Int.* **3**, 1869-1877.
322. Stierle, E., M. Bohnhoff and V. Vavrycuk (2014). Resolution of non-double-couple components in the seismic moment tensor using regional networks—II: application to aftershocks of the 1999 Mw 7.4 Izmit earthquake, *Geophys. J. Int.* **196(3)**, 1878-1888.
323. Stump, B.W. and L.R. Johnson (1977). The determination of source properties by the linear inversion of seismograms, *Bull. Seism. Soc. Am.* **67(6)**, 1489-1502.
324. Tandon, A. N. and H. N. Srivastava (1974). The stress drop and average dislocation of some earthquakes in the Indian-subcontinent, *Pageoph.* **112**, 1051-1057.
325. Thakur, V. C., A. K. Mahajan and V. Gupta (2012). Seismotectonics of 18 September 2011 Sikkim earthquake: a component of transcurrent deformation in eastern Himalaya, *Himalayan Geology* **33(1)**, 89-96.
326. Thin, H.K. and H. Kanamori (1996). Source complexity of the 1994 Northridge earthquake and its relation to aftershock mechanisms, *Bull. Seism. Soc. Am.* **86(1B)**, S84-S92.

327. Tocheport, A., L. Rivera and J. Vander Woerd (2006). A study of the 14 November 2001 Kokoxili earthquake: history and geometry of the rupture from teleseismic data and field observations, *Bull. Seism. Soc. Am.* **96**, 1729–1741.
328. Toksoz, M.N., A.H. Johnston and A. Timur (1978). Attenuation of seismic waves in dry and saturated rocks. I. Laboratory measurements, *Geophys.* **44**, 681–690.
329. Tripathi, J. N., P. Singh, and M. L. Sharma (2012). Variation of Seismic Coda Wave Attenuation in the Garhwal Region, Northwestern Himalaya, *Pure and applied geophysics* **169(1-2)**, 71-88.
330. Tsujiura M., (1978). Spectral analysis of coda waves from local earthquakes, *Bull. Earthquake Res. Inst. Univ. Tokyo* **53**, 1–48.
331. Udías, A. and Buforn, E. (1991). Regional stresses along the Eurasia-Africa plate boundary derived from focal mechanisms of large earthquakes. *pure and applied geophysics* **136(4)**, 433-448.
332. Ugalde, A., J. N. Tripathi, M. Hoshiba and B. K. Rastogi (2007). Intrinsic and scattering attenuation in western India from aftershocks of the 26 January, 2001 Kachchh earthquake, *Tectonophysics* **429(1)**, 111-123.
333. Valdiya, K.S. (1981.) The tectonics of the central sector of the Himalaya. In: H.K. Gupta & F.M. Delany (Eds.), *Zagros–Hindukush–Himalaya: Geodynamic Evolution. Amer. Geophys. Union, Washington* 87–110.
334. Vallee, M. and M. Bouchon (2004). Imaging coseismic rupture in far field by slip patches, *Geophys. J. Int.* **156**, 615–630.
335. Vallina, A. U. (1999). *Principles of Seism.* . Cambridge University Press.
336. Van Eck, T. (1988). Attenuation of coda waves in the Dead Sea region. *Bull. Seism. Soc. Am.* **2**, 770–779.

337. Vavryčuk, V. (2001). Inversion for parameters of tensile earthquakes, *J. Geophys. Res.*, **106 (B8)**, 16.339-16.355.
338. Vavryčuk, V., 2007. On the retrieval of moment tensors from borehole data, *Geophys. Prospect.*, **55**, 381–391.
339. Vavryčuk, V., 2011. Tensile earthquakes: theory, modeling, and inversion, *J. geophys. Res.*, **116(B12)**, B12320,
340. Vavryčuk, V., and D. Kühn (2012), Moment tensor inversion of waveforms: A two-step time-frequency approach, *Geophys. J. Int.*, 190, 1761–1776.
341. Vavryčuk, V., and Kim, S. G. (2014). Nonisotropic radiation of the 2013 North Korean nuclear explosion. *Geophys. Res. Lett.* **41(20)**, 7048-7056.
342. Verma , R.K., M. Mukhopadhyay and , M.S. Ahluwalia (1976). Seismicity, gravity and tectonics of Northeast India and Northern Burma, *Bull. Seism. Soc. Am.* **66**, 1683–1694.
343. Verma, R. K. and G. V. R. Kumar (1987). Seismicity and the nature of plate movement along the Himalayan arc, Northeast India and Arakan-Yoma: a review, *Tectonophysics* **134(1)**, 153-175.
344. Verma, R. K. (1991). Seismicity of the Himalaya and the northeast India, and nature of continent-continent collision, *Physics and Chemistry of the Earth* **18**, 345-370.
345. Wallace, T.C. (1985). A reexamination of the moment tensor solutions of the 1980 Mammoth Lakes earthquakes, *J. Geophys. Res.* **90**, 11,171–11,176
346. Walter, W.R. (1993). Source parameters of the June 29, 1992, Little Skull Mountain earthquake from complete regional waveforms at a single station, *Geophys. Res. Lett.* **20**, 403-406.

347. Wang, Y., K. Sieh, S.T. Tun, K.Y. Lai and T. Myint (2014). Active tectonics and earthquake potential of the Myanmar region, *J. Geophys. Res.: Solid Earth* **119(4)**: 3767-3822.
348. Ward, S.N. (1980b). A technique for the recovery of the seismic moment tensor applied to the Oaxaca, Mexico earthquake of November 1978, *Bull. Seism. Soc. Am.* **70**, 717-734.
349. Wason, H. R. and M. L. Sharma (2000). Source parameters study of local earthquakes in the Garhwal Himalaya based on the digital broadband data, *12WCEE*, 1776 (1-6).
350. Wennerberg, L. (1993). Multiple-scattering interpretations of coda-Q measurements, *Bull. Seism. Soc. Am.* **83**, 279–290.
351. Wenzel, F., M. C. Oncescu, M. Baur, F. Fiedrich, and C. Ionescu (1999). An early warning system for Bucharest, *Seism. Res. Lett.* **70(2)**, 161-169.
352. Wilkie, J. and G. Gibson (1995). Estimation of seismic quality factor Q for Victoria, Australia, *AGSO J. Aust. Geol. Geophys.* **15**, 511–517.
353. Woodgold, C. (1994). Coda-Q in Charlevoix, Quebec, Region. Lapse time dependence and Spatial and temporal comparisons, *Bull. Seism. Soc. Am.* **84**, 1123–1131.
354. Yadav, R. B. S., Bormann, P., Rastogi, B. K., Das, M. C., & Chopra, S. (2009). A homogeneous and complete earthquake catalog for northeast India and the adjoining region. *Seismological Research Letters* **80(4)**, 609-627.
355. Yoshimoto, K., Sato, H., & Ohtake, M. (1993). Frequency-dependent attenuation of P and S waves in the Kanto area, Japan, based on the coda-normalization method. *Geophys. Jo. Int.* **114(1)**, 165-174.
356. Yoshimoto, K., H. Sato, Y. Ito, H. Ito, T. Ohminato and M. Ohtake (1998). Frequency-dependent attenuation of high-frequency P and S waves in the upper crust in western Nagano, Japan, *Pure Appl. Geophys.* **153**, 489–502.

357. Yun, S., W. S. Lee, K. Lee and M. H. Noh (2007). Spatial distribution of coda Q in south Korea, *Bull. Seism. Soc. Am.* **97**, 1012–1018.
358. Zeng, Y., F. Su and K. Aki (1991). Scattered wave energy propagation in a random isotropic scattering medium, I, theory, *J. Geophys. Res.* **96**, 607–619.
359. Zahradnik, J., A. Serpetsidaki, E. Sokos and G.A. Tselentis (2005). Iterative deconvolution of regional waveforms and double-event interpretation of the 2003 Lefkada earthquake, Greece, *Bull. Seism. Soc. Am.* **95**, 159–172.
360. Zahradnik, J., J. Jansky and V. Plicka (2008). Detailed waveform inversion for moment tensors of m 4 events: examples from the Corinth gulf, Greece, *Bull. Seism. Soc. Am.* **98(6)**, 2756–2771.